



I.R.Iran

ISSN:2423-5547
e-ISSN:2423-7469



Journal of Renewable Energy and Environment

Volume 10, Number 1, Winter 2023



Materials and Energy
Research Center



Iranian Association of
Chemical Engineers

Journal of Renewable Energy and Environment

DIRECTOR-IN-CHARGE

H. Omidvar

Amirkabir University of Technology (Tehran Polytechnic), Tehran, Iran

EDITOR-IN-CHIEF

M. Pazouki

Materials and Energy Research Center, Karaj, Iran

EDITORIAL BOARD

M. Ameri, Shahid Beheshti University, Tehran, Iran

S. S. Chandel, Shoolini University, Solan, Himachal Pradesh, India

J. Chaouki, Polytechnique Montréal, Montreal, Canada

H. Ghadami, Materials and Energy Research Center, Karaj, Iran

B. Ghobadian, Tarbiat Modares University, Tehran, Iran

W. K. H. Hogland, Linnaeus University, Kalmar, Sweden

S. M. Hosseinalipoor, Iran University of Science and Technology, Tehran, Iran

H. A. Kazem, Sohar University, Sohar, Sultanate of Oman

K. Kaygusuz, Karadeniz Technical University, Trabzon, Turkey

A. Mostafaeipour, Yazd University, Yazd, Iran

G. H. Najafi, Tarbiat Modares University, Tehran, Iran

M. R. Omidkhan, Tarbiat Modares University, Tehran, Iran

M. H. Panjeshahi, Tehran University, Tehran, Iran

M. Pazouki, Materials and Energy Research Center, Karaj, Iran

R. Roshandel, Sharif University of Technology, Tehran, Iran

M. B. Shafii, Sharif University of Technology, Tehran, Iran

J. Shayegan, Sharif University of Technology, Tehran, Iran

T. Yusaf, Federation University Australia, Ballarat, Australia

S. A. H. Zamzami, Materials and Energy Research Center, Karaj, Iran

EDITORIAL ADVISORY BOARD

N. Azbar, Ege University, Izmir, Turkey

M. El Haj Assad, University of Sharjah, Sharjah, United Arab Emirates

A. Maheri, University of Aberdeen, Aberdeen, United Kingdom

M. Mohanraj, Hindusthan College of Engineering and Technology, Coimbatore, Tamil Nadu, India

A. Sedaghat, Australian College of Kuwait, Kuwait

MANAGING EDITOR

M. Fouladian

LANGUAGE EDITOR

S. Saberi

PAGE DESIGNER

F. Hajizadeh

JOURNAL STAFF

M. Fouladian, V. Hajabdolali Bazzaz, E. Pouladi, R. Chaluei

DISCLAIMER

The publication of articles in *Journal of Renewable Energy and Environment* does not imply that the editorial board, reviewers, or the publisher accept, approve, or endorse the data and conclusions of authors.

Journal of Renewable Energy and Environment: (ISSN: 2423-5547) (e-ISSN: 2423-7469)

Website: www.jree.ir, E-mail: jree@merc.ac.ir

Tel: (+9826)36280040-49 (Ext. 381), Fax: (+9826)36201888

Journal of Renewable Energy and Environment, P. O. Box: 13145-1659, Tehran, Islamic Republic of Iran
Materials and Energy Research Center (MERC); Iranian Association of Chemical Engineers (IACHE)

CONTENTS

Roxana Isabel Bernaola Flores Carmen Elena Flores Barreda Diana Carolina Parada Quinayá Ursula Fabiola Rodríguez Zúñiga	Energy Potential of Agricultural and Forestry By-Products in Peru	1-8
Farhad Amiri Mohammad Hassan Moradi	Improvement of Frequency Stability in the Power System Considering Wind Turbine and Time Delay	9-18
Sapna Kinattinkara Thangavelu Arumugam Nandhini Samiappan Vivek Sivakumar Sampathkumar Velusamy Mohanraj Murugesan Manoj Shanmugamoorthy	Deriving an Alternative Energy Using Anaerobic Co-Digestion of Water Hyacinth, Food Waste, and Cow Manure	19-25
Toyese Friday Oyewusi Gabriel Alebiowu Elizabeth Funmilayo Aransiola Ayowumi Rita Soji-Adekunle Busayo Sunday Adeboye	Effect of Pretreatment on the Physical Properties and Heating Values of Briquettes	26-33
Allen G. Njovana Wenyong Yu Qiyong Shen Jiarui Li Yanyan Zhu Yongsheng Liu	Potential for Battery Energy Storage System in Zimbabwe	34-42
Ghazanfar Shahgholian	A Brief Overview of Microgrid Performance Improvements Using Distributed FACTS Devices	43-58
Mohammad Rahimzadeh Hamid Samadi Nikta Shams Mohammadi	Improving the Efficiency of a Cantilever Energy Scavenger	59-67
Mohammad Rasooli Mavini Hassan Ali Ozgoli Sadegh Safari	Investigation of a Set of Novel Heat Exchanger Configurations of a Heat Recovery Steam Generator to Improve the Energy Efficiency of Combined Cycle Power Plant	68-82

AIMS AND SCOPE

Journal of Renewable Energy and Environment (JREE) publishes original papers, review articles, short communications and technical notes in the field of science and technology of renewable energies and environmental-related issues including:

- Generation
- Storage
- Conversion
- Distribution
- Management (economics, policies and planning)
- Environmental Sustainability

INSTRUCTIONS FOR AUTHORS

Submission of manuscript represents that it had neither been published nor submitted for publication elsewhere and is result of research carried out by author(s). Only the extended and upgraded articles presented in a conference and/or appeared in a symposium proceedings could be evaluated for publication.

Authors are required to include a list describing all the symbols and abbreviations in the paper. Use of the international system of measurement units is mandatory.

- On-line submission of manuscripts results in faster publication process and is recommended. Instructions are given in the JREE web sites: www.jree.ir
- References should be numbered in brackets and appear in sequence through the text. List of references should be given at the end of the paper. All journal articles listed in the References section must follow with article doi.
- Figure captions are to be indicated under the illustrations. They should sufficiently explain the figures.
- Illustrations should appear in their appropriate places in the text.
- Tables and diagrams should be submitted in a form suitable for reproduction.
- Photographs should be of high quality saved as jpg files.
- Tables' illustrations, figures and diagrams will be normally printed in single column width (8 cm). Exceptionally large ones may be printed across two columns (17 cm).



Research Note

Energy Potential of Agricultural and Forestry By-Products in Peru

Roxana Isabel Bernaola Flores, Carmen Elena Flores Barreda, Diana Carolina Parada Quinayá, Ursula Fabiola Rodríguez Zúñiga*

Department of Chemical Engineering, University of Engineering and Technology, Jr. Medrano Silva 165, Barranco, Lima, Peru.

PAPER INFO

Paper history:

Received: 11 January 2022
Revised in revised form: 31 March 2022
Scientific Accepted: 07 April 2022
Published: 27 July 2022

Keywords:

Energy from Agriculture,
Renewable Biofuels,
Circular Economy,
Calorific Value

ABSTRACT

Reducing the demand for fossil fuels and the derived products can be achieved through the development of alternative energy sources. This work presents a countrywide study of the energy potential of lignocellulosic biomass sourced from agro-industrial by-products in the country of Peru. Ranking of the crops that produce the most waste was followed by an energy potential evaluation of carbohydrate conversion and thermochemical conversion. The crops with high calorific values were sugar cane bagasse, wood waste, and coffee husk. The energy potential of the principal lignocellulosic by-products, in terms of tons of oil equivalents per year, resulted from rice straw at 1.45 M, followed by corn residue at 1.13 M and sugar cane residue at 1.10 M. The northern region of Peru generated the highest quantities of rice (straw and husk), banana (husk and rachis), and sugar cane (bagasse and straw) by-products and the southern regions generated the greatest quantities of quinoa residue, all of which could be used as raw materials for biofuels and aggregates for materials. These results indicate that theoretically, this readily available biomass could meet the country's energy demands while promoting sustainability and national energy security.

<https://doi.org/10.30501/jree.2022.323731.1310>

1. INTRODUCTION

Non-renewable fossil fuels, such as coal, oil and natural gas, are currently the main source of energy for the development of public, private, and residential activities. As is well known, consumption of these high-energy fuels generates harmful waste products such as CO₂, greenhouse gas (GHG), NO_x, one of the main components of smog, and SO₂, and the precursor of acid rain. Additionally, the International Energy Agency (IEA) predicts that worldwide oil and gas reserves will fall by up to 60 % by 2030 while energy demand will continue to rise. For example, the growth per capita energy consumption in the United States depletes their fossil-fuel reserves in approximately 10 years [1].

A biofuel is a type of renewable and green fuel, where its energy is derived from biological carbon fixation and can be a solid like wood, liquid like bioethanol and biodiesel, or gas like syngas [2]. Nonetheless, biofuels are considered an effective alternative energy source for decreasing GHG emissions [3]. The most common biofuels produced worldwide are bioethanol, biogas, and biodiesel. New options including biobutanol, biopropanol, and syngas are currently under study [4]. Potential sources of biofuels consist of natural vegetation, cultivated products like fast growing trees and

other crops grown for energy, residues from other agricultural activities such as forestry and food production, as well as other by-product sources such as city, husbandry, and slaughterhouse waste [2].

In recent years, lignocellulosic biomass from forestry and by-products of crop production has been studied for efficient conversion into both renewable energy sources as well as fibers for composite material manufacturing [5]. This waste to biomass repurposing also occurs in the production of organic acids, absorbent materials, fertilizers, high oils, and fermentation products, all comprising important aspects of the bio economy [6]. As such, lignocellulosic biomass sources are considered important platforms to promote energy independence as well as rural development while indirectly helping to reduce the impact of greenhouse gases by fostering food security and process and environmental sustainability [7]. Lignocellulosic waste from the forest sector is most often used in the form of sawdust and chips and as a low-cost energy source in the form of pellets and briquettes [8-10].

On the other hand, the agricultural sector in Peru is one of the main contributors to the national Gross Domestic Product (GDP) and the economies of several regions are dependent directly on this sector. As both agricultural exports and domestic food demand grow, their waste residues will also grow. Currently, much of residual biomass is discarded, incinerated, or repurposed for compost, with a small fraction used as animal feed, fertilizer, and solid and liquid biofuels.

*Corresponding Author's Email: urodriguez@utec.edu.pe (U.F. Rodríguez Zúñiga)

URL: https://www.jree.ir/article_154098.html

Please cite this article as: Bernaola Flores, R.I., Flores Barreda, C.E., Parada Quinayá, D.C. and Rodríguez Zúñiga, U.F., "Energy potential of agricultural and forestry by-products in Peru", *Journal of Renewable Energy and Environment (JREE)*, Vol. 10, No. 1, (2023), 1-8. (<https://doi.org/10.30501/jree.2022.323731.1310>).



The objective of this research is to assess the energy potential and development opportunities for the utilization of lignocellulosic biomass in Peru. The authors hypothesized that biomass feedstock agricultural by-products would be enough to cover the energy demands in terms of ethanol production and heating value. To this end, this study organized its framework as follows. The existing non-renewable and renewable resource energy matrix for Peru is presented, along with current and future projection levels of the agricultural production of crops that could generate useful by-products. A literature review of research on the use of lignocellulosic biomass in Peru is then presented, followed by the energy potential for each crop by-product in terms of Higher Heating Value (HHV). The next section covers chemical characterization of each individual crop by-product and its energy potential in theoretical bioethanol yield. Complementary tons of oil equivalent (TOE) of all the geographical regions is used as an indicator to rank them prospectively considering the availability of feedstock to produce energy.

2. METHODOLOGY

In order to verify the proposed hypothesis, the information resulting from the literature review in the Google Scholar database of the last 7 years and in university thesis repositories on the Internet is presented. Websites from governmental entities such as Ministry of Agriculture and Irrigation (MINAGRI) [11-14] and Ministry of Energy and Mining (MEM) [15-17] were surveyed in order to have national production data organized in tables in the next sections. Ethanol yield was selected to verify the quantity of cellulosic bioethanol that could be produced from agricultural feedstocks. Theoretical ethanol yield from the compositional cellulose (glucan in $\text{mL}\cdot\text{g}^{-1}$) was calculated through this relationship: $[(180 \text{ g of glucose}/162 \text{ g of glucan}) \times (0.51 \text{ g ethanol/g glucose})] / 0.789 \text{ g ethanol per mL}$; assuming 100 % conversion [18]. Complementarily, the energy potential was calculated in terms of the tons of oil equivalent (TOE) that represents the enthalpy of complete combustion of fuel, including the condensation enthalpy [19]. This value is compared to the energy released from burning one ton of crude oil and is equivalent to 41.87 GJ or 11.63 MWh. Both ethanol and TOE (1 TOE = 41.868 GJ) were selected as representative biofuels for the transportation sector.

3. RESULTS AND DISCUSSION

3.1. The energy scenario in Peru

Today, the Peruvian energy matrix is caused by the non-renewable source of natural gas around 65 % in 2018 [15-17]. This year, for example, the national consumption was around $83 \times 10^5 \text{ TJ}$ [17].

According to projections by the Ministry of Energy and Mining [15], energy consumption will be three times greater in 2040, caused by transportation, industrial, and trade sectors [15].

Peru addresses this additional demand by taking advantage of the energy potential of their various biomass resources as other countries have done. Muhammad et al. (2019) [20] in Pakistan and Balat (2010) [21] in Turkey, among others, demonstrated that biomass could play a significant role in sustainably, meeting increased national energy demands.

According to the Peruvian Supreme Decree No 021-2007-EM, biofuels would be commercialized primarily as additives for diesel and gasoline. However, it is also possible to meet the economic demands and sustainable energy requirements of non-transportation activities. Interestingly, Liu et al. (2014) [22] found that a mix of policy and market incentives had a large impact on the type of bioenergy feedstock developed and subsequent GHG emissions reduction. Overall, they found that the use of biomass for electricity generation had a far greater GHG offset potential than its production for vehicle fuel. Already, some Peruvian agroindustry companies currently use sugar cane bagasse as feedstock for steam generators that produce electricity [16].

Additionally, biomass as an energy feedstock has a significant advantage over other energy sources as it can be converted into solid, liquid, or gaseous states. This flexibility, combined with how demand influences technological adaptation, can help further spur innovation in sustainable energy generation [23].

3.2. Peruvian agricultural production and potential generation of by-products

Peru maintains a varied agricultural sector across its coastal, mountainous, and tropical regions, with rice, coffee, and hard yellow corn crops covering the greatest area cultivated, as depicted in Figure 1 [13-24].

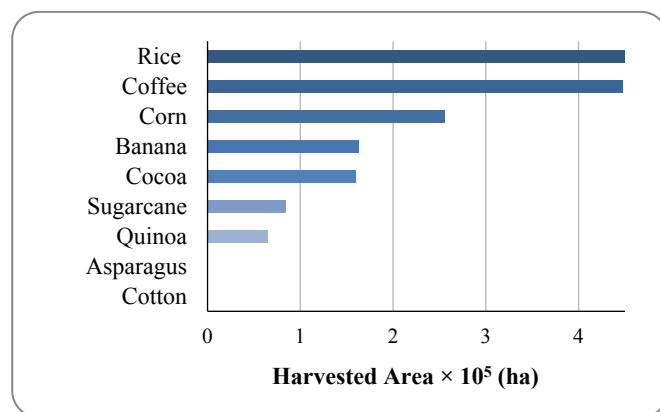


Figure 1. Crop-harvested area in 2018 of the main Peruvian agricultural products

Peru produces other important crops such as asparagus, cocoa, and quinoa which are the 5th, 9th, and 10th leading national agricultural exports by Metric Tons (MT), respectively. Peru leads the world as the largest exporter of fresh, preserved, and frozen asparagus, having the second-largest agricultural area under cultivation after China, and ranked third in yield (MT/ha) [25]. Interestingly, the regions of Ica and La Libertad produce 84.0 % of the area harvested and possible centers of innovation for derived products. With regard to genetic biodiversity, Peru accounts for 60.0 % of the biodiversity (genetic material) of cocoa and 50.0 % of quinoa [14], with Puno and Ayacucho having the largest harvesting area for quinoa.

Considering the harvested area, agricultural and forest residues were calculated in MT (Figure 2) [7, 26-29]. The straw from rice cultivation ($4.27 \times 10^6 \text{ MT}$), the stems and leaves from sugar cane ($3.31 \times 10^6 \text{ MT}$), and the stubble residue from corn ($3.16 \times 10^6 \text{ MT}$) generated the largest quantities of potential by-products in 2018.

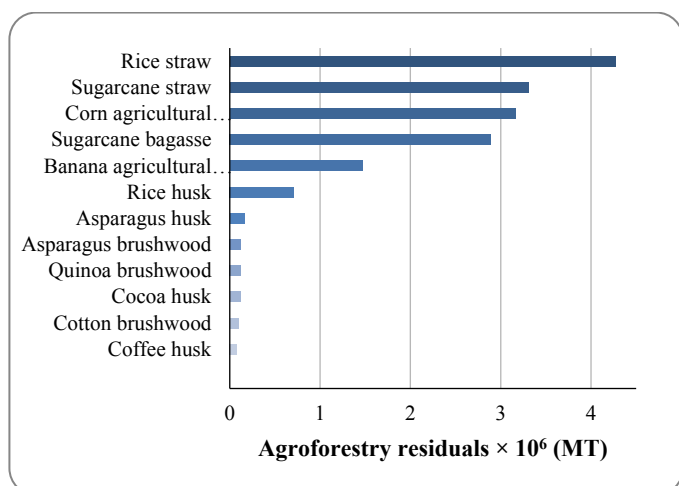


Figure 2. Generation of residuals from Peruvian of agroforestry in 2018

Focusing on 2018 and total crop by-products (MT), as well as listing Harvested Area (ha) and Production (MT) (Table 1), the two crops that generate the greatest quantities of potential residues are sugar cane and rice and are produced predominantly in the San Martín, Piura, and Lambayeque regions, while the third highest quantity of potential residues, corn, is predominantly produced both in the Ancash and Ica regions. It should be noted that sugar cane (bagasse and straw), rice (husk and straw), and asparagus (brushwood and straw) have two different by-products that comprise their total residuals.

Table 1. Crop area, production, and residues of the main crops (2018)

Product	Harvested area (ha × 10 ⁵)	Production (MT × 10 ⁶)	Total Residues (MT × 10 ⁶)
Sugar cane	0.85	10.31	6.20
Rice	4.38	3.56	4.98
Hard yellow corn	2.56	1.27	3.16
Banana	1.63	2.19	1.47
Asparagus	0.31	0.36	0.29
Quinoa	0.65	0.10	0.13
Cocoa	1.60	0.14	0.12
Cotton	0.15	0.04	0.10
Coffee	4.47	0.37	0.07

According to the report "Renewables 2018 Energy Policy Network for the 21st Century", by 2025, Peru aims to have up to 60.0 % of total energy production provided by renewable energy sources including bioenergy [30]. In agreement, the "Peru Natural Gas Sector Report" in 2020 suggested that only 6.0 % of the potential energy from biomass had been utilized, which is a statistic that presents a substantial economic and sustainability opportunity [31].

In terms of the potential growth of national agriculture, The International Coffee Organization predicts that global demand for coffee will increase by 32.0 % by 2030, which can translate into an 87.5 % increase in Peruvian exports [32]. The

International Cocoa Organization (ICCO) predicts that by 2023, global demand for cocoa will increase by 14.3 %. Peru has the potential to meet that demand as it is currently one of the top 10 worldwide cocoa exporters [11] and its production has been increasing at an average annual rate of 10.0 % over the past 13 years (2003-2015) [12]. Based on 2018-2020 figures, the world production of quinoa has a growth rate of 22.6 % and Peru, with an average annual market growth of around 13.0 %, could become the leading producer worldwide [13]. Finally, in 2018, Peru consolidated itself as the world's leading exporter of asparagus (fresh and chilled), and given its two growing seasons and the historical trend of its annual export growth (2005-2015), it is expected to continue in that position into the future [33].

Given that the biomass residues of these crops will follow these growth patterns, their uptake could help contribute to the 60 % target of renewable bioenergy generation proposed in the Renewables 2018 Global Status Report [30].

Studies related to the reuse of lignocellulosic materials in Peru focused on alternatives such as material composites and bioethanol [34-37]. This review shows that no complete overview presents a countrywide evaluation of the energy potential of agro-industrial by-products in Peru. In response to this gap, the framework of the results will present prospective quantification of heat generation through simple combustion using indicators as Heating Value (HV) and tons of equivalent (TOE) by region. The attainable production of cellulosic ethanol production based on the composition of the lignocellulosic biomass (carbohydrates content) is discussed too.

3.3. Heating value (HV) of agricultural by-products

The energy contained in a lignocellulosic material can be measured in terms of calorific value during air combustion and expressed in kJ/kg or kcal/kg [19]. The accumulated plant biomass is not proportional to the energy absorbed during photosynthesis because the amount of the accumulated chemicals differs due to their distinctive energy densities [38]. This difference in carbohydrate generation depends on the species and stage of plant development and it can be characterized by the enthalpy of the complete combustion of a fuel, especially when all carbon is converted into CO₂, all hydrogen is converted into H₂O and is represented as the Higher Heating Value (HHV) [2].

Figure 3 shows the standard HHV values of the lignocellulosic by-products studied in this article, with sugar cane bagasse, wood waste, and coffee husk having the highest values of 4 600.0, 4 413.7, and 4 361.3 kcal/kg, respectively. In addition, the use of sawdust for the production of thermal energy has been studied in equipment such as steam generators, furnaces, and turbines due to their calorific value [20].

Beyond simple combustion, utilization of the heat capacity of biomass can also focus on the combination of technologies that would produce intermediate and final products. The production of coal and bio-oil by pyrolysis, gaseous fuels, and supercritical liquefaction are some other alternatives in thermochemical conversion [39-40]. Although studied since 1788, with the first patent registered by Robert Gardner, gasification and liquefaction are still in the research and development phases, approaching commercialization, with direct combustion and coal co-firing for electricity production projected as the most promising alternative [39, 41].

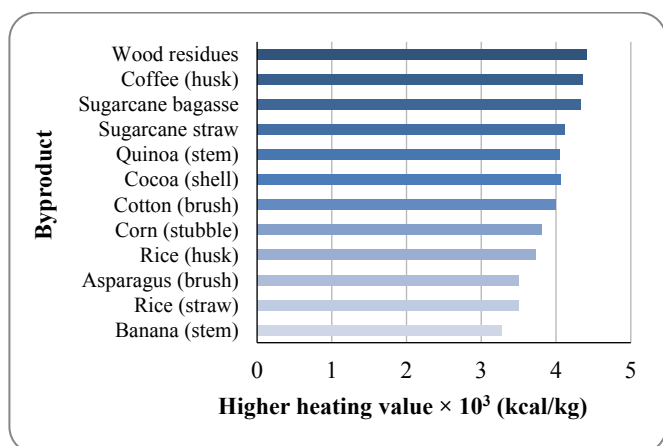


Figure 3. Higher Heating Value (HHV) of major Peruvian agricultural and forest residues

3.4. Characterization of agricultural by-products

To evaluate the energy potential of agriculture and agroforestry by-products, their chemical composition must be determined in terms of the percentage of phenolic content (lignin) and complex carbohydrates (cellulose and hemicellulose). An average composition, on a dry basis, would consist of cellulose (38-50 %), hemicellulose (23-32 %), lignin (15-25 %), and extractives (< 5 %), as reported in different studies corresponding to the principal Peruvian agricultural by-products, as shown in Table 2.

Of complex carbohydrates, cellulose is a polymer composed exclusively of glucose molecules bound by β -glucosidic bonds and hemicellulose is composed of heterogeneous polymers of pentose (xylose, arabinose), hexose (mannose, glucose, and galactose), and sugar acids; all these monomers of sugars can be used in fermentation processes to produce fuels [6, 43, 54].

Lignins are three-dimensional, complex, branched and amorphous heteropolymers formed from phenylpropane units

(coniferyl, cumaryl, and synaprylic alcohols) and have energy properties similar to those of solid fuels such as mineral coal [54, 55]. Their physicochemical characteristics are expressed by proximate analysis, elemental analysis, thermal stability analysis, and calorific value, indicating that they can be used for the production of thermal and electrical energy [5].

The research into the use and transformation of lignin is advancing rapidly. Using different physicochemical extraction procedures, lignin separated from their carbohydrates, and biomass fibers can have different structures, purities, and properties. According to Liao et al. (2020) [56], the three potential uses of lignin can be used for fuel synthesis, for biomaterial as macromolecules, and for pharmaceutical building blocks in aromatics.

In the first user group, lignin serves as a carbon source for energy production in the synthesized fuel. In the second user group, lignin functions in a macromolecular manner by taking advantage of their high molecular mass to produce adhesives, carbon fibers, and polymers including polyurethane foams. The third user group applies technologies to produce polymer building blocks and aromatic monomers such as benzene, phenol, vanillin, and toluene and xylene [57, 58].

The large amounts of lignin found in rice, sugar cane, and corn by-products represent a significant energy source that is currently underutilized in Peru. Lignin contents available from the most significant residues of rice straw, cane residue, and maize are 767×10^3 Mt, 1.4×10^6 Mt, and 696×10^3 Mt, respectively. Given an average calorific potential of 24 MJ/kg of pure and dry lignin, the energy potential amounts to more than 7 billion TJ. However, this biopolymer offers a variety of potential manufacturing routes in a biorefinery scheme and lignin is difficult to isolate and convert into chemical commodities, specialized chemicals, thermal and/or electric power, and advanced biofuels due to its chemical nature [4, 5, 56].

Table 2. Chemical composition of agricultural and agroforestry residues

By-product	Cellulose (%)	Hemicellulose (%)	Lignin (%)	Reference
Rice (straw)	35.6	12.0	15.4	[42]
Corn (agricultural residue)	36.8	30.6	23.1	[43]
Sugar cane (straw)	39.8	28.6	22.5	[44]
Sugar cane (bagasse)	38.0	29.5	21.5	[45]
Banana (pseudostem)	38.5	25.4	5.8	[46]
Quinoa (agricultural residue: stem)	42.1	20.3	13.0	[47]
Rice (husk)	43.5	22.0	17.2	[48]
Asparagus (husk)	31.2	16.8	14.2	[49]
Cotton (bushwood)	37.9	20.4	25.0	[50]
Cocoa (peel)	18.6	13.9	14.2	[51]
Coffee (husk)	36.7	47.4	15.9	[52]
Wood residue: <i>Pinus patula</i>	36.6	25.0	28.5	[53]
Wood residue: <i>Eucalyptus camaldulensis</i>	45.0	17.9	29.5	[53]

3.4.1. Bioethanol yield

Bioethanol is an advantageous fuel used directly as not only an alcohol in specific engines, but also an additive to gasoline,

as it cleans the combustion process, widens flammability limits, and increases octane, flame speeds, and vaporization heat [54, 59]. As such, the process of obtaining bioethanol is a highly studied technological transformation. One way to

increase its production without increasing the planted area is to use the sugars of lignocellulosic biomass as a raw material in the fermentation process. The extraction of these sugars contained in cellulose and hemicellulose encompasses a sequence of stages from chemical pretreatment, chemical, or biological saccharification to conventional fermentation by yeast [43, 55]. While the glucose content to carry out such processes is found in cellulose, it should be noted that other sugars like xylose, an abundant component of most hemicelluloses, can also contribute to the production of bioethanol by using genetically modified yeasts that ferment both compounds [55].

As indicated in the methodology section, the theoretical yield for the production of bioethanol from each by-product was calculated considering the chemical composition of lignocellulosic residues, assuming that all the glucose contained in cellulose is used to produce ethanol. The raw materials with the greatest potential for conversion into ethanol are wood residue, rice husk, and quinoa stalk, yielding 23.0, 22.2, and 21.5 g bioethanol/g total cellulose, respectively as seen in Figure 4.

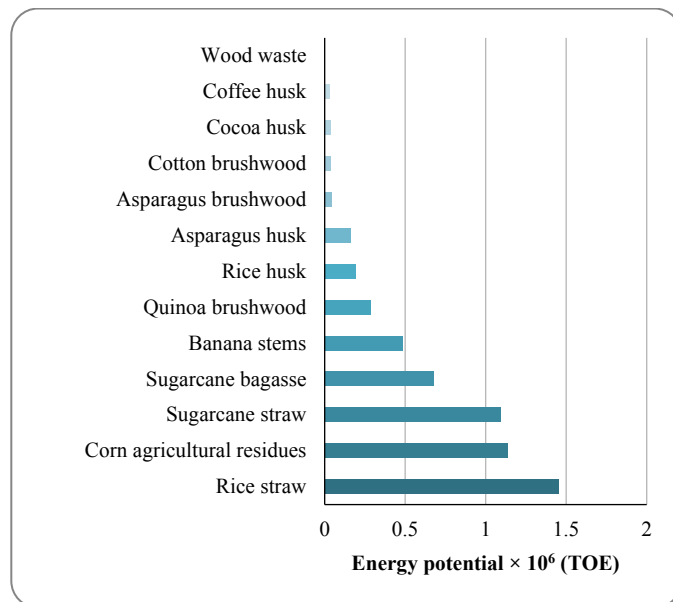


Figure 5. Energy potential (TOE) of major Peruvian agricultural and forest residues

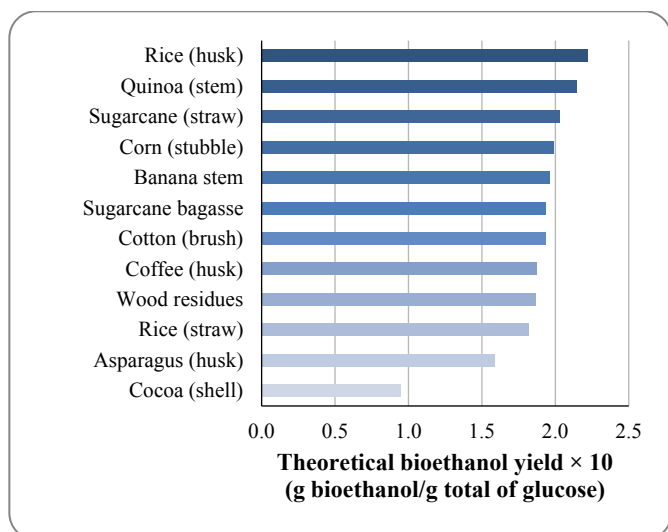


Figure 4. Theoretical bioethanol yield of major Peruvian agricultural and forest residues

In Peru, Peruvian Technical Standard restricts the ethanol content in gasohol to a maximum of 7.8 % and this ethanol is derived from corn (with higher CO₂ emissions than that made from sugar cane) [15-17]. It is demonstrated that lignocellulosic-derived ethanol leads to greenhouse gas savings [43, 54] relative to gasoline and corn ethanol; thus, its use represents an environmental positive impact for the nation.

3.5. Byproduct potential in TOE equivalent by region

Figure 5 shows the energy potential of the main lignocellulosic byproducts in terms of tons of oil equivalent (TOE) per year. As can be seen, rice straw (1.45×10^6), corn agricultural residue (1.13×10^6), sugarcane agricultural residue (1.1×10^6), and sugar cane bagasse (6.80×10^5) formed the classification.

To assess the geographical distribution of the energy potential, Figure 6 shows the distribution in TOE /year by region and biomass availability.

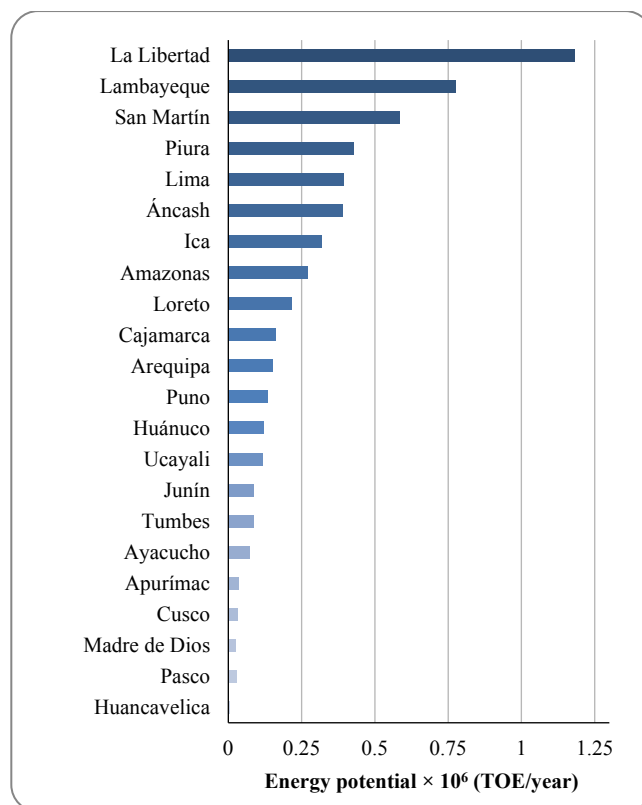


Figure 6. Energy potential (TOE) of Agricultural and Forest Residues by Region

The regions with the greatest energy potential are La Libertad (1.18×10^6 TOE), Lambayeque (7.74×10^5 TOE), San Martín (5.83×10^5 TOE), and Piura (4.29×10^5 TOE) localized in the north of Peru, as can be seen in Figure 7. Due to their location (400-2000 meters above sea level), these regions have tropical climates and landscapes of plains, which promote higher productivity per cultivated hectare and consequently increase the quantity of biomass feedstock for energy potential [60, 61].



Reference	TOE/Year	Main agroforestry residues
	<10000	Rice straw, quinoa brushwood
	100000- 170000	Rice straw, corn residues
	170000 - 400000	Corn residues, sugarcane straw
	> 400000	Rice straw, corn residues

Figure 7. Production of significant agricultural by-products in TOE/year and main agroforestry residues, by geographical region

4. CONCLUSIONS

In Peru, around 1.65×10^7 Mt of agricultural residues and 301 Mt of forest residues are generated annually. The northern region of Peru generates the highest quantities of biomass by-products, mainly rice (straw and husk), banana (husk and rachis), and sugar cane (bagasse and straw), which accounts potentially for more than 4×10^6 TOE per year. This value is equivalent to 20 % to the total national consumption; thus, their development could help reduce fossil fuel dependency, increase the energy security of Peru, and help guide other countries that share similar agricultural profiles.

5. ACKNOWLEDGEMENT

The authors are grateful for the support of the Research Department of the University of Engineering and Technology (UTEC).

REFERENCES

- WWF, The energy report: 100 % renewable energy by 2050, (2011). (http://awsassets.panda.org/downloads/informe_energia_renovable_2010_esp_final_opt.pdf).
- Amiandamhen, S.O., Kumar, A., Adamopoulos, S., Jones, D. and Nilsson, B., "Bioenergy production and utilization in different sectors in Sweden: A state of the art review", *BioResources*, Vol. 15, No. 4, (2020), 9834-9857. (<http://doi.org/10.15376/biores.15.4.Amiandamhen>).
- Dahman, Y., Dignan, C., Fiayaz, A. and Chaudhry, A.L., "An introduction to biofuels, foods, livestock, and the environment", Biomass, biopolymer-based materials, and bioenergy, Woodhead Publishing, (2019), 241-276. (<https://doi.org/10.1016/B978-0-08-102426-3.00013-8>).
- Amezcuá-Allieri, M.A. and Aburto, J., "Conversion of lignin to heat and power, chemicals or fuels into the transition energy strategy", *Lignin-Trends and Applications*, IntechOpen, (2018), 145-161. (<https://www.intechopen.com/chapters/57294>).
- Rebouillat, S. and Pla, F., "A review: on smart materials based on some polysaccharides; within the contextual bigger data, insiders, "improvisation" and said artificial intelligence trends", *Journal of Biomaterials and Nanobiotechnology*, Vol. 10, No. 2, (2019), 41-77. (<https://doi.org/10.4236/jbnb.2019.102004>).
- Iqbal, H., Kyazze, G. and Keshavarz, T., "Advances in the valorization of lignocellulosic materials by biotechnology: An overview", *BioResources*, Vol. 8, No. 2, (2013), 3157-3176. (<https://doi.org/10.15376/biores.8.2.3157-3176>).
- FAO, Bioenergía y seguridad alimentaria, BEFS, Vol. II, (2010). (<http://www.fao.org/3/i1708s/i1708s00.htm>), (Accessed: 5 September 2020).
- Lauri, P., Kallio, A. and Schneider, U., "Price of CO₂ emissions and use of wood in Europe", *Forest Policy and Economics*, Vol. 15, (2012), 123-131. (<https://doi.org/10.1016/j.forpol.2011.10.003>).
- Menardo, S., Bauer, A., Theuretzbacher, F., Piringner, G., Nilsen, P.J., Balsari, P. and Amon, T., "Biogas production from steam-exploded miscanthus and utilization of biogas energy and CO₂ in greenhouses", *BioEnergy Research*, Vol. 6, (2013), 620-630. (<https://doi.org/10.1007/s12155-012-9280-5>).
- Ferreira, L., Otto, R., Silva, F., De Souza, S., De Souza, S. and Junior, O., "Review of the energy potential of the residual biomass for the distributed generation in Brazil", *Renewable and Sustainable Energy Reviews*, Vol. 94, (2018), 440-455. (<http://dx.doi.org/10.1016/j.rser.2018.06.034>).
- MINAGRI-DGPA-DEEIA, "Estudio del cacao en el Perú y en el mundo: un análisis de la producción y el comercio", (2016). (<https://camcafeperu.com.pe/admin/recursos/publicaciones/Estudio-cacao-Peru-y-Mundo.pdf>), (Accessed: 5 November 2019).
- MINAGRI, "El Perú: Centro de origen de la biodiversidad del cacao", (2017). (<http://www.cocoaconnect.org/publication/cocoa-fact-sheet>), (Accessed: 25 November 2021).
- MINAGRI, "Anuario estadístico de producción agrícola", (2018). (https://siea.midagri.gob.pe/portal/phocadownload/datos_y_estadisticas/anuarios/agricola/agricola_2018.pdf), (Accessed: 2 July 2021).
- MINAGRI, "Minagri presenta nueva quinoa con alto contenido en proteínas y calidad de grano", (2020). (<https://www.gob.pe/institucion/midagri/noticias/313516-minagri-presenta-nueva-quinoa-con-alto-contenido-en-proteinas-y-calidad-de-grano>), (Accessed: 20 November 2020).
- MEM, "Nueva matriz energética sostenible para el Perú", (2012). (http://www.minem.gob.pe/minem/archivos/file/DGEE/eficiencia%20energetica/publicaciones/guias/Informe_completo_Estudio_NUMES.pdf), (Accessed: 1 September 2020).
- MEM, "Balance Nacional de Energía", (2017). (<https://www.minem.gob.pe/minem/archivos/file/DGEE/eficiencia%20energetica/publicaciones/BNE%202017.pdf>), (Accessed: 30 May 2020).
- MEM, "Balance Nacional de Energía", (2018). (https://cdn.www.gob.pe/uploads/document/file/98790/BNE_2018.pdf), (Accessed: 18 December 2020).
- Vogel, K.P., Dien, B.S., Jung, H.G., Casler, M.D., Masterson, S.D. and Mitchell, R.B., "Quantifying actual and theoretical ethanol yields for switchgrass strains using NIRS analyses", *BioEnergy Research*, Vol. 4, (2011), 96-110. (<https://doi.org/10.1007/s12155-010-9104-4>).
- Friedl, A., Padouvas, E., Rotter, H. and Varmuza, K., "Prediction of heating values of biomass fuel from elemental composition", *Analytica Chimica Acta*, Vol. 544, (2005), 191-198. (<https://doi.org/10.1016/j.aca.2005.01.041>).
- Saghir, M., Zafar, S., Tahir, A., Ouadi, M., Siddique, B. and Hornung, A., "Unlocking the potential of biomass energy in Pakistan", *Frontiers in Energy Research*, Vol. 7, (2019), 1-18. (<https://doi.org/10.3389/fenrg.2019.00024>).
- Balat, M., "Security of energy supply in Turkey: Challenges and solutions", *Energy Conversion and Management*, Vol. 51, No. 10, (2010), 1998-2011. (<https://doi.org/10.1016/j.enconman.2010.02.033>).
- Liu, T., McConkey, B., Huffman, T., Smith, S., MacGregor, B., Yemshanov, D. and Kulshreshtha, S., "Potential and impacts of renewable energy production from agricultural biomass in Canada", *Applied Energy*, Vol. 130, (2014), 222-229. (<https://doi.org/10.1016/j.apenergy.2014.05.044>).
- Giacchetta, G., Leporini, M. and Marchetti B., "Technical and economic analysis of different cogeneration systems for energy production from biomass", *International Journal of Productivity and Quality Management*, Vol. 13, No. 3, (2014), 289-309. (<https://doi.org/10.1504/IJPMQ.2014.060419>).
- PROMPERÚ, "Desenvolvimiento del comercio exterior agroexportador en el Perú", (2018). (<https://www.siicex.gob.pe/siicex/recursos/sectoresproductivos/Desenvolvimiento%20agroexportador%202018.pdf>), (Accessed: 18 June 2020).

25. Anaya, R., "Situación actual de la exportación de espárragos (*Asparagus officinalis*) en el Perú", Universidad Nacional Agraria La Molina Lima, Perú, (2017). (<http://repositorio.lamolina.edu.pe/handle/20.500.12996/2975>), (Accessed: 15 July 2019).
26. Medina, D.A., Nuñez, M.F.A. and Ordoñez, M.S., "Obtención de enzimas celulasas por fermentación sólida de hongos para ser utilizadas en el proceso de obtención de bioalcohol de residuos del cultivo de banano", *Revista Tecnológica-ESPOL*, Vol. 23, (2010). (<https://doi.org/10.37815/rte>).
27. León-Martínez, T.S., Dopico-Ramírez, D., Triana-Hernández, O. and Medina-Estevez, M., "Paja de la caña de azúcar, Sus usos en la actualidad", *ICIDCA, Sobre los Derivados de la Caña de Azúcar*, Vol. 47, (2013), 13-22. (<https://www.redalyc.org/articulo.oa?id=223128548003>).
28. Ricce, C., Leyva, M., Medina, I., Miranda, J., Saldarriaga, L.F., Rodríguez J. and Jara R.S., "Uso de residuos agroindustriales de La Libertad en la elaboración de un pan integral", *Agroindustrial Science*, Vol. 3, (2013), 41-46.
29. Pinzón Colmenares, I.E., "Estimación de la huella de carbono en los cultivos de quinua (*Chenopodium quinoa*) de los cantones Cayambe y Riobamba ubicados en los Andes Ecuatorianos", Salesian Politecnic University, Quito, Ecuador, (2017). (<https://dspace.ups.edu.ec/handle/123456789/14110>), (Accessed: 10 November 2020)
30. REN21, "Renewables 2018 global status report (Paris: REN21 Secretariat)", (2018). (https://www.ren21.net/wp-content/uploads/2019/05/GSR2018_Full-Report_English.pdf), (Accessed: 20 November 2020)
31. PeruLNG, "Annual Report Peru Ing", (2020). (<https://perulng.com/wp-content/uploads/2021/08/Anual-Report-2020.pdf>), (Accessed: 8 November 2020).
32. Global Coffee Platform, "Statistical Bulletin: Peruvian Coffee", (2017). (<https://www.ico.org/documents/cy2019-20/annual-review-2018-19-e.pdf>), (Accessed: 15 November 2020).
33. Bengoa, M.P., Ramos, M.M. and Shimabukuro, G.J.C., "Plan de negocios para el ingreso a la exportación del espárrago congelado", Pacific University, Lima, Peru, (2016). (<https://repositorio.up.edu.pe/handle/11354/1684>), (Accessed: 15 October 2020).
34. Leturia, M.L.S. and Febres, L.M.C., "Caracterización de biomasa residual de la región Arequipa para la producción de biocombustibles", *Enfoque UTE*, Vol. 6, (2015), 4-42. (<https://doi.org/10.29019/enfoqueute.v6n4.77>).
35. Melgarejo, T.L. and Urquiza, R.A., "Influencia de la temperatura y concentración de ácido sulfúrico en la hidrólisis ácida de raquis del banano, variedad musa cavendish, para la obtención de bioetanol por *saccharomyces cerevisiae* atcc 4126", National University of Santa, Ancash, Peru, (2019). (<http://repositorio.uns.edu.pe/handle/UNS/3389>), (Accessed: 18 November 2020).
36. Rodríguez, G. and Rodríguez García, S.D.L.M., "Extracción y caracterización de bioetanol a partir de biomasa lignocelulósica de caña de azúcar (*Saccharum Officinarum* L.)", University of Piura, Peru, (2015). (<https://repositorio.unp.edu.pe/handle/UNP/394>), (Accessed: 19 November 2020).
37. Baltazar, L.A., "Obtención de biocombustible sólido de segunda generación a partir de tallos de quinua (*Chenopodium quinoa Willd*) y hojas de eucalipto (*Eucalyptus globulus Labill*), con máxima potencia calorífica", National University of the Altiplano, Puno, Peru, (2016). (<http://repositorio.unap.edu.pe/handle/UNAP/3250>), (Accessed: 15 November 2020).
38. Rozenský, L., Hájek, M., Vrba, Z., Pokorný, R., Hansen, J. and Lípa, J., "An analysis of renewable energy consumption efficiency in terms of greenhouse gas production in selected European countries", *BioResources*, Vol. 15, No. 4, (2020), 7714-7729. (<https://doi.org/10.15376/biores.15.4.7714-7729>).
39. Dupont, C., Chiriac, R., Gauthier, G. and Toche, F., "Heat capacity measurements of various biomass types and pyrolysis residues", *Fuel*, Vol. 115, (2014), 644-651. (<https://doi.org/10.1016/j.fuel.2013.07.086>).
40. Reyes, L., Abdelouahed, L., Mohabeer, C., Buvat, J.C. and Taouk, B., "Energetic and exergetic study of the pyrolysis of lignocellulosic biomasses, cellulose, hemicellulose and lignin", *Energy Conversion and Management*, Vol. 244, (2021), 114459. (<https://doi.org/10.1016/j.enconman.2021.114459>).
41. Niksa, S., "Predicting the macroscopic combustion characteristics of diverse forms of biomass in p. p. firing", *Fuel*, Vol. 283, (2021), 118911. (<https://doi.org/10.1016/j.fuel.2020.118911>).
42. González-Rentería, S.M., Soto-Cruz, N.O., Rutiaga-Quiñones, O.M., Medrano-Roldán, H., Rutiaga-Quiñones, J.G. and López-Miranda, J., "Optimization of the enzymatic hydrolysis process of four straw bean varieties (Pinto villa, Pinto saltillo, Pinto mestizo and Flor de mayo)", *Revista Mexicana de Ingeniería Química*, Vol. 10, (2011), 17-28. (http://www.scielo.org.mx/scielo.php?script=sci_arttext&pid=S1665-27382011000100003&lng=es&tln=es).
43. Abascal, F.R., "Estudio de la obtención de bioetanol a partir de diferentes tipos de biomasa lignocelulósica. Matriz de reacciones y optimización", University of Cantabria, Spain, (2017). (<https://repositorio.unican.es/xmlui/bitstream/handle/10902/12178/RAF.pdf?sequence>), (Accessed: 15 November 2020).
44. Wolf, L.D., "Pré-tratamento organossolve do bagaço de cana-de-açúcar para a produção de etanol e obtenção de xilooligômeros", Federal University of São Carlos, Sao Paulo, Brazil, (2011). (<https://repositorio.ufscar.br/handle/ufscar/4071>), (Accessed: 15 November 2019).
45. Rocha, M.D.S., Almeida, R.M.R.G. and da Cruz, A.J.G., "Evaluation of energy potential of the agroindustrial residues from different Brazilian regions", *Engevista*, Vol. 19, (2017), 217-235. (<https://doi.org/10.22409/engevista.v19i1.821>).
46. Adeniyi, A.G., Ighalo, J.O. and Amosa, M.K., "Modelling and simulation of banana (*Musa spp.*) waste pyrolysis for bio-oil production", *Biofuels*, Vol. 12, No. 7, (2021), 879-883. (<https://doi.org/10.1080/17597269.2018.1554949>).
47. Álvarez Narváez, K.M., "Evaluación del uso de saponinas de quinua como agente emulsificante en la producción de micropartículas de manteca de cacao para la liberación controlada de fármacos", Universidad de Quito, (2020), (https://raae.cedia.edu.ec/Record/USFQ_c1b356f09c8ce4ad702955c0931c48a), (Accessed: 8 November 2019).
48. Fernandes, I., Dos Santos, C.A.E., Oliveira, R., Reis, J., Calheiro, D.E., Reis, J.M. and Modolo, R., "Caracterização do resíduo industrial casca de arroz com vistas a sua utilização como biomassa", *6º Fórum Internacional de Resíduos Sólidos*, (2015), 1-9. (<http://www.institutoventuri.org.br/ojs/index.php/firs/article/view/616>).
49. Guo, Q., Wang, N., Liu, H., Li, Z., Lu, L. and Wang, C., "The bioactive compounds and biological functions of *Asparagus officinalis* L. – A review", *Journal of Functional Foods*, Vol. 65, (2020), 103727. (<https://doi.org/10.1016/j.jff.2019.103727>).
50. El Saeidy, E., "Renewable energy in agriculture in Egypt: Technological fundamentals of briquetting cotton stalks as a biofuel", Humboldt-Universität zu Berlin, (2004). (<https://edoc.hu-berlin.de/bitstream/handle/18452/15724/El-Saeidy.pdf?sequence=1>), (Accessed: 1 May 2020).
51. Igbinalodor, R., "Fermentation of cocoa (*Theobroma Cacao* L.) pod husk and its hydrolysate for ethanol production using improved starter cultures", University of Ibadan, Nigeria, (2012). (<http://ir.library.ui.edu.ng/handle/123456789/801>), (Accessed: 10 September 2020).
52. Arias, O.R. and Meneses, C.J., "Caracterización físico-química de residuos agroindustriales (cascarilla de arroz y cascarilla de café), como materia prima potencial para la obtención de bioetanol", Autonomous National University of Nicaragua, Managua, (2016). (<https://repositorio.unan.edu.ni/3793/>).
53. Gómez, E.A., Ríos, L.A. and Peña, J.D., "Effect of wood biomass pretreatment on ethanol yield", *Información Tecnológica*, Vol. 24, No. 5, (2013), 113-122. (<http://dx.doi.org/10.4067/S0718-07642013000500013>).
54. Vasić, K., Knez, Ž. and Leitgeb, M., "Bioethanol production by enzymatic hydrolysis from different lignocellulosic sources", *Molecules*, Vol. 26, (2021), 753. (<http://dx.doi.org/10.3390/molecules26030753>).
55. Robak, K. and Balcerek, M., "Current state-of-the-art in ethanol production from lignocellulosic feedstocks", *Microbiological Research*, Vol. 240, (2020). (<http://dx.doi.org/10.1016/j.micres.2020.126534>).
56. Liao, J.J., Abd Latif, N.H., Trache, D., Brosse, N. and Hussin, M.H., "Current advancement on the isolation, characterization and application of lignin", *International Journal of Biological Macromolecules*, Vol. 162, (2020), 985-1024. (<https://doi.org/10.1016/j.ijbiomac.2020.06.168>).

57. Ragauskas, A.J., Beckham, G.T., Biddy, M.J., Chandra, R., Chen, F., Davis, M.F., Davison, B.H., Dixon, R.A., Gilna, P., Keller, M., Langan, P., Naskar, A.K., Saddler, J.N., Tschaplinski, T.J., Tuskan, G.A., and Wyman, C.E., "Lignin valorization: improving lignin processing in the biorefinery", *Science*, Vol. 344, No. 6185, (2014). (<http://dx.doi.org/10.1126/science.1246843>).
58. Lan, W. and Luterbacher, J.S., "A road to profitability from lignin via the production of bioactive molecules", *ACS Central Science*, Vol. 5, No. 10, (2019), 1642-1644. (<https://doi.org/10.1021/acscentsci.9b00954>).
59. Kim, H. and Choi, B., "The effect of biodiesel and bioethanol blended diesel fuel on nanoparticles and exhaust emissions from CRDI diesel engine", *Renewable Energy*, Vol. 35, (2010), 157-163. (<https://doi.org/10.1016/j.renene.2009.04.008>).
60. INRENA, "Zonas de vida de Holdridge", (1995). (<https://www.senamhi.gob.pe/load/file/01402SENA-9.pdf>), (Accessed: 16 September 2020).
61. SENAMHI, "Clasificación climática de warren thornthwaite", (2020). (<https://www.senamhi.gob.pe/?p=mapa-climatico-del-peru>), (Accessed: 9 August 2020).



Research Article

Improvement of Frequency Stability in the Power System Considering Wind Turbine and Time Delay

Farhad Amiri, Mohammad Hassan Moradi*

Department of Electrical Engineering, Bu-Ali Sina University, P. O. Box: 65178-38695, Hamedan, Hamedan, Iran.

PAPER INFO

Paper history:

Received: 17 January 2022
Revised in revised form: 08 March 2022
Scientific Accepted: 20 March 2022
Published: 06 August 2022

Keywords:

Wind Turbine,
Time Delay,
Load-Frequency Control,
Virtual Damping,
Power System

ABSTRACT

In the power system, frequency stability is critical. The wind turbine oscillates (depending on the wind speed) and is of low inertia. Thus, wind turbines face the issue of power system frequency stability. Since the power system's resources are interconnected via communication networks, the presence of time delay also affects the frequency stability of the power system. When a disturbance occurs in the power system due to load or distributed generation sources (wind turbine), it leads to frequency deviations in the power system, exhibiting low damping speed. Although large conventional generators in the power system provide sufficient inertia and reduce frequency deviation, the damping speed of frequency fluctuations is slow, which may be due to time delays between power system resources. In this paper, virtual damping (a proposed method) is used to accelerate the damping of frequency deviations caused by load disturbances, distributed generation source disturbances, and the time delay between power system resources. The results of the proposed method are compared to those obtained using the conventional method in this field, demonstrating the superiority of the proposed method. The proposed method reduced frequency deviations in the power system caused by disturbances and time delays by 67% (a 67% improvement over existing methods in this field) and increased the damping speed of the frequency deviations by 62% (a 62% improvement over the methods used in this field).

<https://doi.org/10.30501/jree.2022.321859.1308>

1. INTRODUCTION

The conventional energy generation system should be replaced by renewable energy sources since the uncontrolled use of fossil fuels is accompanied by global warming and environmental hazards, besides the danger of their depletion, and because much of the energy derived from these fuels is consumed by buildings [1]. Renewable energy systems impact the process of meeting domestic energy demands [2]. Due to the increased demand for electricity today, distributed generation sources such as wind turbines have made significant inroads into the power system [3, 4]. Wind turbine development has aided human progress throughout history [5, 6]. While incorporating a wind turbine into the power system has numerous benefits, the power system faces several challenges [7, 8]. The issue of frequency control is one of the primary challenges posed by the presence of turbines in the power system [9]. The power system is in a steady state when production and consumption are balanced, and if this equilibrium is lost to a disturbance, the frequency deviates from the nominal value [10]. If the system's frequency fluctuations are not controlled, they can cause significant damage, even up to the point where a production unit shuts

down [11]. The primary control loop is the initial control loop responsible for limiting the frequency drop following a disturbance [10, 12]. This control loop is based on the generator's true frequency-power characteristic and is installed on the generator [10]. The primary control loop constrains the dropped frequency, but is unable to restore it to its nominal value, necessitating the use of another interactive loop termed as the secondary frequency control [13]. The load-frequency control loop can only respond to small-scale and slow changes in load and frequency and is, therefore, incapable of controlling emergencies and the resulting power imbalance. The control of systems during emergencies and rapid changes is investigated in terms of their transient stability and protection [14]. Active power primarily changes the system's frequency, whereas reactive power is insensitive to frequency and is primarily affected by changes in voltage magnitude [15]. As a result, active and reactive powers are managed separately. The loop regulates the Load-Frequency Control (LFC), the actual power, and frequency, and the reactive power and voltage magnitude are also regulated by the Automatic Voltage Regulator (AVR) [16]. The presence of a wind turbine in a power system reduces the system inertia, which later dampens frequency deviations [17]. Even in the presence of wind turbines, large synchronous generators provide sufficient inertia for the power system, but the problem of slow damping frequency deviations persists [18].

*Corresponding Author's Email: mh_moradi@yahoo.co.uk (M.H. Moradi)
URL: https://www.jree.ir/article_154524.html



Several methods have been developed to enhance the frequency stability of the power system in the presence of a wind turbine.

The sliding mode controller is used for Load-Frequency Control (LFC) in a wind turbine-powered power system [19]. Model Predictive Control (MPC) is used to control the load frequency in a power system with a wind turbine [20, 21]. In the presence of a wind turbine, the power system is controlled using a coordinated energy storage source and load-frequency control [22]. The power system and wind turbine controllers are highly complex [23, 24]. A neuro-fuzzy controller is used to coordinate the energy storage source and LFC in the power system in the presence of the wind turbine [25]. An optimized PID controller was used to coordinate the energy storage source and LFC in the power system in the presence of a wind turbine [26]. The methods for controlling the frequency in a power system with wind turbines perform well in the presence of disturbances and uncertainty in system parameters. They do, however, have challenges. These issues include the low damping speed of frequency deviations, the absence of wind turbine participation in the power system's frequency control, and the omission of time delays. Low damping speeds for frequency deviations may result in suboptimal performance of the frequency control system and frequency instability in the power system. The frequency deviation of the European power grid is greater than 0.1 Hz, and the wind turbine must participate in the issue of frequency control and compensate for the power grid's frequency deviations by changing its power [27]. Time delay in the power system is one of the issues that can cause numerous problems during frequency control system operation and result in frequency instability, which is why it is necessary to model time delay when controlling the power system's frequency. As a result, a method for frequency control in the power system is required to address the issues in this field.

The present study discusses the viability of a method for frequency control in a power system with a wind turbine. The proposed method incorporates a virtual damping design on a wind turbine in the power system, thereby increasing the damping speed of power system frequency fluctuations. Among the other advantages of the proposed method are reduced power system frequency fluctuations and active wind turbine operation during control frequency. The proposed method is also designed to consider the effect of time delay. The results of the proposed method are compared to those of conventional methods, demonstrating the superiority of the proposed method in simulation. The proposed method reduced frequency deviations in the power system caused by disturbances and time delays by 67 % (a 67 % improvement over existing methods in this field) and increased the damping speed of the frequency deviations by 62 % (62 % improvement over the methods used in this field). This paper discusses the structure of a power system with a wind turbine, the proposed method, simulation, and results.

2. POWER SYSTEM STRUCTURE WITH THE PRESENCE OF WIND TURBINE

Figure 1 shows the general structure of the power system considering the wind turbine. The studied power system includes several hydropower plants, several non-reheat power plants, some reheat power plants, a number of wind turbines, several Energy Storage Systems (ESS), and different loads. The total amount of power produced in the studied power system is 38000 MW, while the peak load is 29000 MW [26]. Figure 2 shows the dynamic model of the study power system in which different components are modeled using the reduced-order model, which suits the stability analysis of frequency [12].

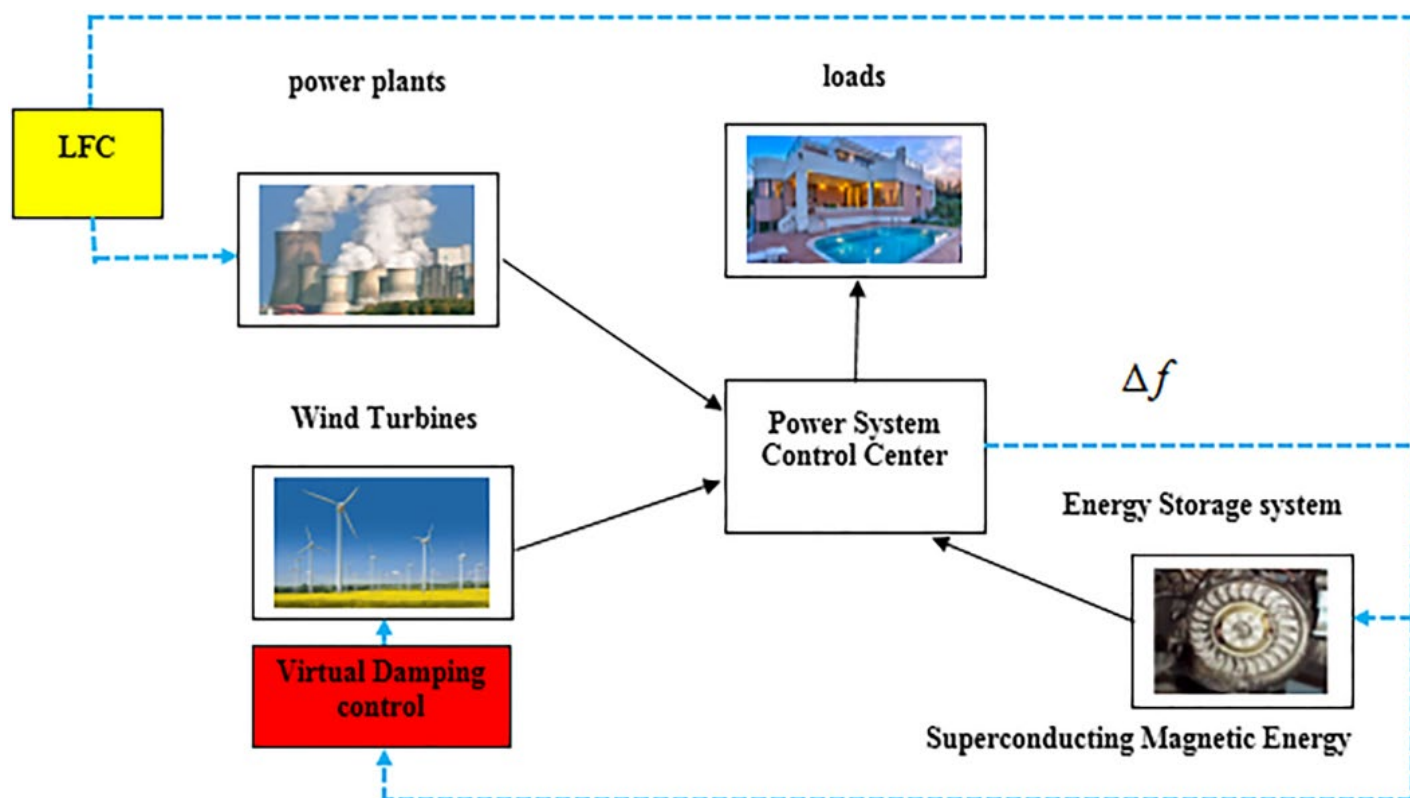


Figure 1. The general structure of the power system considering the wind turbine

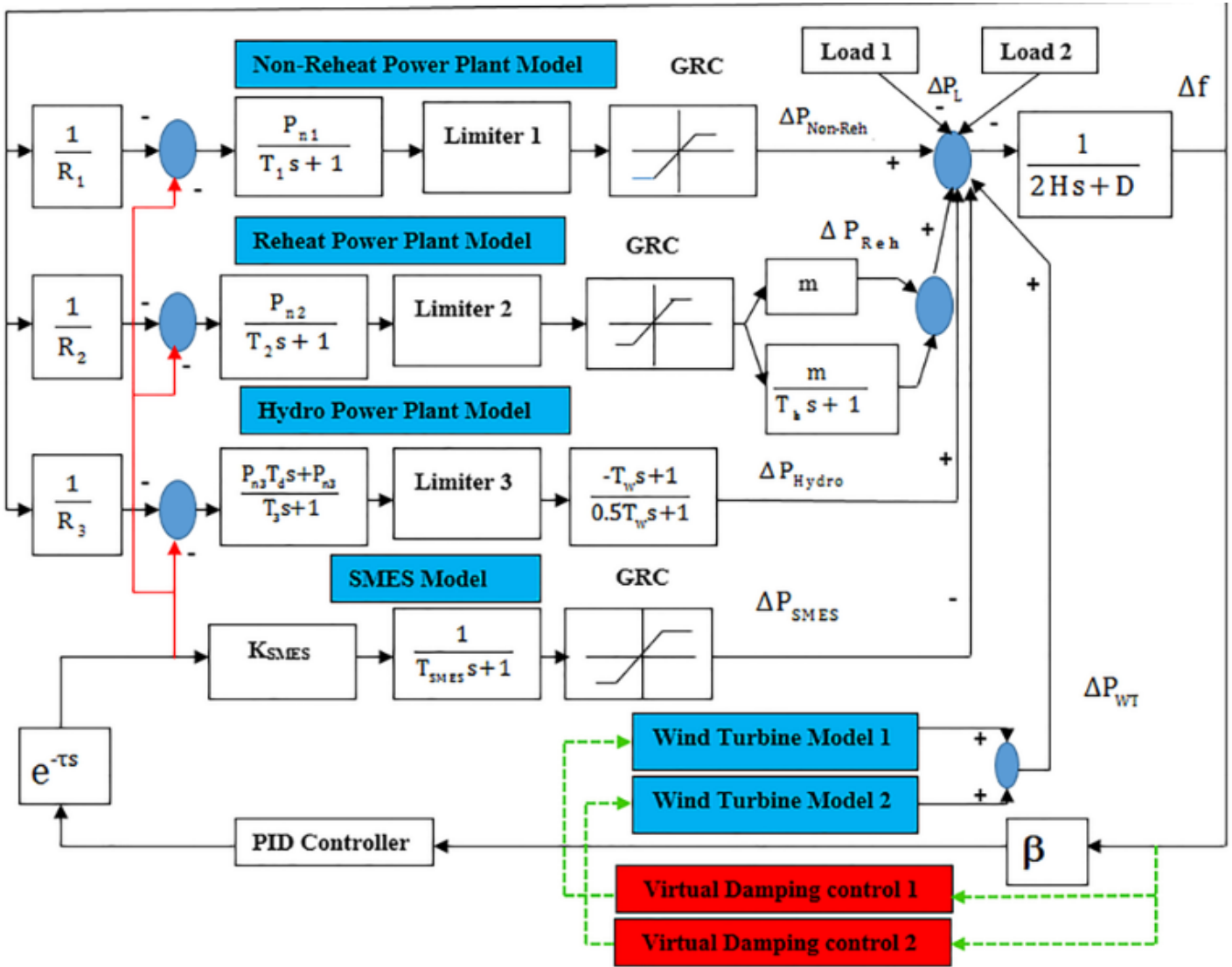


Figure 2. The dynamic model of the study power system

3. PROPOSED METHOD

3.1. The structure of the proposed method

The proposed method (virtual damping for wind turbines) is intended to mitigate frequency deviations caused by load disturbances and distributed generation source disturbances in the power system. It increases the frequency oscillations' damping speed. The proposed method activates the wind turbine during frequency control and also minimizes power system-related frequency deviations caused by disturbances. The dynamic model of the proposed method for wind turbines 1 and 2 is shown in Figure 3. When a disturbance occurs in the power system, feedback is obtained from the frequency deviation multiplied by the virtual Damping gain of wind turbine 1 (D_1) and the virtual Damping gain of wind turbine 2 (D_2). This signal is routed to the inverter of wind turbines 1 and 2. The coefficients D_1 and D_2 , representing the virtual damping control gains for wind turbines 1 and 2, are proportional to the system and determined through system experiments. The proposed method bears no additional economical cost as it is merely a signal that increases the damping of frequency deviations in the power system when a wind turbine is present. During disturbances, the wind turbine operates passively under conventional control methods. To this end, the proposed method activates the wind turbine

during disturbances. When a disturbance enters the power system, this method is used by the wind turbine to obtain feedback from the frequency deviations, reduce the frequency deviations, and enhance the frequency stability of the power system. In Figure 3, $i = 1, 2$, Δf denotes the power system's frequency deviation, D_i is the virtual damping of wind turbines 1 and 2, ΔP_{wi} denotes the output power of wind turbines 1 and 2, and ΔP_{wt} is the output power of inverter wind turbines 1 and 2. The power system parameters in the presence of a wind turbine are listed in Table 1. Simulink MATLAB simulations were used to adjust the virtual damping associated with wind turbines 1 (D_1) and 2 (D_2). As illustrated in Figure 4, load disturbance is introduced into the power system to adjust the wind turbines' virtual damping gain. Additionally, the power system has a time delay ($\tau = 0.5$ sec.). Figure 5 illustrates the power system's frequency response to load disturbances. According to Figure 5, the trial-and-error method was used to determine the virtual damping gain of most turbines (D_1 and D_2). The maximum frequency deviation and settling time associated with the power system's frequency response are depicted in Figures 6 and 7, respectively. According to Figure 6, increasing the wind turbine's virtual damping gain reduces the power system's maximum frequency deviation. Thus, when tuning a wind turbine's virtual damping gain, the higher the gain, the lower the

frequency deviation. According to Figure 7, as the virtual damping gain of a wind turbine increases, the settling time associated with the power system's frequency deviations decreases (higher damping speed). We can achieve a shorter settling time by selecting larger values for the wind turbine's virtual damping gain (higher damping speed). The virtual damping gains associated with wind turbines 1 and 2 are selected to be $D_1=1.5$ and $D_2=1.5$, respectively, based on the

results obtained in the studied power system. A portion of the wind turbine's output must be considered as reserve power to implement the proposed method for frequency control purposes. It is possible to increase the amount of virtual damping gain to the extent that the wind turbine capacity is allowed. 5 % of each wind turbine's capacity is considered reserve power in this paper and the maximum virtual damping gain is selected accordingly.

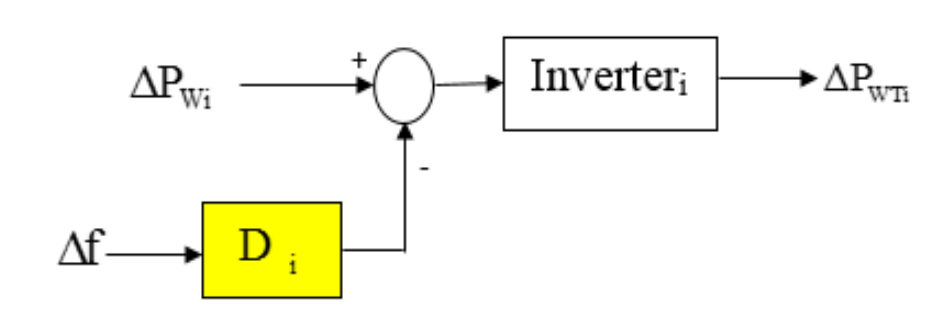


Figure 3. The dynamic model of the proposed method

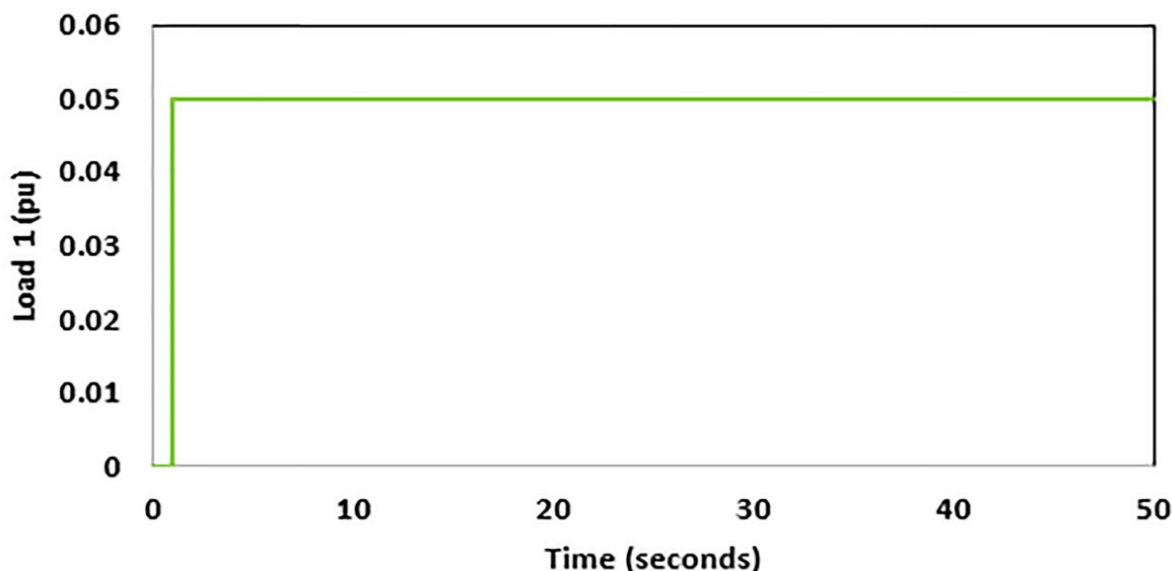


Figure 4. The load disturbance

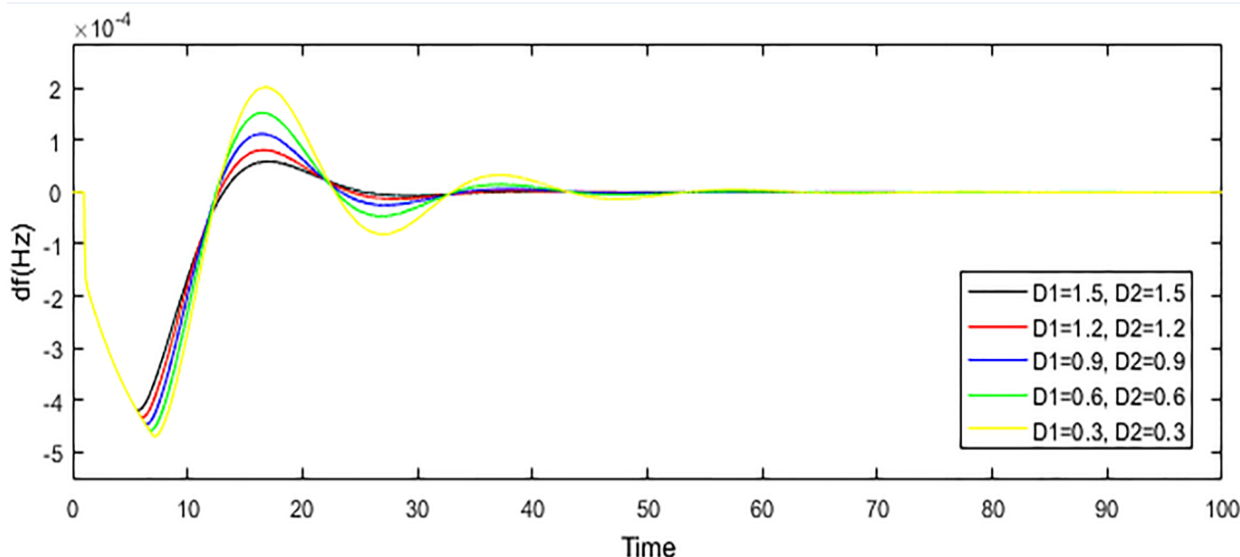


Figure 5. The frequency response of power system

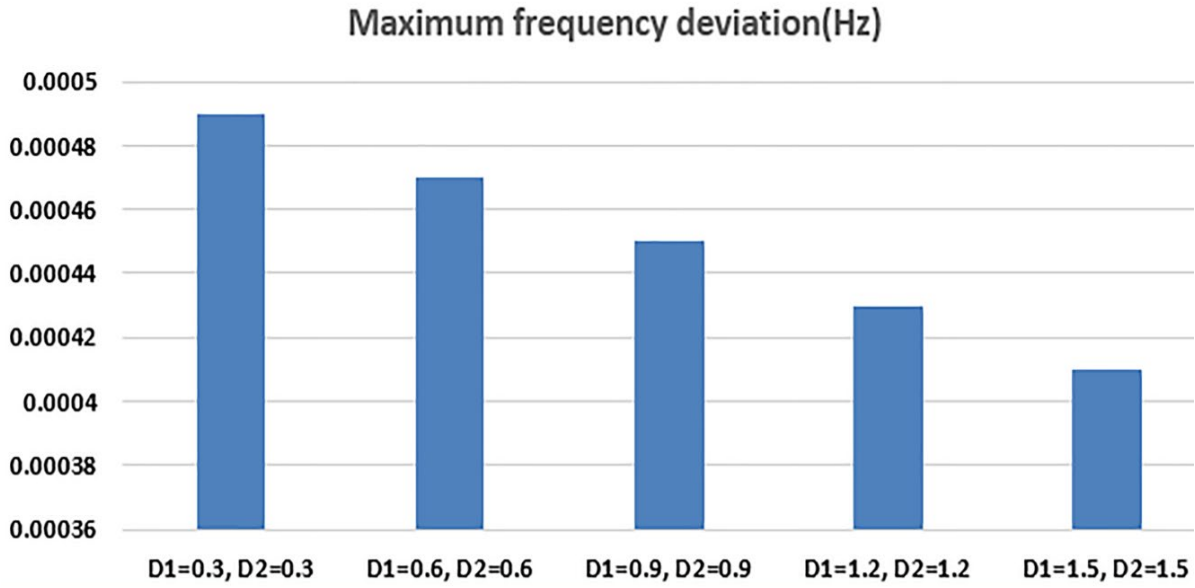


Figure 6. The maximum frequency deviation related to the frequency response of the power system

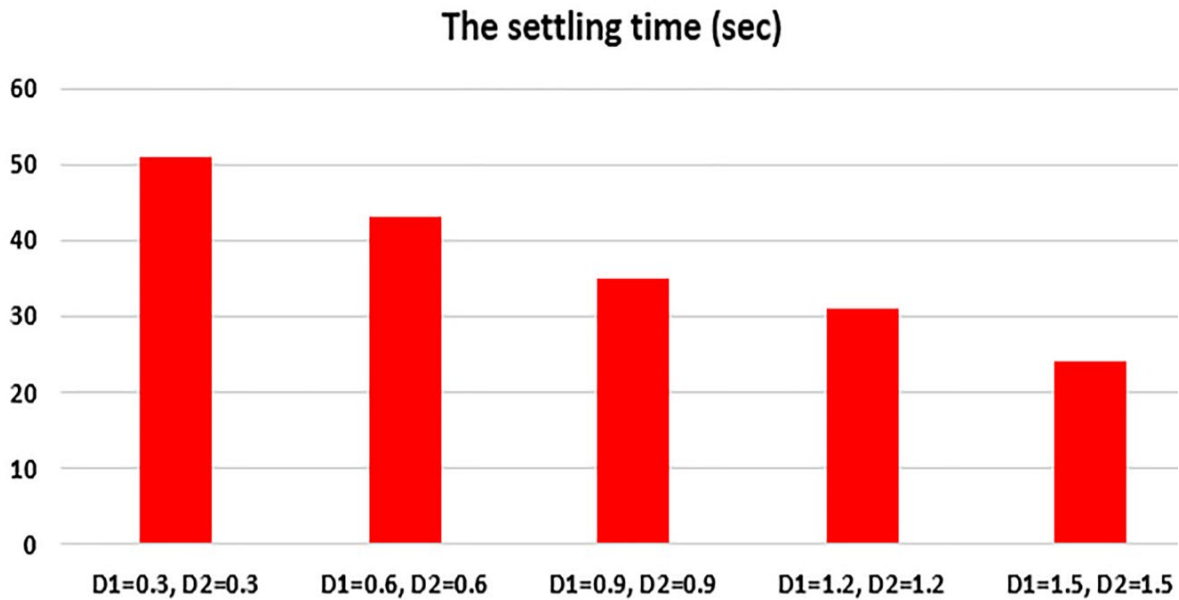


Figure 7. The settling time related to the frequency response of the power system

3.2. State space of the studied power system

Eq. (1) shows the power system's frequency deviation model. Eq. (2) shows the generated power model from the non-reheat power plant. Eqs. (3) and (4) exhibit the generated power model from the reheat power plant. Eqs. (5) and (6) show the hydropower plants' generated power model. Eq. (7) demonstrates the power model of wind turbines. Eq. (8) exhibits the generated power model from superconducting magnetic energy. The system state-space is shown in Eqs. (9) and (10), respectively, for the purpose of designing the proposed method for power systems in the studied power system [26].

$$\Delta f = \frac{1}{2HS + D} [\Delta P_{Reh} + \Delta P_{WT} + \Delta P_{Non-Reh} + \Delta P_{Hydro} - \Delta P_{SMES} - \Delta P_L] \quad (1)$$

$$\Delta P_{Non-Reh} = \frac{P_{n1}}{T_1 s + 1} \times \left[\frac{-1}{R_1} \Delta f - \Delta P_c \right] \quad (2)$$

$$\Delta P_{g2} = \frac{P_{n2}}{T_2 s + 1} \times \left[\frac{-1}{R_2} \Delta f - \Delta P_c \right] \quad (3)$$

$$\Delta P_{Reh} = \left[m + \frac{m}{T_h s + 1} \right] \times \Delta P_{g2} \quad (4)$$

$$\Delta P_{g3} = \frac{P_{n3} T_d s + P_{n3}}{T_3 s + 1} \times \left[\frac{-1}{R_3} \Delta f - \Delta P_c \right] \quad (5)$$

$$\Delta P_{Hydro} = \left[\frac{-T_w s + 1}{0.5 T_w s + 1} \right] \times \Delta P_{g3} \quad (6)$$

$$\Delta P_{WT} = \frac{1}{T_{WT} s + 1} \times \Delta P_{wind} \quad (7)$$

$$\Delta P_{SMES} = \frac{K_{SMES}}{T_{SMES} s + 1} \times \Delta f \quad (8)$$

$$\begin{bmatrix} \dot{\Delta f} \\ \dot{\Delta P}_{\text{Non-Reh}} \\ \dot{\Delta P}_{\text{Reh}} \\ \dot{\Delta P}_{g2} \\ \dot{\Delta P}_{\text{Hydro}} \\ \dot{\Delta P}_{g3} \\ \dot{\Delta P}_{\text{WT}} \\ \dot{\Delta P}_{\text{SMES}} \end{bmatrix} = \frac{2m}{T_h} \begin{bmatrix} \frac{-D}{2H} & \frac{1}{2H} & \frac{1}{2H} & 0 & \frac{1}{2H} & 0 & \frac{1}{2H} & \frac{1}{2H} \\ \frac{-P_{n1}}{T_1 R_1} & \frac{-1}{T_1} & 0 & 0 & 0 & 0 & 0 & 0 \\ \frac{-mP_{n2}}{T_2 R_2} & 0 & \frac{-1}{T_h} & (\frac{2m}{T_h} - \frac{m}{T_2}) & 0 & 0 & 0 & 0 \\ \frac{-P_{n2}}{T_2 R_2} & 0 & 0 & \frac{-1}{T_2} & 0 & 0 & 0 & 0 \\ (\frac{-T_d P_{n3} D}{T_3 R_3 H} + \frac{2P_{n3}}{T_3 R_3}) & (\frac{T_d P_{n3}}{T_3 R_3 H}) & (\frac{T_d P_{n3}}{T_3 R_3 H}) & 0 & (\frac{T_d P_{n3}}{T_3 R_3 H} - \frac{2}{T_w}) & (\frac{2}{T_w} + \frac{2}{T_3}) & 0 & 0 \\ (\frac{T_d P_{n3} D}{2T_3 R_3 H} - \frac{P_{n3}}{T_3 R_3}) & (\frac{-T_d P_{n3}}{2T_3 R_3 H}) & (\frac{-T_d P_{n3}}{2T_3 R_3 H}) & 0 & (\frac{-T_d P_{n3}}{2T_3 R_3 H}) & \frac{-1}{T_3} & 0 & 0 \\ \frac{-D_i}{T_{\text{SMES}}} & 0 & 0 & 0 & 0 & 0 & \frac{-1}{T_{\text{WT}}} & 0 \\ 0 & 0 & 0 & 0 & 0 & 0 & 0 & \frac{-1}{T_{\text{SMES}}} \end{bmatrix} \begin{bmatrix} \Delta f \\ \Delta P_{\text{Non-Reh}} \\ \Delta P_{\text{Reh}} \\ \Delta P_{g2} \\ \Delta P_{\text{Hydro}} \\ \Delta P_{g3} \\ \Delta P_{\text{WT}} \\ \Delta P_{\text{SMES}} \end{bmatrix} + \begin{bmatrix} 0 \\ \frac{-P_{n1}}{T_1} \\ \frac{-mP_{n2}}{T_2} \\ \frac{-P_{n2}}{T_2} \\ \frac{2P_{n3}}{T_3} \\ \frac{-P_{n3}}{T_3} \\ 0 \\ \frac{-K_{\text{SMES}}}{T_{\text{SMES}}} \end{bmatrix} [u]$$

$$+ \begin{bmatrix} 0 & -\frac{1}{2H} \\ 0 & 0 \\ 0 & 0 \\ 0 & 0 \\ 0 & \frac{-T_d P_{n3}}{T_3 R_3 H} \\ 0 & \frac{T_d P_{n3}}{2T_3 R_3 H} \\ \frac{-1}{T_{\text{WT}}} & 0 \\ 0 & 0 \end{bmatrix} \begin{bmatrix} \Delta P_{\text{wi}} \\ \Delta P_L \end{bmatrix}$$

$$y = [1 \ 0 \ 0 \ 0 \ 0 \ 0 \ 0 \ 0] \begin{bmatrix} \Delta f \\ \Delta P_{\text{Non-reh}} \\ \Delta P_{\text{Reh}} \\ \Delta P_{g2} \\ \Delta P_{\text{Hydro}} \\ \Delta P_{g3} \\ \Delta P_{\text{WT}} \\ \Delta P_{\text{SMES}} \end{bmatrix}$$

4. SIMULATION

This paper considers various implementation scenarios for the proposed method. In Scenario (1), the proposed method's performance against load disturbances is evaluated by considering the time delay between the power system's sources. In Scenario (2), the performance of the proposed method against load disturbances and parameter uncertainty is evaluated by considering the time delay between power system resources. In Scenario (3), the performance of the proposed method against power system disturbances (load and wind turbine) is evaluated. Scenario (4) evaluates the performance of the proposed method in the presence of disturbances and uncertainty in system parameters.

Table 1. Power system parameters with the presence of wind turbine [22]

Parameter	Value	Parameter	Value
R ₁	2.5	m	0.5
R ₂	2.5	T _d	5
R ₃	1	T ₁	0.4
β	1	T ₂	0.4
T _w	1	T ₃	90
T _h	6	H	5.7096
P _{n1}	0.2529	P _{n3}	0.1364
P _{n2}	0.6107	P _{w,1}	750KW
P _{w,2}	3000kW	D	0.028
D ₁	1.5	D ₂	1.5

Scenario (1): In this scenario, the performance of the proposed method against load disturbance is investigated by considering the time delay between power system resources. First, the load disturbance according to Figure 8 is applied to the power system considering the time delay ($\tau = 0.5$ sec.). Figure 9 shows the frequency response of the power system to disturbances. According to Figure 9, the maximum frequency deviation using the proposed method is 0.0008 Hz. The maximum frequency deviation using conventional methods (without virtual damping) is 0.0024 Hz. The settling time of

frequency deviations using the proposed method is 12 sec. The settling time of frequency deviations using conventional methods (without virtual damping) is 45 sec. The proposed method has reduced the frequency deviations due to disturbances and time delays of the power system by 67 % and has increased the damping speed of the frequency deviations by 73 % (73 % improvement over the methods used in this field). According to the results of this scenario, the proposed method has a better performance against load disturbance and system time delay.

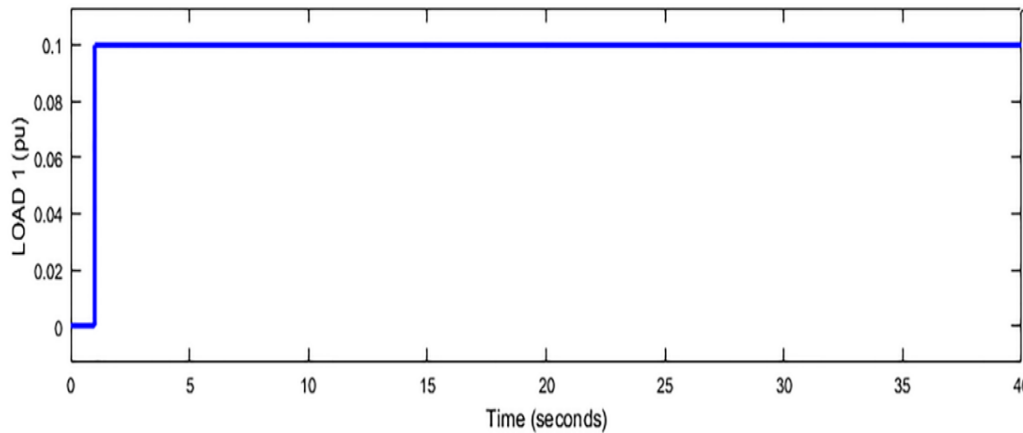


Figure 8. The load disturbance

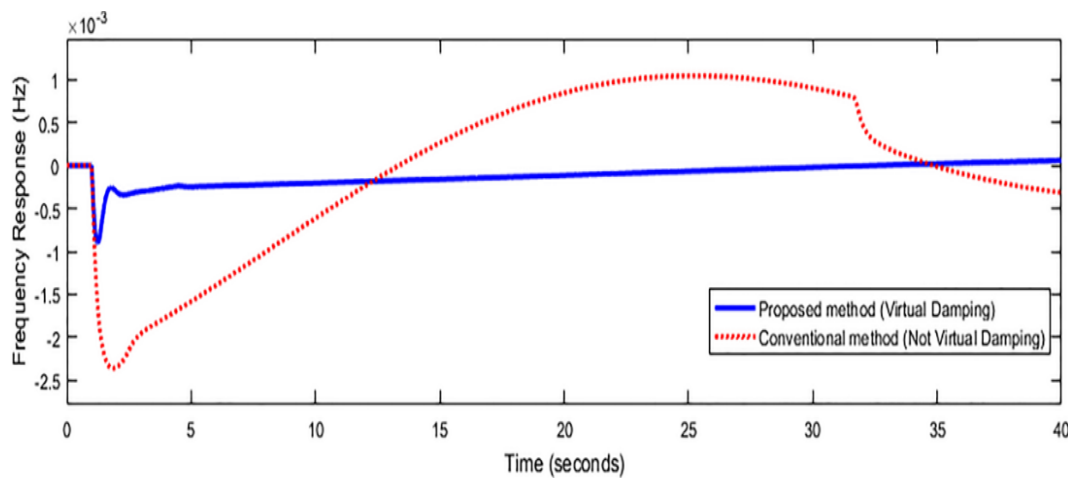


Figure 9. The frequency response of power system, scenario (1)

Scenario (2): In this scenario, the proposed method's performance against load disturbances and uncertainty of system parameters is evaluated by considering the time delay between power system resources. First, the load disturbance is applied to the power system according to Figure 8, considering time delay ($\tau = 0.5$ sec.). The uncertainty of system parameters is considered for power system inertia and power system damping ($D = -30$ %, $H = -30$ %). The frequency response of the power system to disturbances is depicted in Figure 10. According to Figure 10, the proposed method produces a maximum frequency deviation of 0.0011 Hz. The maximum frequency deviation when using conventional methods (without virtual damping) is 0.0031 Hz. The settling time of frequency deviations using the proposed method is 31 sec. The settling time of frequency deviations using conventional methods (without virtual damping) is 78 sec. The proposed method reduced frequency deviations in the power system caused by disturbances and time delays by 65 % and increased the damping speed of the frequency deviations

by 61 % (61 % improvement over the methods used in this field). According to the outcomes of this scenario, the proposed method outperforms existing methods in terms of load disturbance and system time delay.

Scenario (3): The performance of the proposed method against power system disturbances is examined in this scenario. According to Figure 11, the power system is subjected to load disturbances and disturbances from distributed generation sources. Figure 12 illustrates the frequency response of the power system to disturbances. As per Figure 12, the maximum frequency deviation for the proposed method is 0.005 Hz. The maximum frequency deviation when using conventional methods (without virtual damping) is 0.017 Hz. According to the results of this scenario, the proposed method (virtual damping) performed better than conventional methods (without virtual damping) in damping power system frequency fluctuations and was able to dampen the fluctuations more.

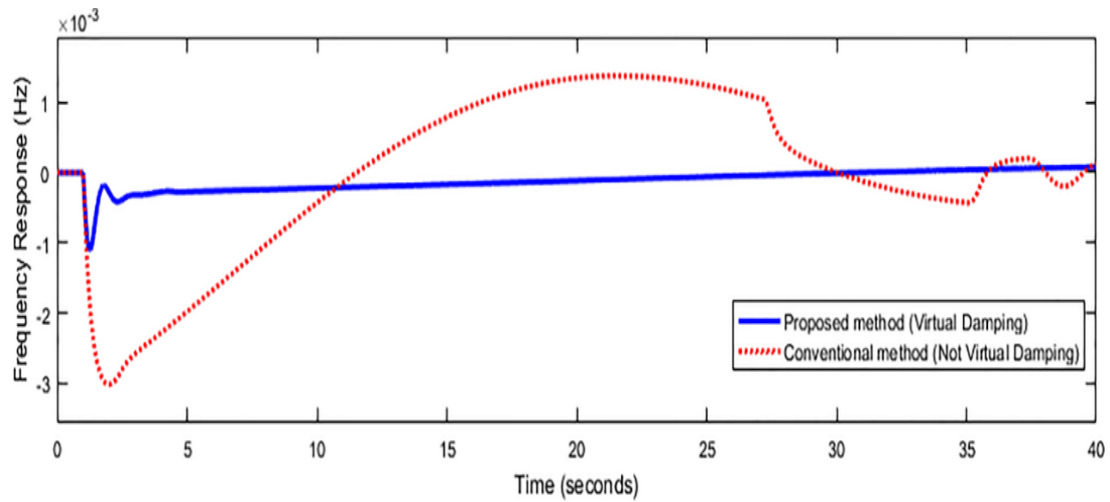


Figure 10. The frequency response of the power system, Scenario (2)

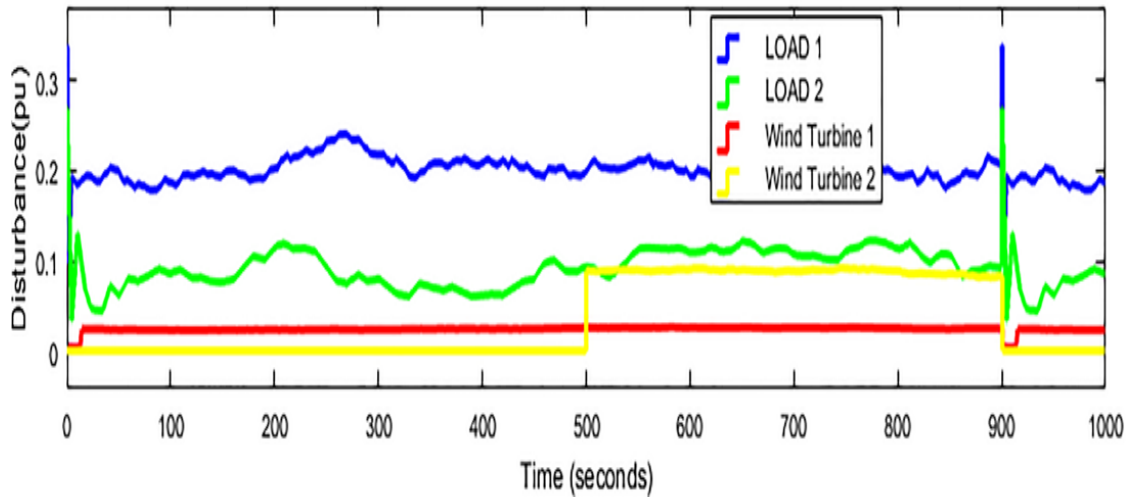


Figure 11. The disturbances in the power system

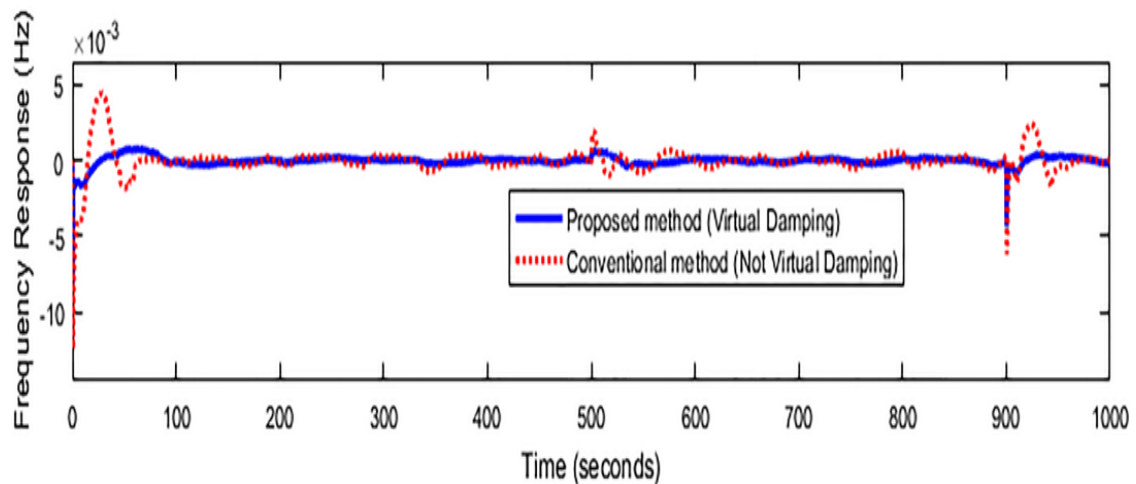


Figure 12. The frequency response of power system, Scenario (3)

Scenario (4): In this scenario, the performance of the proposed method against disturbances and uncertainties related to the parameters of the power system is investigated. The disturbances are entered into the power system according to Figure 11. The uncertainty in the damping parameter of the power system D is considered to be -20% . Figure 13 shows the frequency response of the power system disturbances and the uncertainty of system parameters. As shown in Figure 13,

the maximum frequency deviation using the proposed method is 0.0053 Hz. The maximum frequency deviation using conventional methods (without virtual damping) is 0.022 Hz. The proposed method (virtual damping) has better performance in damping the frequency fluctuations related to the power system than conventional methods (without virtual damping).

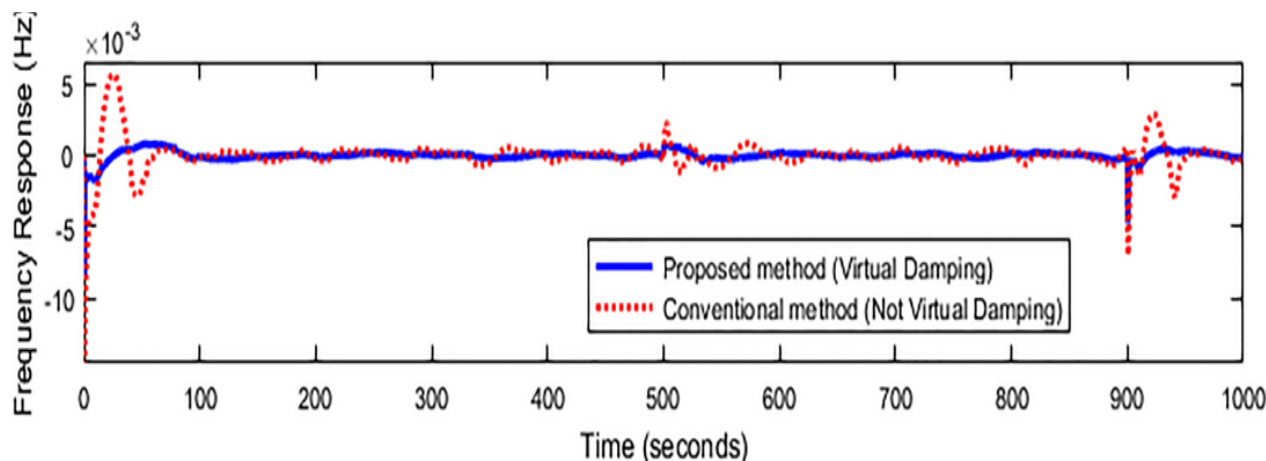


Figure 13. The frequency response of power system, scenario (4)

5. CONCLUSIONS

Distributed generation sources such as wind turbines undeniably impact the power system. The presence of these resources in the power systems poses challenges. The complexity of frequency control is one of the most significant challenges associated with the presence of wind turbines in the power system. Because wind turbines naturally oscillate and are not involved in frequency control. The paper aimed to design and implement a control method (virtual damping) for a wind turbine that has the following advantages:

- Improvement of the damping speed of frequency deviations: Wind turbines reduce the damping speed of frequency deviations caused by disturbances (load and wind turbine), to be then dampened. The presence of this issue may result in power system frequency instability. The proposed method's design (virtual damping) on the wind turbine increases the damping speed associated with the power system's frequency deviations and a decrease in the maximum deviations.
- Wind turbines' proactive role in power system frequency regulation: Wind turbines played no role in the frequency control methods proposed in the power system frequency control field. Due to the presence of wind turbines in today's power systems, this source must be capable of actively controlling the system frequency. According to the proposed method, the wind turbine participates actively in the power system during disturbances, thereby enhancing the frequency stability of the power system.
- Improvement of the power system's frequency stability in the presence of time delay: Time delay in the power system can result in frequency instability. The methods used to control the power system's frequency in the presence of wind turbines do not address the issue of time delay. This paper studied the effects of time delay on the power system. Inclusion of time delay effect results in a more comprehensive frequency response model for controlling the frequency of the power system.

6. ACKNOWLEDGEMENT

This research has received no external funding.

NOMENCLATURE

Δf The power system frequency deviation

$\Delta P_{\text{Non-Reh}}$	The generated power from the non-reheat power plant
ΔP_{Reh}	The generated power from the reheat power plant
ΔP_{g2}	The generated from the governor. 2
ΔP_{g3}	The generated from the governor. 3
ΔP_{Hydro}	The generated power from the hydropower plant
ΔP_L	The load power
ΔP_{SMES}	The generated power from the superconducting magnetic energy
τ	Time delay
R_1	Governor speed regulation non-reheat plant (Hz/pu MW)
R_2	Governor speed regulation reheat plant
R_3	Governor speed regulation hydro plant (Hz/pu MW)
β	Bias factor (pu MW/Hz)
T_w	Water starting time in hydro intake (s)
T_h	Time constant of reheat thermal plant (s)
P_{n1}	Nominal rated power output for the non-reheat plant (MW pu)
P_{n2}	Nominal rated power output for reheat plant (MW pu)
P_{n3}	Nominal rated power output for the hydro plant (MW pu)
$P_{w,1}$	Nominal power of wind turbine 1
$P_{w,2}$	Nominal power of wind turbine 2
m	Fraction of turbine power
T_d	Dashpot time constant of hydro plant speed governor (s)
T_1	Valve time constant of the non-reheat plant (s)
T_2	Steam valve time constant of reheat plant (s)
T_3	Water valve time constant hydro plant (s)
H	Equivalent inertia constant (pu s)
D	System damping coefficient of the area (pu MW/Hz)

REFERENCES

1. Vahdatpour, S., Behzadfar, S., Siampour, L., Veisi, E. and Jahangiri, M., "Evaluation of off-grid hybrid renewable systems in the four climate regions of Iran", *Journal of Renewable Energy and Environment (JREE)*, Vol. 4, No. 1, (2017), 61-70. (<http://dx.doi.org/10.30501/jree.2017.70107>).
2. Mostafaeipour, A., Rezaei, M., Jahangiri, M. and Qolipour, M., "Feasibility analysis of a new tree-shaped wind turbine for urban application: A case study", *Energy & Environment*, Vol. 31, No. 7, (2020), 1230-1256. (<https://doi.org/10.1177/0958305X19888878>).
3. Sedaghat, A., El Haj Assad, M. and Gaith, M., "Aerodynamics performance of continuously variable speed horizontal axis wind turbine with optimal blades", *Energy*, Vol. 77, (2014), 752-759. (<https://doi.org/10.1016/j.energy.2014.09.048>).
4. Sedaghat, A., Samani, I., Ahmadi-Baloutaki, M., El Haj Assad, M. and Gaith, M., "Computational study on novel circulating aerofoils for use in Magnus wind turbine blades", *Energy*, Vol. 91, (2015), 393-403. (<https://doi.org/10.1016/j.energy.2015.08.058>).
5. Lampinen, M.J., Kotiaho, V.W. and El Haj Assad, M., "Application of axial fan theory to horizontal-axis wind turbine", *International Journal of Energy Research*, Vol. 30, No. 13, (2006), 1093-1107. (<https://doi.org/10.1002/er.1208>).

6. Nazari, M.A., El Haj Assad, M., Haghghat, S. and Maleki, A., "Applying TOPSIS method for wind farm site selection in Iran", *Proceedings of 2020 Advances in Science and Engineering Technology International Conferences (ASET)*, (2020, February), 1-4. (<https://doi.org/10.1109/ASET48392.2020.9118223>).
7. Abido, L.K., Bani-Hani, E., El Haj Assad, M., AlShabi, M., Soudan, B. and Oriaje, A.T., "Effects of environmental and turbine parameters on energy gains from wind farm system: Artificial neural network simulations", *Wind Engineering*, Vol. 44, No. 2, (2020), 181-195. (<https://doi.org/10.1177/0309524X19849834>).
8. Amiri, F. and Moradi, M.H., "Designing a fractional order PID controller for a two-area micro-grid under uncertainty of parameters", *Iranian Journal of Energy*, Vol. 20, No. 4, (2018), 49-78. (<https://necjournals.ir/article-1-1212-en.html>).
9. Amiri, F. and Hatami, A., "Nonlinear load frequency control of isolated microgrid using fractional order PID based on hybrid craziness-based particle swarm optimization and pattern search", *Journal of Iranian Association of Electrical and Electronics Engineers*, Vol. 17, No. 2, (2020), 135-148. (http://jiaeee.com/browse.php?a_id=544&slc_lang=en&sid=1&printcase=1&hbnr=1&hmb=1).
10. Amiri, F. and Moradi, M.H., "Designing of the controller for shipboard microgrid based on linear matrix inequality", *Journal of Applied Research in Electrical Engineering*, Vol. 1, No. 2, (2022), 176-186. (<https://doi.org/10.22055/JAREE.2022.39484.1041>).
11. Magdy, G., Shabib, G., Elbaset, A.A. and Mitani, Y., "Renewable power systems dynamic security using a new coordination of frequency control strategy based on virtual synchronous generator and digital frequency protection", *International Journal of Electrical Power & Energy Systems*, Vol. 109, (2019), 351-368. (<https://doi.org/10.1016/j.ijepes.2019.02.007>).
12. Moradi, M.H. and Amiri, F., "Load frequency control in a two area microgrid by optimized model predictive controller", *Journal of Iranian Association of Electrical and Electronics Engineers*, Vol. 19, No. 1, (2022), 125-137. (<https://doi.org/10.52547/jiaeee.19.1.125>).
13. Shahbazi, M. and Amiri, F., "Designing a neuro-fuzzy controller with CRPSO and RLSE algorithms to control voltage and frequency in an isolated microgrid", *Proceedings of 2019 International Power System Conference (PSC)*, (2019), 588-594. (<https://doi.org/10.1109/PSC49016.2019.9081492>).
14. Amiri, F. and Moradi, M.H., "Designing a new robust control for virtual inertia control in the microgrid with regard to virtual damping", *Journal of Electrical and Computer Engineering Innovations (JECEI)*, Vol. 8, No. 1, (2020), 53-70. (<https://doi.org/10.22061/JECEI.2020.6913.347>).
15. Amiri, F. and Moradi, M.H., "Microgrid on the ship: Load frequency-control of the microgrid, taking into account the sea wave energy by the optimized model predictive controller", *Journal of Renewable and New Energy*, Vol. 8, No. 1, (2021), 78-90. (In Farsi). (https://www.jrenew.ir/article_111153_66e20afd3012ff2e42541a303f0f96f7.pdf).
16. Lu, L., Saborio-Romano, O. and Cutululis, N.A., "Torsional oscillation damping in wind turbines with virtual synchronous machine-based frequency response", *Wind Energy*, (2022). (<https://doi.org/10.1002/we.2719>).
17. Moradi, M.H. and Amiri, F., "Virtual inertia control in islanded microgrid by using robust model predictive control (RMPC) with considering the time delay", *Soft Computing*, Vol. 25, No. 8, (2021), 6653-6663. (<https://doi.org/10.1007/s00500-021-05662-z>).
18. Asgari, S., Suratgar, A.A. and Kazemi, M., "Feedforward fractional order PID load frequency control of microgrid using harmony search algorithm", *Iranian Journal of Science and Technology, Transactions of Electrical Engineering*, (2021), 1-13. (<https://doi.org/10.1007/s40998-021-00428-7>).
19. Amiri, F. and Moradi, M.H., "Angular speed control in a hybrid stepper motor using linear matrix inequality", *Computational Intelligence in Electrical Engineering*, Vol. 12, No. 3, (2021), 33-50. (In Farsi). (<https://doi.org/10.22108/isee.2020.122029.1346>).
20. Amiri, F. and Moradi, M.H., "Designing a new robust control method for AC servo motor", *Journal of Nonlinear Systems in Electrical Engineering*, Vol. 7, No. 1, (2020), 55-80. (In Farsi). (<http://journals.sut.ac.ir/jnsee/article-1-326-fa.html>).
21. Ma, M., Zhang, C., Shao, L. and Sun, Y., "Primary frequency regulation for multi-area interconnected power system with wind turbines based on DMPC", *Proceedings of 35th Chinese Control Conference (CCC)*, (2016), 4384-4389. (<https://doi.org/10.1109/ChiCC.2016.7554034>).
22. Amiri, F. and Moradi, M.H., "Coordinated control of LFC and SMES in the power system using a new robust controller", *Iranian Journal of Electrical and Electronic Engineering*, Vol. 17, No. 4, (2021), 1912-1929. (<https://doi.org/10.22068/IJEEE.17.4.1912>).
23. Amiri, F. and Moradi, M.H., "A new control strategy for controlling isolated Microgrid", *Journal of Experimental Medicine*, Vol. 10, No. 4, (2021), 60-73. (<https://doi.org/10.22052/10.4.60>).
24. Afram, A. and Janabi-Sharifi, F., "Theory and applications of HVAC control systems—A review of model predictive control (MPC)", *Building and Environment*, Vol. 72, (2014) 343-355. (<https://doi.org/10.1016/j.buildenv.2013.11.016>).
25. Sharma, M., Bansal, R. K. and Prakash, S., "Robustness analysis of LFC for multi area power system integrated with SMES-TCPS by artificial intelligent technique", *Journal of Electrical Engineering & Technology*, Vol. 14, No. 1, (2019), 97-110. (<https://doi.org/10.1007/s42835-018-00035-3>).
26. Akram, U., Nadarajah, M., Shah, R. and Milano, F., "A review on rapid responsive energy storage technologies for frequency regulation in modern power systems", *Renewable and Sustainable Energy Reviews*, Vol. 120, (2020), 109626. (<https://doi.org/10.1016/j.rser.2019.109626>).
27. European Wind Energy Association, "Wind energy-the facts: A guide to the technology, economics and future of wind power", *Routledge*, (2012). (<https://doi.org/10.4324/9781849773782>).



Research Article

Deriving an Alternative Energy Using Anaerobic Co-Digestion of Water Hyacinth, Food Waste, and Cow Manure

Sapna Kinattinkara ^a, Thangavelu Arumugam ^{b*}, Nandhini Samiappan ^a, Vivek Sivakumar ^c, Sampathkumar Velusamy ^d, Mohanraj Murugesan ^e, Manoj Shanmugamoorthy ^d

^a Department of Environmental Science, PSG College of Arts and Science, P. O. Box: 641014, Coimbatore, India.

^b Department of Environmental Studies, Kannur University, P. O. Box: 670567, Kerala, India.

^c Department of Civil Engineering, Hindustan College of Engineering, P. O. Box: 641032, Coimbatore, India.

^d Department of Civil Engineering, Kongu Engineering College, P. O. Box: 638060, Erode, India.

^e Department of Mechanical Engineering, Hindustan College of Engineering, P. O. Box: 641032, Coimbatore, India.

PAPER INFO

Paper history:

Received: 14 February 2022

Revised in revised form: 07 April 2022

Scientific Accepted: 13 April 2022

Published: 06 August 2022

Keywords:

Anaerobic Digestion,
Bioenergy,
Biogas,
Cow Dung,
Eichhornia Crassipes

ABSTRACT

Increased global energy consumption demands the use of more energy resources, aggravating environmental issues. This study focused on analyzing biogas production from a mixture of cow dung, water hyacinth, and food waste and checking the efficiency of the biogas. The efficiency of biogas production was tested using two alternative settings in the study. The first setup employs Eichhornia crassipes that have been NaOH-treated and mixed with co-digestion substrates such as cow manure and food waste which have been stored at room temperature for 32 days. The second setup contains five different types of substrates such as L1-cow dung, L2-cow dung: water hyacinth, L3-cow dung: food waste, L4-cow dung: water hyacinth: food waste, and L5-water hyacinth. The properties of the Eichhornia crassipes were studied on several biogas substrates, such as pH, temperature, COD, TOC, and NPK tests, as well as total biogas output and methane percentage. The results of the comparison analysis show that the substrate L4 has a high level of NPK (4.7 %) and a higher amount of COD (137600 mg/l). These characteristics enhance the gas yield and methane percentage (85 %). Overall, the water hyacinth mixed with cow dung and food waste exceeded the other four substrates. The total yield of biogas from the first setup was 8.5 litres, the flammability was tested on the 28th day, and the blue flame was obtained. Water hyacinth was removed from aquatic areas and used as an alternative energy source, hence being environmentally friendly.

<https://doi.org/10.30501/jree.2022.327715.1325>

1. INTRODUCTION

Energy is vital to most industrial and commercial wealth organisations and serves as a major component in improving social and economic well-being [1]. Environmental sustainability, economic prosperity, and social equality are all dependent on energy. However, individuals in many developing countries, particularly in rural areas, suffer from energy poverty due to no access to electricity [2]. The shortage of energy can have a negative impact on the country's development, economic growth, lifestyles, health, education, and so on. The economic development of a country is mainly dependent upon the use of energy in industrial, transportation, domestic, and agricultural domains [3]. A high rate of energy consumption in these sectors indicates the development and quality of life in these sectors of the country [4]. In any country, it has been difficult to increase per capita income without raising the use of commercial energy. The

consumption of energy can improve living standards because it provides an essential service to humans [5, 6]. According to the Energy Information Administration, between 2018 and 2050, approximately half of the world's energy consumption will increase [7]. In all industries, non-renewable energy sources like fossil fuels and uranium are still used. These fossil fuels are considered non-sustainable sources, because they produce pollutants that contribute to global warming, according to the Intergovernmental Panel on Climate Change (IPCC). As a result, we focused mostly on alternative energy, which is regarded a renewable and long-term energy source. Solar energy, wind energy, biomass energy, and geothermal energy are examples of renewable energy resources [8].

Biogas is one of the renewable energy sources that is a more sustainable solution which effectively replaces or reduces the demand for coal or natural gas. Humans and animals always generate waste in order to manage the waste, which is used in generating biogas. Recently, energy crops like weeds and agricultural residues have been widely used for biogas production [9]. The water hyacinth (*Eichhornia crassipes*) is

*Corresponding Author's Email: thangavelugis@gmail.com (T. Arumugam)
URL: https://www.jree.ir/article_154525.html



generally considered an aquatic weed, and it is an invasive species that is persistent in the environment and causes aquatic problems [10]. It affects the quality of the water by preventing sunlight and the air-water interface from reaching it. Therefore, these blockages reduce oxygen levels in the water [11]. Several studies have been conducted on biogas production from water hyacinth; methane can be produced under anaerobic conditions. For these reasons, lignocellulose waste can be used and is a significant renewable source [12]. A study conducted on biogas production from anaerobic co-digestion of water hyacinth (*Eichhornia crassipes*) and cow manure revealed that the mesophilic anaerobic fermentation system was operating at $(39\text{ }^{\circ}\text{C} \pm 2\text{ }^{\circ}\text{C})$ [4]. The study in [13] created a fixed dome biogas plant for the creation of biogas from food waste and conducted research on biogas generation from food waste with a co-digester mixture. In many countries, biogas production helps strengthen environmental legislation and regulates the waste recycling process [14]. The main reason behind the use of biogas is to reduce the greenhouse effect by capturing methane as fuel and cutting down on the use of fossil fuels [15]. Moreover, we can get a bio-fertilizer at the end of the process. The objective of this study is to analyze the production of biogas from a mixture of cow dung, water hyacinth, and food waste and to check the efficiency of the biogas. The present study was carried out at three phases: experimental setup, laboratory setup, and analysis of biogas substrates.

2. MATERIALS AND METHODS

2.1. Designing of digester and preparation of biogas substrates

A thirty-five-liter Black Jerry Can was taken for making bio-digester. The plastic tube was fitted with a can cap by using a hose barb coupler and a hose clamp. The barb hose fitting tee was used to connect the outlet of the plastic tube. One outlet of a plastic tube was inserted into 20 L water to measure gas volume. Another outlet was connected to Bunsen burner for checking the flammability. The biogas substrates were made using water hyacinth (*Eichhornia crassipes*), cow dung, and food waste. The water hyacinth was collected from Noyyal River, near Somanur and cow dung, and food waste from the Kasilingampalayam village in Tiruppur district. The sun-dried water hyacinth was chopped into tiny pieces and dried in a hot air oven at $70\text{ }^{\circ}\text{C}$ for 10 hours and pretreated with 1 % NaOH alkali solution. Then, it was mixed with finely ground food waste and cow dung. These mixtures were dissolved using cow urine and made at 3:1 ratio by the volume of cow dung and water hyacinth and food waste mixture. At the end, the total volume was 24 L. The whole process is illustrated in Figure 1.

The mixture was poured into the digester container and it maintained the homogenized mixing. It was conducted between February and March. The digester can was placed at room temperature with adequate sunlight. The pH of the substrates was determined at the initial stage. Moreover, the temperature and volume of gas production were measured on a daily basis. The volume of gas production was measured using water displacement method and the Bunsen burner used to check the flammability. This experimental setup is shown in Figure 2.

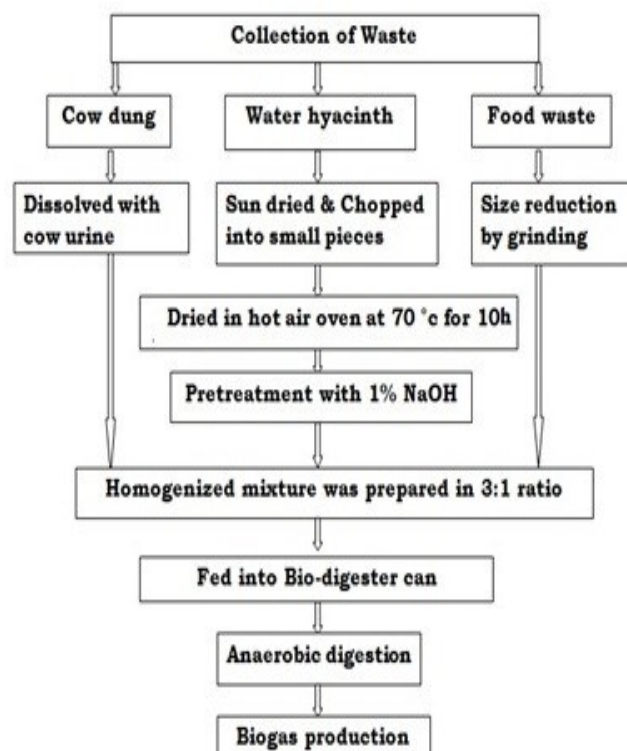


Figure 1. Process followed for preparation of biogas digester



Figure 2. The experimental setup containing a mixture of cow dung and water hyacinth food waste

2.2. Preparation of biogas substrates and setup

The same substrates were taken for laboratory setup. Five clean 750 ml glass bottles were taken and marked by L1 (CD), L2 (CD: WH), L3 (CD: FW), L4 (CD: WH: FW), and L5 (WH), as shown in Figure 3. First, in the case of L1, half of the bottle was filled only with cow dung and cow urine mixing. Second, L2 was filled with a mixture of 3:1 ratio volume of cow dung and 1 % NaOH treated water hyacinth. Third, L3 was filled with a mixture of 3:1 ratio volume of cow dung and food waste. L4 was filled with a mixture of 3:1 ratio of cow dung and 1 % NaOH treated water hyacinth and food waste. Above all the four substrates were mixed with cow urine instead of using water. Finally, L5 was only filled with 1 % NaOH alkali treated water hyacinth. The bottles were placed at room temperature and exposed to direct sunlight. The production of biogas was measured daily using water displacement method and methane content was measured using a saccharometer.



Figure 3. The laboratory setup was prepared with different substrates-L1 (CD), L2 (CD: WH), L3 (CD: FW), L4 (CD:WH: FW), L5 (WH)

2.3. Analysis of biogas substrates

2.3.1. Analysis of physicochemical properties of biogas substrates

The pH of the biogas substrates was measured using a pH meter and the temperature was measured using a room thermometer. The Total organic carbon of the sample was determined based on the Walkley-Black method [10, 11] in Equation (1).

$$\text{Organic Carbon (\%)} = \frac{(\text{Blank}-\text{Sample}) \times N \times 0.003 \times 100 \times C}{\text{Weight of Sample}} \quad (1)$$

C = 1.334, 1.724)

The Chemical Oxygen Demand (COD) of the substrates was analyzed with the help of two hours of reflux condenser digestion under acidic conditions. The chemical oxygen demand of substrates was calculated by the following equation (2) [16].

$$\text{COD} \left(\frac{\text{mg}}{\text{L}} \right) (\%) = \frac{(\text{Blank}-\text{Sample}) \times \text{Normality of FAS} \times 8 \times 1000}{\text{Volume of Sample}} \quad (2)$$

2.3.2. Analysis of total NPK of biogas substrates

The Kjeldahl method was followed to analyze the nitrogen content present in the different biogas substrates (Johan Kjeldahl, 1883). The phosphorus content of the biogas substrates was extracted and measured using UV-Spectrophotometer at 660 nm (EPA 3051 Method). The potassium content of the sample was analyzed by preparing sesquioxide using HCL extraction. Then, potassium was measured under a flame photometer (EPA 3051 method).

2.3.3. Biogas estimation

The water displacement method was used to measure the total biogas level. Moreover, the percentage of methane in the biogas was estimated using a saccharometer filled with saturated KOH. The volume of methane content was noted and the percentage of methane was determined using the following equation (3) [13].

$$\text{Methane Content} = \frac{\text{Volume of Dissolved Biogas}}{\text{Volume of Biogas Injected}} \times 100 \quad (3)$$

The energy generating potential of the biogas was determined by calculating the calorific value of methane. The following equation (4) was used [13].

$$\text{Methane Content} = \% \text{ of Composition of Methane} \times C_{\text{methane}} \quad (4)$$

However, we have: C_{Biogas} - Calorific value of Biogas; C_{Methane} - Calorific value of methane (37 MJ/ m³).

3. RESULTS AND DISCUSSION

3.1. Laboratory setup

3.1.1. Temperature variations

The experiment was carried out for 20 days at room temperature ranging from 26 °C to 42 °C. During the study, the relationship between the temperature and gas production level was noted. When the ambient temperature increases, it gradually increases the gas production level.

3.1.2. pH of biogas substrates

The pH value was taken before and after the anaerobic digestion process. The pH value for the samples ranges from 7.0 to 8.5 (Table 1). The 1 % NaOH pretreatment of water hyacinth helped adjust the pH level. At initial pH, the substrate-L5 (WH) has the highest level of pH 8.5 and the substrate- L4 (CD: WH: FW) has the lowest value of pH 7.0. Moreover, the final value for the same sample (L5- WH) has the highest value of pH 8.5 and the substrates L3 (CD: FW) and L4 (CD: WH: FW) have the lowest value of pH 7.3. Compared to the initial pH, the final pH was increased due to ammonia and H₂S gases which were formed during anaerobic digestion. Sometimes, CO₂ formed into bicarbonate or reacted with some minerals produces buffer conditions, which can increase pH.

3.1.3. Chemical oxygen demand of biogas substrates

The results of the substrates are given in Table 1; their initial level of COD was greatly reduced after the digestion process. The substrate-L4 (CD: WH: FW) contains higher levels of COD and the substrate-L5 (WH) contains low levels of organic matter. After digestion, the substrate-L2 (CD: WH) has a lower COD value, while the substrate-L4 (CD: WH: FW) has a higher level of COD.

3.1.4. Total organic carbon of biogas substrate

The biogas substrate TOC test was conducted based on Walkley and Black method, and the value was given in Table 1. As a result, the substrate-L4 (CD: WH: FW) has a higher level of TOC, while substrate-L5 (WH) has a lower level of TOC. After the digestion process, the final value was taken and the substrate-L3 (CD: FW) had the highest level of TOC while substrate-L5 (WH) contained the lowest level of TOC.

Table 1. Physicochemical properties of biogas substrates

Biogas substrates	pH		COD (mg/L)		TOC (%)	
	Initial	Final	Initial	Final	Initial	Final
L1	7.2	7.6	1,10,000	26,400	10.86	7.75
L2	7.3	7.5	70,000	11,000	10.62	6.20
L3	7.1	7.3	1,60,000	35,200	15.92	13.55
L4	7.0	7.3	1,80,000	42,400	19.03	11.37
L5	8.5	8.5	60,000	48,000	5.68	4.65

3.1.5. Estimation of total NPK

The substrate can be utilized as a fertilizer after it has been digested anaerobically. The time (days) it takes to digest the food is connected to the increase in NPK concentration. The NPK result is shown in Table 2. The NPK content slightly increased after the anaerobic process. The highest level of

NPK is present in the Biogas substrate L4 (CD: WH: FW), while the lowest level is observed in biogas substrates L5 (WH). Here, the substrates L4 were prepared with cow dung, alkali treated water hyacinth, and finely ground food waste. The mixture was dissolved with cow urine to increase gas production while mixing with cow dung [17].

Table 2. Total NPK of biogas substrates

Biogas substrates	Total Kjeldahl nitrogen (%)		Total phosphorus (%)		Total potassium (%)	
	Initial	Final	Initial	Final	Initial	Final
L1	4.90	5.14	1.52	1.78	4.76	4.93
L2	5.11	5.34	1.98	2.07	5.14	5.31
L3	5.63	5.81	2.12	2.24	5.51	5.83
L4	5.84	5.97	2.15	2.31	5.72	5.91
L5	1.93	1.99	0.91	1.08	4.66	4.67

3.1.6. Total gas production and methane estimation

The measurement of biogas production was taken at regular intervals by the water displacement method. At the same time, the percentage of methane was estimated using a

saccharometer, and the calorific value of biogas was calculated using the percentage of methane. These measurements were carried out for the following laboratory setup samples (Table 3).

Table 3. Biogas production from different substrates

Days	SUBSTRATES L1 (CD)		SUBSTRATE L2 (CD: WH)		SUBSTRATE L3 (CD: FW)		SUBSTRATE L4 (CD: WH: FW)	
	Gas production (ml)	Methane (%)	Gas production (ml)	Methane (%)	Gas production (ml)	Methane (%)	Gas production (ml)	Methane (%)
2	92	50	98	48	89	65	85	66
4	108	54	115	56	101	70	103	70
6	123	60	125	62	105	70	110	72
8	128	65	140	70	110	72	120	80
10	130	70	145	75	114	75	133	80
12	129	68	143	80	121	76	140	85
14	111	60	131	80	124	76	141	82
16	95	46	119	75	98	70	138	80
18	41	34	98	50	67	66	97	76
20	33	28	52	50	35	55	52	65

a) Biogas production from substrate L1 (CD)

The sample L1 contains a mixture of cow dung and cow urine. The total biogas production and the methane results are shown in Figure 4. The production of gas was gradually increased and the highest level of gas obtained on Days 8 to 12. The maximum level of methane was 70 % and the gas production was 130 ml. The maximum level of the calorific value of

substrate was 25 MJ/m³. The total yield of gas production was obtained 990 ml.

b) Biogas production from substrate L2 (CD: WH)

The substrate L2 (CD: WH) contains a mixture of cow dung, water hyacinth, and cow urine. The total biogas production and the methane results are shown in Figure 5. The production

of gas was gradually increased and the highest level of gas was obtained on Days 8 to 12. The maximum level of methane 80 % was obtained on Days 12 to 14 and the gas production was 145 ml. The maximum calorific value of L2 was 29 MJ/m³. The total yield of gas production was 1.2 litre.

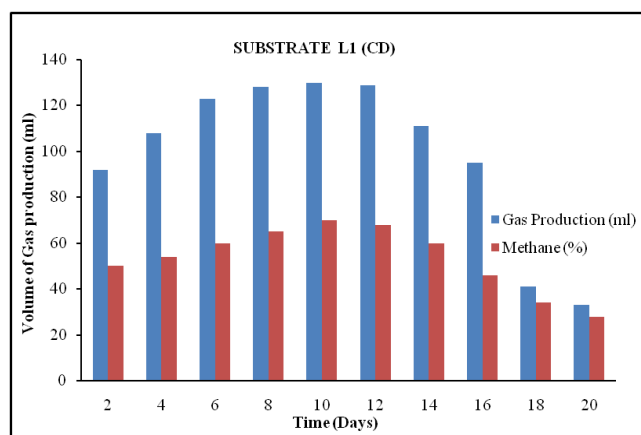


Figure 4. Biogas production from substrates L1 (CD)

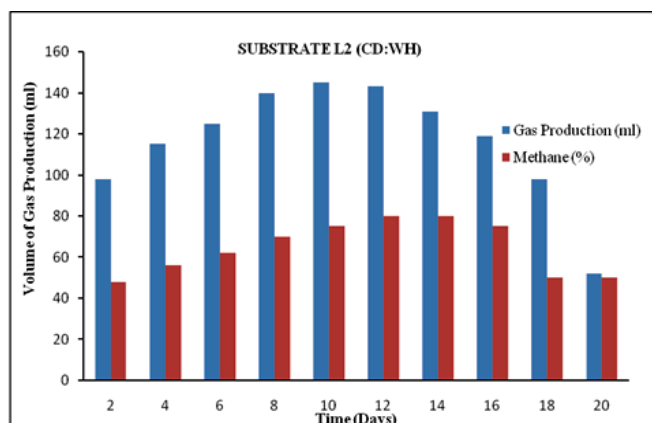


Figure 5. Biogas production from substrate L2 (CD: WH)

c) Biogas production from substrate L3 (CD: FW)

The substrate L3 contains a mixture of cow dung, food waste, and cow urine. The total biogas production and the methane results are shown in Figure 6. The production of gas was gradually increased and it reached the highest level of gas on Days 10 to 14. The maximum level of methane 76 % was obtained on Days 12 to 14 and the gas production was 124 ml. The maximum calorific value obtained in L3 was 28 MJ/m³. The total yield of gas production was obtained at 964 ml.

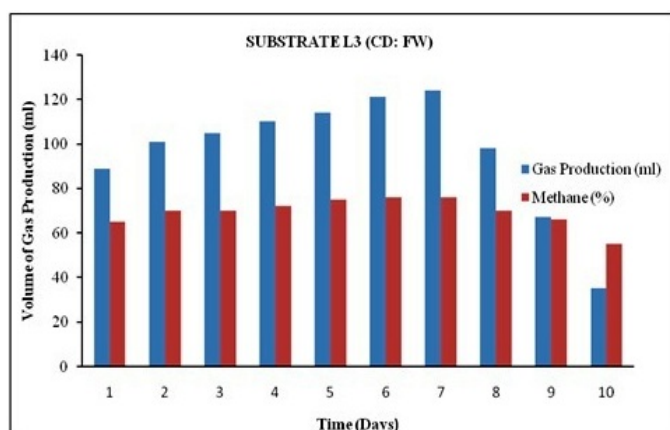


Figure 6. Biogas production from substrates L3 (CD: FW)

d) Biogas production from substrate L4 (CD: WH: FW)

The sample L4 was prepared with cow dung, water hyacinth, food waste, and cow urine. The results of total biogas production and the methane are shown in Figure 7. The production of gas was gradually increased and it reached the highest level of gas on Days 10 to 14. The maximum level of methane 85 % was obtained on Days 12 to 14 and the gas production was 141 ml. The maximum calorific value obtained in L4 was 31 MJ/m³. The total yield of gas production was 1.1 liter.

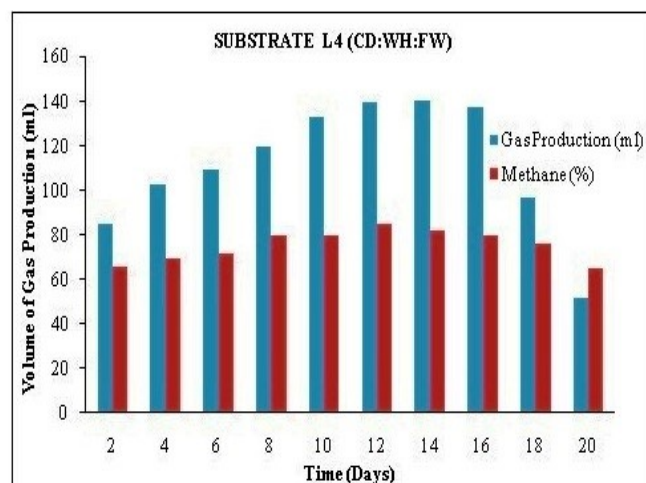


Figure 7. Biogas production from substrate L4 (CD: WH: FW)

e) Biogas production from substrate L5 (WH)

The biogas substrate L5 was only made of water hyacinth. This substrate totally produces 167 ml of gas and there was no methane present in the total gas. Because the pure water hyacinth substrate produces only CO₂ and H₂. Without any co-digestion substrate, it could not show the methane content. Until the presence of high water content (90.08 %) and lignin, there is no chance of methane production [11, 18]. By comparing all the samples, the biogas substrate L4 exhibits the best results, while the L2 shows higher levels of total gas (1166 ml), but the L4 has a higher level of methane (85 %), which was due to high level COD, TOC, and NPK. Moreover, it has an optimum pH. These factors enhance the methane content.

3.2. Experimental setup

3.2.1. Temperature variation

The experimental setup of anaerobic digestion was being conducted for 32 days at room temperature which varied between 29 °C and 45 °C. Reduction in the temperature affects the biogas production.

3.2.2. pH-experimental substrates

The pH of the sample was measured before and after the digestion. The initial and final pH value respectively 7.0 and 7.9. The pH value was increased after digestion, may be due to CO₂, volatile fatty acids.

3.2.3. Total gas production of experimental setup

The total gas production was measured for 32 days using a water displacement method. The volume of gas is shown in Table 4. The gas production was rapidly increased up to Day

16 and then, decreased on Days 18 and 20 due to low temperatures (29 °C and 31 °C) and gradually increased after 20 days. The value remained constant from Days 24 to 30. The total yield of gas production was 8.5 liter. The average production of gas was 265 ml per day. The presence of cow dung and cow urine accelerated the gas production and methane content.

3.2.4. Flammability of biogas

The flammability of the biogas was produced due to the presence of methane. When the methane content reaches the higher level, it produces a stable blue flame used as energy [19]. The experimental sample flammability was checked by attaching the Bunsen burner with the digester shown in Table 4. The gas began to burn on the 10th day and then, the flame was reduced suddenly on the 20th day. Later, it began to produce blue flame after the 28th day. Due to temperature variation, the gas production and methane value was changed. On 25th and 30th days, the ambient temperature range increased up to 40 °C. Therefore, the volume of gas was rapidly increased.

Table 4. Total biogas production (experimental setup)

Days	Gas production (mL)	Days	Gas production (mL)
2	250	18	580
4	280	20	578
6	354	22	603
8	411	24	658
10	472	26	657
12	543	28	661
14	565	30	664
16	590		

4. CONCLUSIONS

Water hyacinth is commonly used to produce biogas in developing countries. There are two benefits to the environment. Firstly, this study obtained renewable energy from waste. Secondly, the water hyacinth was widely distributed in aquatic areas and it caused several issues to the environment. So, there was a need to remove waterweed from the aquatic. The anaerobic digestion process was the best method of disposing of water hyacinth. The biogas was produced from water hyacinth with the help of co-substrates like cow dung and food wastes. This experiment was performed and a compared study was carried out with different substrates. The pH and temperature determine the gas production level. Compared to different substrates (L1-CD, L2-CD: WH, L3-CD: FW, L4-CD: WH: FW, and L5-WH), the substrate L4-CD: WH: FW contains high NPK, higher level of COD. So, it promotes gas production and enhances the methane level (85 %). It gives a calorific value of about 31 MJ/m³. Overall, the water hyacinth with cow dung and food wastes exhibits better results than other substrates. In experimental setup, the flammability was checked and the blue flame was obtained on the 28th day. To sum up, the project was eco-friendly because the water hyacinth was removed from aquatic areas and used as alternative energy, which shows better results.

5. ACKNOWLEDGEMENT

Our sincere thanks to the editor and reviewers for valuable comments to revise this research manuscript.

REFERENCES

- Pachaiyappan, S., Elamvazhuthi, P., Dhamodharan, M. and Sundaram, S., "Biogas production from water hyacinth blended with cow dung", *Indian Journal of Energy*, Vol. 3, No. 1, (2014), 134-139. (https://www.researchgate.net/publication/266912759_Biogasproductionfromwaterhyacinthblendedwith_cowdung).
- Day, R., Walker, G. and Simcock, N., "Conceptualising energy use and energy poverty using a capabilities framework", *Energy Policy*, Vol. 93, (2016), 255-264. (<https://doi.org/10.1016/j.enpol.2016.03.019>).
- Hasanuzzaman, M., Islam, M.A., Rahim, N.A. and Yanping, Y., "Chapter 3: Energy demand", *Energy for sustainable development*, (2020), 41-87. (<https://doi.org/10.1016/B978-0-12-814645-3.00003-1>).
- Dölle, K. and Hughes, T., "Biogas production from anaerobic co-digestion of water hyacinth (*Eichhornia crassipes*) and cow manure", *Journal of Energy Research and Reviews*, Vol. 5, No. 3, (2020), 49-60. (<https://doi.org/10.9734/jenrr/2020/v5i330149>).
- Kunatsa, T. and Xia, X., "Co-digestion of water hyacinth, municipal solid waste and cow dung: A methane optimised biogas-liquid petroleum gas hybrid system", *Applied Energy*, Vol. 304, (2021), 117716. (<https://doi.org/10.1016/j.apenergy.2021.117716>).
- Dölle, K., Hughes, T. and Kurzmann, D.E., "From fossil fuels to renewable biogas production from biomass based feedstock – A review of anaerobic digester systems", *Journal of Energy Research and Reviews*, Vol. 5, No. 3, (2020), 1-37. (<https://doi.org/10.9734/jenrr/2020/v5i330147>).
- Chuang, Y., Lay, C., Sen, B., Chen, C., Gopalakrishnan, K., Wu, J., Lin, C. and Lin, C., "Biohydrogen and biomethane from water hyacinth (*Eichhornia crassipes*) fermentation: Effects of substrate concentration and incubation temperature", *International Journal of Hydrogen Energy*, Vol. 38, No. 27, (2011), 14195-14203. (<https://dx.doi.org/10.1016/j.ijhydene.2011.04.188>).
- Ilo, O., Simatele, M., Nkomo, S., Mkhize, N. and Prabhu, N., "Methodological approaches to optimising anaerobic digestion of water hyacinth for energy efficiency in south africa", *Sustainability (Switzerland)*, Vol. 13, No. 12, (2021). (<https://dx.doi.org/10.3390/su13126746>).
- Fadairo, A. and Fagbenle, R., "Biogas production from water hyacinth blends", *Proceedings of 10th International Conference on Heat Transfer, Fluid Mechanics and Thermodynamics*, Orlando Florida, (2014), 792-799. ([https://repository.up.ac.za/bitstream/handle/2263/44610/Fagbenle_Biog as_2014.pdf;sequence=1#:~:text=The%20results%20showed%20that%20the%20control%20for%20the%20experiment%20produced](https://repository.up.ac.za/bitstream/handle/2263/44610/Fagbenle_Biogas_2014.pdf;sequence=1#:~:text=The%20results%20showed%20that%20the%20control%20for%20the%20experiment%20produced)).
- Zupančič, G. and Roš, M., "Determination of chemical oxygen demand in substrates for anaerobic treatment of solid organic waste", *Waste and Biomass Valorization*, Vol. 3, No. 1, (2012), 89-98. (<https://dx.doi.org/10.1007/s12649-011-9087-1>).
- Gubara, H., Subramanian, P. and Sugumaran, M., "Biogas genesis from vegetable wastes", *International Journal of Current Microbiology and Applied Sciences*, Vol. 7, No. 3, (2018), 1412-1417. (<https://dx.doi.org/10.20546/ijemas.2018.703.169>).
- Ajeh, M., Ogbomida, T., Onochie, U., Akingba, O., Kubeyinje, B., Oerome, O. and Ogbonmwan, S., "Design and construction of fixed dome digester for biogas production using cow dung and water hyacinth", *African Journal of Environmental Science and Technology*, Vol. 14, No. 1, (2020), 15-25. (<https://dx.doi.org/10.5897/ajest2019.2739>).
- Arthur, R., Baidoo, M.F. and Antwi, E., "Biogas as a potential renewable energy source: A Ghanaian case study", *Renewable Energy*, Elsevier, Vol. 36, No. 5, (2011), 1510-1516. (<https://dx.doi.org/10.1016/j.renene.2010.11.012>).
- Fardous, M.R., Nasrin, M.S., Shakil, M.E., Islam, M.S., Hoque, M.A. and Islam, M.Z., "Cow urine for enhancement of biogas production and fertilizer quality of biogas slurry", *Journal of Scientific Research*, Vol. 12, No. 1, (2020), 135-144. (<https://dx.doi.org/10.3329/jsr.v12i1.43031>).
- Njogu, P., Kinyua, R., Muthoni, P. and Nemoto, Y., "Biogas production using water hyacinth (*Eichhornia crassipes*) for electricity generation in

- Kenya", *Energy and Power Engineering*, Vol. 7, (2015), 209-216. (<https://dx.doi.org/10.4236/epe.2015.75021>).
16. Sugumaran, P., Priya, E., Manoharan, D. and Seshadri, S., "Biogas production from water hyacinth blended with cow dung", *Indian Journal of Energy*, Vol. 16, No. 33, (2014), 134-139. (https://www.researchgate.net/publication/266912759_Biogasproductionfromwaterhyacinthblendedwith_cowdung).
 17. Ayanda, O., Ajayi, T. and Asuwaju, F., "Eichhornia crassipes (Mart.) solms: Uses, challenges, threats, and prospects", *Scientific World Journal*, Vol. 2, (2020), 1-12. (<https://doi.org/10.1155/2020/3452172>).
 18. Kulkarni, M.R., Vaidya, R., Srinivas, S., Anand, S. and Narayana, B., "Application of water hyacinth root powder for Congo red dye removal in batch and continuous packed bed operation", *Nanotechnology for Environmental Engineering*, Vol. 6, No. 31, (2021). (<https://doi.org/10.1007/s41204-021-00126-z>).
 19. Nugraha, W.D., Syafrudin., Laksmi Pradita, L., Matin, H., and Budiyo., "Biogas production from water hyacinth (Eichhornia crassipes): The Effect of F/M Ratio", *IOP Conference Series: Earth and Environmental Science*, Vol. 150, (2018). (<https://dx.doi.org/10.1088/1755-1315/150/1/012019>).



Research Article

Effect of Pretreatment on the Physical Properties and Heating Values of Briquettes

Toyese Friday Oyewusi^{a*}, Gabriel Alebiowu^b, Elizabeth Funmilayo Aransiola^c, Ayowumi Rita Soji-Adekunle^d, Busayo Sunday Adeboye^e

^a Department of Agricultural Engineering, Faculty of Engineering, Adeleke University, P.M.B. 250, Ede, Osun State, Nigeria.

^b Department of Pharmaceutics, Faculty of Pharmacy, Obafemi Awolowo University, P.M.B. 13, Ile-Ife, Osun State, Nigeria.

^c Department of Chemical Engineering, Faculty of Technology, Obafemi Awolowo University, P.M.B. 13, Ile-Ife, Osun State, Nigeria.

^d Department of Mechanical Engineering, Faculty of Engineering, Adeleke University, P.M.B. 250, Ede, Osun State, Nigeria.

^e Department of Mechanical Engineering, College of Science, Engineering and Technology, Osun State University, P.M.B. 4494, Osogbo, Osun State, Nigeria.

PAPER INFO

Paper history:

Received: 17 February 2022

Revised in revised form: 12 April 2022

Scientific Accepted: 24 April 2022

Published: 15 August 2022

Keywords:

Carbonized Briquette,
Uncarbonized Briquette,
Density,
Compressive Strength,
Heating Value

A B S T R A C T

Briquettes from agro-residues have been promoted as a better alternative to firewood and charcoals for heating and cooking in the rural communities. In this light, a study was carried out to investigate the effect of pretreatment methods on physical properties and heating values of briquettes produced from corncob. To accomplish this work, an experiment was designed as a $2 \times 3 \times 3 \times 3$ completely randomized with three replicates. The parameters are pretreatment methods (carbonized and uncarbonized), binder types (cassava, corn, and gelatin), binder concentrations (10, 20, 30 %), and compacting pressures (50, 100, and 150 kPa). A charcoal kiln was fabricated to obtain the pretreatment through pyrolysis and a punch and die was also fabricated to facilitate briquette densification. The physical properties tested were limited to moisture content (MC), density and compressive strength and were determined using a conventional method. The heating value of the briquettes produced was determined using bomb calorimeter. The results demonstrated that average moisture content ranged between 5.29-6.58 % and 12.75-13.72 %, mean relaxed density varied from 813-925 kgm^{-3} and 963-1166 kgm^{-3} , compressive strength ranged between 2.27-5.07 MPa and 5.97-10.12 MPa, and heating value ranged between 28.85-32.36 MJkg^{-1} and 27.58-28.80 MJkg^{-1} for carbonized and uncarbonized briquettes, respectively. Briquettes produced from carbonized corncob had a better moisture content and heating value, while briquettes produced from uncarbonized corncob had higher density and compressive strength. The study shows that pretreatment methods under different binder types and concentrations and the compacting pressure significantly affected the briquettes physical properties and heating values. Therefore, this technology can be successfully applied in rural off-grid areas by the government and other stakeholders in the energy sector as part of renewable energy technologies.

<https://doi.org/10.30501/jree.2022.327453.1329>

1. INTRODUCTION

Corncoobs can be described as by-products of corn plant obtained either dry or green. Nigeria is endowed with a huge amount of corn plants which could be roasted or boiled for human consumption upon harvested green. It can also be harvested dry; the grains threshed out of the cob can further be dried and stored or used for human consumption. In whatever forms, the grains are obtained and they allow an enormous quantity of corncoobs which add to environmental wastes. Often, these corncoobs are left on the farm, thereby polluting it and posing health risks to both human and ecology. The current management practice of corncob is usually that of burning in the open or dumping on the farm to decompose; any of these methods apart from resulting in a colossal waste

of resources contribute to environmental degradation and pollution. This corncob can be directly utilized as fuel; however, it is not suitable apparently because it is bulky, uneven, and has low energy density [1]. However, some literature pieces have shown that corncob is a good resource for biofuel due to its lignocellulosic properties [1-3]. Therefore, it is necessary that the corncoobs should be subjected to the conversion process to be able to produce a better fuel in such a way that it will alleviate the problem they pose when used directly.

Briquette technology has been discovered for use as a renewable fuel production from agricultural waste and by-products to solid biofuel in a sustainable way in many developing countries [2]. Briquetting is a densification process for enhancing some physical properties of solid fuel materials and the heating value of biomass [3]. A briquette, defined by Grainger and Gibson [4], is a block of compressed biomass that is used as fuel to start and maintain fire. Briquettes made of biomass that cost nothing to obtain such agricultural wastes

*Corresponding Author's Email: oyewusi.toyese@adelekeuniversity.edu.ng
(T.F. Oyewusi)
URL: https://www.jree.ir/article_154837.html



represent an alternative source for domestic use for rural households or communities. Fuel wood remains a major source of fuel for rural communities since other energy sources (kerosene, gas, and electricity) are either unavailable or grossly inadequate where available and beyond the reach of the masses [1]. Hitherto, collection of fuel wood has grave consequences on forest conservation and sustainable forest resource management. However, briquette production reduces deforestation and its positive effects, thereby turning waste materials into fuel source. However, based on the type of raw materials utilized for the briquette production, they may burn cleaner at a greater heating value than fuel wood and charcoal. Therefore, briquette making has been found to be a promising renewable fuel that supplies additional energy demands for rural, urban, and industrial sectors, thus contributing significantly to expansion of the economy of developing countries.

In recent times, varieties of biomass materials were selected for research. However, a great number of these biomasses were practically applied or utilized with no pretreatment and were found not suitable for large-scale use, particularly in energy production, due to their low energy density. This issue leads to two methods of briquettes production: carbonized (pyrolyzed) and uncarbonized (non-pyrolyzed) methods used in this study. Carbonized method is basically pyrolyzing the biomass to remove volatile matters without or in the limited supply of oxygen. Explicitly, carbonized process entails partial burning of the biomass in an enclosed surrounding to produce char of high-quality carbon. On the other hand, the uncarbonized process is the production of briquettes without carbonizing the biomass without allowing it to pass through any form of heat. The main purpose of biomass pretreatment through pyrolysis is to produce smokeless briquettes that are environmentally friendly with high heating value, which is not feasible or reasonably not achievable for unpretreated biomass. The resulting fine particles obtained at the end of both methods are compacted into regular shape and size, which would not be separated during transportation, storage, or combustion. Fine particles are compressed without the addition of adhesives (binderless briquettes) if the fibres in the material are able to create a strong bond. However, often times, adhesive material is added to facilitate holding the particles of the material together, particularly if the raw material does not have an ability to bond together when compressed. Consequently, addition of adhesive material is to produce a compact briquette, which will suffer less damage during transportation and storage.

The physical properties of briquettes and heating values vary from one method to another and since briquettes can be made of a wide variety of methods, selection of the best briquettes must be made based on the method that has better fuel properties. Therefore, efficient briquette technologies used to extract energy from the biomass and convert it into a more useful form are required, being the essence of this study. Thus, this work aims to investigate the effect of pretreatment methods on the physical properties and heating values of briquettes.

2. MATERIALS AND METHODS

The experiment was designed as $2 \times 3 \times 3 \times 3$ which is completely randomized and replicated three times. These parameters are pretreatment methods (carbonized and uncarbonized), binder types (cassava, corn, and gelatin),

binder concentrations (10, 20, 30 %), and compacting pressure (50, 100, and 150 kPa). The steps followed to achieve this work are shown in Figure 1 and discussed below.

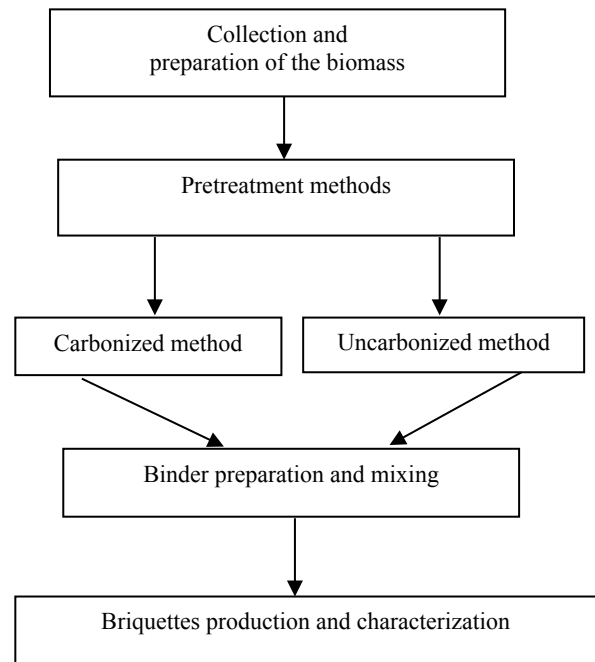


Figure 1. Steps for briquette production

2.1. Collection and preparation of the biomass

The biomass used in this work was the corncob derived from matured *Swan yellow* maize variety harvested from the teaching and research farm of the Obafemi Awolowo University Ile-Ife, Nigeria. The maize was threshed to obtain the corncobs which were later sun dried to 10.08 % (db) moisture content as opined by Eriksson and Prior [5] and ASAE [6]. The moisture content was achieved after drying for five weeks during the dry season of 2020 in Nigeria.

2.2. Pretreatments methods

2.2.1. Carbonized corncob

After collection and drying of the corncobs, they were subjected to pretreatment through pyrolysis facilitated by a fabricated metal kiln of 1.5 m high and 1 m diameter made of 2 mm iron sheet, as presented in Figure 2. An opening was made at the top to allow for the chimney piece and the drum base was closed with a metal sheet and provided with the stand of 120 mm high. The collected corncobs were loosely packed into the kiln and by using a small amount of biomass to create an ignition in the kiln, the top of the kiln was closed tightly to allow fire to spread with a limited supply of air [7]. The disappearance of smoke coming out of the chimney top was evidence of completion of the carbonized process. The carbonized corncobs were allowed to cool and then, crushed using hammer mill and subsequently milled using bur mill to achieve finely particle size that passed through a mesh number of 18 for good binding in line with ASAE [8].

2.2.2. Uncarbonized corncob

For the uncarbonized process, the corncobs were prepared without allowing them to pass through any form of heat apart from pulverizing using hammer mill and then, they were

milled using a bur mill to achieve a finely particle size that passed through a mesh number of 18 [8].

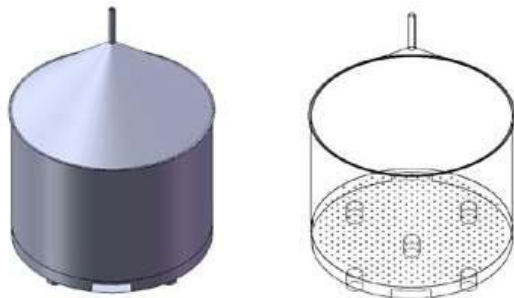


Figure 2. Assembled view of fabricated metal kiln for pyrolysis

2.3. Binder preparation and mixing

Three binders (cassava, corn, and gelatin) at three different proportions of 10, 20, and 30 % (wt/wt) were employed for the mixing. The distilled water of 150 ml was used to dissolve the binders with no form of clog or lump in the binder solution. Using a water bath at 100 °C, the solution was heated for 10 minutes and stirred continuously until it formed an entire binder paste. The wet granulation method, followed by pharmaceutical company, was employed in preparing the granular mass. By using this method, an appropriate number of the corncob fine particles (both in carbonized and uncarbonized forms) were weighed (separately) and carefully stirred together by hand with the binder solution to achieve a homogenous damp mass. After the mixing, the damp mass was allowed to pass through a sieve number 12 and subsequently, oven-dried at 60 °C for 30 minutes. The dried granular mass was sieved using a mesh number 16 to derive granules of uniform size used to produce the briquettes.

2.4. Briquettes production and characterization

A manual method of compaction was used for the production of the briquette. To this end, a mold (punch and die) of 50 mm cylindrical die height and 30 mm internal diameter by 5 mm thickness was fabricated using hardened steel and 0.1 mm allowance was observed for the escape of air. To achieve this

production, the granules were compacted using a hand-powered hydraulic press (Hyspin AWS 22/32 Model) to produce briquettes of uniform shape. For each production, 10 g of the granular mass was employed to fill the mold after that compressed at a different applied pressure of 50, 100, and 150 kPa. The dwelling time for each press during the compaction period was maintained within 120 seconds [9]. The physical properties the briquette determined were limited to moisture content, density, and compressive strength, which were carried out in line with ASTM standards [10]. With ASTM standards, oven dry method was used in determining the moisture content and density was computed as the ratio of mass to volume of the briquette. Instron Universal Testing Machine (Model: 3369) was used in determining the compressive strength. The Oxygen Bomb Calorimeter (Leco AC-350) was used in determining the heating value in accordance with ASTM standards [11]. This was achieved by firing 2 grams each of the briquettes in the Oxygen Bomb Calorimeter connected to a computer set through which the heat values of the briquettes were automatically displayed and recorded. Data collected were analyzed using Statistical Analysis System (SAS) software. The data were analyzed for analysis of variance (ANOVA) using Statistical Analysis System software with input variables including pretreatment methods, binder types, binder concentrations, and compacting pressure. Treatment means and significant differences were evaluated using the Duncan Multiple Range test ($P \leq 0.05$). Correlations were run among parameters to establish their relationships.

3. RESULTS AND DISCUSSION

Table 1 shows ANOVA results with observation that corncob processing method, binder type, binder concentration, compaction pressure, and some of their interactions significantly affected all the briquette's physical properties and heating values. Table 2 presents the treatment means and their significant differences in the moisture content, density, compressive strength, and heating values of the briquettes.

Table 1. The ANOVA results showing the effect of treatments on moisture content, density, compressive strength, and heating value of the briquettes produced

Source	Moisture content (db)	Compressed density (kgm ⁻³)	Relaxed density (kgm ⁻³)	Compressive strength (MPa)	Heating value (MJkg ⁻¹)
PM	<.0001*	<.0001*	<.0001*	<.0001*	<.0001*
PRES	<.0001*	<.0001*	<.0001*	<.0001*	<.0001*
PM*PRES	0.7795	<.0001*	<.0001*	<.0001*	0.1356
CONC	<.0001*	<.0001*	0.0064*	<.0001*	<.0001*
PM*CONC	0.0019*	<.0001*	0.0549	<.0001*	<.0001*
PRES*CONC	0.4602	0.0871	0.9902	<.0001*	<.0001*
PM*PRES*CONC	0.8879	0.1254	0.9957	<.0001*	0.0061*
TYPE	<.0001*	<.0001*	0.0105*	<.0001*	<.0001*
PM*TYPE	<.0001*	<.0001*	<.0001*	<.0001*	<.0001*
PRES*TYPE	0.0021*	<.0001*	0.8810	<.0001*	0.0923
PM*PRES*TYPE	0.2968	0.0004*	0.9609	<.0001*	0.2732
CONC*TYPE	0.0086*	0.1269	0.9998	<.0001*	0.0156*
PM*CONC*TYPE	0.0987	0.2335	0.9968	<.0001*	0.0010*
PRES*CONC*TYPE	0.5710	0.9479	1.0000	<.0001*	0.2940
PM*PRES*CONC*TYPE	0.0171*	0.9934	1.0000	<.0001*	0.1587

PM: Pretreatment Method, TYPE: Binder Type, CONC: Binder Concentration, PRES: Compaction Pressure
 * Factors that are significant at $P < 0.05$

Table 2. The effects of treatments on moisture content, density, compressive strength, and heating value of the briquettes produced

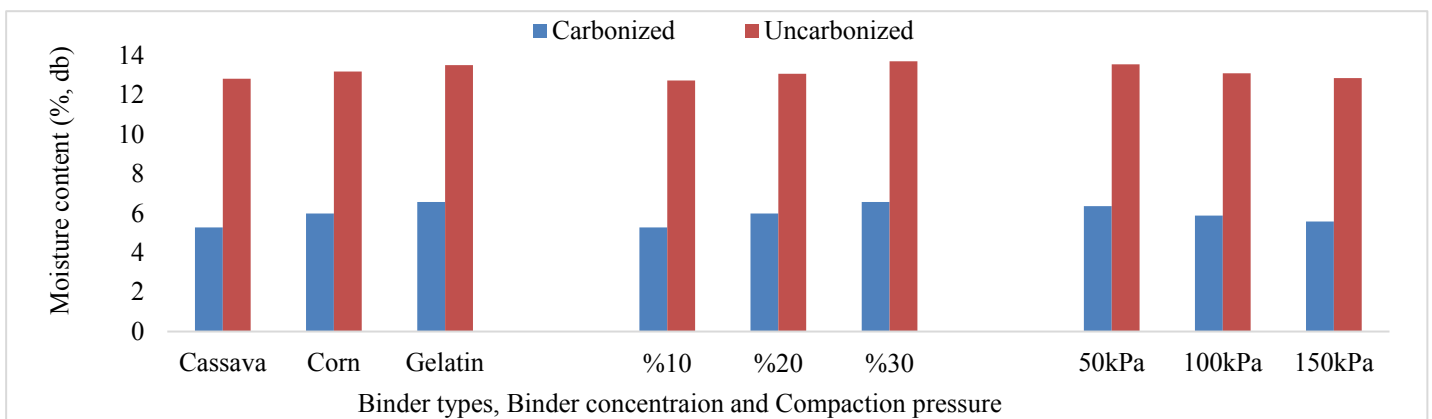
Variable	Moisture content % (db)		Compressed density (kgm ⁻³)		Relaxed density (kgm ⁻³)		Compressive strength (MPa)		Mean heating value (MJkg ⁻¹)	
Pretreatment method										
C	5.95 ^b		1191.85 ^b		863.73 ^b		3.63 ^b		31.13 ^a	
UC	13.19 ^a		1543.29 ^a		1066.71 ^a		7.91 ^a		28.24 ^b	
Binder type	C	UC	C	UC	C	UC	C	UC	C	UC
Cassava	5.29 ^c	12.84 ^c	1307.08 ^a	1421.09 ^c	925.28 ^a	1009.04 ^b	4.65 ^a	6.43 ^c	32.07 ^a	28.49 ^a
Corn	5.99 ^b	13.20 ^b	1170.02 ^b	1659.43 ^a	852.55 ^b	1119.95 ^a	3.37 ^b	9.43 ^a	30.87 ^b	28.26 ^b
Gelatin	6.58 ^a	13.53 ^a	1098.47 ^c	1549.35 ^b	813.37 ^c	1071.14 ^a	2.87 ^c	7.86 ^b	30.45 ^c	27.99 ^c
Binder concentration	C	UC	C	UC	C	UC	C	UC	C	UC
10	6.58 ^a	13.72 ^a	1269.03 ^a	1324.64 ^c	903.17 ^a	1071.19 ^a	4.68 ^a	5.97 ^c	30.68 ^c	28.11 ^c
20	5.99 ^b	13.09 ^b	1195.59 ^b	1560.45 ^b	866.15 ^b	1069.19 ^a	3.79 ^b	7.65 ^b	31.19 ^b	28.25 ^b
30	5.29 ^c	12.75 ^c	1110.95 ^c	1744.79 ^a	821.88 ^c	1059.76 ^a	2.42 ^c	10.12 ^a	31.52 ^a	28.37 ^a
Compacting pressure	C	UC	C	UC	C	UC	C	UC	C	UC
50	5.59 ^c	12.87 ^c	1259.14 ^a	1747.63 ^a	898.49 ^a	1166.33 ^a	5.07 ^a	10.10 ^a	30.77 ^c	28.01 ^c
100	5.89 ^b	13.11 ^b	1197.02 ^b	1547.16 ^b	866.41 ^b	1070.80 ^b	3.55 ^b	7.73 ^b	31.20 ^b	28.27 ^b
150	6.37 ^a	13.57 ^a	1119.41 ^c	1335.08 ^c	826.30 ^c	963.01 ^c	2.27 ^c	5.90 ^c	31.41 ^a	28.45 ^a

* C: carbonized corncob; * UC: uncarbonized corncob
Means with the same letters are not significantly different at a level of 5 %

3.1. Moisture content of the briquettes as affected by processing parameters

The Moisture Content (MC) of the briquettes as affected by processing parameters is shown in Figure 3. It was observed that the average MC varied from 5.29-6.58 % and 12.75-13.72 % for carbonized and uncarbonized briquettes, respectively. The lowest MC was observed for the briquettes produced from carbonized corncob, while higher MC was observed for the briquettes produced from uncarbonized corncob, which is an indication that carbonized process method had the highest effect on the MC of the briquettes produced at a 5 % significant level (Table 2). This implies that the carbonized briquette will ignite faster and produce more heat, according to the conclusion of Akowuah et al. [12]. Cassava binder was observed to perform well at a 10 % concentration for the carbonized and uncarbonized briquettes

produced when 150 kPa pressure was applied. Although there was an increase in MC as binder concentration increased, MC decreased with increased compacting pressure for all briquettes. This may be due to the fact that the feedstock is hygroscopic in form as increasing the concentration also increases the water available, as described by Aransiola et al. [13]. The result of carbonized briquettes agreed with Pallavi et al. [7], which suggested MC of 5-10 % for good quality briquettes. In general, the ignition of briquette is easy when MC is low and burnt without any slag; hence, a greater amount of heating is achieved. Higher MC in briquette causes a substantial amount of heat to be used in vaporizing the excess water which results in occasional tears of briquette into pieces followed by very low heating value, burning rate with quite minor emission of smoke.

**Figure 3.** Moisture content of the briquettes as affected by processing parameters

3.2. Compressed density of the briquettes as affected by processing parameters

The compressed density of the briquettes as affected by processing parameters is shown in Figure 4. The mean values

of compressed density ranged between 1098-1307 kgm^{-3} and 1324-1747 kgm^{-3} for carbonized and uncarbonized corncobs, respectively. The lowest compressed density was observed for briquettes produced from carbonized corncob, while the highest compressed density was observed for briquettes produced from uncarbonized corncob, which is an indication that uncarbonized pretreatment method had highest effect on the briquettes produced (Table 2). However, the carbonized briquette will store more and in a relatively smaller space and good in transportation more than the uncarbonized briquettes. Cassava starch at 30 % binder concentration acts well for carbonized briquettes and corn starch at 10 % binder concentration performs well for uncarbonized briquettes, both under 150 kPa applied pressure. It was discovered that there

was an increase in compressed density as binder concentration increased for briquette produced from carbonized corncob, but compressed density increased with a decrease in the binder concentration for the briquettes produced from uncarbonized corncob.

This might be expected since it is possible that increasing the quantity of binder concentration cause higher resistance in the uncarbonized briquettes during densification causing more pores per unit volume, hence decrease in compressed density. Also, it is noted that at high levels of pressure, compressed densities are high, while they are low at lower pressure; this might be as a result of a significant amount of air being expelled during compaction.

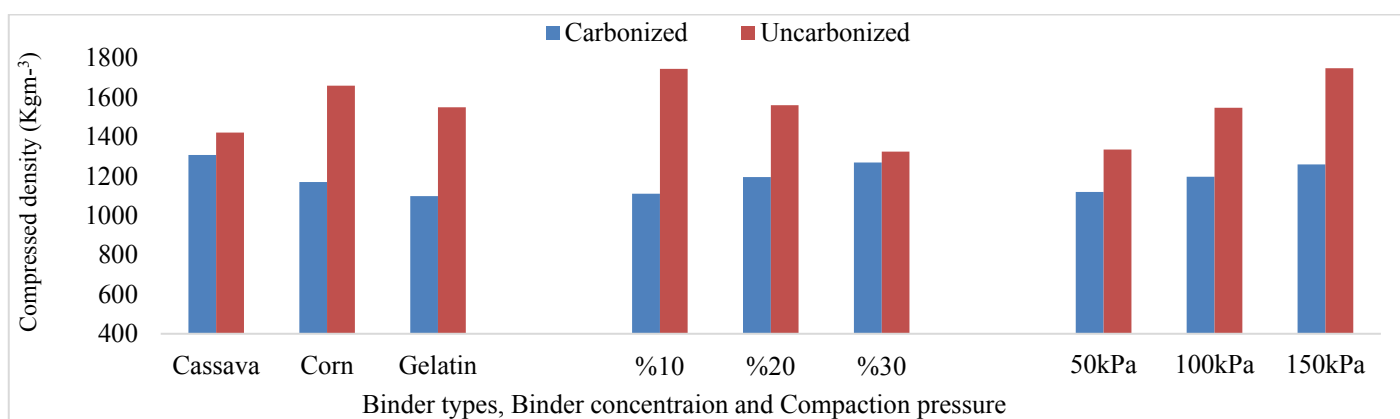


Figure 4. Compressed density of the briquettes as affected by processing parameters

3.3. Relaxed density of the briquettes as affected by processing parameters

The effect of processing parameters on the relaxed density of briquettes is shown in Figure 5. The average relaxed density ranged between 813-925 kgm^{-3} and 963-1166 kgm^{-3} for the carbonized and uncarbonized briquettes, respectively. The values obtained were more than the uncompressed feedstock's initial density, which are 363.64 and 331.33 kgm^{-3} , for carbonized and uncarbonized corncobs, respectively. Therefore, both carbonized and uncarbonized corncobs were able to improve the expected briquettes density as it is required in briquette making from agricultural wastes and the result corresponds to the findings of Eriksson and Prior [5]. Also, the obtained values were higher than the minimum value of 600 kgm^{-3} suggested by Mani et al. [14] and Gilbert et al. [15] for efficient transportation and safe storage. These values are lower than the compressed density of 1098-1307 kgm^{-3} and 1324-1747 kgm^{-3} for carbonized and uncarbonized briquettes, respectively, in this study. The lowest relaxed density was observed for the briquettes produced from carbonized corncob, while the highest compressed density was observed for the briquettes produced from uncarbonized corncob. This indicates that the uncarbonized pretreatment method had the highest effect on the briquettes produced, and both pretreatment methods were significantly different from each other at a significance level of 5 % (Table 2). However, the carbonized briquettes store more in a relatively smaller space and perform well in transportation than the uncarbonized briquettes. Cassava starch at 30 % binder concentration performed well for briquettes produced from carbonized corncob, while corn starch at 10 % binder concentration performed well for briquettes produced from carbonized corncob under compaction pressure of 150 kPa.

Common development of increased relaxed density of carbonized and uncarbonized briquettes was noticed when the applied pressure increased. This is possible due to the strong bond between the feedstock and the binder as a result of increase in pressure and reduction in elastic recovery during relaxation of the briquettes. Also, relaxed density increased as the binder concentration increased for the briquette produced from carbonized corncob, which conforms with works of Sotannde et al. [16] and David et al. [17]; separate studies discovered that density of briquettes was affected by binder concentration. Conversely, relaxed density increased with decreasing binder concentration for the briquettes produced from uncarbonized corncob; this might be expected since a higher binder concentration level can provide higher resistance during compression [17], resulting in the presence of more pore spaces per unit volume of the briquette, thus lower density.

3.4. Compressive strength of the briquettes as affected by processing parameters

The compressive strength of the briquettes as affected by processing parameters is shown in Figure 6. For carbonized and uncarbonized briquettes, the average compressive strength varied from 2.27-5.07 MPa and 5.97-10.12 MPa, respectively.

The lowest compressive strength was observed for briquettes produced from carbonized corncobs, while the highest compressed density was observed for the briquettes produced from uncarbonized corncobs. This depicts that uncarbonized pretreatment method had the highest effect on the compressive strength and both pretreatment methods were significantly different from each other at 5 % level (Table 2). However, the result indicates that briquettes from uncarbonized corncobs suffer less damage during

transportation and storage than briquettes from carbonized corncobs. The compressive strength increased with increasing binder concentration for carbonized briquettes and decreased with increasing binder concentration for the uncarbonized briquettes. Also, compressive strength was the highest with cassava as a binder compared to briquettes made with the other two binders for carbonized briquettes and was the highest with corn as a binder in comparison to briquettes made with the other two binders for uncarbonized briquettes. The compressive strength of the briquettes increased as die

pressure increased for the briquettes produced from both pretreatment methods. The three compacting pressures gave different compressive strength levels; the highest compressive strength was observed for 30 % cassava binder at 150 kPa for carbonized briquettes and 30 % corn binder at 150 kPa for uncarbonized briquettes. This was due to very good sticky binding characteristics of cassava starch and its homogenous mixing with carbonized corncobs and corn starch and its homogenous mixing with uncarbonized corncobs with increase in briquetting pressure.

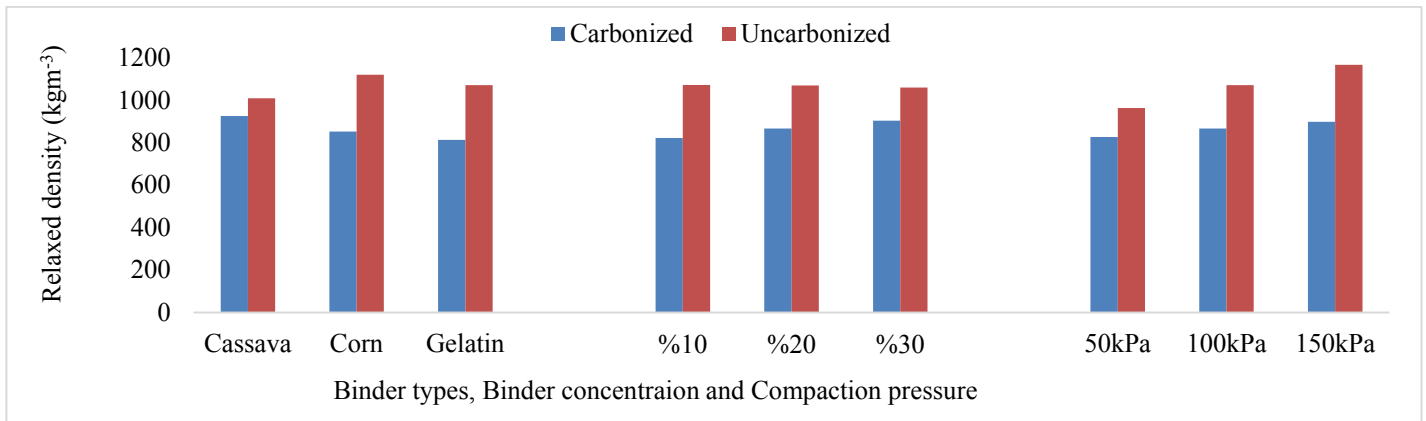


Figure 5. Relaxed density of the briquettes as affected by processing parameters

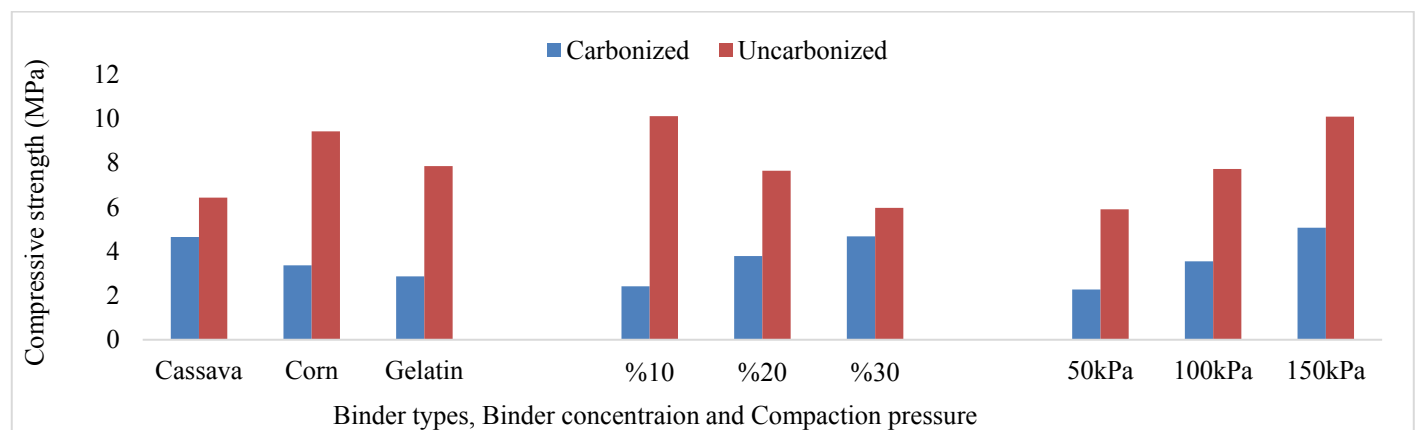


Figure 6. Compressive strength of the briquettes as affected by processing parameters

3.5. Heating value of the briquettes as affected by processing parameters

The effect of processing parameters on the heating value of briquettes is shown in Figure 7. The average heating values achieved in this work ranged between 28.85-32.36 MJkg⁻¹ and 27.58-28.80 MJkg⁻¹ for carbonized and uncarbonized briquettes, respectively. It was observed that the heating values of the uncarbonized briquettes in this study had high values compared to the ones reported in existing literatures which could be an indication of wet granulation method used. The highest heating value was observed for briquettes produced from carbonized corncob, while the lowest was observed for briquettes produced from uncarbonized corncob. This indicates that the carbonized pretreatment method had the highest effect on the heating value of the briquettes produced and both materials were significantly different from each other at a 5 % significance level (Table 2). The highest

heating value of 32.36 MJkg⁻¹ was observed for briquette made from carbonized corncob for 30 % cassava binder at a die pressure of 150 kPa, while briquettes from uncarbonized corncob exhibited the lowest heating value of 28.80 MJkg⁻¹ for the same binder at the same level of binder and pressure. The results of heating values from this study were compared well with the average heating value of 32.43 MJkg⁻¹ from the corncob briquette obtained by Zubairu and Sadiq [18] and with 28.5 MJkg⁻¹ from sawdust briquette by Wakchaure and Mani [19]. All the briquette samples produced in this work were found to have higher heating values, but the heating value of the briquette produced from the carbonized process of corncob competed well with the heating value of fuel wood and charcoal at 31.8 MJkg⁻¹ according to FAO [20]. These energy values can produce enough heat for household cooking and small-scale industrial cottage applications.

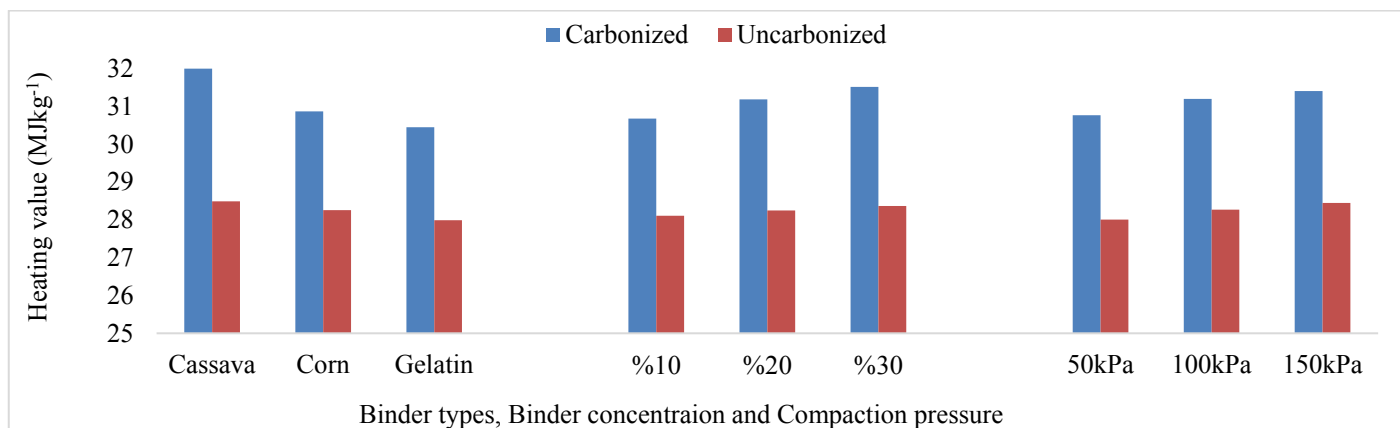


Figure 7. The heating value of the briquettes as affected by processing parameters

4. CONCLUSIONS

This comparative study investigated some physical properties and heating values of briquettes produced from carbonized and uncarbonized processing methods of corncobs using three different types of the binder at three different concentrations and compacting pressures. The results showed that average moisture content ranged between 5.29-6.58 % and 12.75-13.72 %, mean relaxed density varied from 813-925 kgm⁻³ and 963-1166 kgm⁻³, compressive strength ranged between 2.27-5.07 MPa and 5.97-10.12 MPa, and heating value ranged between 28.85-32.36 MJkg⁻¹ and 27.58-28.80 MJkg⁻¹ for carbonized and uncarbonized briquettes, respectively. Based on the results obtained, all the processing parameters studied had significant effects ($P < 0.05$) on the briquette's moisture content, density, compressive strength, and heating value. The briquettes produced from carbonized corncob had a better moisture content (5.29-6.58 %) and heating value (28.85-32.36 MJkg⁻¹), while the briquettes produced from uncarbonized corncob had higher density (1324-1747 kgm⁻³) and compressive strength (5.97-10.12 MPa). Therefore, this study shows that pretreatment methods under different binder types and concentrations and the compacting pressure significantly affected the physical properties and heating values of briquettes. Furthermore, carbonized and uncarbonized corncobs were suitable materials for briquettes production suited for domestic and industrial applications. However, this technology can be successfully applied in rural off-grid areas by the government and other stakeholders in the energy sector as part of renewable energy technologies.

5. ACKNOWLEDGEMENT

This work was carried out in collaboration among all authors.

REFERENCES

1. Wilaipon, P., "Physical characteristics of maize cob briquettes under moderate die pressure", *American Journal of Applied Science*, Vol. 4, No. 12, (2007), 995-998. (<https://thescpub.com/pdf/ajassp.2007.995.998.pdf>).
2. Oyewusi, T.F., Aransiola, E.F., Oyimlola, T.A. and Adesigbin, J.A., "Comparative study of the calorific values and gas emissions of briquettes produced from carbonized and uncarbonized process of corncob", *Journal of the Nigerian Institution of Mechanical Engineers*, Vol. 8, No. 2, (2018), 20-36. (https://www.researchgate.net/publication/341180083_comparative_study_of_the_calorific_values_and_gas_emissions_of_briquettes_produced_from_carbonized_and_uncarbonized_process_of_corncob).
3. Aransiola, E.F., Oyewusi, T.F., Osunbitan, J.A. and Ogunjimi, L.A.O., "Effect of binders and pressures on physical properties of briquettes from carbonized corncob", *Energy Reports*, Vol. 5, (2019), 909-918. (<https://doi.org/10.1016/j.egyr.2019.07.011>).
4. Grainger, L. and Gibson, J., *Coal utilization technology: Economics and policy*, Graham and Trotman Limited, (1981), 179-181. (<https://link.springer.com/book/10.1007/978-94-011-7352-0>).
5. Eriksson, S. and Prior, M., *The briquetting of agricultural wastes for fuel*, FAO Energy and Environment Paper 11, (1990), 121-124. (<http://www.fao.org/docrep/t0275e/t0275e00.htm>).
6. ASAE S269.4, *Cubes, pellets and crumbles – Definitions and methods for determining density, durability and moisture content*, American Society of Agricultural Engineers, (2003), 567-569. (<https://standards.globalspec.com/std/17556/s269-4>).
7. Pallavi, H.V., Srikantaswamy, S., Kiran, B.M., Vyshnavi, D.R. and Ashwin, C.A., "Briquetting agricultural waste as an energy source", *Journal of Environmental Science, Computer Science and Engineering and Technology*, Vol. 2, No. 1, (2013), 160-172. (<https://www.semanticscholar.org/paper/Briquetting-agricultural-waste-as-an-energy-source-Pallavi-Srikantaswamy/b95a39d5be398bc8c4ffe3a7f23c21d16a7844e3?sort=relavance&pdf=true>).
8. ASAE S424.1, *Method of determining and expressing particles size of chopped forage materials by screening*, American Society of Agricultural Engineers, (2003), 567-569. (<https://elibrary.asabe.org/abstract.asp?aid=23583&t=3&dabs=Y&redir=&redirType=>).
9. Oladeji, J.T. and Enweremadu, C.C., "The effects of some processing parameters on physical and combustion characteristics of corncob briquettes", *International Journal of Energy Engineering*, Vol. 2, No. 1, (2012), 22-27. (<https://doi.org/10.5923/j.ijee.20120201.04>).
10. ASTM D1037-93., *Standard test methods of evaluating the properties of wood-based fibre and particle panel material*, American Society of Testing and Materials, (2012), 23-29. (<https://standards.globalspec.com/std/3846840/astm%20D1037-12>).
11. ASTM E711-87, *Test method for gross calorific value of refine derived fuel by the bomb calorimeter*, American Society of Testing and Materials, (1992), 265-271. (<https://ia600603.us.archive.org/6/items/gov.law.astm.e711.1987/astm.e711.1987.pdf>).
12. Akowuah, J., Kemausor, F. and Mitchual, J.S., "Physio-chemical characteristics and market potential of sawdust charcoal briquettes", *International Journal of Energy and Environmental Engineering*, Vol. 3, No. 20, (2012), 1-6. (<https://link.springer.com/article/10.1186/2251-6832-3-20>).
13. Oyewusi, T.F., Aransiola, E.F., Olaley, T.E., Osunbitan, J.A. and Ogunjimi, L.A.O., "A comparative study on the physical properties of briquettes from carbonized and uncarbonized corncobs", *Proceedings of the 7th Obafemi Awolowo University, Faculty of Technology Conference*, Ile-Ife, Nigeria, (2019), 127-135. (https://www.researchgate.net/publication/342523225_a_comparative_study_on_the_physical_properties_of_briquettes_produced_from_carbonized_and_uncarbonized_corncob_material).
14. Mani, S., Tabil, L.G. and Sokhansanj, S., "Specific energy requirement for compacting corn stover", *Bioresource Technology*, Vol. 97, No. 12, (2006), 1420-1426. (<https://doi.org/10.1016/j.biortech.2005.06.019>).

15. Gilbert, P., Ryu, C., Sharif, V. and Switchenbank, J., "Effect of processing parameters on pelletization of herbaceous crops", *Fuel*, Vol. 88, (2009), 1491-1497. (<https://doi.org/10.1016/j.fuel.2009.03.015>).
16. Sotannde, O., Oluyeye, G., and Abah, B., "Physical and combustion properties of briquettes from sawdust of azadirachta indica", *Journal of Forestry Research*, Vol. 21, (2010), 63-67. (<https://doi.org/10.1007/s11676-010-0010-6>).
17. David, K.C., Daudi, M.N. and Jason, M.G., "Effect of binder types and amount on physical and combustion characteristics", *International Journal of Engineering Research Science, and Technology*, Vol. 2, No. 1, (2013), 12-20. (<https://www.semanticscholar.org/paper/EFFECT-OF-BINDER-TYPES-AND-AMOUNT-ON-PHYSICAL-AND-Chirchir-Nyaanga/df9578ad09bfb93bdc5ed91f2bce9634b3cc14d4>).
18. Zubairu, A. and Sadiq, A., "Production and characterization of briquette charcoal by carbonization of agro-waste", *Energy and Power*; Vol. 4, No. 2, (2014), 41-47. (<https://doi.org/10.5923/j.ep.20140402.03>).
19. Wakchaure, G.C. and Mani, I., "Thermal and storage characteristics of biomass briquettes with organic binders", *Journal of Agricultural Engineering*, Vol. 48, No. 4, (2011), 24-30. (https://www.researchgate.net/publication/235946165_Thermal_and_Storage_Characteristics_of_Biomass_Briquettes_with_Organic_Binders).
20. Food and Agricultural Organization, FAO, "Industrial Charcoal Production, TCP/CRO/3101 (A) Development of a sustainable charcoal industry, Zagreb, Croatia", (2021). (<https://pdfcoffee.com/faoindustrial-charcoal-production-pdf-free.html>), (Accessed: 19 December 2021).



Technical Note

Potential for Battery Energy Storage System in Zimbabwe

Allen G. Njovana, Wenying Yu*, Qiying Shen, Jiarui Li, Yanyan Zhu, Yongsheng Liu*

Institute of Solar Energy, Shanghai University of Electric Power, P. O. Box: 200090, Shanghai, China.

PAPER INFO

Paper history:

Received: 24 August 2021

Revised in revised form: 28 December 2021

Scientific Accepted: 08 January 2022

Published: 20 August 2022

Keywords:

Battery Energy Storage System,

Solar Photovoltaic,

BESS Investments,

Levelized Cost of Energy Storage,

Lithium-Iron Phosphate,

Zimbabwe

ABSTRACT

This study aims to assess the potential of coupling solar PV power plants with Battery Energy Storage System (BESS) to curtail load-shedding and provide a stable and reliable baseload power generation in Zimbabwe. Data from geographical surveys, power plant proposals, and investment information from related sources were reviewed and applied accordingly. Areas considered to be of good potential to employ the use of BESS were identified considering such factors as feasibility of PV plants, proximity to transmission lines, the size of a town or neighborhood, and energy demands for BESS Return On Investment (ROI) calculations. Previous studies have proven that 10 % of the suitable land for PV systems has the capability to generate thirty times the current power demand of the nation operating even with the least efficiency. In recent years, coupling renewable energy sources with a suitable energy storage system yielded improved performances, giving consumers a reliable, stable, and predictable grid. BESS technologies on the utility scale have improved in recent years, giving more options with improved safety, and decreasing the purchase costs, too.

<https://doi.org/10.30501/jree.2022.294957.1230>

1. INTRODUCTION

Zimbabwe is currently experiencing power outages that have a drastic impact on the nation's development, economy, education, and health systems. There have been no significant investments in power generation besides the growth of the country's population and migration to urban centres (urbanization) that have increased the power demands. Electricity accessibility and rural electrification are below standard due to the high demand of electricity in urban centers which are prioritized first though load shedding continues. Initially, hydropower and coal-fired power plants generating respectively at a ratio of 38 % to 62 % were able to sufficiently meet the energy demands in the country before the major factors came into consideration [1]. Currently, Zimbabwe's power supply companies cannot generate enough energy to meet the national demands or pay for adequate power imports from South Africa or Mozambique due to the growing number of energy consumers. The national electricity demand as of May 2021 was estimated between 1800 MW and 2200 MW depending on season, yet the generated power from the Kariba hydropower and all the thermal power plants in the country only amounts to 1200 MW [2]. After a hiatus, the Zimbabwean government introduced new renewable energy policies with the aim of eradicating power outages in the country, and the Infrastructure Development Bank of

Zimbabwe issued proposals to seek partners develop small-scale PV plants as alternatives to improve the country's grid and reduce the load-shedding crisis.

Due to the decent amount of unhindered solar radiation of approximately 6.5 kWh/m² DNI daily available in Zimbabwe, there are high possibilities of solar PV panels producing more electrical energy than required during the day [3]. Like any other country, high energy consumption periods (peak-loads) are experienced during morning and evening hours when there is little to no sunlight. The proposed small-scale PV plants are capable of improving the grid but will not be able to meet the energy demands of the country; therefore, the introduction of Energy Storage Systems (ESSs) should be considered. Energy storage is essential in PV systems to overcome the intermittency of the energy generated by the system which could be caused due to daily, monthly, or seasonal solar irradiance fluctuations. Other countries can offer several ESS alternatives for PV plants like Pumped Storage Hydropower (PSH) or grid-storage, but for a country like Zimbabwe, grid storage is impractical since the grid is already failing to meet the demands. Also, PSH entails construction of large water reservoirs and alteration of topographies, which result in high capital expenditures (CAPEX) as well as a long duration of time until the constructions are finished. Other ESSs are not technically and economically favorable considering Zimbabwe's current economic situation. Considering these factors and the advances in Battery Energy Storage System (BESS) technology in the past years, BESS utility has the capability to increase the stability and resiliency of the grid,

*Corresponding Authors' Email: ywyshdl@shiep.edu.cn (W.Y. Yu) and ysliu@shiep.edu.cn (Y.S. Liu)

URL: https://www.jree.ir/article_155040.html



thus meeting consumers' energy demands and possibly offering a Lower Levelized Cost of Electricity (LCOE).

This study addresses the following BESS application objectives:

- How much electricity does Zimbabwe need?
- Identification of the functions of a BESS;
- Discussion and selection of the ideal BESS technology for Zimbabwe's situation;
- Selection of a suitable location and method of coupling BESS with the PV system;
- Assessment of the economic and technical barriers hindering the employment of BESS technology;
- BESS sizing and economic analysis including Capital Expenditure (CAPEX) and Operation Expenditure (OPEX);
- Advising policy-makers and potential investors on the potential for BESS in Zimbabwe.

2. ZIMBABWE ENERGY CONSUMPTION AND GENERATION

According to International Energy Agency (IEA) 2019 data, 18 % of the total power used in Zimbabwe was imported from neighboring countries. Total annual imports depend on certain aspects like climate and turbine breakdowns since Zimbabwe's electricity generation derives mainly from hydropower and coal-fired thermal power plants. In 2017, Southern Africa received less rainfall compared to the previous years and experienced high temperatures under which all the factors had a significant impact on hydropower generation. Kariba Dam water levels decreased because of low rainfall and high evaporation rate caused by intense heat. In the year 2000, Zimbabwe had the highest import rate of over 5000 GWh and the rate declined due to the extension of the Kariba South Dam hydropower and high implementation of individual off-grid system. The country has never been able to export electricity as the grid cannot meet the nation's energy demands.

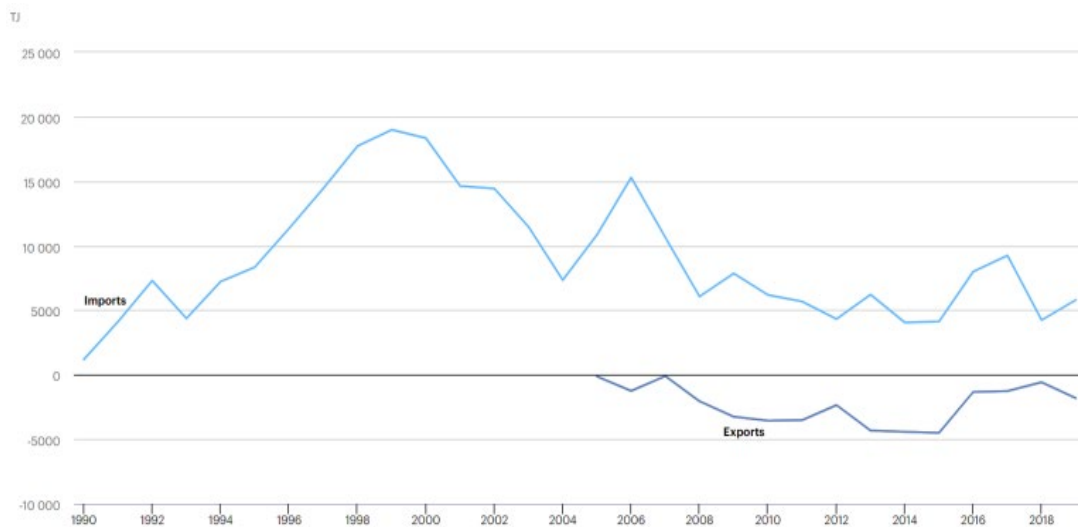


Figure 1. Electricity imports vs. exports, Zimbabwe 1990-2019 [IEA]

The country's population is estimated at 14.8 million and national electricity access stands at 41 %, leaving most of the population without access to electricity. Electricity consumption per capita in 2020 was estimated at 1,320 kWh, (830 kWh less than the required) and the total annual generation at 8,200 GWh (1.3 GWh less). Most of Zimbabwe's electricity is generated through coal thermal power and hydropower plants at a ratio of 58 % to 38 %,

respectively. Biofuels and oil currently have a total capacity of less than 5 % combined, although the biofuels sector is experiencing great investments. Zimbabwe receives 3000 hours of sun per year and the most radiated region receives up to 6.5 kWh/m²; this proves the great potential of solar energy generation through both solar photovoltaic (PV) and solar thermal compared to other renewable sources given they are easily affected by climate change.



Figure 2. Electricity generation by source, Zimbabwe 1990-2019 [IEA]

3. BESS FUNCTIONS

Energy storage systems have the ability of storing energy using thermal, mechanical, chemical, and electrochemical solutions. BESS typically utilizes an electrochemical solution to store electrical energy in a chemical form, which enjoys significant benefits since both electrical and chemical energies share the same common carrier and electron. This makes batteries a commonly used system to store excess electricity from different sources. BESS is able to mitigate the sharp fluctuations of variable renewable energy resources for on-grid systems, provides ancillary services for the system, complements, and extends the operating hours of the system in a reliable and cost-effective manner. Before implementing BESS, there is a need for identifying locations where it is necessary to use storage (based on energy demand statistics) for grid balancing and peak shaving instead of conventional network reinforcement. The following represent a few critical functions that an energy storage system is expected to perform:

Integration into the grid: Just like other renewable sources, solar energy is variable which makes it hard for electricity providers to plug it directly into the electricity grid without a storage medium, thus guaranteeing a constant and smooth supply of electricity to consumers. In most cases, grids balance the supply and demand of electricity and thus benefit the most from dispatchable sources of energy (so far, fossil fuels that could be burned on demand or diesel gensets provide that sort of convenience) [4]. Energy storage makes solar energy and other renewable energy sources more dispatchable (available on-demand grid operators) at any time of the day and hence, more cost-competitive with traditional fuel options. In Zimbabwe, the ageing thermal power plants have resulted in recurring power plant breakdowns leaving consumers in unexpected blackouts. Unsteady diesel imports also affect genset operators. All these prove the best potential for BESS in Zimbabwe.

Peak demand: Responding to peak demands requires the ability to generate power quickly, considering batteries they have an extremely fast response time compared to other ESSs. The energy stored in the batteries is immediately available and can be discharged and used to meet peak demand depending on the battery capacity and storage duration. This helps use the stored renewable power for peak generation to meet consumer demands and avoid grid disruptions or blackouts.

Load/Time shifting: PV modules generate power only during the daytime with the peak at noon hours, which is when electricity demand is also the lowest, while the peak energy demand is often located during evening hours, when the solar irradiation is low or not available. Solar power needs to be “time-shifted” to be available during high demand, and this can be achieved by means of utility-scale energy storage [5]. Thus, BESS allows shifting energy usage by charging batteries with solar energy and discharging them during peak load when electricity is also more expensive.

Figure 3 shows less power demand during the day hours when there is enough sunshine for the PV arrays to generate power; therefore, excess power generated will charge the BESS. During the peak demand, PV arrays will not be generating power; therefore, the BESS discharges and meets the energy demands.

Energy autonomy and emergency backup: For communities living in areas without access to electricity grid, combined

renewable energy plus storage systems may be the best option to provide for constant supply of electricity and keep operations running during power outages. This autonomous approach can be realized on both distributed (house/community) and utility (area/region) scales. In such situations, a BESS would be required to have a high energy capacity (amount of stored energy) and a long duration energy storage capacity with a decent rate of charge or discharge (power capacity) to provide a stable and constant power supply.

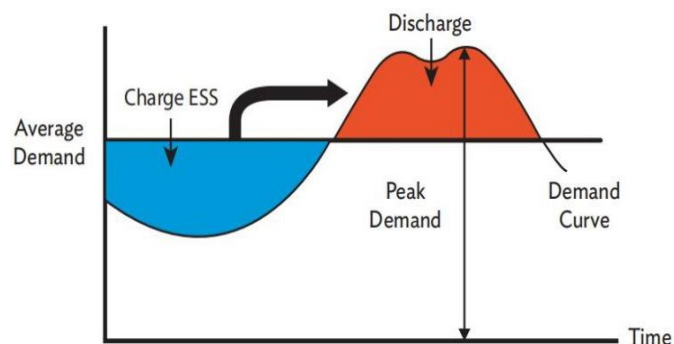


Figure 3. BESS use for load/time shifting [5]

Peak shaving: In a commercial/community setting, the most important application of energy storage is peak shaving. A higher percentage of the utility bills are made up of demand charges that are mostly experienced during early or later hours of the day when there is no availability of sunlight for solar energy generation. Solar arrays alone are not always a sufficient solution to meet these demands as they are affected by time of the day, weather, and season. BESS can guarantee no power disruptions from the grid during peak times. Thus, peak shaving helps the utility meet demand without having to ramp up expensive peaking gensets. In this case, network operators should be required to identify locations where it is necessary to use storage for peak shaving based on energy consumption data instead of conventional network reinforcement.

In general, peak load problems could be reduced, electrical stability improved, and power quality disturbances eliminated. Energy storage offers a flexible and multifunctional role in the grid of electric power supply by ensuring more efficient management of available power for consumers. As supply from PV components varies due to its intermittency, energy must be provided to rapidly restore the frequency to the desired limits [6]. This application is ideal for high-power batteries because they can respond quickly and the energy requirement is low. Energy storage can be applied at the power plant where the RES is in support of the transmission network at various points in the distribution areas.

4. BESS TECHNOLOGY

Electrochemical batteries come in many different forms of technologies: some are more applicable to utility-scale energy storage, while others are only applicable to certain devices or equipment. Applicability to large systems depends on such factors as life span, charge, and discharge (round trip) efficiency, ability to scale up with no ill effects or performance loss, design and operation mode, power densities, and Depth of Discharge (DOD). Utility-scale BESS requires energy storage ranging from a few megawatt-hours (MWh) to hundreds of MWh and the technology must be able

to discharge quickly to match the fluctuations of the variable solar resource during the day or respond quickly to an unexpected power cut at any time of the day providing an Uninterruptible Power Supply (UPS) [7]. Considering the factors and the requirements of a BESS, the two technologies that have a greater potential in Zimbabwe are lithium-ion batteries and flow batteries based on their performance, energy density, safety, and applicability. However, flow batteries are subject to significant technical and economic setbacks in comparison to standard solid-state batteries which make it difficult to implement them in Zimbabwe. In recent years, lithium-ion (Li-ion) batteries are commonly used, and they dominate most of the market growth and their costs are decreasing as technology advances and manufacturing efficiency increases which makes them affordable and an ideal technology for Zimbabwe's investment [8].

Li-ion batteries have a growing share in storage capacity additions and are largely driven by the declining cost of Li-ion technology in recent years, which, in turn, is expedited by the ramp-up in production to meet the growing demand of batteries for electric vehicles [9]. The introduction of the cell-

to-pack technology in 2019 led to a further decline in costs of Li-ion batteries although it is currently significant in the EV industry. Compared to other batteries, lithium batteries offer more advantages which are more favorable for a large-scale BESS. Lithium batteries are available in different types with different properties; however, for this assessment, lithium-iron phosphate (LiFePO_4)/(LFP) batteries are selected amongst lithium batteries. LFP batteries can withstand more charge-discharge cycles of nearly over 5000 cycles at 80 % Depth of Discharge (DOD) compared to batteries like lead-acid batteries [10]. Although LFP batteries have a relatively lower energy density (watt-hours per kilogram "Wh/kg") than other Li-ion batteries, they still offer a high round trip efficiency of up to 95 % and a longer life span of 10-15 years depending on the area of application [11]. LFP batteries are much safer than other Li-ion batteries due to their thermal and chemical stability, making them incombustible in the event of mishandling, short circuiting, high temperatures, or overcharging, which is probable due to high solar irradiance in Zimbabwe although LFP batteries are equipped with a Battery Management System (BMS).



Figure 4. Modularity of LFP batteries [12]

Figure 4 shows the modularity of lithium-batteries including the LFP batteries. The cells are enclosed in modules and mounted on a rack. Each rack has its own BMS which ensures

that each cell remains within the safe limits, and it is enclosed together in a container to form a powerpack [12].

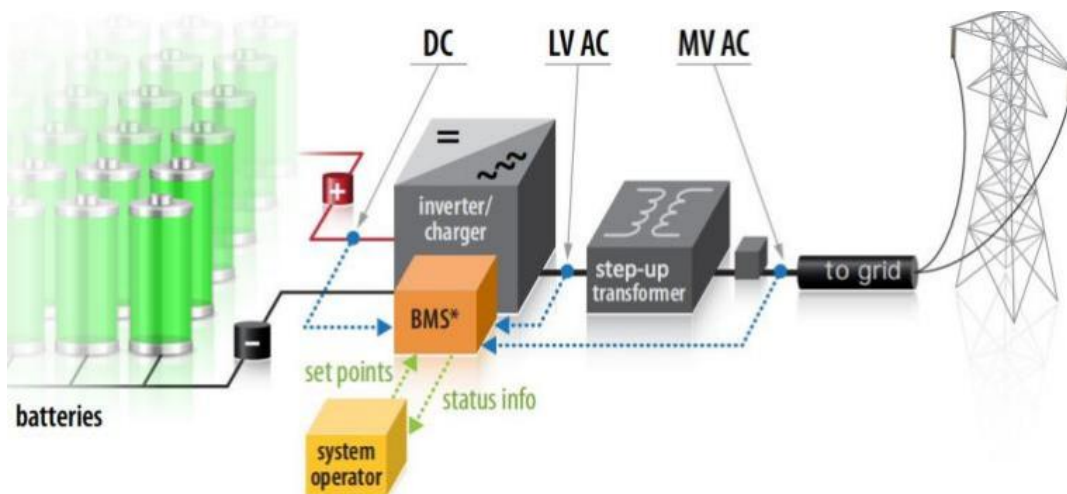


Figure 5. BESS directly connected to the grid [19]

A BESS is composed of different levels, namely Energy Management System (EMS), battery system, and Power Conversion System (PCS), which need to be considered for both operation and investment [13]. The battery system is composed of containers with several battery packs inter-connected in series and parallel to reach the desired value of current and voltage. The BMS controls the proper operation of each cell to allow the system to work within a desired voltage, current, and temperature so as not to pose any danger for the system itself but ensure viable operation of the

batteries. The system also calibrates and equalizes the State of Charge (SoC) of the cells. The BESS is connected to the inverters to convert the power from DC to AC. In each BESS, there is a specific power electronic level, called PCS (Power Conversion System), that is usually grouped in a conversion unit including all the auxiliary services needed for the proper monitoring [14]. Depending on the size of the system, there is a step-up transformer connection from low-voltage to high-voltage to meet the required transmission voltage.

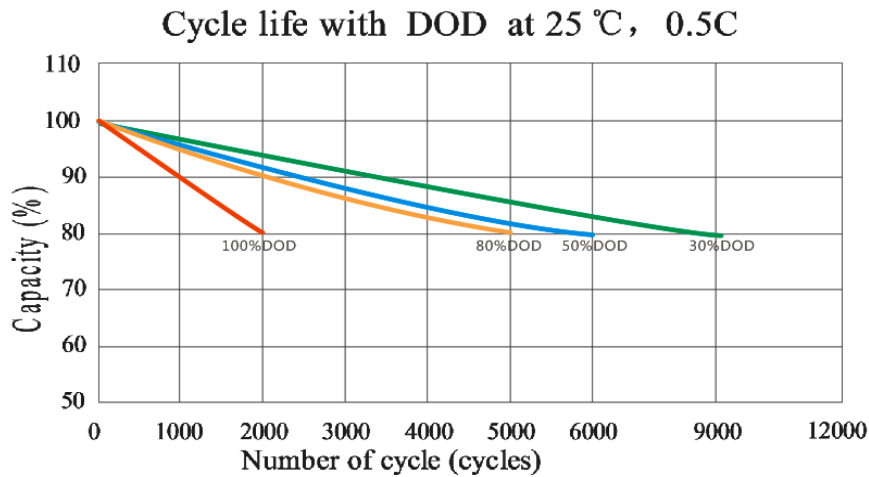


Figure 6. LFP batteries cycles based on DOD [15]

The long service life of LFP batteries makes it possible to use LiFePO₄ in utility-scale energy storage applications. Given that the BESS will operate at a constant temperature of around 25 °C at 80 % DOD, 0.5C (charge or discharge rate), this can result in 4500-5000 cycles, which is equivalent to approximately 10-12 years [15]. As shown in Figure 6, LFP battery’s lifespan depends on the DOD, operation temperature, the C-rate.

Mounting a BESS to a utility PV system requires different methods of coupling, which can be split into two main categories: AC coupling and DC coupling.

AC coupling with the BESS involves coupling using an AC bus. The AC bus is located after the PV array where power is converted to AC using an inverter. With this system method, the power supplied to the grid is maximized by discharging both the battery and PV at maximum power [16]. They offer the ability to be dispatched independently or together. AC coupling is more common when the BESS is deployed in the same area of distribution, i.e., near load/consumers, which is more advantageous for the BESS operator.

5. BESS COUPLING AND LOCATION

5.1. BESS coupling

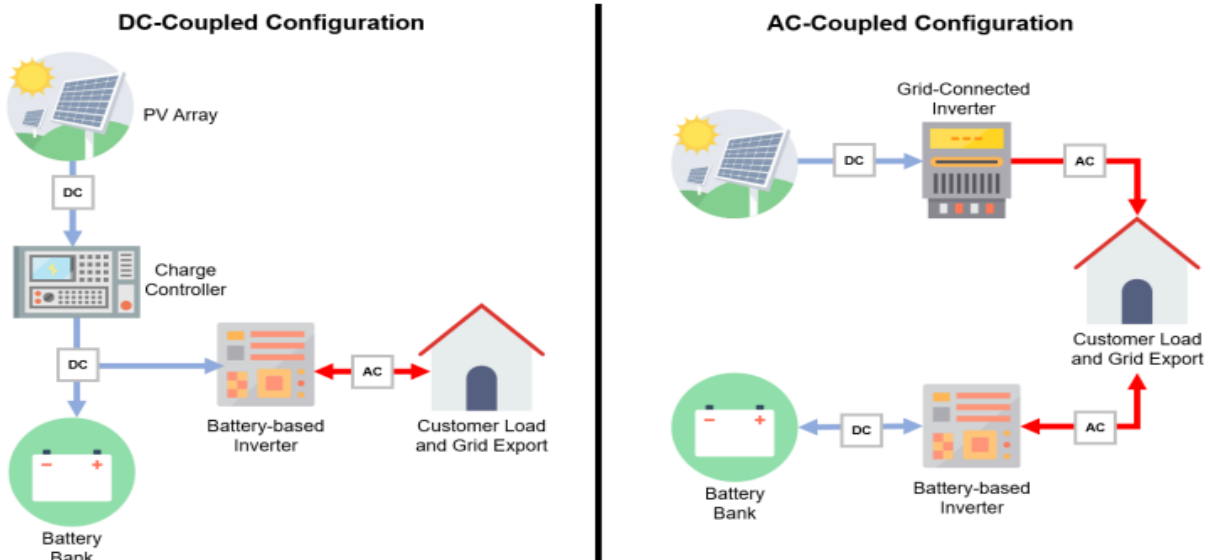


Figure 7. BESS AC and DC coupling [16]

An alternative approach involving coupling energy storage to PV arrays with a DC-to-DC converter can help maximize production and profits for existing and new utility-scale installations. DC-Coupled utility-scale solar plus storage leads to higher round-trip efficiencies and lower cost of integration with existing PV arrays and at the same time, opens new revenue streams not possible with traditional AC-coupled storage [16]. DC coupled BESS, on the other hand, can be co-located with the PV plant as it requires a direct connection using a DC bus, which may have a few limitations.

5.2. BESS location

BESS coupling is dependent on the deployment location of the BESS itself. There are three main ways a utility-scale BESS can be deployed: within the area of distribution that is near load centers; co-located with Renewable Energy Source (RES) (in this case PV plant), or in the transmission network. There are important implications in the siting of the BESS based on the services the system can best provide, and the most appropriate location for the BESS also depends on its intended purpose. Technically, a BESS can provide a broad range of services in any locations; therefore, an important analysis of the costs, safety, and benefits of multiple locations is required to determine the optimal siting to meet system needs [17].

5.3. Area of distribution near load centers

After costs and dispatchability analysis for the ideal BESS location, energy storage systems located within the distribution area where the consumers/energy demand is or co-located with the RES offer a stable grid depending on the BESS operation parameters. BESSs that are in the distribution network have the capability to provide all the services offered by a transmission-network sited storage, in addition to several services related to congestion and power quality issues [18]. It may be difficult to site other energy storage system technologies near load/consumers to provide peaking capacity due to concerns about safety, emissions, or land use. However, BESS and typically LFP batteries can be co-located near load with fewer siting challenges than others due to their

high tolerance to different working conditions and the safety they offer. Since the BESS is deployed near the load site, electrical losses in transmission and distribution can be greatly reduced while capacity and energy value are increased; therefore, generated electricity can efficiently reach the intended consumers with minor loss. Distribution-level BESS systems can also provide local power quality services and support improved resilience during extreme weather events [19]. This siting can work effectively for both power providers that operate the BESS and the RES and for private BESS operators as it offers profitable arbitrage opportunities by charging the battery storage during off-peak hours when electricity is cheap and discharging during expensive peak hours. Investments in transmission and distribution are also deferred, leading to reduced CAPEX.

Taking Zimbabwe's residential system into consideration, suburbs are put into three main categories: low-density suburbs, medium-density suburbs, and high-density suburbs. In this case, the ideal suburbs to deploy a load site BESS will be in high density suburbs as they are highly populated areas; therefore, there are more consumers than other suburbs and furthermore, these are the suburbs that experience the highest power cuts during peak demands when the grid is unable to meet all the demands. The siting challenges are very limited and the BESS itself is scalable; as a result, a BESS deployed in high-density suburbs has a greater chance of high Return On Investment (ROI). Medium-density suburbs, on the other hand, may be an ideal location for small-sized BESS as well since the suburbs are less populated and have a great percentage of the population invested in individual on-grid PV systems with energy storage systems connected Behind-The-Meter (BTM). Low-density suburbs are the least populated suburbs that experience nearly no power interruptions and have a great percentage of the population with individual off-grid PV systems.

To summarize, the BESS located in high-density suburbs can be charged during off-peak hours when there is excess electricity generation. The BESS will be connected to the grid which will be transmitting PV power from the PV plant. Below is an example of a BESS located far from the RES, but close to the load center.



Figure 8. BESS located near load center

5.4. Co-located with Renewable Energy Source (RES)

In most cases, RES plants are located far from load centers as their location depends on the availability of adequate supply of natural resource like wind or solar. Solar PV plants require vast open land that is not prone to any sunlight hindrance, which is mostly available far from the urban centers where the electricity demand is located. For the generated energy to reach the demand/consumer area, significant transmission capacity is required. Considering the variability of Variable Renewable Energy (VRE) resources, the transmission capacity used to deliver the power may be underutilized for large periods of the year resulting in low ROI due to increased transmission value. A BESS can reduce the transmission

capacity needed to integrate these resources and increase the utilization of the remaining capacity by using storage to charge excess generation during periods of high resource availability and discharge during periods of low resource availability [20]. In this case, it is cost effective to co-locate RES plant and the BESS in an area where there is an existing transmission capacity.

In this case, the BESS is deployed in the same location as that of the PV system. The PV system will generate power and transmit it to the BESS via DC-DC coupling. The BESS will charge and transmit power to the grid. Figure 9 below shows a BESS co-located with the PV plant.



Figure 9. BESS co-located with PV plant

6. BESS DEPLOYMENT BARRIERS

In the meantime, there are no commercial or pilot BESS that has been designed and operated on a utility scale in Zimbabwe. Generally, there is little development or investments in storing excess energy produced in the country. The main barriers of the deployment of energy storage can be grouped into three different categories: technical barriers, regulatory barriers, and economic barriers.

6.1. Technical barriers

Large-scale electrochemical energy storages are still emerging technologies that are experiencing rapid changes and advancements regularly and, in some cases, show more investment risks for investors than conventional generator investments. These risks include the technical aspects of BESS, which can be less understood by stakeholders but comprehensible for the engineering team as they are changing faster than other technologies in recent years. Zimbabwe has always been relying on biofuels, hydroelectricity, and thermal power; therefore, investments in thermal energy storage and mechanical energy storage such as pumped storage hydro-electric for the newly opened PV plants are more favorable since the storage systems operation and maintenance procedures are just the same as the current running power plants; however, their response times are slower than the fast-ramping capabilities of BESS. Furthermore, the import of key repairs like turbines and generators may be impacted by the acute foreign currency shortages that constantly recur. Although the battery technology itself requires to be imported, the long lifespan

offered specifically by LFP batteries makes it possible for the BESS operator to rely on importations and it also allows the investors to catch up with the new battery technologies available at given times. The gaps in data and analysis capabilities and lack of adequate tools can deter investments and possibly stop battery storage from being considered for services that can be provided by better well-known conventional generators [21-22]. Technical know-how of the battery cells, chemical properties, reactions, and operation parameters may be required before implementing them on a large scale.

6.2. Regulatory barriers

Storage could also be technically able to provide essential grid services, if no regulations or guidelines explicitly state that storage must provide certain services or meet certain requirements. Without a guarantee that services provided by a BESS project can be compensated, storage operators and financing institutions might be unwilling to make the necessary capital investments as they will view it a risk. Among other requirements, the rules must be flexible enough to ensure access to the market for storage systems operators, taking into consideration their unique operating and technical characteristics. Restrictions or lack of clarity around the way how storage can be used across generation, transmission, and distribution roles can lead to investors investing in too big or too small BESS and deploy them in wrong locations. Zimbabwe Energy Regulation Authority (ZERA) has encouraged small-scale Independent Power Providers (IPP) to sell excess generated electricity to Zimbabwe Electricity

Supply Authority (ZESA); however, there are terms on how much power can one sell to ZESA. The amount of power an IPP can sell to ZESA is unlimited; however, there is a set minimum amount of power an IPP can negotiate to sell to ZESA which has been the biggest limitation for IPPs as they are incapable of investing in large-scale systems. Furthermore, to guarantee ZESA with a stable power supply as an IPP, it requires the implementation of BESS in which a lot of IPP cannot afford to invest currently.

The range of various services ESS can often provide cuts across multiple markets and compensation sources. In some jurisdictions, providing services across different compensation sources is restricted by certain regulations [23-24].

6.3. Economic barriers

Although BESS has the capability to provide the same services as those of a conventional grid, it is impossible for an IPP to implement a BESS independently as power distribution requires to be regulated by the power distribution authorities; thus, consumers may be required to apply for the shift from local grid and connect them to BESS. Furthermore, the presence of batteries in the market could distort the pricing formation which could affect storage systems and conventional generators. The one-tariff regime implemented in Zimbabwe could work effectively with thermal or hydro power; however, if a BESS is coupled with a PV system, tariffs may be expected to vary for baseload and peak demand as this will allow a decent ROI and give investors interests to increase the storage capacity and replace batteries after their lifespan. Battery systems can provide certain services much faster and more accurately than conventional resources, which may not be reflected in compensation for the service [25-26]. Similarly, BESS is uniquely suited to produce up or down regulation, given their larger operating range over which to supply regulating reserves (due to their lack of a minimum stable level and capability to supply up and down regulation that may be over their nameplate capacity based on whether they are charging or discharging) [27-28].

To summarize all the barriers, the unavailability of practical references to gain accurate data and knowledge of BESS application benefits has an impact on the investment and deployment of the system. There are currently no policy measures and institutional structures that guide investments in energy storage in Zimbabwe since these will be new and experimental projects. Since utility-scale energy storage is still considered a new technology, there is a possibility of lack of technological know-how and skills based on large-scale BESS in the country. While other barriers require government and policy intervention, other issues such as lack of know-how can be tackled by intensive trainings and with reference to other operational projects around the world, some of which have been operational for several years.

7. BESS TECHNO-ECONOMIC ANALYSIS

There are two major costs in the investment of a BESS: the capital expenditure (CAPEX) and the operation expenditure (OPEX). The CAPEX of a BESS is made of a onetime investment that is required to bring the whole BESS into an operating state and it can be separated into direct (C_{direct}) and indirect ($C_{indirect}$) costs. Here, the C_{direct} costs of the BESS are related to the total cost of battery modules or battery packs ($C_{batteries}$), the balance of plant (CBOP) including BMS, the

total cost of Power Conditioning System (PCS) (CPCS) required when converting the generated DC power into AC power and the installation costs ($C_{installation}$) of all the BESS equipment. The BOP costs are the civil work costs only. Given that the BESS is coupled on the DC side, the cost of the PCS is not taken as it is integrated with the RES (PV) PCS. The indirect costs are the engineering costs ($C_{engineering}$) associated with the contractors, the tax costs (CTAX) including municipal fees to be paid if the system is deployed in a residential area near consumers, and the project installation or process contingency costs ($C_{contingency}$). BESS CAPEX calculations are done through the equations below:

$$CAPEX_{BESS} = C_{direct} + C_{indirect}$$

$$C_{direct} = C_{batteries} + C_{PCS} + C_{BOP} + C_{installation}$$

$$C_{indirect} = C_{engineering} + C_{TAX} + C_{contingency}$$

Operation expenditure (OPEX) of a BESS has fixed costs and variable costs that can be presented as labor and engineering costs (C_{labor}) associated with the system operation, the O&M costs which mainly consist of operation and maintenance of the PCS, and replacement ($C_{O\&M}$). Since equipment wear with operation, there are decommissioning and disposal costs ($C_{disposal}$) to be incurred.

$$OPEX_{BESS} = C_{labor} + C_{O\&M} + C_{disposal}$$

After several years of use (4-12 years), the BESS will need to be replaced due to the underperformance of the system or the fact that the battery modules may have reached their operational lifespan; this replacement can be equal to C_{direct} or less since the cost of batteries is decreasing yearly.

8. CONCLUSIONS

Zimbabwe has a great potential for high solar PV production and since the grid is failing to meet the nation's energy demands, BESS has a greater potential for stabilizing the grid. However, considering Zimbabwe's situation where electricity tariffs and distribution are mostly governed by Zimbabwe Energy Regulatory Authority (ZERA), arbitrage where in other countries a private BESS operator charges the BESS during off-peak hours when electricity is cheap and discharges during expensive peak hours might be infeasible since ZERA and Zimbabwe Electricity Supply Authority (ZESA) passed a one-tariff regime whether it is off-peak hours or peak hours and an additional 6 % that goes towards the Rural Electrification Agency (REA). On the other hand, power absorbed and delivered by a BESS may also require to be regulated by ZERA with the aim of preventing irregular tariffs. Given that a BESS operator or ZESA itself has coupled the grid with a BESS, it is possible that the 6 % REA levy can be removed with the guarantee of putting fault and contingency into consideration to ensure safety and stability of the grid in return. According to Zimbabwe National Statistics Agency (ZimStat) data, Zimbabwe's electrical energy imports reached 192 %, which is equal to US\$192.3 million in 2020; however, due to the Covid-19 pandemic, energy demands decreased, and the grid started to stabilize. The reduced business hours in 2021 lowered the energy demand, which is proof that the application of BESSs to serve both commercial

and communal grids can help stabilize the grid.

Since Independent Power Providers (IPPs) in Zimbabwe have been efficiently producing energy for their consumption, there is a high potential for having efficient IPP managed BESSs only if ZESA/ZERA gives incentives to private BESS operators. Investors may be compensated in several ways and may experience a decent return on investment (ROI) within a short period of time depending on the location, targeted consumers, and size of the energy storage system. Instead of a flat tariff system, ZESA uses a stepped tariff system where every individual is entitled to a certain amount of discounted kWh with the aim of making electricity affordable for everyone, especially the less fortunate, although these kWh capacities are not enough to last long. After the discounted power is used up, the more power used by a consumer, the more expensive it becomes. In this case, if a BESS is privately operated, ZESA can pay the predetermined price and recover through retail electricity rates plus an additional REA levy paid by consumers. BESSs have a high possibility for curtailing energy problems in Zimbabwe and provide a better stable and reliable grid for the consumers and might also lower the LCOE in the future since battery costs continue to decline and Zimbabwe is considered to have the largest lithium deposits in Africa as of 2021 that are yet to be exploited.

9. ACKNOWLEDGEMENT

This work is supported by the National Natural Science Foundation of China (No. 51971128), Program of Shanghai Academic/Technology Research Leader (No. 20XD1401800), Science and Technology Commission of Shanghai Municipality (No. 19020501000).

REFERENCES

- "Zimbabwe set for real solar growth", (2020). (<https://www.py-magazine.com/2020/01/24/zimbabwe-set-for-real-solar-growth/>), (Accessed: 24 Jan. 2020).
- Jones, D., "Refurbishment delays hamper Zimbabwe energy prospects", (2021). (<https://allafrica.com/stories/202105200809.html#:~:text=Victoria%20Falls%20---%20THE%20expansion%20of%20release%20finances%20to%20the%20contractor>), (Accessed: 20 May 2021).
- World Bank, "Global solar atlas 2.0", Solar resource data: Solargis, (2019). (<https://xs.studiodahu.com/scholar?q=Global+Solar+Atlas+2.0%2C+Solar+resource+data%2C+Solargis>)
- Menictas, C., Skyllas-Kazacos, M. and Mariana Lim, T., "Advances in batteries for medium and large-scale energy storage", *Elsevier Ltd.*, (2014), 563-586. (<https://doi.org/10.1016/C2013-0-16429-X>).
- Handbook on battery energy storage system, (2018). (<https://dx.doi.org/10.22617/TCS189791-2>), (Accessed: Dec. 20218).
- Energy storage impacts of electrochemical utility-scale battery energy storage systems on the bulk power system, (2021), 5-12. (<https://www.readkong.com/page/energy-storage-impacts-of-electrochemical-utility-scale-1520315>).
- DiOrio, N., Dobos, A. and Janzou, S., "Economic analysis case studies of battery energy storage with SAM", (2015), 5-7. (<https://www.nrel.gov/docs/fy16osti/64987.pdf>).
- Battery University, "Types of lithium-ion", (2015). (<https://batteryuniversity.com/article/bu-205-types-of-lithium-ion>).
- Curry, C., "Lithium-ion battery costs and market", (2017). (<https://data.bloomberglp.com/bnef/sites/14/2017/07/BNEF-Lithium-ion-battery-costs-and-market.pdf>), (Accessed: 4 Jul. 2017).
- Ioakimidis, C.S., Murillo-Marrodán, A., Bagheri, A., Thomas, D. and Genikomsakis, K.N., "Life cycle assessment of a lithium iron phosphate (LFP) electric vehicle battery in second life application scenarios", *Sustainability*, Vol. 11, No. 9, (2019). (<https://doi.org/10.3390/su11092527>).
- Accardo, A., Dotelli, G., Musa, M.L. and Spessa, E., "Life cycle assessment of an NMC battery for application to electric light-duty commercial vehicles and comparison with a sodium-nickel-chloride battery", *Applied Sciences*, Vol. 11, No. 3, (2021). (<https://doi.org/10.3390/app11031160>).
- Andrey, A. and Anna, P., "Efficient energy management and energy saving with a BESS (Battery Energy Storage System)", (2021). (<https://www.integrasources.com/blog/energy-management-and-energy-saving-bess/>), (Accessed: 16 Aug. 2021).
- Tumino, P., "The architecture of battery energy storage systems", (2020). (<https://eepower.com/technical-articles/the-architecture-of-battery-energy-storage-systems/>), (Accessed: 23 Sep. 2020).
- Xavier, L.S., Amorim, W., Cupertino, A.F., Mendes, V.F., do Boaventura, W.C. and Pereira, H.A., "Power converters for battery energy storage systems connected to medium voltage systems: A comprehensive review", *BMC Energy*, Vol. 7, No. 4 (2019), 1778-1790. (<https://doi.org/10.1186/s42500-019-0006-5>).
- "Life cycle of lithium iron phosphate batteries". (<https://www.powertechsystems.eu/home/tech-corner/lithium-iron-phosphate-lifepo4/>).
- Ptiera, "Technical aspects of battery energy storage systems for integration in distribution circuits in New York state", (2019). (<https://www.ptiera.com/distribution-systems/technical-aspects-of-battery-energy-storage-systems-for-integration-in-distribution-circuits-in-new-york-state/>), (Accessed: 13 Feb. 2019).
- "Practical considerations for siting utility-scale battery projects", (2016). (<https://www.powermag.com/practical-considerations-siting-utility-scale-battery-projects/>), (Accessed: 1 May 2016).
- Alzahrani, A., Alharthi, H. and Khalid, M., "Minimization of power losses through optimal battery placement in a distributed network with high penetration of photovoltaics", *Energies*, Vol. 13, No. 1, (2019). (<https://doi.org/10.3390/en13010140>).
- "Grid-scale battery storage", (2019). (<https://www.nrel.gov/docs/fy19osti/74426.pdf>), (Accessed: Sep. 2019).
- "Determine optimal sites project size, technology and economics for utility-scale (generation+) battery system deployment", (2019). (https://www.irena.org/media/Files/IRENA/Agency/Publication/2019/Sep/IRENA_Utility-scale-batteries_2019.pdf).
- Advanced lithium-ion battery research and development. (<https://materials.waters.com/li-ion/>).
- Cole, W., Frazier, W.A. and Augustine, C., "Cost projections for utility-scale battery storage: 2021 update", National Renewable Energy Laboratory, (2021). (<https://www.nrel.gov/docs/fy21osti/79236.pdf>), (Accessed: Jun. 2016).
- Samu, R., Fahrioglu, M. and Ozansoy, C., "The potential and economic viability of wind farms in Zimbabwe", *International Journal of Green Energy*, Vol. 16, No. 15, (2019), 1539-1546. (<https://doi.org/10.1080/15435075.2019.1671424>).
- Denholm, P., Sun, Y. and Mai, T., "An introduction to grid services: Concepts, technical requirements, and provision from wind", Golden, CO: National Renewable Energy Laboratory, (2019), 1-52. (<https://doi.org/10.2172/1493402>).
- Battery Energy Storage Systems (BESS): Ancillary services and beyond, (2018). (<https://innovationweek.irena.org/-/media/Files/IRENA/Innovation-Week/SessionalDocuments/IRENA-IW18--Electricity-storage--01---Duboviks--BESS--06-Sept-2018.pdf>), (Accessed: 6 Sep. 2018).
- Ibrahim, H. and Ilinca, A., "Techno-economic analysis of different energy storage technologies", In *Energy Storage: Technologies and Applications*, edited by Ahmed Zobaa, (2013). (<https://doi.org/10.5772/52220>).
- Why battery management systems are important in lithium iron phosphate batteries, (2018). (<https://reliionbattery.com/blog/why-battery-management-systems-are-important-in-lithium-iron-phosphate-batteries/>), (Accessed: 27 Nov. 2018).
- DiOrio, N., Dobos, A., Janzou, S., Nelson, A. and Lundstrom, B., "Techno-economic modelling of battery energy storage in SAM", (2015), 1-36. (<https://doi.org/10.2172/1225314>).



Review Article

A Brief Overview of Microgrid Performance Improvements Using Distributed FACTS Devices

Ghazanfar Shahgholian ^{a,b*}

^a Department of Electrical Engineering, Najafabad Branch, Islamic Azad University, Najafabad, Iran.

^b Smart Microgrid Research Center, Najafabad Branch, Islamic Azad University, Najafabad, Iran.

PAPER INFO

Paper history:

Received: 26 December 2021

Revised in revised form: 28 February 2022

Scientific Accepted: 24 March 2022

Published: 27 August 2022

Keywords:

Microgrid,
Distributed Flexible AC Transmission System,
Performance,
Connection Mode

ABSTRACT

Distributed flexible ac transmission system (D-FACTS) is a light-weight version of FACTS, which it is easily allocated and costs less than flexible ac transmission system (FACTS) devices. They have potential benefits to improve the system stability and improvement in power quality in microgrid (MG). The integration of distributed energy sources, loads, electrical energy storage devices, and electronic power devices, as well as the operation of microgrids in connected or island-connected modes has expanded their use. It is a small main grid that can generate electricity when disconnected from the main network. In addition, microgrids reduce the high investment costs required to upgrade the network. The application of DFACTS devices for improving the microgrid operation has been investigated by some researches. This paper provides a review of impact and role of various DFACTS devices in the function of microgrids, which has been reported in recent years in various pieces of the literature. DFACTS devices with their properties are described. Finally, a useful reference and framework for the study is provided for future expansion of DFACTS devices so as to improve the performance of the microgrid.

<https://doi.org/10.30501/jree.2022.321435.1305>

1. INTRODUCTION

Power systems are generally centralized, consisting of large power plants, and power is transmitted to consumption through long-distance transmission lines [1-10]. The demand for clean and free-of-contamination electric power is increasing day by day with the ongoing developments and advances [11-14]. A microgrid (MG) is a controllable local electrical network that can work independently or collaboratively with other small networks [15, 16]. It is a complex non-linear system with inter-coupling of thermodynamics, chemical energy, and electrostatics [17-22].

Many types of renewable energy resources are utilized as power generators in MGs [23-27]. Thus, an MG is able to reduce the loss of transmission to improve the efficiency of grids and resolve energy crisis [28, 29]. It must, also, be capable to power flow control and supervise energy storage [30, 31]. The ability to export to or import energy from the main network is a must [32-35].

An MG system consists of different power quality issues [36-38]. Power quality problems can also be very costly for both utility and the customer [39]. Frequency changes, voltage fluctuations, voltage distortions, flicker, and voltage

disturbances reduce the quality of energy supplied to consumers in an MG [40-43]. Figure 1 shows the classification of power quality problems and their impacts on grid-connected MG systems [44, 45].

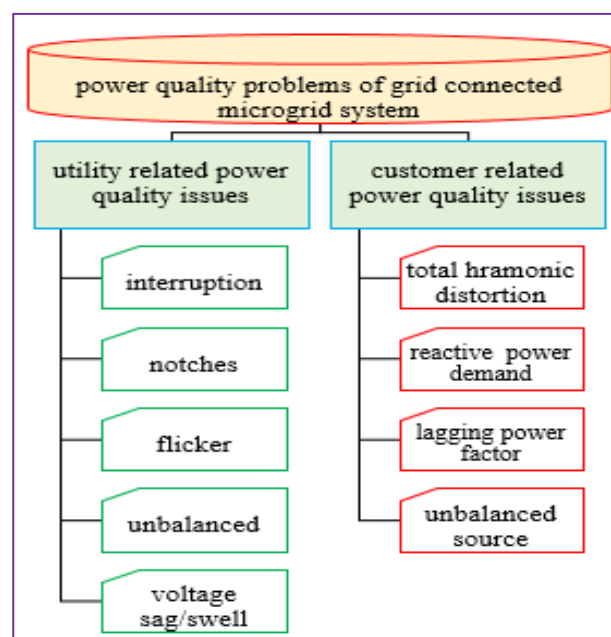


Figure 1. Power quality of MG system

*Corresponding Author's Email: shahgholian@iaun.ac.ir (Gh. Shahgholian)

URL: https://www.jree.ir/article_155308.html



1.1. Short summary of FACTS devices

FACTS devices are used in AC transmission networks to increase power transmission capability, stability, and control of networks [46, 47]. These devices are connected to the transmission system in terms of connection to four categories, according to Figure 2. The important advantages of FACTS controllers include the following: the ability to increase power transmission capability, restrict electricity to designated routes, improve transient and dynamic stability, reduce damping power system fluctuations, and adjust system voltage and flexible system operation with simple controls [48-60].

1.2. Importance of DFACTS devices

DFACTS device is used in distribution system, while FACTS device is used in transmission systems [61-67]. These devices are designed and installed to improve power quality anywhere in the power distribution system [68, 69]. DFACTS are used to improve the system stability and power quality improvement in MGs [70, 71].

Figure 3 shows a reduction in the MG power losses in the islanding mode due to the use of the DFACTS. The improvement in power factor values is shown in Figure 4. As can be seen, the power factor in heavy load has increased to 0.8 and at light load, the power factor has increased to unity [72].

1.3. Innovation and contributions

There are several papers results about DFACTS from various aspects of application in MG. This paper provides a comprehensive review of various DFACTS devices for performance improvement of MG that have been reported in

the literature during recent years. The significance and the novelty of the work is as follows:

- Use of this paper review as an initial platform for research work on microgrids in industry.
- Review of DFACTS devices used by microgrids for enhancing power quality.
- Comprehensive review of DFACTS types.
- Review of the available types for application of different compensators.

1.4. Paper organization and structure

In Section 1, the whole subject of the study is mentioned. The structure and operation of an MG are investigated in Section 2. A classification of the most relevant MGs can be also found in this section. In Section 3, a brief overview of the application of DFACTS in power system is made, where the features and structure are stated. The effect of DFACTS on behavior of the MG is discussed in Section 4. Finally, the conclusion of the research is presented in Section 5.

2. CHARACTERISTICS OPERATING OF MICROGRID

MG is a controllable and independent power system, which is a localized group of distributed energy resources, loads, energy storage devices, inverters, and protection devices [73, 74]. Figure 5 depicts the typical structure of an MG. The MG connects to the network in a PCC whose aim is to maintain the same voltage as the main grid. It is characterized by a variety of parameters such as mode of operation, distribution system, source, scenario, and sizes, as shown in Figure 6 [75].

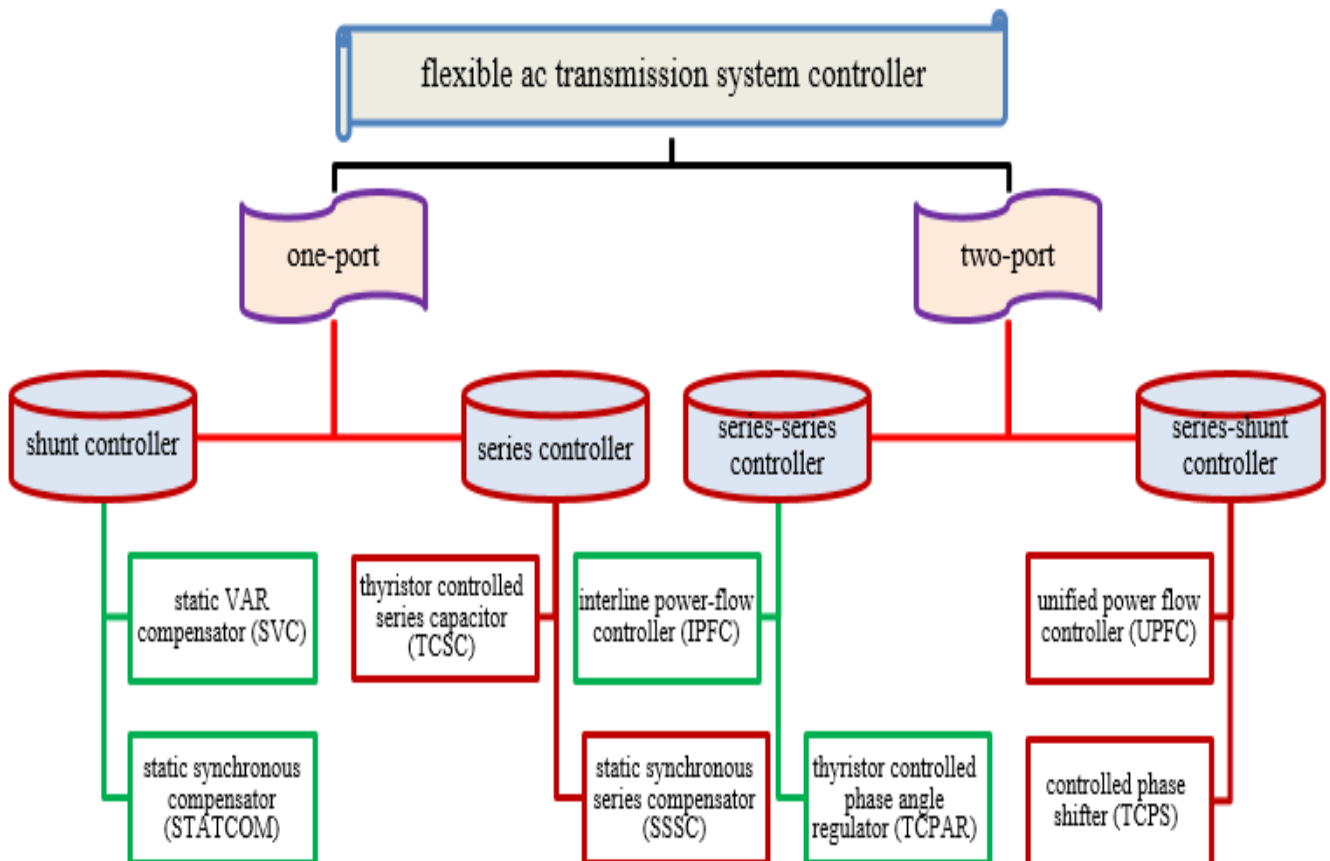


Figure 2. Classification of facade devices based on the type of connection

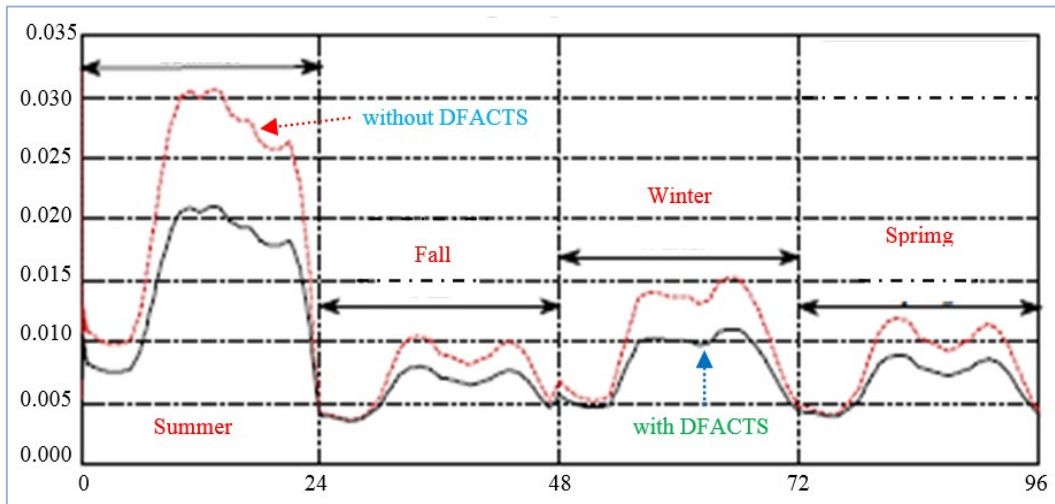


Figure 3. MG power loss profile

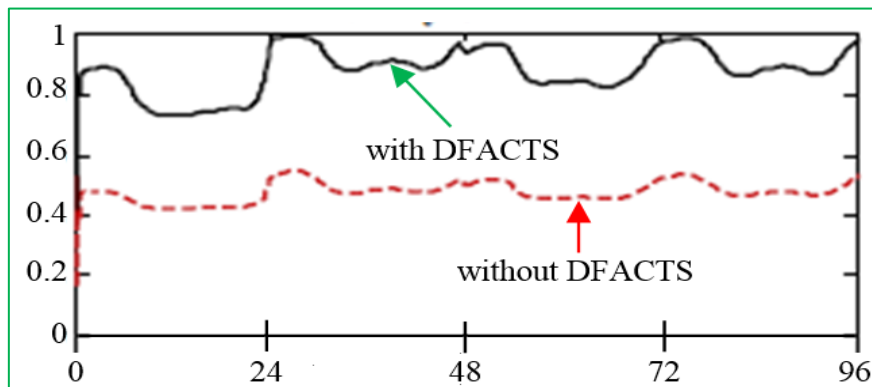


Figure 4. Power factor profile at the utility grid bus

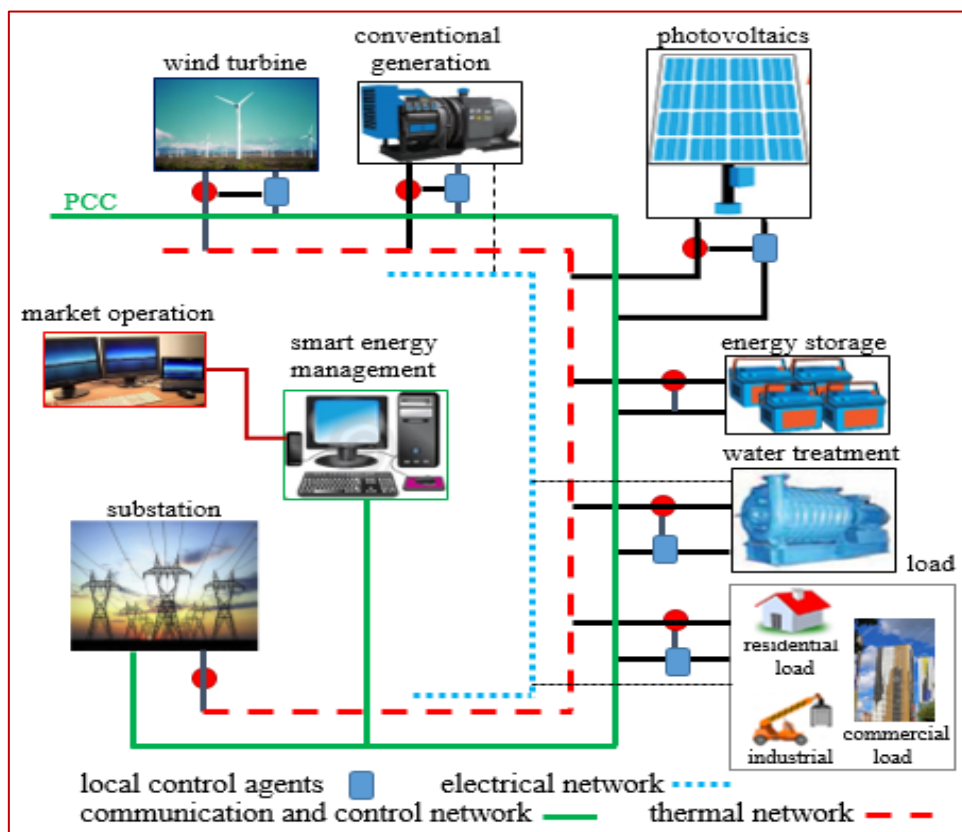


Figure 5. Microgrid architecture

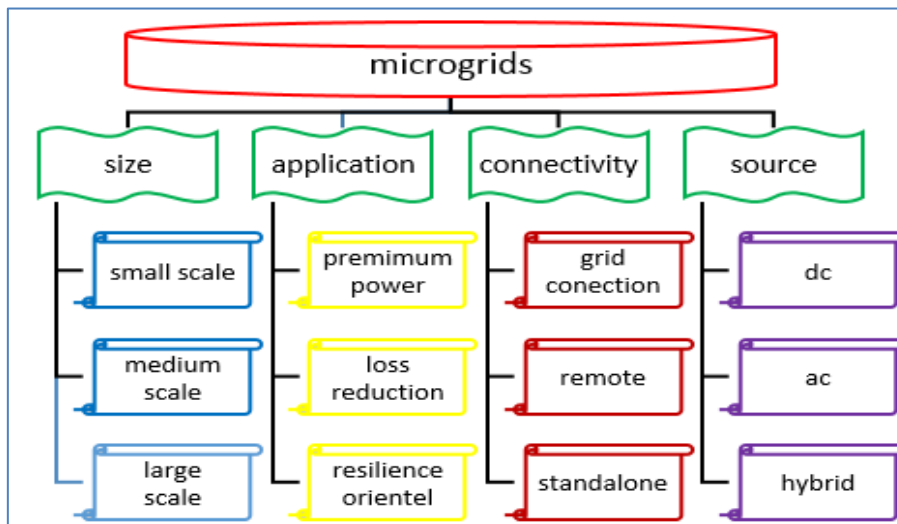


Figure 6. Microgrid types

This classification has been performed based on the studies found in the literature. MGs are classified based on location to remote MGs and urban MGs. MGs are divided into different types and classes in terms of their controlling topology [76]. With regard to power, the MG is classified as an ac power system [77], a dc power system [78, 79], or a hybrid system [80, 81] which reveal their advantages and disadvantages upon its application.

The operating modes for MGs are recognized and defined as follows: grid-connected mode, transition to island mode, island mode, and reconnection mode [82, 83]. Therefore, in the event of reduced power quality or network faults, microgrid increases the reliability of energy sources [84]. In the grid-connected mode, the power flow of MGs is bidirectional. While in the islanded mode, the power supply of MGs must meet the demand of load [85, 86]. Depending on their topology, MG control can be divided into three classes: simple (or virtual prime mover), master control (or physical prime mover), and peer-to-peer control (or distributed control).

3. OVERVIEW OF DFACTS DEVICES

The devices for improving the quality of power and reliability of supply can be divided into three categories: (a) passive mitigation devices such as transformers and rotating machine; (b) DC system; and (c) power-based electronics. DFACTS

devices such as Unified Power Quality Compensator (UPQC) [87, 88], Distributed Power Flow Controller (DPFC) [89], Dynamic Voltage Restorer (DVR) [90-91], DSSC [92, 93], and DSTATCOM [94-96] have many potential benefits in a power system. They are applied to low-voltage distribution systems.

3.1. Introduction of DFACTS devices

DFACTS devices are divided into four categories based on the type of connection: series, shunt, series-shunt, and series-series. This section briefly explains the DFATCS types.

3.1.1. Unified power quality conditioner

UPQC is a major custom power device. It is a multifunction power conditioner [97, 98]. The UPQC power circuit consists of a common dc-link capacitor and two filters including a shunt active power filter and a series active power filter. One of the methods to compensate for various disturbances in the power system such as voltage disturbances in the power supply, correcting voltage fluctuations, and preventing the harmonic flow of load is the use of UPQC [99]. Schematic structure of the UPQC is shown in Figure 7. Several applications of UPQC in the power systems are listed in Table 1.

Table 1. Various applications of UPQC in the power system

Ref.	Subject	Suggested method	Contributions (Cause of use in power system)
[100]	Improvement of power quality	Adaptive frequency passiveness control	The application of UPQC to improve power quality in the manufacturing industry indicates that the adaptive frequency passiveness control method is used.
[101]	Effect mitigating of supply voltage sags	Power injection method	A UPQC-Q control structure is provided so as to achieve the minimum active power injection. Also, this method takes into consideration the limitations of the phase difference during voltage sag events.
[102]	Power quality enhancement	Adaptive JAYA algorithm	An online tuning method is adopted for PI control gains in PV-UPQC shunt and serial converter controllers. The JAYA adaptive algorithm has two independent objective functions.

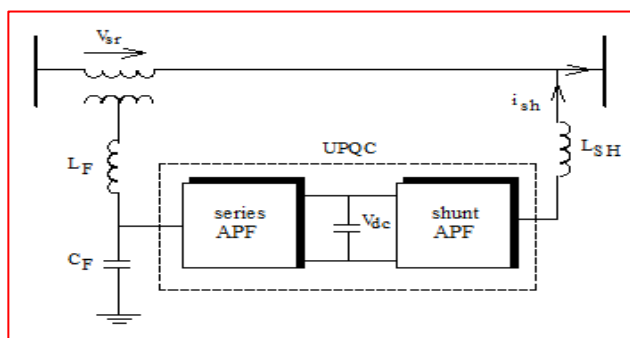


Figure 7. UPQC system configuration

3.1.2. Dynamic voltage restorer

The two main parts of DVR are the power circuit and control circuit. It is a series compensation device composed of an energy storage system with a dc link, a filter circuit, an inverter, and a series voltage injection transformer [103, 104]. A schematic diagram of the DVR is shown in Figure 8.

The coupling transformer is connected in series to the grid to correct the voltage disturbances during faulty grid conditions [105]. Several DVR applications in power systems are listed in Table 2.

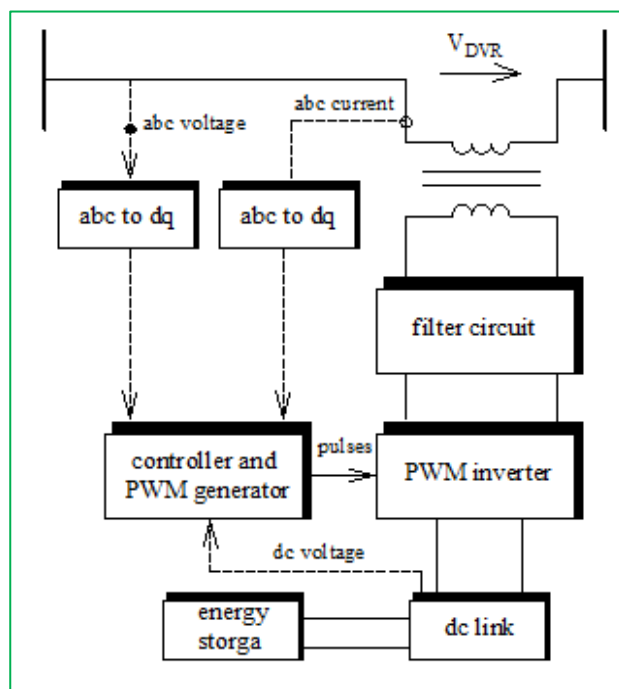


Figure 8. Schematic structure of the DVR compensator

Table 2. Various applications of DVR in the power system

Ref.	Subject	Suggested method	Contributions (Cause of use in power system)
[106]	Voltage droop compensation and automatic power recovery	Adaptive control	An improved control structure is proposed for sensitive loads to improve voltage quality using DVR during the voltage compensation stage and maximum active power absorption during the energy self-recovery stage.
[107]	Enhanced voltage sag compensation	Compensation of phase jump with minimum active power injection	An increased compensation method is proposed that reduces the load voltage phase jump while improving the overall bending compensation time.
[108]	Balanced voltage sag compensation	Discrete-time domain control	The proposed control strategy is implemented with two nested regulators in the synchronous reference frame.
[109]	Fault ride improve	Hybrid genetic algorithm optimized	Custom DVR enhances the regulation of network voltage in unusual conditions.

3.1.3. Distributed static series compensator

DSSC is a low power device that can act as a variable impedance [110]. It is connected in series providing active power flow control through transmission line [111]. DSSC structure is similar to Static Synchronous Series Compensator (SSSC) differentiating in power rating, but has the same capability as the SSSC. The distributed concept of the DSSC provides much lower cost and higher reliability than the SSSC [112, 113]. DSSC basic structure is shown in Figure 9. Several applications of DSSC in power systems are listed in Table 3.

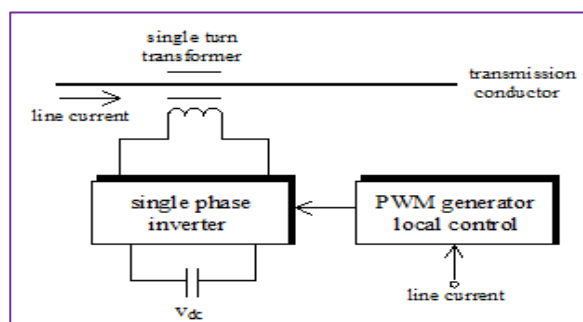


Figure 9. Schematic structure of the DSSC

Table 3. Various applications of DSSC in the power system

Ref.	Subject	Suggested method	Contributions (Cause of use in power system)
[114]	Loadability and reliability in power system	Flow model of DC load	The load flow model is used to find the optimal location for the DSSC and linear integer linear programming is used to solve the optimization problem.
[115]	Active power flow control	Line reactance changing	To achieve the desired flow controlled performance, the distribution of DSSC modules is used to operate by effectively changing the interface reaction.
[116]	Control of power flow in grid	Change the impedance of the line	DFACTS is proposed as an alternative approach to realize cost-effective energy flow control.

3.1.4. Distributed power flow controller

DPFC can be installed directly on the conductor. Using the control center located in the control post, the DPFC installed on the lines can be controlled. A DPFC controlled for operation is reactive voltage injection mode and series reactor mode. DPFC is derived from UPFC, which includes adjustment of line impedance, transmission angle, and bus

voltage [117]. The converter inside the DPFC is independent and the required DC voltage is supplied by its own DC capacitor.

Figure 10 shows the schematic diagram of the DPFC. The DPFC consists of one shunt converter and several series converters [118]. Several applications of DPFC in power systems are listed in Table 4.

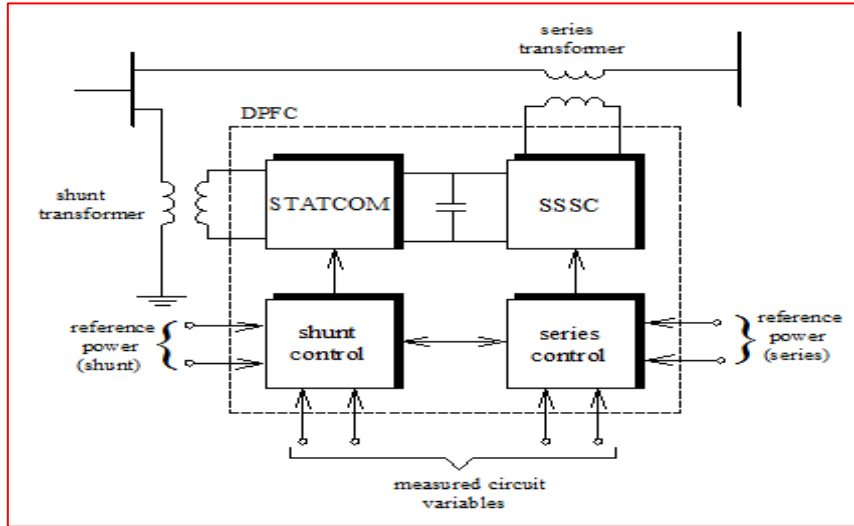


Figure 10. Schematic structure of the DPFC

Table 4. Various applications of DPFC in the power system

Ref.	Subject	Suggested method	Contributions (Cause of use in power system)
[119]	Improve power system stability	Optimization problem using PSO	An oscillation damping controller is designed for DPFC to damp LFOs, in which the optimal design problem is considered as an optimization problem.
[120]	Energy balance	Multi-objective coordinated control	A multi-objective coordinated control equation is proposed in which the equation minimizes the variance between the actual value of the control target and its given value to ensure that the DC capacitor voltage, both in the series and shunt side, is stable at target value.
[121]	Increase system loading capability	Linear programming of complex integers	An optimal DPFC configuration method is proposed to increase system load according to economic performance, in which DPFC investment and system loading behavior are analyzed and optimal solutions are used.

3.1.5. Distribution static synchronous compensator

DSTATCOM is a voltage source converter and is used as a shunt connection. This compensator is used to compensate for the bus voltage in distribution networks and it improves power factor and reactive power control [122, 123].

It works through exchanging the reactive power between the DSTATCOM and the power system [124]. DSTATCOM basic structure is shown in Figure 11. Several applications of DSTATCOM in power systems are listed in Table 5.

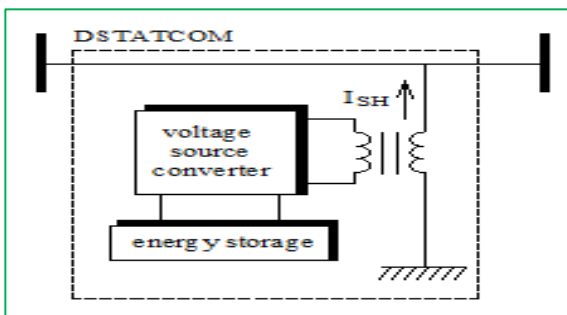


Figure 11. Schematic structure of the DSTATCOM

3.1.6. Solid-state circuit breaker

SSCB is a semiconductor-based protection device with no moving parts to cut off the fault current [129, 130]. Solid state circuit breakers are divided into two groups: hybrid circuit breaker and all SSCBs [131, 132]. The SSCBs solve the problem of slow reactive devices [133]. It is suitable for voltage systems at both high and low levels. A typical of the solid-state DC circuit breaker is shown in Figure 12 [134, 135]. Several applications of SSCB in power systems are listed in Table 6.

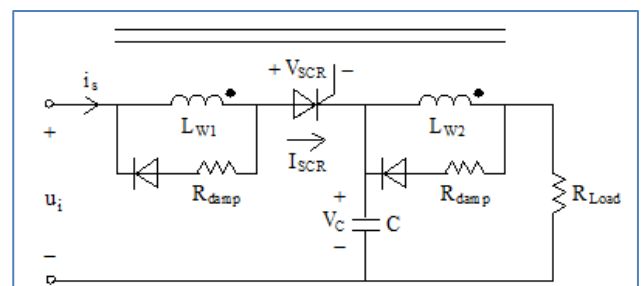


Figure 12. Schematic structure of the SSCB

Table 5. Various applications of DSTATCOM in the power system

Ref.	Subject	Suggested method	Contributions (Cause of use in power system)
[125]	Loss reduction and voltage profile	Direct load flow	A DG is placed optimally for reduction of losses in the network and under voltage at several buses is solved by the optimal placement of DSTATCOM.
[126]	Improve dynamic response and power quality	PSO-tuned PI controller	The PI controller set to PSO works better than the traditional PI controller set to the Ziegler-Nichols technique.
[127]	Power quality enhancement	Composite observer based control technique	This method is used to reduce reactive power, balance the load, and reduce harmonic distortion.
[128]	DSTATCOM nonlinear controller	Hybrid optimization	The basis of nonlinear control is partial feedback linearization, which is used to better regulate the DC capacitor voltage in DSTATCOM.

Table 6. Various applications of SSCB in the power system

Ref.	Subject	Suggested method	Contributions (Cause of use in power system)
[136]	Protection against short circuit	Switches design	Implementation of a simplified prototype of SSCB as a fault current limiter with DG is studied.
[137]	DC fault protection for modular multi-level	Advanced planning stage	The concept of protection for SSC and DC high voltage systems based on the overhead transmission is proposed and analysed.
[138]	Systematic evaluation of solid-state devices	Hybrid circuit breakers	Due to the simplicity of the control circuit and the switching resistance due to dv/dt , voltage controlled devices are selected.

3.2. Summary of the review study of DFACTS

Some of the available review studies on application of the DFACTS in power system are mentioned in Table 7.

Table 7. A review run on studies on different aspects of DFACTS

Ref.	Specifications (Summary of the review studies)
[139]	The impact of installing DFACTS devices by studying the linear sensitivities of power system quantities has been investigated.
[140]	Various conventional and adaptive algorithms used to control DFACTS devices for improvement of power quality in utility grids with renewable energy penetration are reviewed and discussed.
[141]	A survey on the optimal allocation of DSTATCOM in distribution networks is presented. Reducing power loss, reducing voltage deviation, improving reliability standards, and increasing voltage stability are some of the goals of using DFACTS.
[142]	For DVR with flywheel energy storage, input-output linearization ac voltage controller theory and performance are presented.
[143]	Various challenges related to SSCB design from the perspective of general applications and comparison of several SSB technologies based on key criteria are discussed.

4. LITERATURE REVIEW

Several researchers have studied the effect of DFACTS devices on the improvement the performance of MGs [144, 145]. In this section, upon reviewing the research, the application of each device in improving the performance of the MG is examined.

4.1. Improved MG performance

In this section, various indicators associated with MG performance improvement by DFACTS devices are mentioned.

4.1.1. Grid voltage disturbances

Grid voltage disturbances are the most common power quality problems in industrial distribution systems. The voltage disturbances of the network include voltage sags, swells, flicker, and harmonics.

At the moment of voltage droop, the rms value of the line voltage decreases, which lasts for a period of one half cycle of voltage up to 500 ms.

The objective of [146] is to investigate reactive power compensation in MG for voltage sag/swell mitigation using UPQC such that the MG is developed with two DGs units, a PV-cell and a wind generator, to give the output voltage equal to a typical 3-phase 4-wire distribution system.

To manage power quality in an MG, a DVR compensation strategy based on three basic strategies was presented in [147] and its method protects against sensitive voltage droops against main voltage droop with phase jump.

A DC microgrid-integrated DVR system to mitigate the grid voltage sag and swell was presented in [148]; compared to the conventional DVR designated by pure energy storage, the DC microgrid extends the DVR performance.

The utilization of the custom power device specifically DVR in mitigating the problem of voltage sags and swells occurring in MG was proposed in [149], in which the MG was modeled and simulated under different loading conditions causing power quality problems. Moreover, for the performance of DVR in overcoming the problems, reactive power compensation was analyzed.

The voltage profiles of the IEEE 69-buses without DSTACOM and the multiple DSTATCOM effect under various load conditions are shown in Figures 13 and 14 [150].

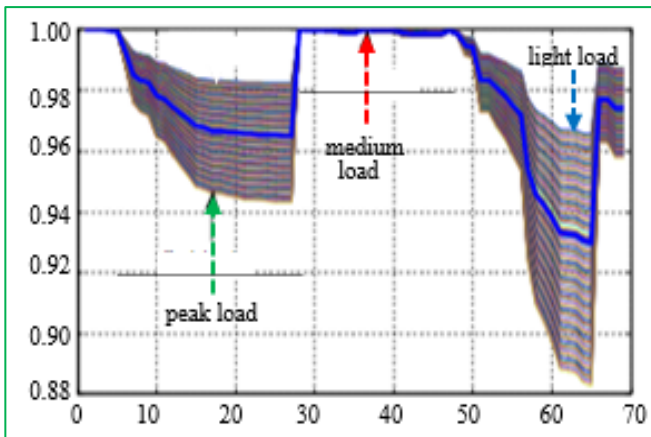


Figure 13. Voltage profile in system without DSTATCOM for different load variations

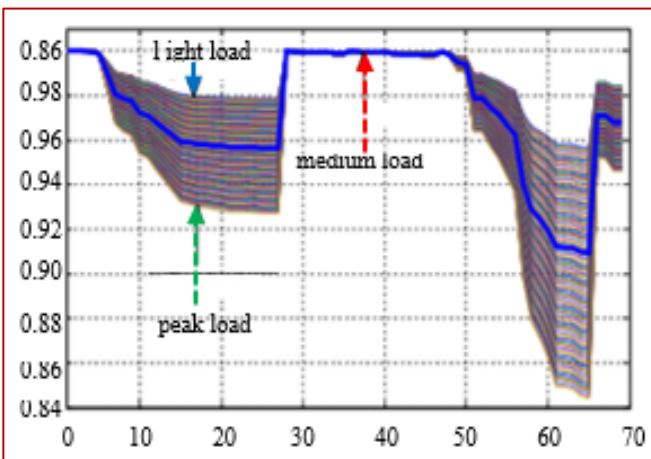


Figure 14. Voltage profile in system equipped with DSTATCOM for different load variations

The x-axis and the y-axis show voltage in perunit and bus number, respectively. As can be seen, the specifications of the distribution system have been improved using DSTATCOM. Figure 15 shows the reactive current variations through the distribution transformers of MG system with three DGs due to a fault at one of the busbars. Accordingly, the operation of DFACTS in MG1 and MG2 reduced the reactive current flowing out of MG3, which does not have a DFACTS connected mode.

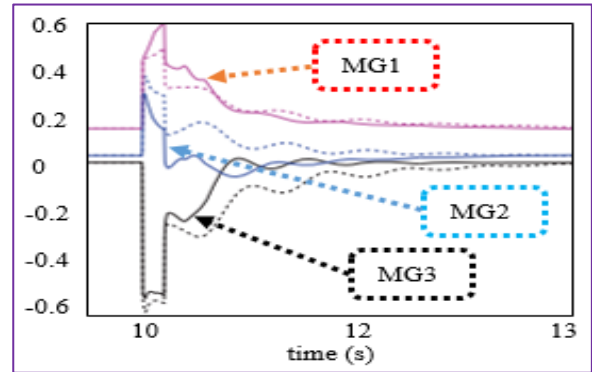


Figure 15. Reactive current variations with and without DSTATCOM

4.1.2. Improvement of Low-Voltage Ride-Through Capability

In a high-penetration MG under some minor or temporary faults, improved LVRT capability can help strengthen force support and reduce system instability [151]. The LVRT characteristics of MGs in different operating conditions were investigated in [152], in which the DSTATCOM at different locations of the MG was used to compensate for voltage drop to provide additional reactive power.

Various methods can be used to increase the LVRT capability of fixed-speed induction generator-based wind turbines, some of which were presented in [153], where DVR series connection and STATCOM shunt connection in simulation results had very efficient approaches to increasing LVRT capability.

DVR was used in between the source voltage and critical or sensitive load in the MG system to improve the LVRT capability in [154], where in case of using DVR, it usually requires the series transformer, energy storage system, and converter.

In order to increase the power quality and modify the ability of LVRT in a three-phase medium voltage network, the use of DVR was proposed in [155], where the network is connected to a hybrid distributed generation system and there are WTG, PV plants and sensitive load at the same PCC. A comparison between SFCL and DVR for LVRT improvement of an MG was presented in [156]; according to the demonstrated results, in power stabilization, SFCL exhibited better control effects. Figure 16 shows the frequency characteristics of the MG under the fault. As is seen, two devices can both mitigate the fault current from the microgrid to the PCC. Figure 17 shows the load power variation curves of the microgrid before and after the fault.

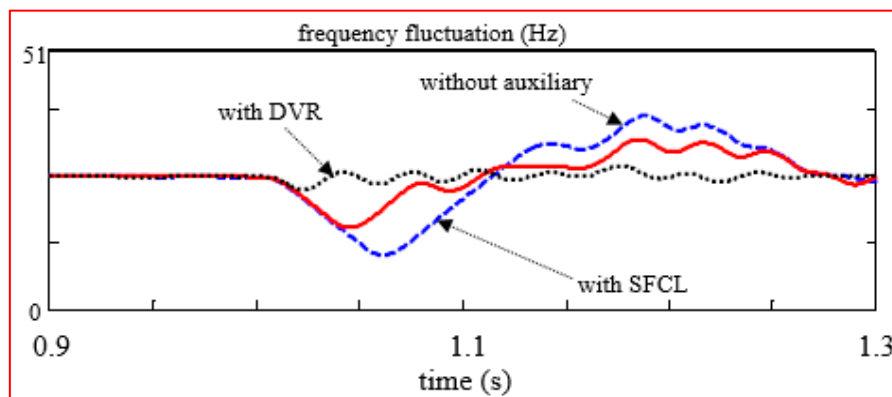


Figure 16. Frequency fluctuation in microgrids under the short-circuit fault

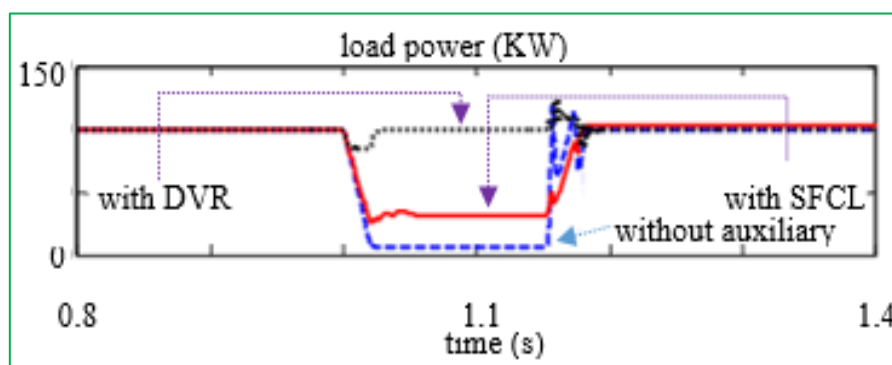


Figure 17. Load power in microgrids under the short-circuit fault

4.1.3. Power quality profile enhancement

When the microgrid is connected to the main grid, the impact of power quality issues is concerning and that can be a major issue for research. The major power quality problems are low power factor, high harmonic in distribution system, voltage flicker, active power and reactive power, increased reactive power required, and system voltage fluctuations [157].

In order to compensate for the power quality problems created in the system connected to the microgrid, the use of UPQC device was investigated in [158], where an ANFIS was used to increase the UPQC compensation capacity based on the voltage estimate of link DC and its voltage regulation.

For non-conventional sources based MGs, adaptive management of the voltage and reactive power required for them was presented in [159], where UPFC was used to investigate the hybrid MG and analysis of the test system and the tuned parameters of the PI controller of UPFC were with fuzzy.

An online method to adjust tracking of DSTATCOM set point in MGs by monitoring the PCC voltage and distributed resources currents was presented in [160], where online control of DSTATCOM was obtained through reinforcement learning algorithm. Based on the most modern power conditioning equipment such as UPQC in the microgrid energy system, the use of fuzzy logic method was proposed in [161] where the MG working in conjunction with this method was employed to track disruption in smart grids and improve system quality with high flexibility.

In order to improve the power quality and reduce fluctuations when changing the microgrid connection modes, UPQC was used in [162], where UPQC integration and control was done using the control method in distribution generation-based MG systems.

The performance of stand-alone hybrid renewable energy system was enhanced in [163] using an optimal PI controller of DVR. There are three energy sources in this hybrid system including wind turbines, fuel cells, and solar PV cells. In all the three sources, the voltage, current, and power waveforms were enhanced. Also, WTG dynamics improvement and continuous performance of three sources in fault conditions were achieved. This indicates an increase in system performance. Figures 18 and 19 show the current and rms voltage of the fuel cell, respectively, and illustrate the effect of DVR when a three-phase fault with a fault clearing time of 0.05 seconds is applied to the system. Fault clearing time ranges between 0.5 and 0.55 seconds.

4.1.4. Reliability enhancement

There are two types of objective functions used to solve the optimization problem: reliability indicators and system cost. Reliability enhancement is one of the benefits of MG system because it can work in grid-connected and islanding modes [164].

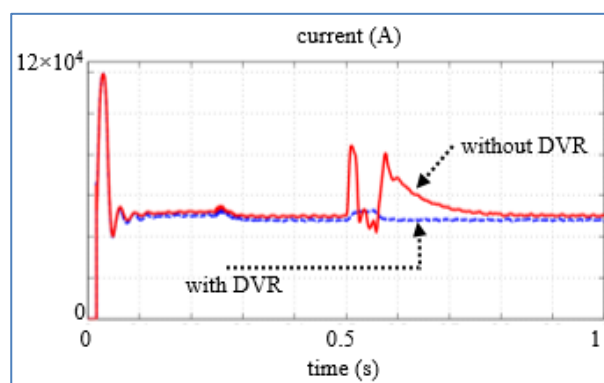


Figure 18. Influence of DVR on fuel cell output current at the three-phase fault

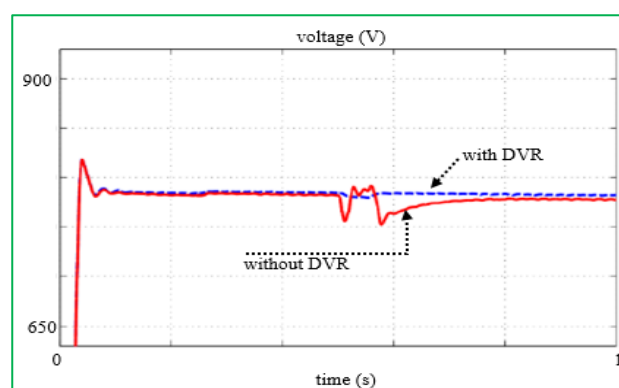


Figure 19. Influence of DVR on fuel cell output voltage at the three-phase fault

To improve the reliability and limit the fault current, a compensator was proposed as an interface between the main grid and the MG in [165]. To inject voltage when in the fault in the main network resurfaces in two different places, i.e., the main network and MG, the DVR is used to ensure normal operation.

A bidirectional dc SSCB to realize the bidirectional flow of energy was proposed in [166], which guaranteed higher dc MG operating efficiency.

4.1.5. Optimal scheduling

The goal of optimal scheduling is to optimize specific objective functions by planning the deployment of DGs, responsive loads, and power exchanges between the MG and the main network [167, 168].

Optimal scheduling of MG was presented in [169], where uncertain parameters for modeling based on a stochastic method include solar radiation, wind speed, and loads, and to transfer more power to the upstream grid, the compensator (DVR) is placed in line between the main grid and the microgrid.

To help the PV penetrate higher, a multi-objective method for programming microgrids was studied in [170]. In order to control the volt/var process, the existing control devices such as under-load tap changer and DSTATCOM were coordinated.

4.1.6. Dynamic stability

A number of approaches to enhancing microgrid stability exist: using different control methods, supplying the required reactive power, cutting off the load, and reducing its amount and distributed energy storage systems [171, 172]. Due to the weak inertia of the equivalent system, autonomous MG control and management is more difficult and requires public network support [173, 174].

An MG test system with DFACTS is considered to study the dynamic stability in [175] under various fault and load change conditions, in which the proposed method was given for control based on browser optimization and fuzzy logic.

The effect of an STATCOM on the frequency of islanded MGs based on frequency control using fuzzy cooperative control was investigated in [176], in which to achieve fast frequency control, instantaneous power balance between

generation and consumption could be supplied through energy storage systems such as battery with a proper frequency control method.

An impact method to stabilize reactive power changes in islanded MGs was applied using advanced FACTS device and the UPFC connected to the MG was proposed in [177], leading to voltage instability control.

An SDTATCOM was presented in [178] to reduce the changes in the positive and negative sequence components of the main voltage and fundamental frequency. In this respect, the installation location of DSTATCOM in a low-voltage MG was discussed.

4.1.7. Short-circuit protection

Due to the development of commercially viable equipment with fast performance and the need for coordination and reliability, proper short-circuit protection in MGs is important.

A short-circuit protection methodology based on SSCBs that provides FCL in low-voltage dc MGs was evaluated in [179], where SSCB solutions based on IGCT were possible for low-voltage microgrids according to the simulation results in a simple dc MG system, but it is necessary to connect several devices in parallel to open fast-rising fault currents.

An improved topology of the SSCB in dc MG was proposed in [180]. To determine the position of the fault, it is able to inject the signal into the faulty line.

4.2. Review study of DFACTS in microgrid

Some of the available review studies on the application of the DFACTS for improving the performance in MGs are mentioned in Table 8.

Table 8. A review of studies on DFACTS in microgrids

Ref.	Research topic	Specifications (Summary of the review studies)
[181]	Protection dc microgrid	The benefits and shortfalls of the wide bandgap SSCBs and its application with PV generators were investigated.
[182]	Power quality improvement	The techniques commonly used for power quality enhancement of MGs were presented. Methodologies such as PSO, filters, controllers, compensators, and DFACTS devices were analyzed.
[183]	Improve stability and power quality	A number of DFACTS devices were reviewed in terms of function. DFACTS devices can contribute to building independent and high-quality microgrids along with stability and quality improvement.
[184]	Reactive power compensation methods	Challenges and issues related to power quality in the microgrid were investigated. Compensation methods were expressed using various control techniques, algorithms, and devices.

5. CONCLUSIONS

Microgrids have many advantages over conventional power grid networks. An MG reduces power losses in the distribution system and improves network power capacity and reliability. Also, it provides local support for voltage and frequency regulation. In this paper, several researches that are related to MG and DFACTS were studied and reviewed. To use the DFACTS devices, they were mounted on transmission towers or connected to conductors. They have been widely used in distribution systems to improve the system performance. They offer many potential benefits for MG operations. Further, this paper also throws light on the major role of DFACTS in microgrid performance, some of its limitations, and future prospects.

6. ACKNOWLEDGEMENT

The author would like to thank the respected journal executive, journal editor, and referees for making suggestions to improve the quality of the paper. This research has been conducted at the Smart Microgrid Research Center, Najafabad Branch, Islamic Azad University, Najafabad, Iran.

NOMENCLATURE

ANFIS	Adaptive Neuro Fuzzy Inference System
DFACTS	Distributed Flexible AC Transmission System
DG	Distributed Generator
DPFC	Distributed Power Flow Controller
DSSC	Distributed Static Series Compensator
DSTATCOM	Distribution Static Synchronous Compensator
DVR	Dynamic Voltage Restorer
FACTS	Flexible AC Transmission System
FCL	Fault-Current Limiting

HVDC	High-Voltage DC
IGCT	Integrated Gate-Commutated Thyristor
IGCT	Integrated Gate-Commutated Thyristor
LFO	Low Frequency Oscillation
LVRT	Low-Voltage Ride-Through
MG	Microgrid
PCC	Point of Common Coupling
PI controller	Proportional-Integral Controller
PSO	Particle Swarm Optimization
PV	Photovoltaic
SFCL	Superconducting Fault Current Limiter
SSCB	Solid-State Circuit Breaker
SSSC	Static Synchronous Series Compensator
UPQC	Unified Power Quality Compensator
WBG	Wide Bandgap
WTG	Wind Turbine Generator

REFERENCES

- Vaez-Zadeh, S. and Zamanifar, M., "Efficiency optimization control of IPM synchronous motor drives with online parameter estimation", *Journal of Intelligent Procedures in Electrical Technology*, Vol. 2, (2011), 57-65. (<https://www.sid.ir/paper/573404/en>).
- Shahgholian, Gh., Rezaei, M.H., Etesami, A. and Yousefi, M.R., "Simulation of speed sensor less control of PMSM based on DTC method with MRAS", *Proceedings of the IEEE/IPEC*, Vol. 1, (2010), 40-45. (<http://dx.doi.org/10.1109/IPEC2010.5697127>).
- Peiravan, Z., Delshad, M. and Amini, M.R., "A new soft switching interleaved flyback converter with parallel coupled inductors and recovery leakage inductance energy", *Journal of Intelligent Procedures in Electrical Technology*, Vol. 13, (2022), 31-47. (<https://dorl.net/dor/20.1001.1.23223871.1401.13.50.2.3>).
- Hosseini, E., Shahgholian, Gh., Mahdavi-Nasab, H. and Mesrinejad, F., "Variable speed wind turbine pitch angle control using three-term fuzzy controller", *International Journal of Smart Electrical Engineering*, Vol. 11, (2022), 63-70. (<https://dorl.net/dor/20.1001.1.22519246.2022.11.02.2.0>).
- Faiz, J., Shahgholian, Gh. and Ehsan, M., "Stability analysis and simulation of a single-phase voltage source UPS inverter with two-stage cascade output filter", *European Transactions on Electrical Power*, Vol. 18, (2008), 29-49. (<https://doi.org/10.1002/etep.160>).
- Mirtalaei, S., Mohtaj, M. and Karami, H., "Design and implementation of a high step-up boost-sepic hybrid converter with soft switching", *Journal of Intelligent Procedures in Electrical Technology*, Vol. 6, (2016), 27-34. (<https://dorl.net/dor/20.1001.1.23223871.1394.6.24.3.3>).
- Moradi Nezhad, S., Saghafi, H., Delshad, M. and Sadeghi, R., "Nonparametric correlative-probabilistic microgrid power energy management based sine-cosine algorithm", *IEEE Access*, Vol. 9, (2021), 156323-156336. (<https://doi.org/10.1109/ACCESS.2021.3123981>).
- Shahgholian, Gh., and Shafaghi, P., "State space modeling and eigenvalue analysis of the permanent magnet DC motor drive system", *Proceedings of the IEEE/ICECT*, Vol. 1, Kuala Lumpur, Malaysia, (2010), 63-67. (<https://doi.org/10.1109/ICECTECH.2010.5479987>).
- Ghasemi, M., Roosta, A. and Fani, B., "Coordinated control of FACTS devices by using ADALINE neural network to enhance the transient stability of power system", *Journal of Intelligent Procedures in Electrical Technology*, Vol. 3, (2012), 27-40. (<https://dorl.net/dor/20.1001.1.23223871.1391.3.9.4.3>).
- Shabani, S., Delshad, M. and Sadeghi, R., "A soft switched non-isolated high step-up dc-dc converter with low number of auxiliary elements", *Journal of Intelligent Procedures in Electrical Technology*, Vol. 13, (2022), 125-138. (<https://dorl.net/dor/20.1001.1.23223871.1401.13.51.8.1>).
- Samadinasab, S., Namdari, F. and Bakshipoor, M., "A novel approach for earthing system design using finite element method", *Journal of Intelligent Procedures in Electrical Technology*, Vol. 8, (2017), 54-63. (<https://dorl.net/dor/20.1001.1.23223871.1396.8.29.6.0>).
- Badal, F.R., Das, P., Sarker, S.K. and Das, S.K., "A survey on control issues in renewable energy integration and microgrid", *Protection and Control of Modern Power Systems*, Vol. 4, (2019), 1-27. (<https://doi.org/10.1186/s41601-019-0122-8>).
- Ahmadpour, A., Shenava, S.S., Dejamkhooy, A. and Mokaramian, E., "Electromagnetic force analysis of transformer on the ferroresonance due to consecutive 3-phase short-circuit faults using finite element method (FEM)", *Journal of Intelligent Procedures in Electrical Technology*, Vol. 11, (2020), 47-60. (<https://dorl.net/dor/20.1001.1.23223871.1399.11.41.4.3>).
- Fooladgar, M., Rok-Rok, E., Fani, B. and Shahgholian, Gh., "Evaluation of the trajectory sensitivity analysis of the DFIG control parameters in response to changes in wind speed and the line impedance connection to the grid DFIG", *Journal of Intelligent Procedures in Electrical Technology*, Vol. 5, (2015), 37-54. (<https://dorl.net/dor/20.1001.1.23223871.1393.5.20.4.9>).
- Abedi, A., Rezaie, B., Khosravi, A. and Shahabi, M., "A novel local control technique for converter-based renewable energy resources in the stand-alone dc micro-grids", *Journal of Renewable Energy and Environment*, Vol. 7, No. 2, (2020), 52-63. (<https://dx.doi.org/10.30501/jree.2020.107365>).
- Zamanian, S., Sadi, S., Ghaffarpour, R. and Mahdavian, A., "Inverter-based microgrid dynamic stability analysis considering inventory of dynamic and static load models", *Journal of Intelligent Procedures in Electrical Technology*, Vol. 11, (2021), 91-109. (<https://dorl.net/dor/20.1001.1.23223871.1399.11.44.6.1>).
- Hosseini, E. and Shahgholian, Gh., "Partial- or full-power production in WECS: A survey of control and structural strategies", *European Power Electronics and Drives*, Vol. 27, (2017), 125-142. (<https://doi.org/10.1080/09398368.2017.1413161>).
- Haghshenas, Gh., Mirtalaei, S.M.M., Mordmand, H. and Shahgholian, Gh., "High step-up boost-flyback converter with soft switching for photovoltaic applications", *Journal of Circuits, Systems, and Computers*, Vol. 28, No. 1, (2019), 1-16. (<http://dx.doi.org/10.1142/S0218126619500142>), (ISSN: 0218-1266).
- Hosseini, E. and Shahgholian, Gh., "Different types of pitch angle control strategies used in wind turbine system applications", *Journal of Renewable Energy and Environment (JREE)*, Vol. 4, (2017), 20-35. (<https://dx.doi.org/10.30501/jree.2017.70103>).
- Mahdavian, M., Shahgholian, Gh., Janghorbani, M., Soltani, B. and Wattanapongsakorn, N., "Load frequency control in power system with hydro turbine under various conditions", *Proceedings of 12th International Conference on Electrical Engineering/Electronics, Computer, Telecommunications and Information Technology (ECTI-CON)*, Hua Hin, Thailand, (2015), 1-5. (<http://dx.doi.org/10.1109/ECTICon.2015.7206938>).
- Aghadavoodi, E. and Shahgholian, Gh., "A new practical feed-forward cascade analyze for close loop identification of combustion control loop system through RANFIS and NARX", *Applied Thermal Engineering*, Vol. 133, (2018), 381-395. (<http://dx.doi.org/10.1016/j.applthermaleng.2018.01.075>).
- Hosseini, E. and Shahgholian, Gh., "Output power levelling for DFIG wind turbine system using intelligent pitch angle control", *Automatika*, Vol. 58, (2017), 363-374. (<http://dx.doi.org/10.1080/00051144.2018.1455017>).
- Khani, K. and Shahgholian, Gh., "Analysis and optimization of frequency control in isolated microgrid with double-fed induction-generators based wind turbine", *Journal of International Council on Electrical Engineering*, Vol. 9, (2019), 24-37. (<http://dx.doi.org/10.1080/22348972.2018.1564547>).
- Yengijeh, N.P., Moradi CheshmehBeigi, H. and Hajizadeh, A., "Inertia emulation with the concept of virtual supercapacitor for islanded dc microgrid", *Proceedings of the IEEE/IWEC*, Vol. 1, Shahrood, Iran, (2021). (<http://dx.doi.org/10.1109/IWEC52400.2021.9467013>).
- Shahgholian, Gh., "An overview of hydroelectric power plant: Operation, modeling, and control", *Journal of Renewable Energy and Environment (JREE)*, Vol. 7, (2020), 14-28. (<https://dx.doi.org/10.30501/jree.2020.221567.1087>).
- Bagheri, S. and Moradi CheshmehBeigi, H., "DC microgrid voltage stability through inertia enhancement using a bidirectional dc-dc converter", *Proceedings of the IEEE/IWEC*, Vol. 1, Shahrood, Iran, (2021), 1-5. (<https://dx.doi.org/10.1109/IWEC52400.2021.9467032>).
- Keyvani-Boroujeni, B., Fani, B., Shahgholian, Gh. and Alhelou, H.H., "Virtual impedance-based droop control scheme to avoid power quality and stability problems in VSI-dominated microgrids", *IEEE Access*, Vol. 9, (2012), 144999-145011. (<https://doi.org/10.1109/ACCESS.2021.3122800>).
- Karimi, H., Fani, B. and Shahgholian, Gh., "Coordinated protection scheme based on virtual impedance control for loop-based microgrids",

- Journal of Intelligent Procedures in Electrical Technology*, Vol. 12, (2021), 15-32. (https://jipet.iaun.iau.ir/article_678745.html?lang=en).
29. Shahgholian, Gh. and Ebrahimi-Salary, M., "Effect of load shedding strategy on interconnected power systems stability when a blackout occurs", *International Journal of Computer and Electrical Engineering*, Vol. 4, No. 2, (2012), 212-216. (<http://dx.doi.org/10.7763/IJCEE.2012.V4.481>).
 30. Abbasi, M., Nafar, M. and Simab, M., "Management and control of microgrids connected to three-phase network with the approach of activating current limitation under unbalanced errors using fuzzy intelligent method with the presence of battery, wind, photovoltaic and diesel sources", *Journal of Intelligent Procedures in Electrical Technology*, Vol. 13, (2022), 59-71. (https://jipet.iaun.iau.ir/article_682223.html?lang=en).
 31. Gorji, S., Zamanian, S. and Moazzami, M., "Techno-economic and environmental base approach for optimal energy management of microgrids using crow search algorithm", *Journal of Intelligent Procedures in Electrical Technology*, Vol. 11, (2020), 49-68. (https://jipet.iaun.iau.ir/article_674939.html?lang=en).
 32. Shahgholian, Gh., Arezoomand, M. and Mahmoodian, H., "Analysis and simulation of the single-machine infinite-bus with power system stabilizer and parameters variation effects", *Proceedings of the IEEE/ICIAS*, Vol. 1, Kuala Lumpur, Malaysia, (2007), 161-171. (<http://dx.doi.org/10.1109/ICIAS.2007.4658368>).
 33. Shahgholian, Gh., "Analysis and simulation of dynamic performance for DFIG-based wind farm connected to a distribution system", *Energy Equipment and Systems*, Vol. 6, No. 2, (2018), 117-130. (<https://dx.doi.org/10.22059/ees.2018.31531>).
 34. Fayazi, H., Fani, B., Moazzami, M. and Shahgholian, Gh., "An offline three-level protection coordination scheme for distribution systems considering transient stability of synchronous distributed generation", *International Journal of Electrical Power and Energy Systems*, Vol. 131, (2021), 107069. (<https://dx.doi.org/10.1016/j.ijepes.2021.107069>).
 35. Kiani, A., Fani, B. and Shahgholian, Gh., "A multi-agent solution to multi-thread protection of DG-dominated distribution networks", *International Journal of Electrical Power and Energy Systems*, Vol. 130, (2021), 106921. (<https://dx.doi.org/10.1016/j.ijepes.2021.106921>).
 36. Singh, B., Al-Haddad, K. and Chandra, A., "A review of active filters for power quality improvement", *IEEE Transactions on Industrial Electronics*, Vol. 46, No. 5, (1999), 960-971. (<http://dx.doi.org/10.1109/41.793345>).
 37. Kadam, S.S. and Kanse, Y.K., "DSTATCOM for power quality improvement", *Proceedings of the IEEE/ICSDNET*, Vol. 1, Kottayam, India, (2018), 1-5. (<http://dx.doi.org/10.1109/ICSDNET.2018.8821066>).
 38. Fayazi, H., Moazzami, M., Fani, B. and Shahgholian, Gh., "Coordination of protection equipment in synchronous generator-based microgrids with regard to maintaining first swing stability", *Journal of Intelligent Procedures in Electrical Technology*, Vol. 14, (2023), 1-14. (https://jipet.iaun.iau.ir/article_682345.html).
 39. Omar, A.I., Aleem, S.H.E.A., El-Zahab, E.E.A., Algablawy, M. and Ali, Z.M., "An improved approach for robust control of dynamic voltage restorer and power quality enhancement using grasshopper optimization algorithm", *ISA Transactions*, Vol. 95, (2019), 110-129. (<http://dx.doi.org/10.1016/j.isatra.2019.05.001>).
 40. Patrao, I., Figueres, E., Garcerá, G. and González-Medina, R., "Microgrid architectures for low voltage distributed generation", *Renewable and Sustainable Energy Reviews*, Vol. 43, (2015), 415-424. (<https://doi.org/10.1016/j.rser.2014.11.054>).
 41. Micallef, A., "Review of the current challenges and methods to mitigate power quality issues in single-phase microgrids", *IET Generation, Transmission and Distribution*, Vol. 13, No. 1, (2019), 2044-2054. (<https://doi.org/10.1049/iet-gtd.2018.6020>).
 42. Shahgholian, Gh., Mahdavian, M., Emami, A. and Ahmadzade, B., "Improve power quality using static synchronous compensator with fuzzy logic controller", *Proceedings of the IEEE/ICEMS*, Beijing, China, (2011), 1-5. (<https://doi.org/10.1109/ICEMS.2011.6073830>).
 43. Mahdavian, M. and Jabbari, M., "Design and implementation of a shunt active power filter for enhancing power quality", *Journal of Intelligent Procedures in Electrical Technology*, Vol. 1, No. 4, (2011), 25-32. (https://jipet.iaun.iau.ir/article_550750.html?lang=en).
 44. Shahgholian, Gh. and Izadpanahi, N., "Improving the performance of wind turbine equipped with DFIG using STATCOM based on input-output feedback linearization controller", *Energy Equipment and Systems*, Vol. 4, No. 1, (2016), 65-79. (<http://dx.doi.org/10.22059/EES.2016.20128>).
 45. Samal, S. and Hota, P.K., "Design and analysis of solar PV-fuel cell and wind energy based microgrid system for power quality improvement", *Journal Cogent Engineering*, Vol. 4, (2017), 1-21. (<http://dx.doi.org/10.1080/23311916.2017.1402453>).
 46. Shahgholian, Gh., Shafaghi, P., Moalem, S. and Mahdavian, M., "Damping power system oscillations in single-machine infinite-bus power system using a STATCOM", *Proceeding of the IEEE/ICCEE*, Vol. 1, Dubai, United Arab Emirates, (2009), 130-134. (<http://dx.doi.org/10.1109/ICCEE.2009.30>).
 47. Faiz, J. and Shahgholian, Gh., "Modeling and damping controller design for static var compensator", *Proceedings of the IEEE/POWERENG*, Vol. 1, Riga, Latvia, (2015), 405-409. (<http://dx.doi.org/10.1109/PowerEng.2015.7266351>).
 48. Parastvand, H., Bass, O., Masoum, M.A.S., Chapman, A. and Lachowicz, S., "Cyber-security constrained placement of FACTS devices in power networks from a novel topological perspective", *IEEE Access*, Vol. 8, (2020), 108201-108215. (<https://doi.org/10.1109/ACCESS.2020.3001308>).
 49. Kamarposhti, M.A., Shokouhandeh, H., Colak, I., Band, S.S. and Eguchi, K., "Optimal location of FACTS devices in order to simultaneously improving transmission losses and stability margin using artificial bee colony algorithm", *IEEE Access*, Vol. 9, (2021), 125920-125929. (<https://doi.org/10.1109/ACCESS.2021.3108687>).
 50. Bone, G., Pantoš, M. and Mihalič, R., "Newtonian steady state modeling of FACTS devices using unaltered power-flow routines", *IEEE Transactions on Power Systems*, Vol. 34, (2019), 1216-1226. (<https://doi.org/10.1109/TPWRS.2018.2876407>).
 51. Nazaripouya, H. and Mehraeen, S., "Modeling and nonlinear optimal control of weak/islanded grids using FACTS device in a game theoretic approach", *IEEE Transactions on Control Systems Technology*, Vol. 24, No. 1, (2016), 158-171. (<https://doi.org/10.1109/TCST.2015.2421434>).
 52. Frolov, V., Thakurta, P.G., Backhaus, S., Bialek, J. and Chertkov, M., "Operations- and uncertainty-aware installation of FACTS devices in a large transmission system", *IEEE Transactions on Control of Network Systems*, Vol. 6, No. 3, (2019), 961-970. (<https://doi.org/10.1109/TCNS.2019.2899104>).
 53. Shahgholian, Gh., Maghsoodi, M. and Movahedi, A., "Fuzzy and proportional integral controller design for thyristor controlled series capacitor and power system stabilizer to improve power system stability", *Revue Roumaine des Sciences Techniques Serie Electrotechnique et Energetique*, Vol. 61, (2016), 418-423. (<https://www.semanticscholar.org/paper/FUZZY-AND-PROPORTIONAL-INTEGRAL-CONTROLLER-DESIGN-Shahgholian-Maghsoodi/010bcb370f286a5c11c09c6238e32be0d4546f99>).
 54. Motaghi, A., AalIzadeh, M. and Abbasian, M., "Reactive power compensation and reducing network transmission losses by optimal placement of parallel and series FACTS devices with fuzzy-evolutionary method", *Journal of Intelligent Procedures in Electrical Technology*, Vol. 9, (2019), 27-38. (https://jipet.iaun.iau.ir/article_620188.html?lang=en).
 55. Kazemi-Zahrani, A. and Parastegari, M., "Designing PSS and SVC parameters simultaneously through the improved quantum algorithm in the multi-machine power system", *Journal of Intelligent Procedures in Electrical Technology*, Vol. 8, (2017), 68-75. (https://jipet.iaun.iau.ir/article_597478.html?lang=en).
 56. Ghasemi, S. and Gholipoor, E., "Reactive power optimization in the presence of FACTS devices using evolutionary algorithms based on fuzzy logic", *Journal of Intelligent Procedures in Electrical Technology*, Vol. 6, (2015), 45-54. (<https://dori.net/dor/20.1001.1.23223871.1394.6.23.6.4>).
 57. Zanjani, S., Azimi, Z. and Azimi, M., "Assessment and analyze hybride control system in distribution static synchronous compensator based current source converter", *Journal of Intelligent Procedures in Electrical Technology*, Vol. 2, (2011), 59-67. (<https://dori.net/dor/20.1001.1.23223871.1390.2.7.7.5>).
 58. Barati, H., Saki, R. and Mortazavi, S., "Intelligent control of UPFC for enhancing transient stability on multi-machine power systems", *Journal of Intelligent Procedures in Electrical Technology*, Vol. 1, (2010), 3-12. (<https://dori.net/dor/20.1001.1.23223871.1389.1.1.1.0>).
 59. Shahgholian, Gh., Hamidpour, H. and Movahedi, A., "Transient stability promotion by FACTS controller based on adaptive inertia weight

- particle swarm optimization method", *Advances in Electrical and Electronic Engineering*, Vol. 16, (2018), 57-70. (<https://doi.org/10.15598/aece.v16i1.2369>).
60. Shahgholian, Gh. and Faiz, J., "Coordinated control of power system stabilizer and FACTS devices for dynamic performance enhancement-State of art", *Proceedings of the IEEE/IEPS*, Kyiv, Ukraine, (2016), 1-6. (<https://doi.org/10.1109/IEPS.2016.7521865>).
 61. Shahgholian, Gh. and Movahedi, A., "Coordinated control of TCSC and SVC for system stability enhancement using ANFIS method", *International Review on Modelling and Simulations*, Vol. 4, No. 5, (2011). (https://www.researchgate.net/publication/286221971_Coordinated_control_of_TCSC_and_SVC_for_system_stability_enhancement_using_A_NFIS_method).
 62. Peddakapu, K., Mohamed, M.R., Sulaiman, M.H., Srinivasarao, P., Veerendra, A.S. and Leung, P.K., "Performance analysis of distributed power flow controller with ultra-capacitor for regulating the frequency deviations in restructured power system", *Journal of Energy Storage*, Vol. 31, (2020), 101676. (<https://doi.org/10.1016/j.est.2020.101676>).
 63. Shahgholian, Gh., Mahdavian, M., Noorani Kalteh, M. and Janghorbani, M., "Design of a new IPFC-based damping neurocontrol for enhancing stability of a power system using particle swarm optimization", *International Journal of Smart Electrical Engineering*, Vol. 3, (2014), 73-78. (<https://dori.net/dor/20.1001.1.22519246.2014.03.02.2.4>).
 64. Faiz, J., Shahgholian, Gh. and Torabiyani, M., "Design and simulation of UPFC for enhancement of power quality in transmission lines", *Proceedings of the IEEE/POWERCON*, Vol. 1, Zhejiang, China, (2010), 1-5. (<http://dx.doi.org/10.1109/POWERCON.2010.5666588>).
 65. Shahgholian, Gh., Eshtehardiha, S., Mahdavinab, H. and Yousefi, M.R., "A novel approach in automatic control based on the genetic algorithm in STATCOM for improvement power system transient stability", *Proceedings of the IEEE/ICIS*, Vol. 1, Varna, (2008), 14-19. (<https://doi.org/10.1109/IS.2008.4670419>).
 66. Jafari, E., Marjanian, A., Silaymani, S. and Shahgholian, Gh., "Designing an emotional intelligent controller for IPFC to improve the transient stability based on energy function", *Journal of Electrical Engineering and Technology*, Vol. 8, (2013), 478-489. (<https://doi.org/10.5370/JEET.2013.8.3.478>).
 67. Shahgholian, Gh., Mardani, E., Mahdavian, M., Janghorbani, M., Azadeh, M. and Farazpey, S., "Impact of PSS and STATCOM on dynamic parameters of power system based on neuro-fuzzy controllers", *Proceedings of the IEEE/ECTICON*, Chiang Mai, Thailand, (2016), 1-4. (<https://doi.org/10.1109/ECTICON.2016.7561243>).
 68. Li, B., Xiao, G., Lu, R., Deng, R. and Bao, H., "On feasibility and limitations of detecting false data injection attacks on power grid state estimation using D-FACTS devices", *IEEE Transactions on Industrial Informatics*, Vol. 16, (2020), 854-864. (<http://dx.doi.org/10.1109/TII.2019.2922215>).
 69. Shahgholian, Gh., Faiz, J., Fani, B. and Yousefi, M.R., "Operation, modeling, control and applications of static synchronous compensator: A review", *Proceedings of the IEEE/IPEC*, Vol. 1, Singapore, (2010), 596-601. (<http://dx.doi.org/10.1109/IPECON.2010.5697064>).
 70. Ning, G., He, S., Wang, Y., Yao, L. and Wang, Z., "A novel distributed flexible ac transmission system controller based on active variable inductance (AVI)", *Proceedings of the IEEE/PESC*, Vol. 1, Jeju, South Korea, (2006), 1-4. (<http://dx.doi.org/10.1109/pesc.2006.1711970>).
 71. Bruno, S., Carne, G.D. and Scala, M.L., "Distributed FACTS for power system transient stability control", *Energies*, Vol. 13, 1-16. (<http://dx.doi.org/10.3390/en13112901>).
 72. Abdelsalam, A.A., Gabbar, H.A. and Sharaf, A.M., "Performance enhancement of hybrid AC/DC microgrid based D-FACTS", *Electrical Power and Energy Systems*, Vol. 63, (2014), 382-393. (<https://doi.org/10.1016/j.ijepes.2014.06.003>).
 73. Shahgholian, Gh., Fani, B., Keyvani, B., Karimi, H. and Moazzami, M., "Improve the reactive power sharing by uses to modify droop characteristics in autonomous microgrids", *Energy Engineering and Management*, Vol. 9, (2019), 64-71. (https://energy.kashanu.ac.ir/index.php?slc_lang=en&sid=1).
 74. Fayazi, H., Moazzami, M., Fani, B. and Shahgholian, Gh., "A first swing stability improvement approach in microgrids with synchronous distributed generators", *International Transactions on Electrical Energy Systems*, Vol. 31, (2021), e12816. (<http://dx.doi.org/10.1002/2050-7038.12816>).
 75. Shahgholian, Gh., "A brief review on microgrids: Operation, applications, modeling, and control", *International Transactions on Electrical Energy Systems*, Vol. 31, (2021), e12885. (<https://doi.org/10.1002/2050-7038.12885>).
 76. Keyvani-Boroujeni, B., Shahgholian, Gh. and Fani, B., "A distributed secondary control approach for inverter-dominated microgrids with application to avoiding bifurcation-triggered instabilities", *IEEE Journal of Emerging and Selected Topics in Power Electronics*, Vol. 8, No. 4, (2020), 3361-3371. (<http://doi.org/10.1109/JESTPE.2020.2974756>).
 77. Shafiee, Q., Nasirian, V., Vasquez, J.C., Guerrero, J.M. and Davoudi, A., "A multi-functional fully distributed control framework for ac microgrids", *IEEE Transactions on Smart Grid*, Vol. 9, No. 4, (2018), 3247-3258. (<http://dx.doi.org/10.1109/TSG.2016.2628785>).
 78. Wang, Z., Liu, F., Chen, Y., Low, S.H. and Mei, S., "Unified distributed control of stand-alone dc microgrids", *IEEE Transactions on Smart Grid*, Vol. 10, No. 1, (2019), 1013-1024. (<http://dx.doi.org/10.1109/TSG.2017.2757498>).
 79. Ahmadi, R. and Ferdowsi, M., "Improving the performance of a line regulating converter in a converter-dominated DC microgrid system", *IEEE Transactions on Smart Grid*, Vol. 5, (2014), 2553-2563. (<http://dx.doi.org/10.1109/TSG.2014.2319267>).
 80. Wang, J., Jin, C. and Wang, P., "A uniform control strategy for the interlinking converter in hierarchical controlled hybrid AC/DC microgrids", *IEEE Transactions on Industrial Electronics*, Vol. 65, (2018), 6188-6197. (<http://dx.doi.org/10.1109/TIE.2017.2784349>).
 81. Aprilia, E., Meng, K., Hosani, M.A., Zeineldin, H.H. and Dong, Z.Y., "Unified power flow algorithm for standalone ac/dc hybrid microgrids", *IEEE Transactions on Smart Grid*, Vol. 10, (2019), 639-649. (<http://dx.doi.org/10.1109/TSG.2017.2749435>).
 82. Kamali, M., Fani, B., Shahgholian, Gh., Gharehpertian, G.B. and Shafiee, M., "Harmonic compensation and micro-grid voltage and frequency control based on power proportional distribution with adaptive virtual impedance method", *Journal of Intelligent Procedures in Electrical Technology*, Vol. 14, (2023), 33-60. (In Farsi). (http://jipet.iaun.ac.ir/article_688614.html?lang=en).
 83. Karimi, H., Shahgholian, Gh., Fani, B., Sadeghkhani, I. and Moazzami, M., "A protection strategy for inverter interfaced islanded microgrids with looped configuration", *Electrical Engineering*, Vol. 101, No. 3, (2019), 1059-1073. (<https://doi.org/10.1007/s00202-019-00841-6>).
 84. Xiao, Z., Wu, J. and Jenkins, N., "An overview of microgrid control", *Journal Intelligent Automation and Soft Computing*, Vol. 16, (2010), 199-212. (<https://portal.arid.my/Publications/fbedd8d3-ea1b-48.pdf>).
 85. Shuai, Z., Sun, Y., Shen, Z.J., Tian, W., Tu, C., Li, Y. and Yin, X., "Microgrid stability: Classification and a review", *Renewable and Sustainable Energy Reviews*, Vol. 58, (2016), 167-179. (<https://doi.org/10.1016/j.rser.2015.12.201>).
 86. Sadegehan, M., Fani, B., Sadeghkhani, I. and Shahgholian, Gh., "A local power control scheme for electronically interfaced distributed generators in islanded microgrids", *Iranian Electric Industry Journal of Quality and Productivity*, Vol. 8, No. 3, (2020), 47-58. (<http://dx.doi.org/10.29252/iejqp.8.3.47>).
 87. Xu, Y., Xiao, X., Sun, Y. and Long, Y., "Voltage sag compensation strategy for unified power quality conditioner with simultaneous reactive power injection", *Journal of Modern Power Systems and Clean Energy*, Vol. 4, (2016), 113-122. (<http://dx.doi.org/10.1007/s40565-016-0183-x>).
 88. Campanhol, L.B.G., da Silva, S.A.O., de Oliveira, A.A. and Bacon, V.D., "Power flow and stability analyses of a multifunctional distributed generation system integrating a photovoltaic system with unified power quality conditioner", *IEEE Transactions on Power Electronics*, Vol. 34, (2019), 6241-6256. (<https://doi.org/10.1109/TPEL.2018.2873503>).
 89. Naidu, R.P.K. and Meikandasivam, S., "Power quality enhancement in a grid-connected hybrid system with coordinated PQ theory & fractional order PID controller in DPFC", *Sustainable Energy, Grids and Networks*, Vol. 21, (2020), 100317. (<http://dx.doi.org/10.1016/j.segan.2020.100317>).
 90. Hossam-Eldin, A.A., Abdallah, E.N., Elgamal, M.S. and Aboras, K.M., "Fault ride-through of grid-connected THIPWM fired DCMLI-based DFIG using parallel switched feedback-controlled DVR", *IET Generation, Transmission and Distribution*, Vol. 14, (2020), 945-954. (<http://dx.doi.org/10.1049/iet-gtd.2019.0215>).
 91. Mansoor, M., Mariun, N., Toudeshki, A., Wahab, N.I.A. and Hojabri, M., "Innovating problem solving in power quality devices: A survey

- based on dynamic voltage restorer case (DVR)", *Renewable and Sustainable Energy Reviews*, (2017). (<http://dx.doi.org/10.1016/j.rser.2016.12.022>).
92. Dorostkar-Ghamsari, M., Fotuhi-Firuzabad, M. and Aminifar, F., "Probabilistic worth assessment of distributed static series compensators", *IEEE Transactions on Power Delivery*, Vol. 26, (2011), 1734-1743. (<https://doi.org/10.1109/TPWRD.2011.2127497>).
 93. Amini, A. and Kargar, A., "Reduction of sub-synchronous resonances with D-FACTS devices using intelligent control", *Journal of Intelligent Procedures in Electrical Technology*, Vol. 7, (2016), 3-14. (https://jipet.iaun.iau.ir/article_561188.html?lang=en).
 94. Singh, B., Arya, S.R. and Jain, C., "Simple peak detection control algorithm of distribution static compensator for power quality improvement", *IET Power Electronics*, Vol. 7, No. 7, (2014), 1736-1746. (<http://dx.doi.org/10.1049/iet-pel.2013.0494>).
 95. Mahdavian, M. and Shahgholian, Gh., "State space analysis of power system stability enhancement with used the STATCOM", *Proceedings of the IEEE/ECTI*, Vol. 1, Chiang Mai, Thailand, (2010), 1201-1205. (<https://ieeexplore.ieee.org/document/5491668>).
 96. Noori, A., Zhang, Y., Nouri, N. and M. Hajivand, "Hybrid allocation of capacitor and distributed static compensator in radial distribution networks using multi-objective improved golden ratio optimization based on fuzzy decision making", *IEEE Access*, Vol. 8, (2020), 162180-162195. (<https://doi.org/10.1109/ACCESS.2020.2993693>).
 97. Gayatri, M.T.L., Parimi, A.M. and Kumar, A.V.P., "Microgrid reactive power compensation using UPQC with common DC link energy restored by PV array", *Proceedings of the IEEE/ICETETS*, Pudukkottai, India, (2016), 1-8 (<http://dx.doi.org/10.1109/ICETETS.2016.7603079>).
 98. Gowrishankar, A. and Ramasamy, M., "SPV-based UPQC with modified power angle control scheme for the enhancement of power quality", *Journal of Circuits, Systems and Computers*, Vol. 29, No. 04, Article No. 2050064, (2020). (<https://doi.org/10.1142/S0218126620500644>).
 99. Khadkikar, V. and Chandra, A., "A new control philosophy for a unified power quality conditioner (UPQC) to coordinate load-reactive power demand between shunt and series inverters", *IEEE Transactions on Power Delivery*, Vol. 23, (2008), 2522-2534. (<http://dx.doi.org/10.1109/TPWRD.2008.921146>).
 100. Rajarajan, R. and Prakash, R., "A reformed adaptive frequency passiveness control for unified power quality compensator with model parameter ability to improve power quality", *Microprocessors and Microsystems*, Vol. 73, (2020), 102984. (<http://dx.doi.org/10.1016/j.micpro.2019.102984>).
 101. Lee, W.C., Lee, D.M. and Lee, T.K., "New control scheme for a unified power-quality compensator-q with minimum active power injection", *IEEE Transactions on Power Delivery*, Vol. 25, (2010), 1068-1076. (<http://dx.doi.org/10.1109/TPWRD.2009.2031556>).
 102. Dash, S.K. and Ray, P.K., "Power quality improvement utilizing PV fed unified power quality conditioner based on UV-PI and PR-R controller", *CPSS Transactions on Power Electronics and Applications*, Vol. 3, (2018), 243-253. (<http://dx.doi.org/10.24295/CPSSPEA.2018.00024>).
 103. Sebastian, P. and Nair, U., "Improved low voltage ride through capability of a fixed speed wind generator using dynamic voltage restorer", *Procedia Technology*, Vol. 25, (2016), 767-774. (<http://dx.doi.org/10.1016/j.protcy.2016.08.171>).
 104. Hassanein, W.S., Ahmed, M.M., Raouf, M.O., Ashmawy, M.G. and Mosaad, M.I., "Performance improvement of off-grid hybrid renewable energy system using dynamic voltage restorer", *Alexandria Engineering Journal*, Vol. 59, No. 3, (2020), 1567-1581. (<http://dx.doi.org/10.1016/j.aej.2020.03.037>).
 105. Jerin, A.R.A., Palanisamy, K., Umashankar, S. and Thirumoorthy, A.D., "Power quality improvement of grid connected wind farms through voltage restoration using dynamic voltage restorer", *International Journal of Renewable Energy Research*, Vol. 6, (2016), 53-60. (<https://doi.org/10.20508/ijrer.v6i1.3070.g6759>).
 106. Tu, C., Guo, Q., Jiang, F., Chen, C., Li, X., Xiao, F. and Gao, J., "Dynamic voltage restorer with an improved strategy to voltage sag compensation and energy self-recovery", *CPSS Transactions on Power Electronics and Applications*, Vol. 4, (2019), 219-229 (<http://dx.doi.org/10.24295/CPSSPEA.2019.00021>).
 107. Rauf, A.M. and Khadkikar, V., "An enhanced voltage sag compensation scheme for dynamic voltage restorer", *IEEE Transactions on Industrial Electronics*, Vol. 62, (2015), 2683-2692. (<http://dx.doi.org/10.1109/TIE.2014.2362096>).
 108. Torres, A.P., Roncero-Sánchez, P., Vázquez, J., López-Alcolea, F.J. and Molina-Martínez, E.J., "A discrete-time control method for fast transient voltage-sag compensation in DVR", *IEEE Access*, Vol. 7, (2019), 564-577. (<http://dx.doi.org/10.1109/ACCESS.2019.2955177>).
 109. Sitharthan, R., Sundarabalan, C.K., Devalalaji, K.R., Nataraj, S.K. and Karthikeyan, M., "Improved fault ride through capability of DFIG-wind turbines using customized dynamic voltage restorer", *Sustainable Cities and Society*, Vol. 39, (2018), 114-125. (<http://dx.doi.org/10.1016/j.scs.2018.02.008>).
 110. Brissette, A., Maksimović, D. and Levron, Y., "Distributed series static compensator deployment using a linearized transmission system model", *IEEE Transactions on Power Delivery*, Vol. 30, (2015), 1269-1277. (<http://dx.doi.org/10.1109/TPWRD.2014.2362764>).
 111. Gaigowal, S.R. and Renge, M.M., "DSSC: A distributed power flow controller", *Energy Procedia*, Vol. 117, (2017), 745-752. (<http://dx.doi.org/10.1016/j.egypro.2017.05.190>).
 112. Khazaie, J., Mokhtari, M., Khalilyan, M. and Nazarpour, D., "Sub-synchronous resonance damping using distributed static series compensator (DSSC) enhanced with fuzzy logic controller", *International Journal of Electrical Power and Energy Systems*, Vol. 43, (2012), 80-89. (<http://dx.doi.org/10.1016/j.ijepes.2012.05.009>).
 113. Pashaie, A., Zahawi, B. and Giaouris, D., "Distributed static series compensation for distribution network line voltage profile improvement", *Proceedings of the IEEE/PES*, Vol. 1, Manchester, UK, (2011), 1-4. (<http://dx.doi.org/10.1109/ISGTEurope.2011.6162823>).
 114. Dorostkar-Ghamsari, M., Fotuhi-Firuzabad, M., Aminifar, F., Safdarian, A. and Lehtonen, M., "Optimal distributed static series compensator placement for enhancing power system loadability and reliability", *IET Generation, Transmission and Distribution*, Vol. 9, (2015), 1043-1050. (<http://dx.doi.org/10.1049/iet-gtd.2014.0958>).
 115. Divan, D.M., Brumsickle, W.E., Schneider, R.S., Kranz, B., Gascoigne, R.W., Bradshaw, D.T., Ingram, M.R. and Grant, I.S., "A distributed static series compensator system for realizing active power flow control on existing power lines", *IEEE Transactions on Power Delivery*, Vol. 22, (2007), 642-649. (<http://dx.doi.org/10.1109/TPWRD.2006.887103>).
 116. Divan, D. and Johal, H., "Distributed FACTS- A new concept for realizing grid power flow control", *IEEE Transactions on Power Electronics*, Vol. 22, (2007), 2253-2260. (<http://dx.doi.org/10.1109/TPEL.2007.909252>).
 117. Shahgholian, Gh., Mahdavian, M., Janghorbani, M., Eshaghpour, I. and Ganji, E., "Analysis and simulation of UPFC in electrical power system for power flow control", *Proceedings of the IEEE/ECTICON*, Vol. 1, Phuket, Thailand, (2017), 62-65. (<https://doi.org/10.1109/ECTICON.2017.8096173>).
 118. Yuan, Z., Haan, S.W.H., Ferreira, J.B. and Cvoric, D., "A FACTS device: Distributed power-flow controller (DPFC)", *IEEE Transactions on Power Electronics*, Vol. 25, (2010), 2564-2572. (<http://dx.doi.org/10.1109/TPEL.2010.2050494>).
 119. Safari, A., Soulat, B. and Ajami, A., "Modeling and unified tuning of distributed power flow controller for damping of power system oscillations", *Ain Shams Engineering Journal*, Vol. 4, (2013), 775-782. (<http://dx.doi.org/10.1016/j.asej.2013.02.003>).
 120. Tang, A., Shao, Y., Xu, Q., Zheng, X., Zhao, H. and Xu, D., "Multi-objective coordination control of distributed power flow controller", *CSEE Journal of Power and Energy Systems*, Vol. 5, (2019), 348-354. (<http://dx.doi.org/10.17775/CSEEJPES.2018.01450>).
 121. Dai, J., Tang, Y., Liu, Y., Ning, J., Wang, Q., Zhu, N. and Zhao, J., "Optimal configuration of distributed power flow controller to enhance system loadability via mixed integer linear programming", *Journal of Modern Power Systems and Clean Energy*, Vol. 7, (2019), 1484-1494. (<http://dx.doi.org/10.1007/s40565-019-0568-8>).
 122. Shahgholian, Gh., Haghjoo, E., Seifi, A. and Hassanzadeh, I., "The improvement DSTATCOM to enhance the quality of power using fuzzy-neural controller", *Journal of Intelligent Procedures in Electrical Technology*, Vol. 2, (2011), 3-16. (https://jipet.iaun.iau.ir/article_550725.html?lang=en).
 123. Shahgholian, Gh. and Azimi, Z., "Analysis and design of a DSTATCOM based on sliding mode control strategy for improvement of voltage sag in distribution systems", *Electronics*, Vol. 5, No. 3, (2016), 1-12. (<http://dx.doi.org/10.3390/electronics5030041>).
 124. Patel, N., Gupta, N. and Babu, B.C., "Photovoltaic system operation as DSTATCOM for power quality improvement employing active current

- control", *IET Generation, Transmission and Distribution*, Vol. 14, No. 17, (2020), 3518-3529. (<http://dx.doi.org/10.1049/iet-gtd.2019.1487>).
125. Iqbal, F., Khan, M.T. and Siddiqui, A.S., "Optimal placement of DG and DSTATCOM for loss reduction and voltage profile improvement", *Alexandria Engineering Journal*, Vol. 57, No. 2, (2018), 755-765. (<http://dx.doi.org/10.1016/j.aej.2017.03.002>).
 126. Eswaran, T. and Kumar, V.S., "Particle swarm optimization (PSO)-based tuning technique for PI controller for management of a distributed static synchronous compensator (DSTATCOM) for improved dynamic response and power quality", *Journal of Applied Research and Technology*, Vol. 15, No. 2, (2017), 173-189. (<http://dx.doi.org/10.1016/j.jart.2017.01.011>).
 127. Arya, S.R., Singh, B., Niwas, R., Chandra, A. and Al-Haddad, K., "Power quality enhancement using DSTATCOM in distributed power generation system", *IEEE Transactions on Industry Applications*, Vol. 52, No. 6, (2016), 5203-5212. (<http://dx.doi.org/10.1109/TIA.2016.2600644>).
 128. Tolabi, H.B., Hosseini, R. and Shakarami, M.R., "A robust hybrid fuzzy-simulated annealing-intelligent water drops approach for tuning a distribution static compensator nonlinear controller in a distribution system", *Journal Engineering Optimization*, Vol. 48, (2016), 1-20. (<https://doi.org/10.1080/0305215X.2015.1080579>).
 129. Cairoli, P., Pan, Z., Tschida, C., Wang, Z., Ramanan, V.R., Raciti, L. and Antoniazzi, A., "Solid-state circuit breaker protection for dc shipboard power systems: breaker design, protection scheme, validation testing", *IEEE Transactions on Industry Applications*, Vol. 56, No. 2, (2020), 952-960. (<http://dx.doi.org/10.1109/TIA.2019.2962762>).
 130. Li, B., He, J., Li, Y. and Li, R., "A novel solid-state circuit breaker with self-adapt fault current limiting capability for LVDC distribution network", *IEEE Transactions on Power Electronics*, Vol. 34, No. 4, (2019), 3516-3529. (<http://dx.doi.org/10.1109/TPEL.2018.2850441>).
 131. Liu, F., Liu, W., Zha, X., Yang, H. and Feng, K., "Solid-state circuit breaker snubber design for transient overvoltage suppression at bus fault interruption in low-voltage dc microgrid", *IEEE Transactions on Power Electronics*, Vol. 32, No. 4, (2017), 3007-3021. (<http://dx.doi.org/10.1109/TPEL.2016.2574751>).
 132. Song, S., Kim, J., Choi, S., Kim, I. and Choi, S., "New simple-structured ac solid-state circuit breaker", *IEEE Transactions on Industrial Electronics*, Vol. 65, No. 11, (2018), 8455-8463. (<http://dx.doi.org/10.1109/TIE.2018.2809674>).
 133. Shen, Z.J., Sabui, G., Miao, Z. and Shuai, Z., "Wide-bandgap solid-state circuit breakers for dc power systems: Device and circuit considerations", *IEEE Transactions on Electron Devices*, Vol. 62, No. 2, (2015), 294-300. (<http://dx.doi.org/10.1109/TED.2014.2384204>).
 134. Li, W., Wang, Y., Wu, X. and Zhang, X., "A novel solid-state circuit breaker for on-board dc microgrid system", *IEEE Transactions on Industrial Electronics*, Vol. 66, No. 7, (2019), 5715-5723. (<http://dx.doi.org/10.1109/TIE.2018.2854559>).
 135. Anselmo, I.S. and Rashid, M.H., "Solid-state circuit breakers for d.c. microgrid applications", *Proceedings of the IEEE/ICECCE*, Vol. 1, Istanbul, Turkey, (2020), 1-4. (<https://doi.org/10.1109/ICECCE49384.2020.9179267>).
 136. Nasereddine, R., Amor, I., Massoud, A. and Ben Brahim, L., "AC solid state circuit breakers for fault current limitation in distributed generation", *Proceedings of the IEEE/GCC*, Doha, Qatar, (2013). 446-449. (<https://doi.org/10.1109/IEEEGCC.2013.6705820>).
 137. Stumpe, M., Tünnerhoff, P., Dave, J., Schnettler, A., Ergin, D., Schön, A., Würflinger, K. and Schettler, F., "DC fault protection for modular multi-level converter-based HVDC multi-terminal systems with solid state circuit breakers", *IET Generation, Transmission and Distribution*, Vol. 12, No. 12, (2018), 3013-3020. (<https://doi.org/10.1049/iet-gtd.2017.1322>).
 138. Milojković, J., Litovski, V. and Blond, S.L., "Low-voltage circuit breakers based on WBG solid-state devices", *Journal of Circuits, Systems and Computers*, Vol. 27, (2018), 1850020. (<https://doi.org/10.1142/S0218126618500202>).
 139. Rogers, K.M. and Overbye, T.J., "Some applications of distributed flexible ac transmission system (D-FACTS) devices in power systems", *Proceedings of the IEEE/NAPS*, Vol. 1, Calgary, AB, Canada, (2008), 1-8. (<http://dx.doi.org/10.1109/NAPS.2008.5307314>).
 140. Chawda, G.S., Shaik, A.G., Mahela, O.P., Padmanaban, S. and Holm-Nielsen, J.B., "Comprehensive review of distributed FACTS control algorithms for power quality enhancement in utility grid with renewable energy penetration", *IEEE Access*, Vol. 8, (2020), 107614-107634. (<http://dx.doi.org/10.1109/ACCESS.2020.3000931>).
 141. Sirjani, R. and Jordehi, A.R., "Optimal placement and sizing of distribution static compensator (D-STATCOM) in electric distribution networks: A review", *Renewable and Sustainable Energy Reviews*, Vol. 77, (2017), 688-694. (<http://dx.doi.org/10.1016/j.rser.2017.04.035>).
 142. Gamba, P., Silva, J.F., Pinto, S.F. and Margato, E., "Input-output linearization and PI controllers for ac-ac matrix converter based dynamic voltage restorers with Flywheel Energy Storage: a comparison", *Electric Power Systems Research*, Vol. 169, (2019), 214-228. (<http://dx.doi.org/10.1016/j.epsr.2018.12.023>).
 143. Rodrigues, R., Du, Y., Antoniazzi, A. and Cairoli, P., "A review of solid-state circuit breakers", *IEEE Transactions on Power Electronics*, Vol. 36, (2021), 364-377. (<http://dx.doi.org/10.1109/TPEL.2020.3003358>).
 144. Li, P., Li, Y. and Yin, Z., "Realization of UPQC H_o coordinated control in microgrid", *International Journal of Electrical Power and Energy Systems*, Vol. 65, (2015), 443-452. (<http://dx.doi.org/10.1016/j.ijepes.2014.10.032>).
 145. Khadem, S.K., Basu, M. and Conlon, M.F., "Intelligent islanding and seamless reconnection technique for microgrid with UPQC", *IEEE Journal of Emerging and Selected Topics in Power Electronics*, Vol. 3, (2015), 483-492. (<http://dx.doi.org/10.1109/JESTPE.2014.2326983>).
 146. Gayatri, M.T.L., Parimi, A.M. and Kumar, A.V.P., "Utilization of unified power quality conditioner for voltage sag/swell mitigation in microgrid", *Proceedings of the IEEE/PESTSE*, Vol. 1, Bangalore, India, (2016), 1-6. (<http://dx.doi.org/10.1109/PESTSE.2016.7516475>).
 147. Li, Z., Li, W. and Pan, T., "An optimized compensation strategy of DVR for micro-grid voltage sag", *Protection and Control of Modern Power Systems*, Vol. 1, (2016), 1-8. (<http://dx.doi.org/10.1186/s41601-016-0018-9>).
 148. Wang, B., Ye, J., Manandhar, U., Ukil, A. and Gooi, H.B., "A DC microgrid integrated dynamic voltage restorer with model predictive control", *Proceedings of the IEEE/ACEPT*, Vol. 1, Singapore, (2017), 1-5. (<http://dx.doi.org/10.1109/ACEPT.2017.8168554>).
 149. Gayatri, M.T.L., Parimi, A.M. and Kumar, A.V.P., "Application of dynamic voltage restorer in microgrid for voltage sag/swell mitigation", *Proceedings of the IEEE/PCITC*, Vol. 1, Bhubaneswar, India, (2015), 750-755. (<http://dx.doi.org/10.1109/PCITC.2015.7438096>).
 150. Yuvaraj, T., Ravi, K. and Devabalaji, R., "DSTATCOM allocation in distribution networks considering load variations using bat algorithm", *Ain Shams Engineering Journal*, Vol. 8, (2017), 391-403. (<http://dx.doi.org/10.1016/j.asej.2015.08.006>).
 151. Mali, S., James, S. and Tank, I., "Improving low voltage ride-through capabilities for grid connected wind turbine generator", *Energy Procedia*, Vol. 54, (2014), 530-540. (<http://dx.doi.org/10.1016/j.egypro.2014.07.294>).
 152. Jayawardena, A.V., Meegahapola, L.G., Robinson, D.A. and Perera, S., "Low-voltage ride-through characteristics of microgrids with distribution static synchronous compensator (DSTATCOM)", *Proceedings of the IEEE/AUPEC*, Vol. 1, Wollongong, NSW, Australia, (2015), 1-6. (<http://dx.doi.org/10.1109/AUPEC.2015.7324823>).
 153. Moghadasi, A., Sarwat, A. and Guerrero, J.M., "A comprehensive review of low-voltage-ride-through methods for fixed-speed wind power generators", *Renewable and Sustainable Energy Reviews*, Vol. 55, (2016), 823-839. (<http://dx.doi.org/10.1016/j.rser.2015.11.020>).
 154. Omar, R. and Rahim, N.A., "Power quality improvement in low voltage distribution system using dynamic voltage restorer (DVR)", *Proceedings of the IEEE/Tai Chung*, Vol. 1, Taichung, Taiwan, (2010), 973-978. (<http://dx.doi.org/10.1109/ICIEA.2010.5515734>).
 155. Benali, A., Khiat, M., Allaoui, T. and Denaï, M., "Power quality improvement and low voltage ride through capability in hybrid wind-pv farms grid-connected using dynamic voltage restorer", *IEEE Access*, Vol. 6, (2018), 68634-68648. (<http://dx.doi.org/10.1109/ACCESS.2018.2878493>).
 156. Chen, L., Chen, H., Yang, J., Zhu, L., Tang, Y., Koh, L.H., Xu, Y., Zhang, C., Liao, Y. and Ren, L., "Comparison of superconducting fault current limiter and dynamic voltage restorer for LVRT improvement of high penetration microgrid", *IEEE Transactions on Applied Superconductivity*, Vol. 27, (2017), 1-7. (<http://dx.doi.org/10.1109/T-ASC.2017.2656624>).
 157. Prabaakaran, K., Chitra, N. and Kumar, A.S., "Power quality enhancement in microgrid- A survey", *Proceedings of the*

- IEEE/ICCPCT*, Nagercoil, India, (2013), 126-131. (<https://doi.org/10.1109/ICCPCT.2013.6528830>).
158. Kumar, A.S., Rajasekar, S. and Ajay-D-VimalRaj, P., "Power quality profile enhancement of utility connected microgrid system using ANFIS-UPQC", *Procedia Technology*, Vol. 21, (2015), 112-119. (<http://dx.doi.org/10.1016/j.protcy.2015.10.017>).
159. Gandhar, S., Ohri, J. and Singh, M., "Dynamic reactive power optimization of hybrid micro grid in islanded mode using fuzzy tuned UPFC", *Journal of Information and Optimization Sciences*, Vol. 41, (2020), 305-315. (<http://dx.doi.org/10.1080/02522667.2020.1721620>).
160. Bagheri, M., Nurmanova, V., Abedinia, O. and Naderi, M.S., "Enhancing power quality in microgrids with a new online control strategy for DSTATCOM using reinforcement learning algorithm", *IEEE Access*, Vol. 6, (2018), 38986-38996. (<http://dx.doi.org/10.1109/ACCESS.2018.2852941>).
161. Benachaiba, C., Haidar, A.M.A., Habab, M. and Abdelkhalik, O., "Smart control of UPQC within microgrid energy system", *Energy Procedia*, Vol. 6, (2011), 503-512. (<http://dx.doi.org/10.1016/j.egypro.2011.05.058>).
162. Harshitha, M.R., Sharmila, R.S., Shivasharanappa, G.C. and Prakash, R., "UPQC with islanding and grid connection for microgrid applications", *International Journal of Scientific and Research Publications*, Vol. 6, (2016), 214-220. (<https://journals.pen2print.org/index.php/ijr/article/view/5691>).
163. El-Raouf, M.O.A. Mosaad, M.I., Al-Ahmar, M.A., Mallawany, A.L. and El-Bendary, F.M., "Optimal PI controller of DVR to enhance the performance of hybrid power system feeding a remote area in Egypt", *Sustainable Cities and Society*, Vol. 47, (2019), 101469. (<https://doi.org/10.1016/j.scs.2019.101469>).
164. Gludetch, S. and Tayjasanant, T., "Optimal placement of protective devices for improving reliability indices in microgrid system", *Proceedings of the IEEE/APPEEC*, Kowloon, China, (2013), 1-6. (<https://doi.org/10.1109/APPEEC.2013.6837303>).
165. Syed, I. and Khadkikar, V., "A dynamic voltage restorer (DVR) based interface scheme for microgrids", *Proceedings of the IEEE/IECON*, Dallas, TX, USA, (2014), 5143-5149. (<http://dx.doi.org/10.1109/IECON.2014.7049283>).
166. Wang, Y., Li, W., Wu, X. and Wu, X., "A novel bidirectional solid-state circuit breaker for dc microgrid", *IEEE Transactions on Industrial Electronics*, Vol. 66, No. 7, (2019), 5707-5714. (<http://dx.doi.org/10.1109/TIE.2018.2878191>).
167. Ramli, M.A.M. and Bouchekara, H.R.E.H., "Solving the problem of large-scale optimal scheduling of distributed energy resources in smart grids using an improved variable neighborhood search", *IEEE Access*, Vol. 8, (2020), 77321-77335. (<https://doi.org/10.1109/ACCESS.2020.2986895>).
168. Bai, W., Eke, I. and Lee, K.Y., "Optimal scheduling of distributed energy resources by modern heuristic optimization technique", *Proceedings of the IEEE/ISAP*, San Antonio, TX, USA, (2017), 1-6. (<https://doi.org/10.1109/ISAP.2017.8071407>).
169. Jirdehi, M.A., Tabar, V.S., Hemmati, R. and Siano, P., "Multi objective stochastic microgrid scheduling incorporating dynamic voltage restorer", *International Journal of Electrical Power and Energy Systems*, Vol. 93, (2017), 316-327. (<http://dx.doi.org/10.1016/j.ijepes.2017.06.010>).
170. Hamidi, A., Golshannavaz, S. and Nazarpour, D., "D-FACTS cooperation in renewable integrated microgrids: A linear multiobjective approach", *IEEE Transactions on Sustainable Energy*, Vol. 10, (2019), 355-363. (<http://dx.doi.org/10.1109/TSSTE.2017.2723163>).
171. Hossain, M.A., Pota, H.R., Hossain, M.J. and Blaabjerg, F., "Evolution of microgrids with converter-interfaced generations: challenges and opportunities", *International Journal of Electrical Power and Energy Systems*, Vol. 109, (2019), 160-186. (<https://doi.org/10.1016/j.ijepes.2019.01.038>).
172. Majumder, R., "Some aspects of stability in microgrids", *IEEE Transactions on Power Systems*, Vol. 28, No. 3, (2013), 3243-3252. (<https://doi.org/10.1109/TPWRS.2012.2234146>).
173. Tang, X., Deng, W. and Qi, Z., "Investigation of the dynamic stability of microgrid", *IEEE Transactions on Power Systems*, Vol. 29, No. 2, (2014), 698-706. (<http://dx.doi.org/10.1109/TPWRS.2013.2285585>).
174. Shahgholian, Gh., Dehghani, M. and Behzadfar, N., "The effect of STATCOM controller for improving dynamic performance of wind farm in power system", *International Journal Natural and Engineering Sciences*, Vol. 4, No. 2, (2020), 1-20. (<https://www.ijnes.org/index.php/ijnes/article/view/577>).
175. Choudhury, S., Bhowmik, P. and Rout, P.K., "Economic load sharing in a D-STATCOM integrated islanded microgrid based on fuzzy logic and seeker optimization approach", *Sustainable Cities and Society*, Vol. 37, (2018), 57-69. (<http://doi.org/10.1016/j.scs.2017.11.004>).
176. Rahmani, M., Faghihi, F., Moradi CheshmehBeigi, H. and Hosseini, S.M., "Frequency control of islanded microgrids based on fuzzy cooperative and influence of STATCOM on frequency of microgrids", *Journal of Renewable Energy and Environment (JREE)*, Vol. 5, No. 4, (2018), 27-33. (<http://dx.doi.org/10.30501/jree.2018.94119>).
177. Gandhar, S., Ohri, J. and Singh, M., "Improvement of voltage stability of renewable energy sources-based microgrid using ANFIS-tuned UPFC", *Advances in Energy and Built Environment*, Vol. 36, (2020), 133-143. (http://dx.doi.org/10.1007/978-981-13-7557-6_11).
178. Lee, T., Hu, S. and Chan, Y., "Design of D-STATCOM for voltage regulation in microgrids", *Proceedings of the IEEE/PCCE*, Atlanta, GA, USA, (2010), 3456-3463. (<http://dx.doi.org/10.1109/ECCE.2010.5618339>).
179. Munasib, S. and Balda, J.C., "Short-circuit protection for low-voltage DC microgrids based on solid-state circuit breakers", *Proceedings of the IEEE/PEDG*, Vol. 1, Vancouver, BC, Canada, (2016), 1-7. (<https://doi.org/10.1109/PEDG.2016.7527062>).
180. Liu, W., Liu, F., Zha, X., Huang, M., Chen, C. and Zhuang, Y., "An improved SSCB combining fault interruption and fault location functions for dc line short-circuit fault protection", *IEEE Transactions on Power Delivery*, Vol. 34, No. 3, (2019), 858-868. (<http://dx.doi.org/10.1109/TPWRD.2018.2882497>).
181. Almutairy, I., "Solid state circuit breaker protection devices for DC microgrid in review", *Proceedings of the IEEE/ICEDSA*, Vol. 1, Ras Al Khaimah, United Arab Emirates, (2016), 1-3. (<https://doi.org/10.1109/ICEDSA.2016.7818478>).
182. Urquiza, J., Singh, P., Kondrath, N., Hidalgo-León, R. and Soriano, G., "Using D-FACTS in microgrids for power quality improvement: A review", *Proceedings of the IEEE/ETCM*, Vol. 1, Salinas, Ecuador, (2017), 1-6. (<http://dx.doi.org/10.1109/ETCM.2017.8247546>).
183. Wang, J., Wang, Z., Xu, L. and Wang, Z., "A summary of applications of D-FACTS on microgrid", *Proceedings of the IEEE/APPEEC*, Vol. 1, Shanghai, China, (2012), 1-6. (<http://dx.doi.org/10.1109/APPEEC.2012.6307225>).
184. Gayatri, M.T.L., Parimi, A.M. and Kumar, A.V.P., "A review of reactive power compensation techniques in microgrids", *Renewable and Sustainable Energy Reviews*, Vol. 81, (2018), 1030-1036. (<http://dx.doi.org/10.1016/j.rser.2017.08.006>).



Technical Note

Improving the Efficiency of a Cantilever Energy Scavenger

Mohammad Rahimzadeh ^{a*}, Hamid Samadi ^b, Nikta Shams Mohammadi ^c

^a Department of Mechanical Engineering, Faculty of Engineering, Golestan University, P. O. Box: 49138-15759, Gorgan, Golestan, Iran.

^b Department of Mechanical Engineering, Babol University of Technology, P. O. Box: 47148-73113, Babol, Mazandaran, Iran.

^c Department of Electrical Engineering, Shahrood University of Technology, P. O. Box: 36199-95161, Shahrood, Semnan, Iran.

PAPER INFO

Paper history:

Received: 16 December 2021

Revised in revised form: 01 May 2022

Scientific Accepted: 21 May 2022

Published: 27 August 2022

Keywords:

Piezoelectric,
Cantilever Beam,
Energy Harvesting,
Voltage,
Unimorph

ABSTRACT

Energy harvesting from ambient vibrations using piezoelectric cantilevers is one of the most popular mechanisms for producing electrical energy. Recently, efforts have been made to improve the performance of energy harvesters. The output voltage dramatically depends on the geometrical and physical parameters of these devices. In addition, improved performance is often achieved by operating at or near the resonance point. So, this paper aims to reduce the natural frequency to match the environmental excitation frequency and increase the harvested energy. For this purpose, different geometrical and physical parameters are studied to determine the impact of each parameter. These parameters include the length, thickness, density, and Young's modulus of each layer. The beam is considered a unimorph cantilever with rectangular configuration and the study is performed using COMSOL Multiphysics software. The results are compared with those obtained by an analytical approach. The results show that changing the parameters made the natural frequency of the system vary in the range of 20 Hz to 200 Hz and increased the output voltage up to 20 V.

<https://doi.org/10.30501/jree.2022.320113.1300>

1. INTRODUCTION

Rapid advances in electronic devices and sensors have intensified the efforts for portable energy sources [1]. The high costs of constant battery replacement and the limited final weights of devices have increased the attempts at supplying energy from ambient vibrations such as vibration of the wing of a UAV during flight, traffic and wind induced vibrations in tall bridges, vibration coming from rotating tires of a vehicle, heart beats and blood pressure fluctuations in the human body, and vibration due to walking or physical exercise [2]. In general, mechanical energy can be converted into electrical energy through three mechanisms, namely electromagnetic [3], electrostatic, and piezoelectric [4]. At the same time, piezoelectric materials have been considered for use to boost the output voltage because they need no electrical sources [5].

The capability to harvest energy from the environment is significant, especially in high-tech industries like aerospace. For instance, Eugeni et al. [6] modeled a piezoelectric energy harvester on a fluid stream and developed it for use in wireless sensors. In another study, Liu et al. [7] developed energy harvesting arrays consisting of several piezoelectric elements to monitor traffic and energy harvesting. These arrays were examined to simulate the effects of loads and speeds of different vehicle axles. The impacts of piezoelectric

configurations on the harvested amount of energy were then studied. The impacts of temperature on the output signals of the arrays were also analyzed. The experimental results indicated that the output voltage increased gradually as the load and frequency increased. With rapid developments in artificial intelligence technologies and the Internet of Things, wearable electronic devices have attracted a great deal of attention. Piezoelectric-based nanogenerators have great potential for use as human health monitoring sensors and biomechanical energy harvesters in wearable electronics due to their high flexibility, low weight, high reliability, and high accuracy [8, 9]. Piezoelectric materials are used as actuators, sensors, and energy harvesters in various medical devices. Natural piezoelectric materials have different properties from mineral piezoelectric materials. The high mechanical properties and flexibility of natural piezoelectric materials are very important and practical in various applications of medical equipment. Natural piezoelectric materials are used in medical sensors, which are located close to internal organs such as the heart due to the need for proper flexibility [10]. As discussed earlier, the exceptional capabilities and properties of piezoelectric materials have made them easy to use in different fields [11]. However, it is necessary to know everything about the field of use, limitations, and conditions of the system for the application of piezoelectric materials [12]. Hence, the parameters of energy harvesting systems must be appropriately designed [13].

*Corresponding Author's Email: m.rahimzadeh@gu.ac.ir (M. Rahimzadeh)

URL: https://www.jree.ir/article_155304.html



In the conventional design of energy scavengers based on piezoelectric materials, a cantilever beam configuration is used with a piezoelectric layer [14]. Creating high strain energy and reducing natural frequencies in this configuration are the main reasons for employing such a beam to harvest energy [15]. Nevertheless, the natural frequencies in these mechanisms range from several hundred Hz to several kHz. Of note, the excitation frequencies of environmental resources are usually not very high. A way of solving this problem is to use proof mass at the free end of the beam. This method helps reduce the resonant frequency of the energy harvesting system [16]. Moreover, the geometry of the beam structure and properties of the materials used have substantial impacts on an energy harvesting performance [17]. In recent studies, beams have been used in various geometrical shapes such as rectangular and triangular shapes. Moreover, it is possible to increase the harvested energy by applying optimization methods to the geometrical parameters of the beams [18]. The output power depends significantly on the properties of materials and the geometrical parameters of the beam [19]. Stress and strain increase as the geometrical properties of the beam change; therefore, higher levels of voltage and power can be harvested from a specific piezoelectric material [20]. According to the research results, the natural frequency of a triangular beam is lower than that of a rectangular or trapezoidal beam under the same conditions. Furthermore, the thickness of the beam layer affects the performance of an energy harvester performance. The beam structure is usually in the form of an elastic layer with a piezoelectric patch (unimorph) or an elastic layer with two piezoelectric patches on either side of the elastic layer (bimorph) [21, 22].

An energy harvesting system must be appropriately designed in an environment exposed to ambient vibrations due to the adaption of that system to environmental conditions. Efficiency improvement is important in the design and analysis of energy harvesters. Efficiency is defined as the ratio of the output electrical energy to the input mechanical energy. Despite several studies on the efficiency analysis of energy harvesters, the effects of geometric and physical parameters on the performance of energy harvesters have not been explored simultaneously through analytical and numerical (FEM) approaches. In this study, different multiplication factors were applied to geometrical and physical parameters such as beam length, thickness, density, and Young's modulus to measure the effect of each on the energy harvesting process. The resulting information of these simulations can lead to a more appropriate design of an energy scavenger. Based on the separate analysis of the effect of each parameter on the energy harvesting process, it is possible to select the appropriate material and geometry of the energy harvester to meet the needs and conditions of each environment. The energy harvester beam was considered rectangular and unimorph.

2. ELECTROMECHANICAL MODEL OF THE ENERGY HARVESTER

One of the most common models of energy harvesting is a cantilever beam with a piezoelectric layer, which is shown in Figure 1. The beam has the width of b and length of L . It also consists of an elastic layer with the thickness of h_s and a piezoelectric layer with the thickness of h_p . The electrodes cover the entire surface of the piezoelectric layer, which does not slip with respect to the beam.

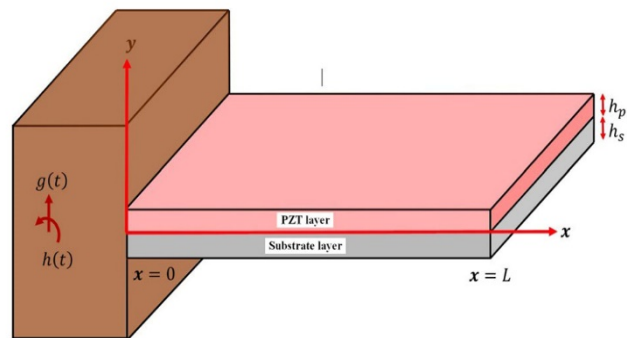


Figure 1. The schematic view of an energy scavenger under base vibrations

The general motion of the beam under forced vibrations including the base motion and its transverse displacements can be expressed as in Equation 1 [23]:

$$w(x, t) = w_b(x, t) + w_r(x, t) \quad (1)$$

where $w_b(x, t)$ is the motion of the base of the beam and $w_r(x, t)$ is the transverse displacement of the beam related to the clamped end. Moreover, the motion of the beam base is defined as in the following equation:

$$w_b(x, t) = g(t) + xh(t) \quad (2)$$

where $g(t)$ is the translational motion of the beam along the Y-axis and $h(t)$ is the rotation of the beam around the Z-axis. The equation of motion assuming the Euler-Bernoulli beam theory can be expressed as follows [23]:

$$\begin{aligned} \frac{\partial^2 M(x, t)}{\partial x^2} + C_s I \frac{\partial^5 w_{rel}(x, t)}{\partial x^4 \partial t} + C_a \frac{\partial w_{rel}(x, t)}{\partial t} \\ + m \frac{\partial^2 w_{rel}(x, t)}{\partial t^2} \\ = -m \frac{\partial^2 w_b(x, t)}{\partial t^2} - C_a \frac{\partial w_b(x, t)}{\partial t} \end{aligned} \quad (3)$$

The bending moment $M(x, t)$ is calculated as follows:

$$M(x, t) = - \int_{h_a}^{h_b} T_1^s b y \, dy - \int_{h_b}^{h_c} T_1^p b y \, dy \quad (4)$$

where T_1^s and T_1^p denote stress in the elastic and piezoelectric layers, respectively.

$$T_1^s = Y_s S_1^s \quad (5)$$

$$T_1^p = Y_p (S_1^p - d_{31} E_3) \quad (6)$$

where d_{31} refers to the piezoelectric constant and E_3 denotes the electric field, whereas S_1^s indicates the strain in the elastic layer. Furthermore, S_1^p shows the strain in the piezoelectric layer. Replacing the values obtained in Equation 4 yields the following equations:

$$M(x, t) = \int_{h_a}^{h_b} Y_s b \frac{\partial^2 w_{rel}(x, t)}{\partial x^2} y^2 dy \quad (7)$$

$$+ \int_{h_b}^{h_c} Y_p b \frac{\partial^2 w_{rel}(x, t)}{\partial x^2} y^2 dy$$

$$- \int_{h_b}^{h_c} v(t) Y_p b \frac{d_{31}}{h_p} y dy$$

$$M(x, t) = YI \frac{\partial^2 w_{rel}(x, t)}{\partial x^2} + \vartheta v(t) \quad (8)$$

where Y_s denotes Young's modulus of the substrate layer, Y_p Young's modulus of the piezoelectric material, I the moments of inertia of the beam cross-section, and m the linear mass density of the beam. The bending stiffness of the composite beam and electromechanical coupling can be obtained from the following equations:

$$YI = b \left[\frac{Y_s(h_b^3 - h_a^3) + Y_p(h_c^3 - h_b^3)}{3} \right] \quad (9)$$

$$\vartheta = -\frac{Y_p d_{31} b}{2h_p} (h_c^2 - h_b^2) \quad (10)$$

$$M(x, t) = YI \frac{\partial^2 w_{rel}(x, t)}{\partial x^2} + \vartheta v(t) [H(x) - H(x - L)] \quad (11)$$

Figure 2 demonstrates the beam cross-section.

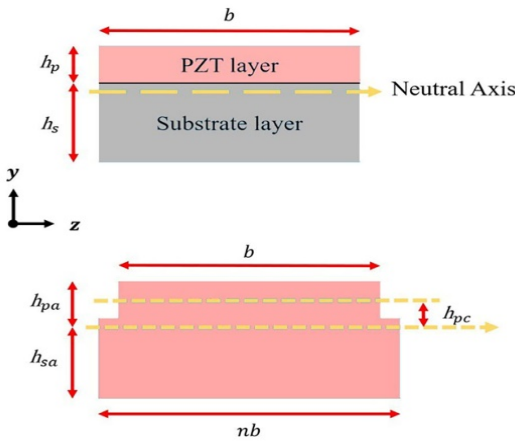


Figure 2. The cross-section of an energy scavenger and its equivalent cross-section

The following equations can be employed to find the position of the neutral axis [23]:

$$n = \frac{Y_s}{Y_p} \quad (12)$$

$$h_{pa} = \frac{h_p^2 + 2nh_p h_s + nh_s^2}{2(h_p + nh_s)} \quad (13)$$

$$h_{sa} = \frac{h_p^2 + 2h_p h_s + nh_s^2}{2(h_p + nh_s)} \quad (14)$$

$$h_{pc} = \frac{nh_s(h_p + h_s)}{2(h_p + nh_s)} \quad (15)$$

To maintain the relationship between electrical and mechanical parameters of the system, it is necessary to define the piezoelectric constitutive relations [24]:

$$D_3 = d_{31} T_1 + \varepsilon_{33}^T E_3 \quad (16)$$

$$D_3(x, t) = d_{31} Y_p S_1(x, t) - \varepsilon_{33}^S \frac{v(t)}{h_p} \quad (17)$$

$$S_1(x, t) = -h_{pc} \frac{\partial^2 w_{rel}(x, t)}{\partial x^2} \quad (18)$$

$$D_3(x, t) = -d_{31} Y_p h_{pc} \frac{\partial^2 w_{rel}(x, t)}{\partial x^2} - \varepsilon_{33}^S \frac{v(t)}{h_p} \quad (19)$$

In the above equations, D_3 refers to the electric displacement, whereas ε_{33}^T represents the permittivity, and E_3 denotes the electric field. Moreover, current $i(t)$ and voltage $v(t)$ can be calculated in accordance with the amount of electric charge $q(t)$.

$$q(t) = \int_A D \cdot ndA = - \int_{x=0}^L \left(d_{31} Y_p h_{pc} \frac{\partial^2 w_{rel}(x, t)}{\partial x^2} + \varepsilon_{33}^S b \frac{v(t)}{h_p} \right) dx \quad (20)$$

$$i(t) = \frac{dq(t)}{dt} = - \int_{x=0}^L d_{31} Y_p h_{pc} b \frac{\partial^3 w_{rel}(x, t)}{\partial x^2 \partial t} dx - \frac{\varepsilon_{33}^S b L}{h_p} \frac{dv(t)}{dt} \quad (21)$$

$$\frac{\varepsilon_{33}^S b L}{h_p} \frac{dv(t)}{dt} + \frac{v(t)}{R_1} = - \int_{x=0}^L d_{31} Y_p h_{pc} b \frac{\partial^3 w_{rel}(x, t)}{\partial x^2 \partial t} dx \quad (22)$$

$$v(t) = R_1 i(t) = -R_1 \left[\int_{x=0}^L d_{31} Y_p h_{pc} b \frac{\partial^3 w_{rel}(x, t)}{\partial x^2 \partial t} dx - \frac{\varepsilon_{33}^S b L}{h_p} \frac{dv(t)}{dt} \right] \quad (23)$$

In the above equations, h_{pc} refers to the distance between neutral axis and the piezoelectric layer center, whereas R_1 indicates the electrical resistance of the circuit. To solve the

governing equations, the transverse motion of the beam can be written as a convergent series of eigenfunctions:

$$w_{\text{rel}}(x, t) = \sum_{r=1}^n \phi_r(x) \eta_r(t) \quad (24)$$

$$\phi_r(x) = \sqrt{\frac{1}{mI}} \left[\cosh \frac{\lambda_r}{L} x - \cos \frac{\lambda_r}{L} x - \sigma_r \left(\sinh \frac{\lambda_r}{L} x - \sin \frac{\lambda_r}{L} x \right) \right] \quad (25)$$

$$\eta_r(t) = \frac{[m\omega^2(\gamma_r^w Y_0 + \gamma_r^\theta \theta_0) - \chi_r V_0] e^{j\omega t}}{\omega_r^2 - \omega^2 + j2\zeta_r \omega_r \omega} \quad (26)$$

where $\phi_r(x)$ represents the mass normalized eigenfunction, and $\eta_r(t)$ indicates the modal coordinate of the cantilever beam. Herein, λ_r 's can be specified by solving the characteristic equation:

$$1 + \cos \lambda \cosh \lambda = 0 \quad (27)$$

$$\sigma_r = \frac{\sinh \lambda_r - \sin \lambda_r}{\cosh \lambda_r + \cos \lambda_r} \quad (28)$$

where:

$$\omega_r = \lambda_r^2 \sqrt{\frac{YI}{mL^4}} \quad (29)$$

$$\gamma_r^w = \int_0^L \phi_r(x) dx \quad (30)$$

$$\gamma_r^\theta = \int_0^L x \phi_r(x) dx \quad (31)$$

Assuming:

$$h(t) = \theta_0 e^{j\omega t} \quad (32)$$

$$g(t) = Y_0 e^{j\omega t} \quad (33)$$

$$v(t) = V_0 e^{j\omega t} \quad (34)$$

$v(t)$ can be defined as follows:

$$V_0 = \frac{\sum_{r=1}^{\infty} \frac{j m \omega^3 \phi_r (\gamma_r^w Y_0 + \gamma_r^\theta \theta_0)}{\omega_r^2 - \omega^2 + j 2 \zeta_r \omega_r \omega}}{\sum_{r=1}^{\infty} \frac{j \omega \chi_r \phi_r}{\omega_r^2 - \omega^2 + j 2 \zeta_r \omega_r \omega} + \frac{1 + j \omega \tau_c}{\tau_c}} \quad (35)$$

$$v(t) = \frac{\sum_{r=1}^{\infty} \frac{j m \omega^3 \phi_r (\gamma_r^w Y_0 + \gamma_r^\theta \theta_0) e^{j\omega t}}{\omega_r^2 - \omega^2 + j 2 \zeta_r \omega_r \omega}}{\sum_{r=1}^{\infty} \frac{j \omega \chi_r \phi_r}{\omega_r^2 - \omega^2 + j 2 \zeta_r \omega_r \omega} + \frac{1 + j \omega \tau_c}{\tau_c}} \quad (36)$$

$$\frac{v(t)}{-\omega^2 Y_0 e^{j\omega t}} = \frac{\sum_{r=1}^{\infty} \frac{-j m \omega \phi_r \gamma_r^w}{\omega_r^2 - \omega^2 + j 2 \zeta_r \omega_r \omega}}{\sum_{r=1}^{\infty} \frac{j \omega \chi_r \phi_r}{\omega_r^2 - \omega^2 + j 2 \zeta_r \omega_r \omega} + \frac{1 + j \omega \tau_c}{\tau_c}} \quad (37)$$

where:

$$\phi_r = -\frac{d_{31} Y_p h_p c h_p}{\epsilon_{33}^s L} \int_{x=0}^L \frac{d^2 \phi_r(x)}{dx^2} dx = -\frac{d_{31} Y_p h_p c h_p}{\epsilon_{33}^s L} \frac{d \phi_r(x)}{dx} \Big|_{x=L} \quad (38)$$

3. PROBLEM STATEMENT

Table 1 presents the geometrical and mechanical characteristics of the unimorph beam. To study the effects of scavenger parameters such as length, thickness, Young modulus, and density on lowest resonant frequency and harvester performance, a comparative study has been carried out by considering some multiplication factors. Better insight can be achieved by multiplying each parameter by factors 0.5, 1, and 1.5, whereas others are deemed to be constant. This approach, for the design of an energy scavenger, leads to a more appropriate selection of materials and geometrical properties. Hence, it is possible to obtain a greater amount of energy. The numerical simulations were performed in COMSOL Multiphysics software (Figure 3). Additionally, the load resistance was considered $R_1 = 10^6 \Omega$ in this study.

Table 1. The mechanical and geometrical characteristics of the piezoelectric and substrate layers

Parameter	Substrate layer	PZT layer
Young modulus (GPa)	100	66
Density (Kg/m3)	7165	7800
Length (mm)	100	100
Width (mm)	20	20
Thickness (mm)	0.5	0.4

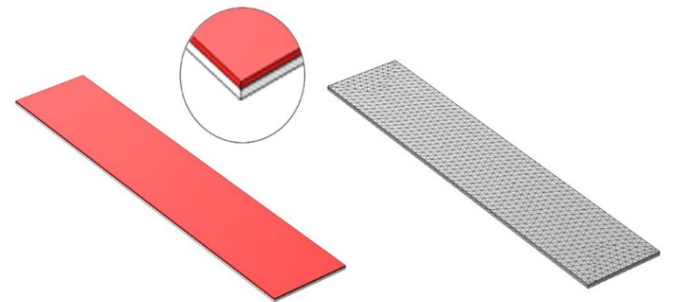


Figure 3. The geometrical and meshed model of the rectangular beam

4. RESULTS AND DISCUSSION

Table 2 shows the analytical and numerical (COMSOL) natural frequencies of the harvester. As can be seen, the

results are in good agreement. The numerical first natural frequency was found to be 47.82 Hz in COMSOL, whereas it was analytically calculated to be 47.81 Hz. Figure 4 depicts the numerical mode shapes 1-3 of the energy scavenger. Figure 5 plots the analytical output voltage at 0-400 Hz for resistive loads of 500 Ω, 5 kΩ, and 50 kΩ logarithmically. As can be seen, the output voltage was maximized at the natural frequencies. In addition, a rise in the resistive load raised the output voltage. This is evident throughout the frequency range, including the second natural frequency. Figure 6 depicts the numerical output voltage of the harvester at 0-400 Hz for the same resistive loads in COMSOL. The logarithmic voltage was obtained to be -0.938, -0.012, and 0.576 V at resistive loads of 500 Ω, 5 kΩ, and 50 kΩ, respectively, at the first natural frequency. At the second natural frequency, however, the logarithmic voltage was found to be -1.501, -0.650, and -0.325 V at resistive loads of 500 Ω, 5 kΩ, and 50 kΩ, respectively. Figure 7 compares the numerical and analytical output voltages at 0-400 Hz for a resistive load of 50 kΩ. As can be seen, the numerical and analytical results were in good agreement. The slight difference between the output voltage results at the second natural frequency arose from the use of a constant damping ratio throughout the frequency range in the numerical model in COMSOL.

Table 2. Comparing the values of natural frequencies obtained from COMSOL Multiphysics and MATLAB

	COMSOL Multiphysics	Matlab
1 st natural frequency (Hz)	47.82	47.81
2 nd natural frequency (Hz)	299.65	299.61
3 rd natural frequency (Hz)	838.81	838.92

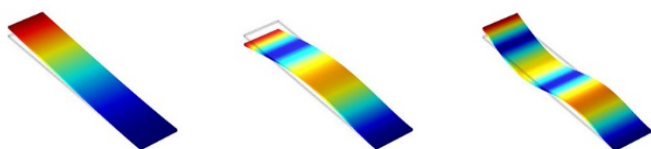


Figure 4. The first three mode shapes of the unimorph cantilever scavenger

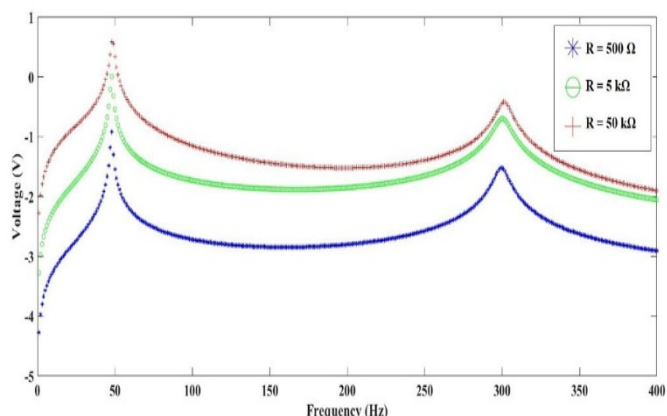


Figure 5. The voltage output versus the frequency for the unimorph cantilever beam within the range of 0 to 400 Hz through the analytical method

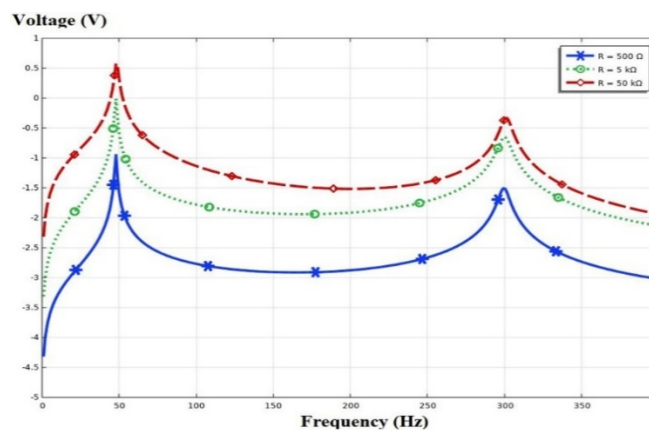


Figure 6. The voltage output versus the frequency for the unimorph cantilever beam within the range of 0 to 400 Hz from COMSOL Multiphysics

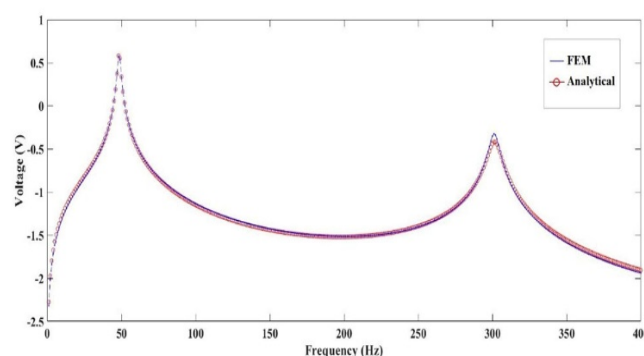


Figure 7. The voltage output versus the frequency for the unimorph cantilever beam within the range of 0 to 400 Hz for $R_1 = 50 \text{ k}\Omega$ through the analytical method and simulation from COMSOL Multiphysics

Figure 8 plots the analytical output voltage for 10-210 Hz at a resistive load of 1 MΩ and different lengths. As can be seen, a 50 % reduction (increase) in the initial harvester length (i.e., 100 mm) reduced (increased) the output voltage and increased (reduced) the natural frequency. Since ambient vibration typically occurs at low frequencies, an increase in the beam length would enhance harvester performance. Figure 9 depicts the numerical output voltage for 10-210 Hz at a resistive load of 1 MΩ and different lengths. According to Figure 9, the numerical output voltage was calculated to be 2.921, 10.679, and 22.423 V at length factors of 0.5, 1.0, and 1.5, respectively; a rise in the energy scavenger length from 100 to 150 mm led to a 110 % increase in the output voltage. The numerical results show good agreement with the analytical calculations.

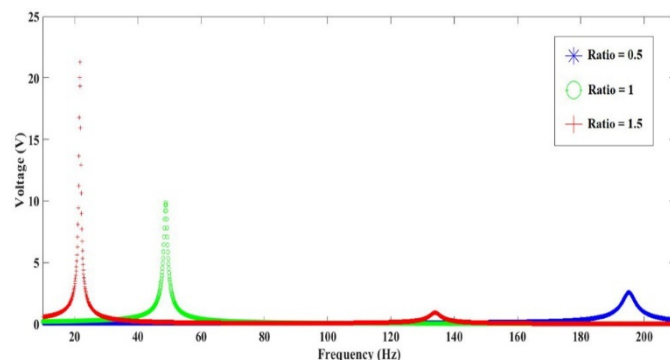


Figure 8. The voltage versus the frequency for variations in the beam length through the analytical method

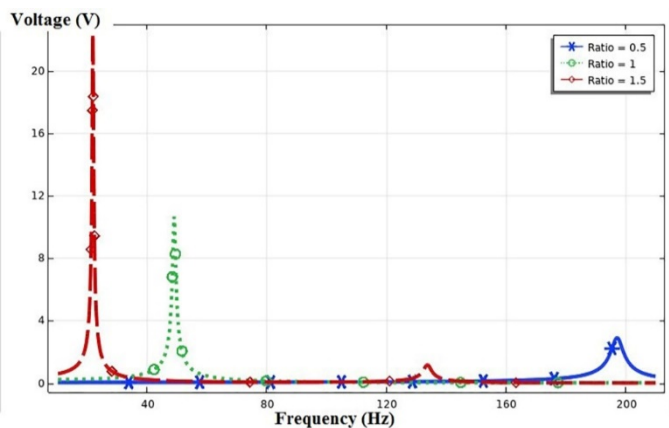


Figure 9. The voltage versus the frequency for variations in the beam length through the finite elements

Figure 10 plots the analytical output voltage at 30-70 Hz for substrate layer thicknesses of 0.25, 0.50, and 0.75 mm (ratios 0.5, 1.0, and 1.5). As shown in Figure 10, a reduction in the substrate thickness diminished the natural frequency and elevated the output voltage of the energy scavenger. Although the decreased substrate thickness led to only a slight rise in the output voltage, it could be considered for performance improvement as the natural frequency of the energy scavenger would substantially decline. The output voltage was maximized (8.8 V) at a substrate thickness of 0.75 mm. Figure 11 plots the analytical output voltage at 35-65 Hz for piezoelectric layer thicknesses of 0.2, 0.4, and 0.6 mm (factors 0.5, 1.0, and 1.5). As can be seen, a decrease (rise) in the thickness of the piezoelectric layer decreased (raised) the output voltage and reduced (increased) the natural frequency of the harvester. This is not efficient in the performance improvement of the harvester as the output voltage undergoes a small rise, while the natural frequency substantially increases.

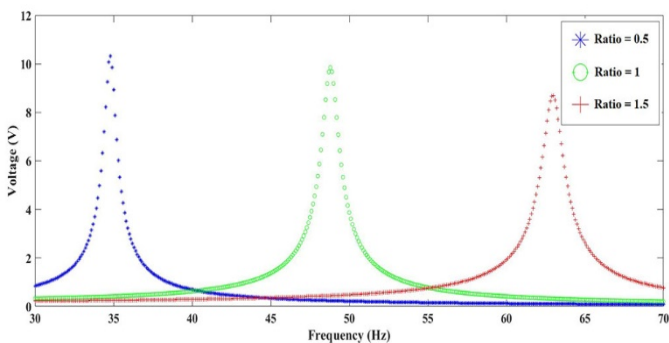


Figure 10. The voltage versus the frequency for variations in the substrate thickness through the analytical method

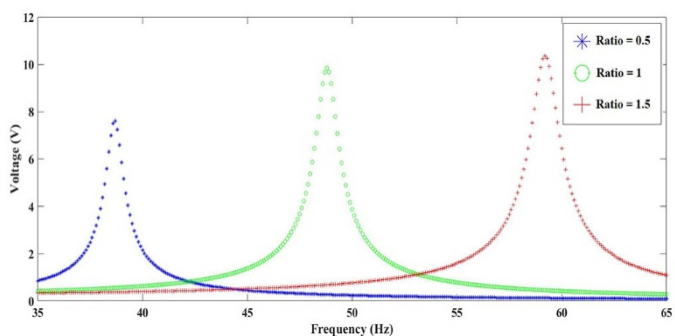


Figure 11. The voltage versus the frequency for variations of the piezoelectric layer thickness through the analytical method

Figure 12 shows the numerical output voltage at 35-65 Hz for piezoelectric layer thicknesses of 0.2, 0.4, and 0.6 mm (ratios 0.5, 1.0, and 1.5). The numerical results were in good agreement with the analytical calculations. The maximum numerical output voltage was found to be 9.338 V at a piezoelectric layer thickness of 0.2 mm.

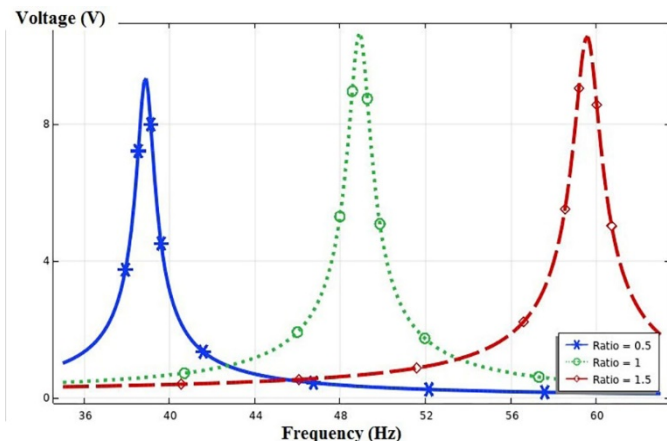


Figure 12. The generated voltage versus the frequency for variations of the piezoelectric layer thickness from COMSOL Multiphysics

Figure 13 represents the analytical output voltage at 40-55 Hz for substrate elasticity moduli of 50, 100, and 150 GPa (ratios 0.5, 1.0, and 1.5). A reduction in the elasticity modulus not only diminished the natural frequency of the harvester but also resulted in a slight rise in the output voltage. This can be assumed as a performance improvement criterion of such harvesters. The reduced elasticity modulus of the substrate layer at a ratio of 0.5 increased the maximum voltage to 10.609 V and reduced the natural frequency to 41.1 Hz.

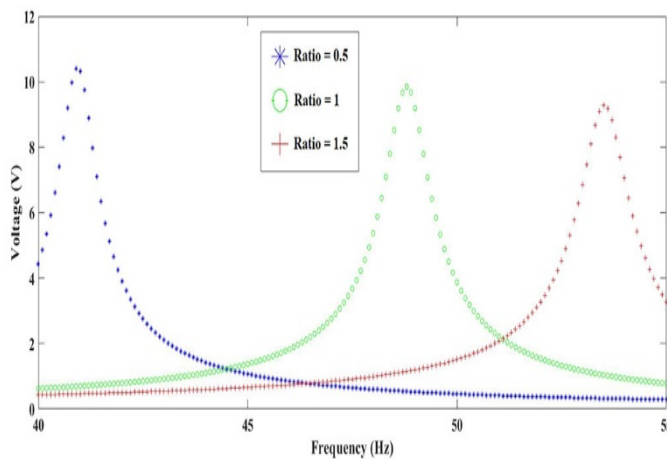


Figure 13. The voltage versus the frequency for variations in substrate Young's modulus through the analytical approach

Figure 14 shows the numerical results at 40-55 Hz in COMSOL. The numerical and analytical results show good agreement. Figure 15 plots the analytical voltage output at 37-60 Hz for piezoelectric layer elasticity moduli of 33, 66, and 99 GPa (ratios 0.5, 1.0, and 1.5). It was found that a reduction in the elasticity modulus of the piezoelectric layer reduced not only the maximum output voltage but also the natural frequency. This can be considered for reducing the natural frequency to the ambient excitation frequency range to improve harvester performance. A 50 % decrease in the elasticity modulus of the piezoelectric layer diminished the voltage to 9.2 V.

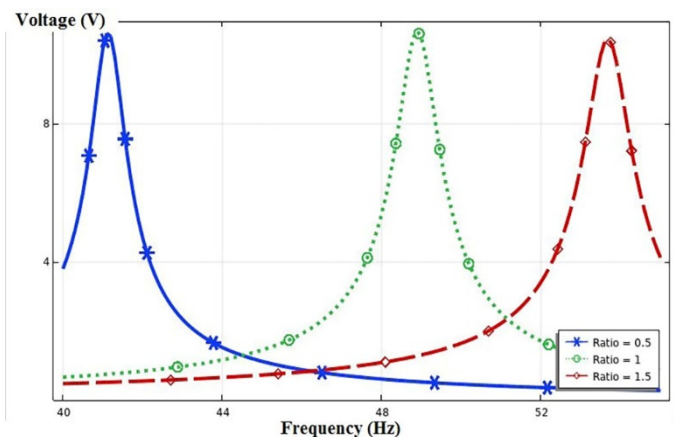


Figure 14. The voltage versus the frequency for variations in substrate Young's modulus from COMSOL Multiphysics

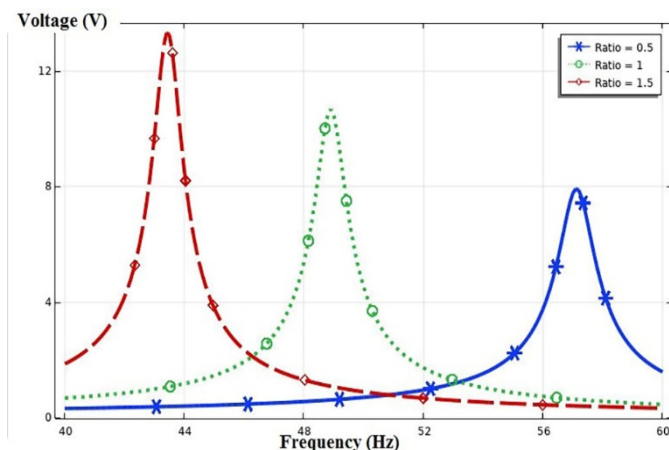


Figure 17. The voltage versus the frequency for variations in the density of the substrate layer from COMSOL Multiphysics

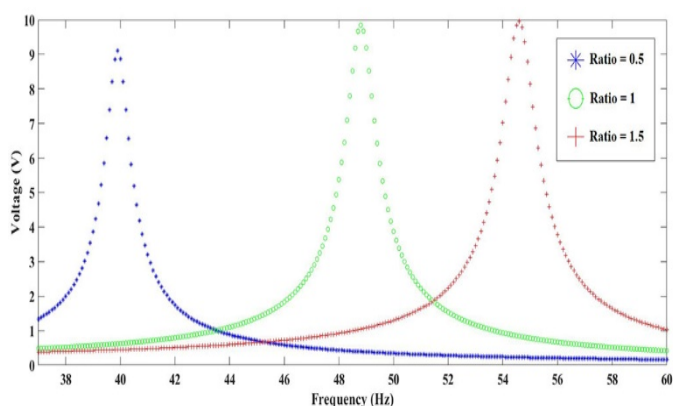


Figure 15. The voltage versus the frequency for variations in piezoelectric Young's modulus through the analytical approach

Figures 16 and 17 compare the analytical and numerical output voltages at 40-60 Hz for substrate layer densities of 3582.5, 7165, and 10747.5 kg/m³ (ratios 0.5, 1.0, and 1.5). As can be seen, the analytical and numerical (COMSOL) results well agree. A rise in the substrate density was found to raise the output voltage and diminish the natural frequency. Thus, increased substrate density could be assumed as an effective measure to improve harvester performance. A 50 % rise in the substrate density increased the analytical output voltage to 12.4 V. Furthermore, factors of 0.5, 1.0, and 1.5 in the substrate density led to numerical output voltages of 7.928, 10.679, and 13.327 V and numerical natural frequencies of 57.1, 48.9, and 43.4 Hz, respectively.

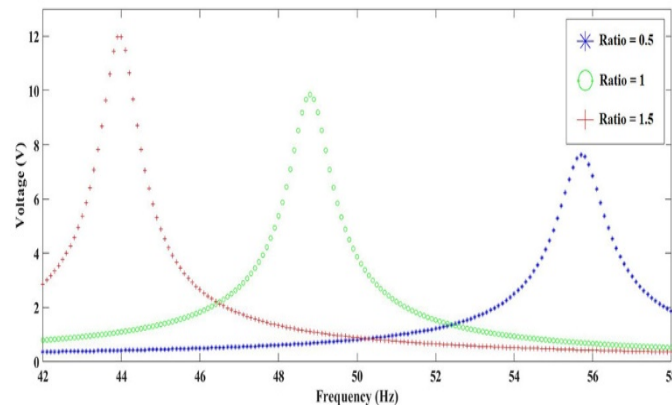


Figure 18. The voltage versus the frequency for variations in the density of the piezoelectric layer through the analytical approach

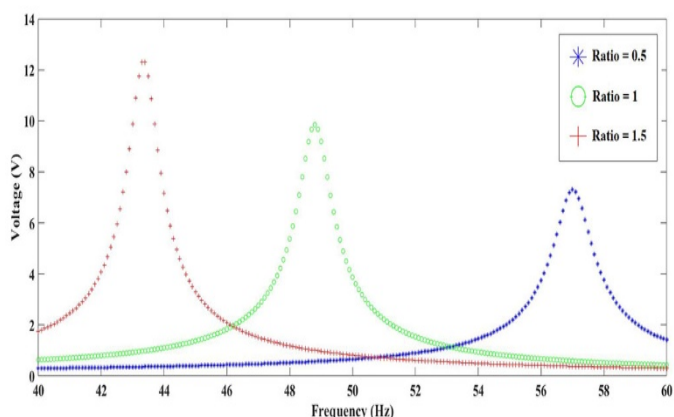


Figure 16. The voltage versus the frequency for variations in the density of the substrate layer through the analytical approach

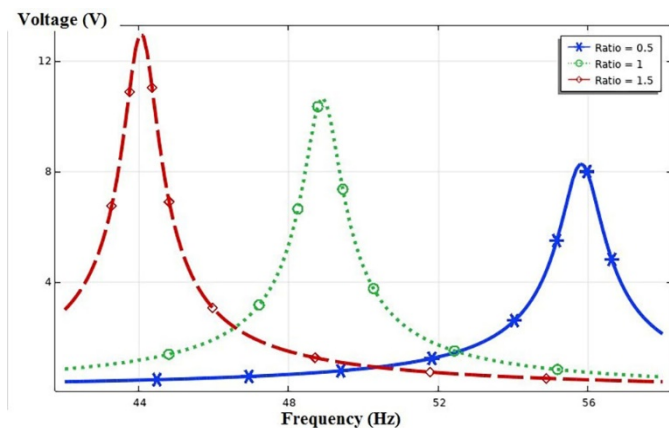


Figure 19. The voltage versus the frequency for variations in the density of the piezoelectric layer from COMSOL Multiphysics

Figures 18 and 19 compare the analytical and numerical output voltages at 42-58 Hz for piezoelectric layer densities of 3900, 7800, and 11700 (ratios 0.5, 1.0, and 1.5). Likewise, an increase in the density of the piezoelectric layer not only increased the output voltage but also substantially reduced the natural frequency. Piezoelectric layer density ratios 0.5, 1.0, and 1.5 resulted in numerical output voltages of 8.283, 10.679, and 12.977 V and numerical natural frequencies of 55.8, 48.9, and 44.0, respectively. Table 3 shows variations in the output voltage and resonant frequency of the energy harvester for the two approaches of changing physical and geometric parameters.

Table 3. Percentage variations in the output voltage and resonant frequency of the cantilever energy scavenger due to changes in physical and geometric parameters

Parameter	Symbol/Unit	Quantity 1	Quantity 2	Quantity change (%)	Natural frequency change (%)	Output voltage change (%)
Length	l (mm)	50	100	+50	-152.57	+265.65
Piezoelectric thickness	h_p (mm)	0.2	0.4	+50	+25.71	+14.35
Substrate thickness	h_s (mm)	0.25	0.5	+50	+40.52	- 4.44
Piezoelectric density	ρ_p (kg/m ³)	3900	7800	+50	-12.37	+28.98
Substrate density	ρ_s (kg/m ³)	3582.5	7165	+50	-12.36	+34.68
Piezoelectric Young modulus	Y_p (Gpa)	33	66	+50	+22.29	+8.92
Substrate Young modulus	Y_s (Gpa)	50	100	+50	+18.98	+0.66

5. CONCLUSIONS

The performance of an energy scavenger was analyzed in this study by changing the geometrical and mechanical parameters of a unimorph cantilevered beam. The analysis of the energy harvester was done using COMSOL Multiphysics finite element software besides an analytical approach. According to the results, increasing the beam length led to a noticeable decrease in natural frequency, whereas the output voltage increased. Moreover, the output voltage decreased upon an increase in the thickness of the substrate layer. However, increasing the thickness of the piezoelectric layer increased the harvested energy. Furthermore, decreasing Young's modulus of the substrate layer or increasing Young's modulus of the piezoelectric layer increased the harvested energy. Finally, increasing the density of the piezoelectric layer or that of the substrate layer increased the output voltage and reduced the resonant frequency value. The results can be taken into account to design better energy harvesters and improve their performance.

6. ACKNOWLEDGEMENT

We thank our colleagues who provided insight and expertise that greatly assisted the research.

NOMENCLATURE

b	Beam width (m)
C	Damping
D_3	Electric displacement
d_{31}	Piezoelectric constant (pm/V)
E_3	Electric field
h	Beam thickness (m)
I	Moments of inertia
i	Electric current (A)
L	Beam length (m)
M	Internal bending moment
m	Mass per unit length of the beam
q	Electric charge
R_1	Load resistance (Ω)
S	Strain
T	Stress
v	Output voltage (V)
w	General motion of the beam
Y	Young's modulus (GPa)
Greek letters	
Φ_r	Mass normalized eigenfunction
θ	Electromechanical coupling

ϵ_{33}^T	Permittivity (nF/m)
ρ	Density (kg/m ³)
λ	Dimensionless frequency number
η_r	Modal coordinate of the clamped-free beam

REFERENCES

- Fakhzan, M.N. and Muthalif, A.G., "Harvesting vibration energy using piezoelectric material: Modeling, simulation and experimental verifications", *Mechatronics*, Vol. 23, No. 1, (2013), 61-66. (<https://doi.org/10.1016/J.MECHATRONICS.2012.10.009>).
- Yang, Z., Zhou, S., Zu, J. and Inman, D., "High-performance piezoelectric energy harvesters and their applications", *Joule*, Vol. 2, No. 4, (2018), 642-697. (<https://doi.org/10.1016/j.joule.2018.03.011>).
- Williams, C.B., Shearwood, C., Harradine, M.A., Mellor, P.H., Birch, T.S. and Yates, R.B., "Development of an electromagnetic micro-generator", *Proceedings of IEEE-Circuits, Devices and Systems*, Vol. 148, No. 6, (2001), 337-342. (<https://doi.org/10.1049/ip-cds:20010525>).
- Roundy, S., Wright, P.K. and Rabaey, J., "A study of low level vibrations as a power source for wireless sensor nodes", *Computer Communications*, Vol. 26, No. 11, (2003), 1131-1144. ([https://doi.org/10.1016/S0140-3664\(02\)00248-7](https://doi.org/10.1016/S0140-3664(02)00248-7)).
- Pradeesh, E.L. and Udhayakumar, S., "Effect of placement of piezoelectric material and proof mass on the performance of piezoelectric energy harvester", *Mechanical Systems and Signal Processing*, Vol. 130, (2019), 664-676. (<https://doi.org/10.1016/j.ymssp.2019.05.044>).
- Eugeni, M., Elahi, H., Fune, F., Lampani, L., Mastroddi, F., Romano, G.P. and Gaudenzi, P., "Numerical and experimental investigation of piezoelectric energy harvester based on flag-flutter", *Aerospace Science and Technology*, Vol. 11, No. 10, (2020), 933. (<https://doi.org/10.1016/j.ast.2019.105634>).
- Liu, Z., Cao, Y., Sha, A., Wang, H., Guo, L. and Hao, Y., "Energy harvesting array materials with thin piezoelectric plates for traffic data monitoring", *Construction and Building Materials*, Vol. 302, (2021), 124-147. (<https://doi.org/10.1016/j.conbuildmat.2021.124147>).
- Zhao, Z., Dai, Y., Dou, S.X. and Liang, J., "Flexible nanogenerators for wearable electronic applications based on piezoelectric materials", *Materials Today Energy*, Vol. 20, (2021), 100690. (<https://doi.org/10.1016/j.mtener.2021.100690>).
- Su, H., Wang, X., Li, C., Wang, Z., Wu, Y., Zhang, J. and Zheng, H., "Enhanced energy harvesting ability of polydimethylsiloxane-BaTiO₃-based flexible piezoelectric nanogenerator for tactile imitation application", *Nano Energy*, Vol. 83, (2021), 105809. (<https://doi.org/10.1016/j.nanoen.2021.105809>).
- Nguyen, T.D., Deshmukh, N., Nagarath, J.M., Kramer, T., Purohit, P.K., Berry, M.J. and McAlpine, M.C., "Piezoelectric nanoribbons for monitoring cellular deformations", *Nature Nanotechnology*, Vol. 10, No. 1038, (2012), 587-593. (<https://doi.org/10.1038/nnano.2012.112>).
- Jamshidi, R. and Jafari, A.A., "Conical shell vibration control with distributed piezoelectric sensor and actuator layer", *Composite Structures*, Vol. 117, (2021), 96-117. (<https://doi.org/10.1016/j.isatra.2021.01.037>).

12. Rui, X., Zeng, Z., Zhang, Y., Li, Y., Feng, H., Huang, X. and Sha, Z., "Design and experimental investigation of a self-tuning piezoelectric energy harvesting system for intelligent vehicle wheels", *IEEE Transactions on Vehicular Technology*, Vol. 69, No. 2, (2020), 1440-1451 (<https://doi.org/10.1109/TVT.2019.2959616>).
13. Wang, K.F., Wang, B.L., Gao, Y. and Zhou, J.Y., "Nonlinear analysis of piezoelectric wind energy harvesters with different geometrical shapes", *Archive of Applied Mechanics*, Vol. 90, (2020), 721-736. (<https://doi.org/10.1007/s00419-019-01636-8>).
14. Pradeesh, E.L., Udhayakumar, S. and Sathishkumar, C., "Investigation on various beam geometries for piezoelectric energy harvester with two serially mounted piezoelectric materials", *SN Applied Sciences*, Vol. 1, No.1648, (2019), 1-11. (<https://doi.org/10.1007/s42452-019-1709-4>).
15. Zhang, S., Liu, Y., Deng, J., Tian, X. and Gao, X., "Development of a two-DOF inertial rotary motor using a piezoelectric actuator constructed on four bimorphs", *Mechanical Systems and Signal Processing*, Vol. 149, (2021). (<https://doi.org/10.1016/j.ymssp.2020.107213>).
16. Moon, K., Choe, J., Kim, H., Ahn, D. and Jeong, J., "A method of broadening the bandwidth by tuning the proof mass in a piezoelectric energy harvesting cantilever", *Sensors and Actuators, A: Physical*, Vol. 276, (2018), 17-25. (<https://doi.org/10.1016/j.sna.2018.04.004>).
17. Zhang, G., Gao, S., Liu, H. and Niu, S., "A low frequency piezoelectric energy harvester with trapezoidal cantilever beam: theory and experiment", *Microsystem Technologies*, Vol. 23, (2017), 3457-3466. (<https://doi.org/10.1007/s00542-016-3224-5>).
18. Karadag, C.V., Ertarla, S., Topaloglu, N. and Okyar, A.F., "Optimization of beam profiles for improved piezoelectric energy harvesting efficiency", *Structural and Multidisciplinary Optimization*, Vol. 63, (2021), 631-643. (<https://doi.org/10.1007/s00158-020-02714-0>).
19. Lee, M.S., Kim, C.I., Park, W.I., Cho, J.H., Paik, J.H. and Jeong, Y.H., "Energy harvesting performance of unimorph piezoelectric cantilever generator using interdigitated electrode lead zirconate titanate laminate", *Energy*, Vol. 179, (2019), 373-382. (<https://doi.org/10.1016/j.energy.2019.04.215>).
20. Alameh, A.H., Gratuze, M. and Nabki, F., "Impact of geometry on the performance of cantilever-based piezoelectric vibration energy harvesters", *IEEE Sensors Journal*, Vol. 19, No. 22, (2019), 10316-10326. (<https://doi.org/10.1109/JSEN.2019.2932341>).
21. Rua Taborda, M.I., Elissalde, C., Chung, U.C., Maglione, M., Fernandes, E., Salehian, A. and Debéda, H., "Key features in the development of unimorph stainless steel cantilever with screen-printed PZT dedicated to energy harvesting applications", *International Journal of Applied Ceramic Technology*, Vol. 17, No. 6, (2020), 2533-2544. (<https://doi.org/10.1111/ijac.13588>).
22. Ahoor, Z.H., Ghafarirad, H. and Zareinejad, M., "Nonlinear dynamic modeling of bimorph piezoelectric actuators using modified constitutive equations caused by material nonlinearity", *Mechanics of Advanced Materials and Structures*, Vol. 28, No. 8, (2021), 763-773. (<https://doi.org/10.1080/15376494.2019.1590885>).
23. Erturk, A. and Inman, D.J., "A distributed parameter electromechanical model for cantilevered piezoelectric energy harvesters", *Journal of Vibration and Acoustics*, Vol. 130, No. 4, (2008), 1-15. (<https://doi.org/10.1115/1.2890402>).
24. Rahimzadeh, M., Samadi, H. and Mohammadi, N.S., "Analysis of energy harvesting enhancement in piezoelectric unimorph cantilevers", *Sensors*, Vol. 21, No. 24, (2021), 1-16. (<https://doi.org/10.3390/s21248463>).



Research Article

Investigation of a Set of Novel Heat Exchanger Configurations of a Heat Recovery Steam Generator to Improve the Energy Efficiency of Combined Cycle Power Plant

Mohammad Rasooli Mavini^a, Hassan Ali Ozgoli^{b*}, Sadegh Safari^a

^a Department of Energy Engineering, Faculty of Natural Resources and Environment, Science and Research Branch, Islamic Azad University (IAU), P. O. Box: 14515-775, Tehran, Tehran, Iran.

^b Department of Mechanical Engineering, Iranian Research Organization for Science and Technology (IROST), P. O. Box: 33535-111, Tehran, Tehran, Iran.

PAPER INFO

Paper history:

Received: 24 January 2022

Revised in revised form: 08 May 2022

Scientific Accepted: 28 May 2022

Published: 28 September 2022

Keywords:

HRSG,

CHP,

Configuration Analysis,

Energy Efficiency,

Environment Analysis

ABSTRACT

In this study, various configuration designs of a Heat Recovery Steam Generator (HRSG) are examined to enhance the energy efficiency of a Combined Cycle Power Plant (CCPP). A novel approach to investigating ten applicable configurations of a dual pressure HRSG is used thoroughly to explore the best practice models from the energy-conserving perspective. Further, a fuel consumption assessment has been conducted to identify the best performance of the cycle and investigate the minimum pollutants released by each Heat Recovery Steam Generator (HRSG). The results revealed that four out of ten scenarios expressed considerably better performance in terms of fuel consumption, steam production, energy efficiency, and environmental considerations. Further, it was found that compared to conventional configurations, not only the selected scenarios managed to improve the low-pressure steam generation, but also 30 % fuel consumption saving in supplementary firing was achieved as both economic and environmental benefits. Moreover, the carbon dioxide saving potential for the best scenario is 51.37 kgCO₂ MWh⁻¹; consequently, the environmental benefit of it is calculated to be about 133,418 \$ MWh⁻¹.

<https://doi.org/10.30501/jree.2022.326260.1317>

1. INTRODUCTION

The upsurging consumption of fossil fuel has sparked some serious environmental problems on the global scale. Enhancing efficiency and mitigating pollutants are considered as the main concerns in any design of power generation plants. Therefore, improvement of thermal efficiency and reduction of fuel consumption of conventional cycles have gained much attention in tackle climate crises. There is no doubt that a Heat Recovery System (HRS), at any stage, plays a key role in conserving energy, not to mention the pivotal role of a Heat Recovery Steam Generator (HRSG) that is widely used as a critical component in various types of Combined Cycles (CC) [1]. Research on minimizing energy consumption and developing combined power generation systems in order to achieve better performance has deep roots in the literature [2, 3]. Some studies have highlighted the significance of recovering waste heat [4] and energy [5] into the cycle to improve energy efficiency, while many efforts have been made in the case of industrial sectors [6, 7]. Moreover, employing renewable energy sources in thermal cycles as well as using modern technologies such as gasifiers [8], fuel cells [9], and storage systems [10, 11] have attracted

the attention of many researchers. In previous literature, it is widely considered as a good way to supply the required fuel of thermal and power systems using renewable resources such as biomass and biogas to mitigate the environmental consequences [12]. Ultimately, the application of integrated cycles such as Combined Heat and Power (CHP) and poly-generation systems has been considered as a significant purpose of optimizing energy consumption and reducing environmental issues associated with the Combined Cycle Power Plants (CCPPs) [13], given that these systems are still broadly adopted as a key player in supplying electricity demand in every corner of the world. The main reason behind this broad application is ample resources of the Nature Gas (NG) which is available in huge amount and it gives higher overall thermal efficiency [14]. Given that the Heat Recovery Steam Generator (HRSG) is an indispensable part of these cycles and its function is to recover the waste heat present in the exhaust gases of the gas turbine and to generate the steam to run a steam power cycle, it is broadly highlighted in previous studies. Table 1 lists a review of the literature regarding the optimum performance analysis of CCPPs. It offers the design parameters, objectives, examination method, and the outstanding results and observations.

Moreover, effective parameters in the best feasible layout will be selected by considering the environmental aspects as

*Corresponding Author's Email: a.ozgoli@irost.org (H.A. Ozgoli)

URL: https://www.jree.ir/article_158101.html

Please cite this article as: Rasooli Mavini, M., Ozgoli, H.A. and Safari, S., "Investigation of a set of novel heat exchanger configurations of a heat recovery steam generator to improve the energy efficiency of combined cycle power plant", *Journal of Renewable Energy and Environment (JREE)*, Vol. 10, No. 1, (2023), 68-82. (<https://doi.org/10.30501/jree.2022.326260.1317>).



the main algorithm. Various heat exchanger layouts of the HRSG in a CCPP have been investigated to examine the maximum amount of generated steam at different pressure levels. In this regard, assessing the fuel consumption to

identify the best performance of the cycle and investigating the minimum pollutants released of each HRSG configuration are accomplished.

Table 1. Literature review of optimum performance analysis of CCPPs

Design parameters	Considerations	Examination approach	Key Findings	Ref.
Mass flow rate, HRSG inlet gas temperature	Cycle efficiency	Thermodynamic and parametric analyses	Increasing the inlet gas to the HRSG until 650 °C is favorable. Increase in this temperature reduces the efficiency.	[15]
Temperature, steam pressure and pinch point	Energetic and exeric efficiency	Thermodynamic methodology	By increasing the pinch point, the power to heat ratio also increases; however, the first-law and second-law efficiency decreases while the pinch point increases. Also, reheat process has received considerable improvement in output power and thermal power production.	[16]
pressure ratio, cycle temperature ratio, number of reheats and cycle pressure drop	Power-output, thermal efficiency, and exergy destruction	Thermodynamic analysis using second law	The efficiency and power output reach maximum at an intermediate pressure ratio. 50 % of the overall cycle exergy destruction occurs in the combustion chamber.	[17]
Operating conditions and cost related to fuel consumption, investment, and maintenance	Cost, and mass flowrate	Thermo-economic optimization using genetic algorithm	Various methods are investigated to establish how to reduce the objective function.	[18]
Mass flow rate, HRSG inlet gas temperature and pressure	Increasing efficiency over than 60 % without resorting new GT	Thermodynamic analysis and parametric study	Optimization of HRSG is sufficient to obtain the efficiency of a CCPPs in the order of 60 %. Gas to gas recuperation enhances the overall efficiency to 65 %.	[19]
Turbine Inlet Temperature (TIT), and pinch points the steam turbine inlet pressure	Optimization of the triple-pressure reheat combined cycle, irreversibility reduction of a HRSG	Thermodynamic analysis and parametric study	Optimal triple-pressure reheat CC is 1.7 % higher in efficiency than the reduced irreversibility triple-pressure reheat CC.	[20]
Inlet temperature to HRSG, pressure level, cost	HRSG pressure levels on exergy efficiency of combined cycle power plants	Thermo-economic optimization	Exergy destruction rate in HRSG is affected by an increase in the number of pressure levels and causes sensible improvement in exergy efficiency of the whole cycle.	[21]
Compression ratio, stack temperature and cooling steam ratio, temperature values of turbine inlet	Overall thermal efficiency and power output of the GT cycle were optimized	Thermodynamics optimization	The combined cycle gas turbine plants indicates better power output at 400 MW.	[22]
Ambient conditions	Electricity power generation and consumption of the fuel of the gas turbine cycle	Thermodynamic and parametric analysis	In comparison to the annual production in ISO conditions, the loss in electricity generation is about 2.87-0.71 %.	[23]
Steam quality at steam turbine outlet	Overall output power and efficiency	Multi-Objective Optimization (MOO) for the comprehensive thermodynamic analysis	The steam turbine inlet temperature and pressure increase when the steam quality at the steam turbine outlet increases.	[24]

A challenging problem that arises in this domain is the optimization of HRSG which not only is significantly important for the design of CCPPs but also plays a particular role in maximizing the power delivered to the Steam Turbine (ST) and improves the overall performance of the power cycle. As discussed earlier, achieving higher electric and thermal efficiency of the CCPPs requires optimizing the entire plant, and the three key components comprising the Gas Turbine (GT), HRSG, and Steam Turbine (ST). However, among the three mentioned component plants, the

performance of the GT is of priority as the predominant influencer in the performance; most of the previous research studies in this field aim to solve this problem. However, the HRSG has rarely been studied directly. Furthermore, few studies have focused on different configurations of it as the HRSG component of the CCPPs can be made on order particularly for each GT unit, while the GT and ST can be selected from the set of commercially available range plants [24].

Based on the aforementioned explanations, no comprehensive study has been performed on the optimal configuration of heat exchangers in the HRSG system, so far. In the proposed new approach, the arrangement of HRSG heat exchangers in terms of thermal efficiency has been evaluated simultaneously with the electrical efficiency of the whole CCGP. The mathematical model described in this study makes it possible to determine the optimal configuration of the HRSG heat exchanger. In this way, heat exchangers of each pressure level can be placed in.

2. MATERIAL AND METHOD

2.1. System description

Figure 1 shows a chemotic flow diagram of a dual-pressure CCGT Power Plant. A CCGT Power Plant, generally, can be divided into three major subsystems: upstream cycle (Brayton cycle), downstream cycle (Rankin cycle), and HRSG. The system also includes other auxiliary equipment such as a

pump, condenser, and cooling tower. In the upstream cycle, fresh air enters the compressor where compressed and leaves with higher temperature and pressure than the inlet point. In the combustion chamber, the compressed air and fuel, typically Natural Gas (NG) or diesel fuels, contribute to the combustion reaction. Then, combustion products will be expanded in the gas turbine for both generating electrical power employing generator and producing mechanical work for running the compressor. Further, the hot exhaust gas flow of GT, which is still capable of doing work, enters into the HRSG. In this study, there are several heat exchangers in dual pressure HRSG to use the thermal energy of this stream by passing through steps in the economizer, evaporator, and super heater. Eventually, superheat steam is produced to run High-Pressure (HP) and Low-Pressure (LP) steam turbines. The steam turbine sends its energy to the generator drive shaft, where it is converted into additional electricity.

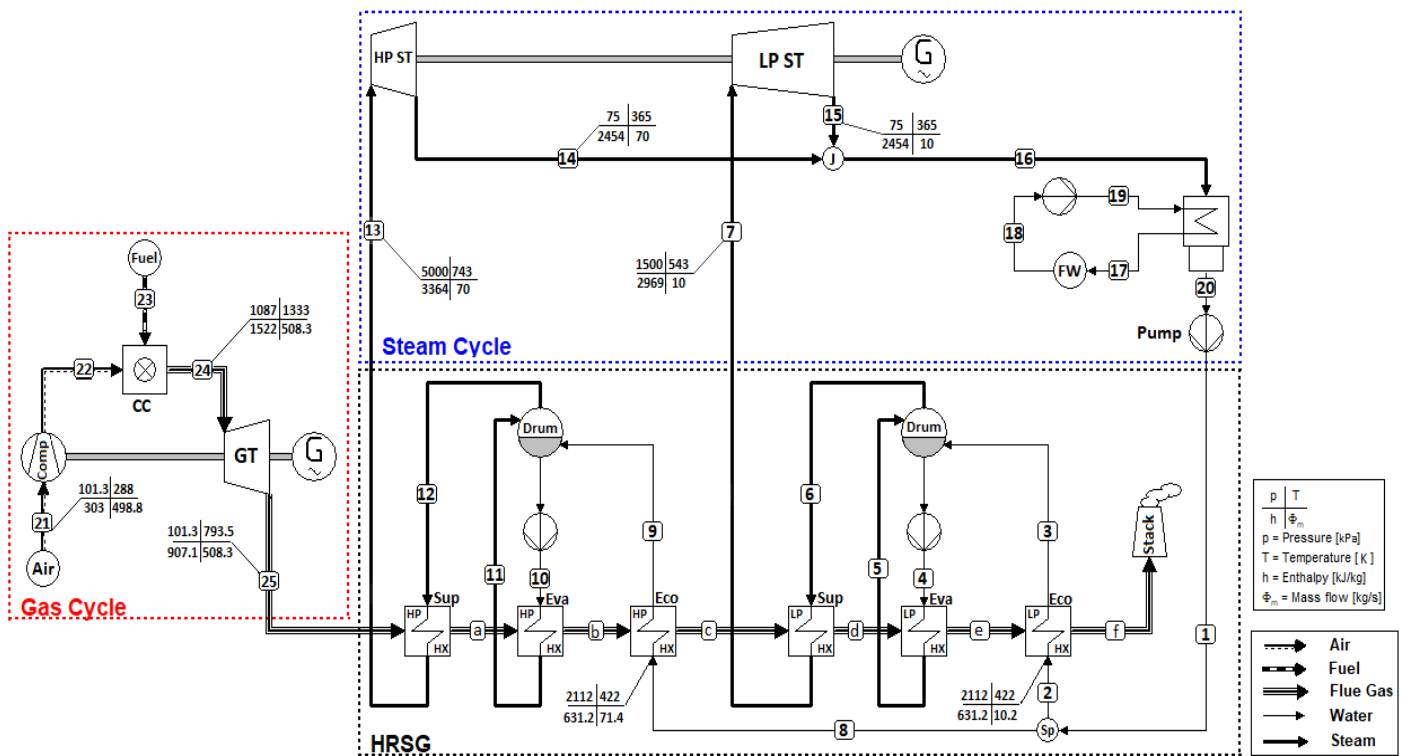


Figure 1. Schematic flow diagram of a dual-pressure CCGT power plant

2.2. Model assumptions

Several principal assumptions are considered to solve the model of the CCGT Power Plant. These assumptions which simplify the developed model and accelerate the calculation process are listed as follows:

- All processes have been done in a steady flow and steady-state conditions.
- Natural gas is considered as supplied fuel to the system.
- The ISO ambient condition (Temperature of 288 K and pressure of 101.3 kPa) is assumed.
- Siemens GT-V94.2 is used in Bryton Cycle.
- 5 % pressure drop is presumed in the both combustion chamber and HRSG.
- The HRSG unit is considered as a two-pressured unit.
- The blowdown of HP and LP drums is assumed 2 %.

- AP is considered to be characterized by 15 degrees.
- 0.86 and 0.90 are assumed as isentropic efficiency of compressor and isentropic efficiency of gas turbine, respectively.

These assumptions are employed throughout the analysis to derive the corresponding equations of each system component [18, 25, 26].

2.3. System modeling

The model was developed in Engineering Equation Solver (EES), which provided thermodynamic properties required to model and evaluate the performance of the CCGT Power Plant. For simplification, the calculation process model is divided into three major subsystems. Then, these sections are connected to provide an appropriate basis for both thermodynamic and environmental analyses of the system.

Further, first, the system subsections including compression and combustion, Gas Turbinr, dual-pressure HRSG, and Steam Turbine are explained by considering such design parameters as Compressor Pressure Ratio (CPR), Turbine Inlet Temperature (TIT), electricity power demand, blowing down amounts of high- and low-pressure drums, HP, and LP steam temperature and superheat approach temperature difference. Next, the environmental model is discussed. This study developed a mathematical model of an industrial gas turbine, validated the results through comparison of the actual performance of the Fars CCGT power plant located in Iran,

and employed the same Siemens V94.2 turbines to produce electricity. Of note, the mentioned GT model is vastly used in the majority of power plants in Iran.

2.3.1. Combined cycle gas turbine power plant

In order to perform energetic analysis on the CCGT Power Plants, it is required to consider equations that are dominant at each component of the cycle. The equations regarding Compressor, Gas Turbine (GT), and Combustion Chamber (CC) are briefly presented in Table 2 [25].

Table 1. Governing equations on CCGT power plant [25]

CCGT power plant relations	Equations No.
$T_{ACout} = T_{ACin} \left\{ 1 + \frac{1}{\eta_{AC}} \left[RPC^{\frac{\gamma_{air}-1}{\gamma_{air}}} - 1 \right] \right\}$	(1)
$\dot{w}_{AC} = \dot{m}_{air} C_{p_{air}} (T_{ACout} - T_{ACin})$	(2)
$C_p = a + b \frac{T}{100} + c \left(\frac{T}{100} \right)^{-2}$	(3)
$a = \sum_{i=1}^{noc} a_i \times mf_i$	(4)
$b = \sum_{i=1}^{noc} b_i \times mf_i$	(5)
$c = \sum_{i=1}^{noc} c_i \times mf_i$	(6)
$RPC = \frac{P_{out}}{P_{in}}$	(7)
$Heat\ Rate = \frac{3412}{\eta_{th}} \left[\frac{Btu}{kWh} \right]$	(8)
$\dot{m}_{Fuel} = \frac{PW_{GT} \times Heat\ Rate}{LHV}$	(9)
$O_{2theo} = [2CH_4 + 3.5C_2H_6 + 5C_3H_8 + 6.5C_4H_{10} + 8C_5H_{12}] \times \dot{m}_{Fuel}$	(10)
$\dot{m}_{airtheo} = \frac{O_{2theo}}{0.21} \times MW_{air}$	(11)
$\dot{m}_{airAct} = \dot{m}_{airtheo} \times \left(\frac{Excess\ Air\ \%}{100} + 1 \right)$	(12)
$T_{GTout} = T_{GTin} \left\{ 1 - \eta_{GT} \left[1 - RPT^{\frac{1-\gamma_{FG}}{\gamma_{FG}}} \right] \right\}$	(13)
$\dot{w}_{GT} = \dot{m}_g C_{p_{FG}} (T_{GTin} - T_{GTout})$	(14)
$RPT = RPC \times (1 - \Delta P)$	(15)
$\dot{Q} - \dot{W} = \sum \dot{m}_{out} h_{out} - \sum \dot{m}_{in} h_{in}$	(16)
$H_{ACin} = a(T_{ACin} - T_{Ref}) + \frac{b}{100} (T_{ACin}^2 - (T_{ACin} \times T_{Ref})) + c(100)^2 \left(\frac{1}{T_{ACin}} - \frac{T_{Ref}}{T_{ACin}^2} \right) + H_{Ref}$	(17)
$S_{ACin} = a \ln \left(\frac{T_{ACin}}{T_{Ref}} \right) + \frac{b}{100} \times T_{ACin} \times \ln \left(\frac{T_{ACin}}{T_{Ref}} \right) + c(100)^2 \left(\frac{1}{T_{ACin}^2} \right) \ln \left(\frac{T_{ACin}}{T_{Ref}} \right) - R_{air} \ln \left(\frac{P_{ACin}}{P_{Ref}} \right) + S_{Ref}$	(18)
$S'_{ACout} = a \ln \left(\frac{T'_{ACout}}{T_{ACin}} \right) + \frac{b}{100} \times T'_{ACout} \times \ln \left(\frac{T'_{ACout}}{T_{ACin}} \right) + c(100)^2 \left(\frac{1}{T'_{ACout}^2} \right) \ln \left(\frac{T'_{ACout}}{T_{ACin}} \right) - R_{air} \ln \left(\frac{P_{ACout}}{P_{ACin}} \right) + S_{ACin}$	(19)
$\eta_{ACisen} = \frac{H'_{ACout} - H_{ACin}}{H_{ACout} - H_{ACin}}$	(20)
$\dot{m}_{CCout} h_{CCout} = \dot{m}_{CCin} h_{CCin} + \dot{m}_{Fuel} \times [(\eta_{CC} \times LHV) + (C_{p_{Fuel}} \times T_{Fuel})]$	(21)
$H_{GTin} = a'(T_{GTin} - T_{ACout}) + \frac{b'}{100} (T_{GTin}^2 - (T_{GTin} \times T_{ACout})) + c'(100)^2 \left(\frac{1}{T_{GTin}} - \frac{T_{ACout}}{T_{GTin}^2} \right) + H_{ACout}$	(22)

$S_{GT_{in}} = a' \ln \left(\frac{T_{GT_{in}}}{T_{AC_{out}}} \right) + \frac{b'}{100} \times T_{GT_{in}} \times \ln \left(\frac{T_{GT_{in}}}{T_{AC_{out}}} \right) + c'(100)^2 \left(\frac{1}{T_{GT_{in}}^2} \right) \ln \left(\frac{T_{GT_{in}}}{T_{AC_{out}}} \right) - R_{FG} \ln \left(\frac{P_{GT_{in}}}{P_{AC_{out}}} \right) + S_{AC_{out}}$	(23)
$S'_{GT_{out}} = a' \ln \left(\frac{T'_{GT_{out}}}{T_{GT_{in}}} \right) + \frac{b'}{100} \times T'_{GT_{out}} \times \ln \left(\frac{T'_{GT_{out}}}{T_{GT_{in}}} \right) + c'(100)^2 \left(\frac{1}{T'_{GT_{out}}^2} \right) \ln \left(\frac{T'_{GT_{out}}}{T_{GT_{in}}} \right) - R_{FG} \ln \left(\frac{P_{GT_{out}}}{P_{GT_{in}}} \right) + S_{GT_{in}}$	(24)
$H'_{GT_{out}} = a'(T'_{GT_{out}} - T_{GT_{in}}) + \frac{b'}{100} (T'_{GT_{out}}^2 - (T'_{GT_{out}} \times T_{GT_{in}})) + c'(100)^2 \left(\frac{1}{T'_{GT_{out}}} - \frac{T_{GT_{in}}}{T'_{GT_{out}}^2} \right) + H_{GT_{in}}$	(25)
$\eta_{GT_{isen}} = \frac{H_{GT_{in}} - H_{GT_{out}}}{H_{GT_{in}} - H'_{GT_{out}}}$	(26)

Here, the RPC term in Equation (7) is the ratio of outlet air pressure to inlet air pressure that, according to the specifications of Siemens GT-V94.2, is equal to 11.31 [26]. To calculate the consumed fuel in a combustion chamber with regard to the heat rate, Equations (8) and (9) are used as follows [26]; then, the combustion equations can be written and solved as demonstrated in Equations (10-12) [26]. After solving Equations (8-12), required oxygen for combustion reaction will be obtained. Finally, by considering excess oxygen which is used to ensure complete combustion and increase mass flow rate, the actual amount of oxygen and air suction in the compressor will be obtained [26]. Since our work is always extracted from the expanding high pressure gas in the gas turbine system, outlet temperature and generated work are determined using Equations (13) to (15) [26, 27]. Further, the mass and energy balance equations for each component can be obtained from Equations (16) [26]. The calculation of enthalpy of flow in the inlet and outlet of each component is required for each correspondent equation of mass and energy balance as well as other cycle's components [26]. The enthalpy and entropy of the hot stream entering the gas turbine are obtained from Equations (22-25) [26].

Based on Equation (26) and isentropic efficiency of the gas turbine, the actual enthalpy of exhausted flow from the gas turbine can be obtained. The actual temperature of the outlet flow in the gas turbine as well as the entropy of the outlet stream from the gas turbine are in operating condition. Then, by considering the enthalpy of flow at the inlet and outlet of the gas turbine, the produced work by the turbine can be calculated using Equation (14) and in relation to the cycle. Finally, the net power generated by Gas Cycle (GC) as well as thermal efficiency of the gas cycle can be obtained by means of Equations (27) and (28), respectively [26].

$$W_{netGC} = W_{GT} - W_{AC} \quad (27)$$

$$\eta_{thGC} = \frac{W_{netGC}}{Q_{in}} \quad (28)$$

In the steam cycle, the generated work by turbines can be obtained based on energy equation. With having pre-defined temperature and pressure of steam in LP and HP superheated conditions, the enthalpy of steams can be calculated. Then, by employing Equation (29), the work of steam turbine can be obtained. Further, according to the description given above, the net efficiency of the combined cycle power plant is calculated from integration of gas turbine cycle and steam cycle as described in Equations (30) to (32) [19, 26].

$$W_{ST} = \dot{m}_{HP}(h_{HP_{in}} - h_{HP_{out}}) + \dot{m}_{LP}(h_{LP_{in}} - h_{LP_{out}}) \quad (29)$$

$$\eta_{ST} = \frac{W_{ST} - W_{Pump}}{Q_{inST}} \quad (30)$$

$$\eta_{CCPP} = \frac{W_{GT} - W_{AC} + W_{ST} - W_{Pump}}{Q_{inCCPP}} \quad (31)$$

$$\eta_{Electrical} = \frac{W_{GT} - W_{AC} + W_{ST}}{Q_{inCCPP}} \quad (32)$$

2.3.2. Dual pressure HRSG

Two paths for exchanging heat in HRSG should be considered. The first path is where the hot exhausted gas flow from the gas turbine enters the HRSG unit and it moves towards the stack and eventually vents into the environment after passing through the exchanger tubes inside it. The second path is where the entering water to the HRSG unit passes through the inside of heat exchanger tubes until it is turned to superheated steam which will drive the steam turbine. In the base scenario of (A), for modeling superheated part and high-pressure evaporator, the following equations are employed [25]:

$$\begin{aligned} \dot{m}_{FG} \times C_{pFG} \times (T_a - T_c) \\ = \dot{m}_{HP}(h_{12} - h_{11}) + \dot{m}_{HP}(h_{11} - h_9) \\ + \dot{m}_{HP}(1 + BLD_{HP} \%)(h_9 - h_8) \end{aligned} \quad (33)$$

In addition, for high-pressure economizer, low-pressure super heater, and the evaporator, we have Equation (34) as follows [25]:

$$\begin{aligned} \dot{m}_{FG} \times C_{pFG} \times (T_c - T_f) \\ = \dot{m}_{HP}(1 + BLD_{HP} \%)(h_8 - h_7) \\ + \dot{m}_{LP}(h_6 - h_5) + \dot{m}_{LP}(h_5 - h_3) \\ + \dot{m}_{LP}(1 + \% BLD_{LP})(h_3 - h_2) \end{aligned} \quad (34)$$

Through Equations (33) and (34), the production values of high-pressure and low-pressure superheated steam will be obtained [24].

$$\begin{aligned} \dot{m}_{DB} \times C_{pFG} \times (T_{c_{new}} - T_f) \\ = \dot{m}'_{HP}(1 + BLD_{HP} \%)(h_8 - h_7) \\ + \dot{m}'_{LP}(h_6 - h_5) + \dot{m}'_{LP}(h_5 - h_3) \\ + \dot{m}'_{LP}(1 + BLD_{LP} \%)(h_3 - h_2) \end{aligned} \quad (35)$$

After calculating the corrected temperature at point C, the HRSG input temperature is modified through Equation (36) [25]:

$$\begin{aligned} \dot{m}_{DB} \times C_{pFG} \times (T_{a_{new}} - T_{c_{new}}) \\ = \dot{m}'_{HP}(h_{12} - h_{11}) + \dot{m}'_{HP}(h_{11} - h_9) \\ + \dot{m}'_{HP}(1 + BLD_{HP} \%) (h_9 - h_8) \end{aligned} \quad (36)$$

In the end, the temperature of the inlet flow into the HRSG that should produce the amount of required steam at different pressure levels will be determined. Also, by solving the mass and energy balance equations for the duct burner, the amount of auxiliary fuel that provides the supplementary firing system will be calculated. Then, the amount of air for delivering complete combustion can be calculated.

$$\begin{aligned} \dot{m}_{FG} \times h_{GT_{out}} + \dot{m}_{FA} \times h_{FA} \\ + \dot{m}_{AxFuel} \times \left(LHV + (C_{pFuel} \times T_{Fuel}) \right) \\ = \dot{m}_{DB} \times C_{pFG} \times T_{a_{new}} \end{aligned} \quad (37)$$

$$\dot{m}_{FA} = \frac{\dot{m}_{AxFuel}}{MW_{Fuel}} \times 10.96 \times MW_{air} \quad (38)$$

$$\dot{m}_{DB} = \dot{m}_{FG} + \dot{m}_{FA} + \dot{m}_{AxFuel} \quad (39)$$

2.4. Environmental modeling

The less a system generates CO₂ emissions, the more environmentally-friendly the plant is [12]. In order to analyze the combustion products, the combustion equation must first be written and solved for each compartment of fuel to obtain the quantities of combustion products. In this equation, the amount of carbon dioxide and argon in the combustion air has been monitored. According to the general combustion equation for fuel, the following equation is given [28].

$$\begin{aligned} C_x H_y + n \times \left(1 + \left(\frac{\text{Excess air } \%}{100} \right) \right) \\ \times (O_2 + 3.72 \times N_2 + 0.04 \times AR \\ + 0.0014 \times CO_2) \\ = n_1 \times CO_2 + n_2 \times H_2O + n_3 \times N_2 \\ + n_4 \times AR + n_5 \times O_2 \end{aligned} \quad (40)$$

To evaluate the environmental expenses associated with CO₂ emissions in conventional systems, Equation (41) is simply employed [27]. Herein, \dot{z}_{CO_2} is the environmental damage cost, \dot{m}_{CO_2} potential emission of CO₂, and C_{CO_2} is the unit damage cost which is equal to 0.024 \$/kg [29]. Therefore, the carbon emission saving potential of the present study can be calculated for each configuration design through Equation (42), where $\Omega_{CO_2_{ref}}$ is the CO₂ emission from a base scenario which is scenario (A) in this study. The environmental benefit (BEN_{env}) of the best scenario designed can be calculated using Equation (43) [8, 27].

$$\dot{z}_{CO_2} = \dot{m}_{CO_2} \times C_{CO_2} \quad (41)$$

$$\Omega_{CO_2_{potential}} = \Omega_{CO_2_{ref}} - \Omega_{CO_2_{sys}} \quad (42)$$

$$BEN_{env} = \dot{z}_{CO_2} \times \Omega_{CO_2_{potential}} \quad (43)$$

3. METHODOLOGY

3.1. Solution methodology

In this work, a solution methodology is illustrated and indicated in Figure 2. The key intention of the proposed

methodology is to offer the operation solutions based on technical model for engineers. The technical proposed model will be solved in three consecutive steps by employing all the required equations in a structured manner, as illustrated in Figure 2. Later, power and efficiency of each component as well as the pollutant emission for the winner scenario as dependent variables will be determined.

3.2. Input parameters and validation

The model developed in the preceding sections is used to simulate and evaluate the performance of the CCGT power plant. The model input parameters of the Bryton cycle of the studied plant are listed in Table 3. More details may be found in [18, 26]. Initial values for the CCGT power plant are presented in Table 4 and more details can be found in [25, 26].

In order to ensure the model validation and accuracy, some modeling results of the CCGT power plant are compared to those of the installed CCGT power plant in south of Iran, and the results are shown in Table 5. It is observed that the presented results reasonably agree with the actual outcomes of the installed plants.

Besides, in Table 6, the values of the specific heat capacity have been calculated with minor difference from the measured values. As a result, the enthalpy of the flow can be accurately estimated. Thus, another major parameter of HRSG modeling, which is the enthalpy of hot gas flow entering it, was obtained with high accuracy.

3.3. Scenario description

Regarding the layout of heat exchangers in HRSG, 10 designed scenarios are presented and discussed in Table 7 labelled from (A) to (J). It is worth noting that among them, two scenarios of (G) and (H) have been presented and evaluated from different aspects in previous studies, whereas others are examined in the present study to explore the best configuration in terms of energy improvement. First of all, in scenario (A), a low-pressure economizer, evaporator, and super heater as well as a high-pressure economizer, evaporator, and super heater are arranged along the length of HRSG and from the end to the first part close to the outlet of the gas turbine, while in scenario (B), it is shown that they are in the same order, except that the high-pressure economizer is fed from the output of low-pressure economizer, as depicted schematically below. Next, in scenario (D), the same layout of scenario (C) is considered; however, as is shown earlier, the high-pressure economizer inlet will be supplied from the low-pressure economizer as previously discussed. For a better understanding of the scenarios, Figure 3 presents the base scenario and Table 7 shows the all scenarios and their associated changes.

Further, in scenario (E), low-pressure super heater is delivered to the beginning part of HRSG ahead of HP superheater, while in scenario (F), the economizers are connected. Furthermore, in scenario (G), the high-pressure economizer is moved ahead of the low-pressure superheater and after the low-pressure evaporator. In scenario (H), the outlet of the low-pressure economizer is connected to the inlet of the high-pressure economizer with the same arrangement; in scenario (I), the low-pressure super heater is moved forward, but the other heat exchangers have the same arrangement of first scenario (A). Finally, in scenario (J), the inlet and outlet of economizers are connected.

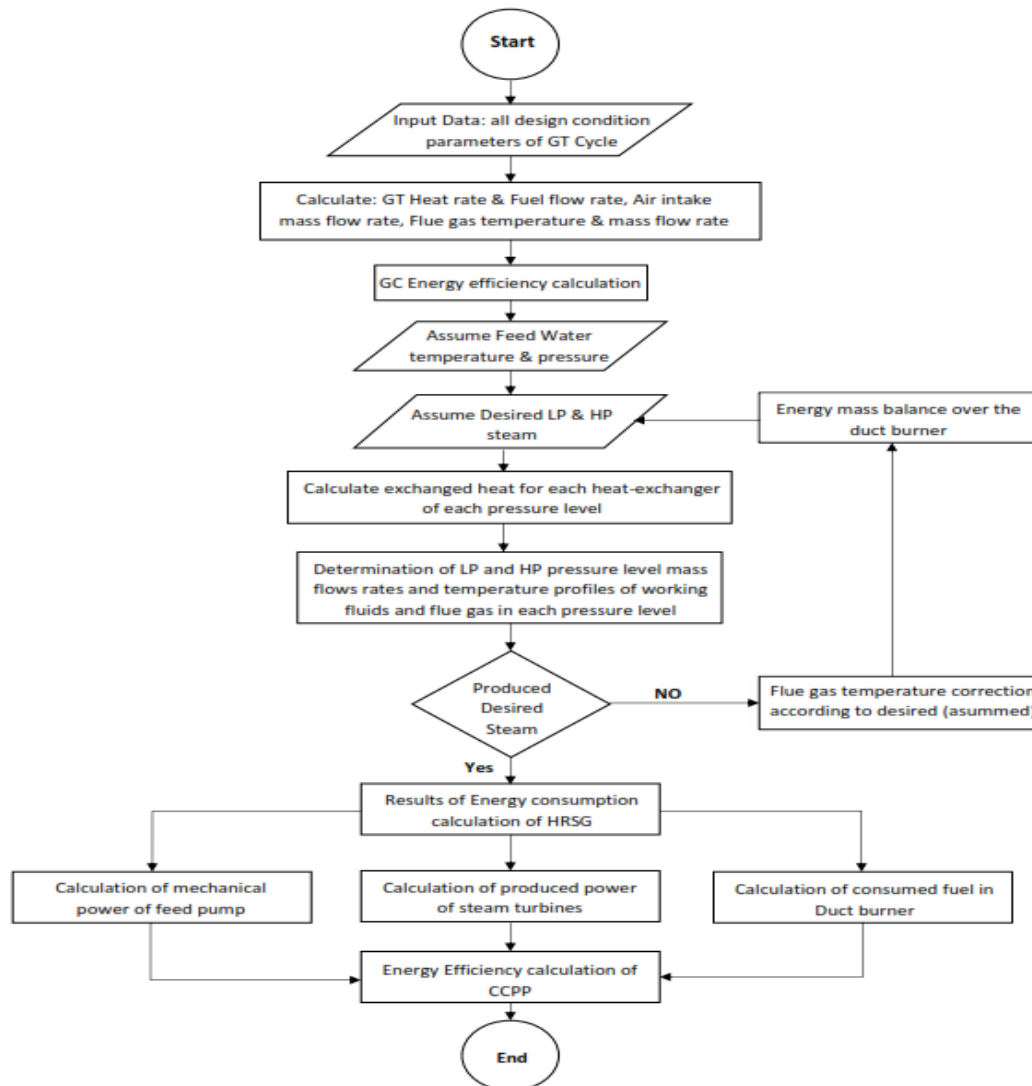


Figure 2. Solution procedure of the CCGT power plant model

Table 3. Model input parameters for the Brayton cycle [18, 26]

Parameters	Value	Unit
Compressor isentropic efficiency	87	%
Compressor flow rate	500	[kg/s]
Combustion chamber efficiency	99	%
Excess air	210	%
Fuel flow rate	9.56	[kg/s]
Pressure ratio of cycle	11.30	-
Pressure loss	5	%
Turbine isentropic efficiency	90	%
Turbine inlet temperature	1333	[K]

Table 4. Initial values for modeling of the presented CCGP

Parameter	Value	Unit
Electricity power demand	159,000	[kW]
Ambient air temperature	288.15	[K]
Ambient air pressure	101.30	[kPa]
Reference temperature	273.15	[K]
Reference pressure	101.30	[kPa]
Approach temperature	15	[K]
Fuel temperature	293.15	[K]

Table 5. Thermo-physical property of medium fluid in the BC

Items	Model results		Fars power plant		Relative error(%)
	Inlet	Outlet	Inlet	Outlet	
Compressor					
Temperature [K]	304.95	626.9	304.9	629.95	0.48
Pressure [kPa]	101.30	1145	-	-	-
Mass flow rate [kg/s]	498.81	498.8	504.4	504.40	1.11
Enthalpy [kJ/kg]	303.01	647.5	305.3	640.51	-1.08
Combustion chamber					
Temperature [K]	594.3	1333	640	1333	0
Pressure [kPa]	1145	1087	-	-	-
Mass flow rate [kg/s]	498.8	508.3	504	513.5	1.01
Enthalpy [kJ/kg]	612.00	1522	-	-	-
Gas Turbine					
Temperature [K]	1333	796.7	1333	809.95	1.63
Pressure [kPa]	1087	101.3	-	-	-
Mass flow rate [kg/s]	508.3	508.3	513.5	513.50	1.01
Enthalpy [kJ/kg]	1522	907.1	-	873.24	-3.87

Table 6. The specific heat capacity comparison with Fars power plant

Specific heat	Calculated [J/kg. K]	Measured [J/kg. K]	Relative error (%)
N ₂	1.037	1.039	0.19
O ₂	0.910	0.916	0.65
Ar	0.521	0.520	-0.19
CO ₂	0.827	0.835	0.95
Dry air	1.001	1.005	0.39

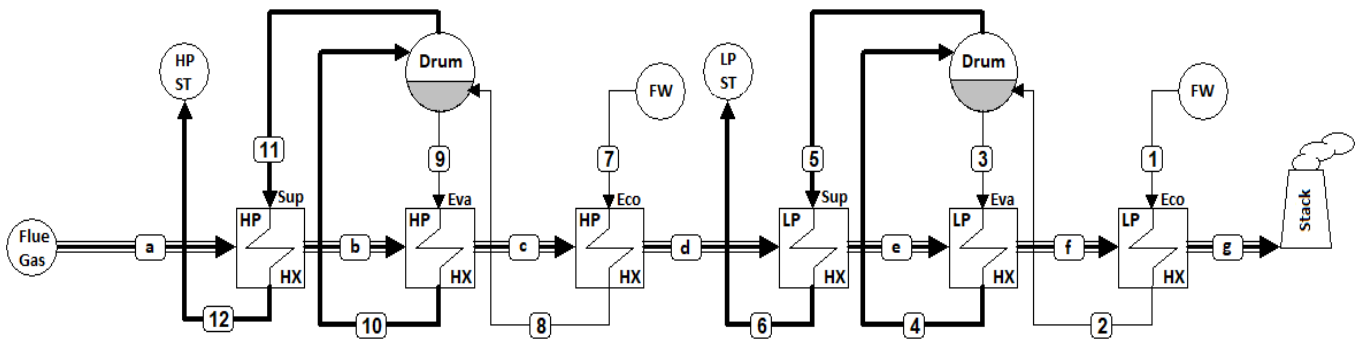


Figure 3. Base scenario of (A)

Table 7. Scenario comparison and highlighting the changes in each scenario with the previous one

Scenario comparison	Previous layout	New layout
Scn. B Vs. Scn. A		
	Using low-pressure economizer preheated water for high-pressure economizer input	
Scn. C Vs. Scn. A		
	Placement of high-pressure economizer after the low-pressure economizer	
Scn. D Vs. Scn. C		
	Application of low-pressure economizer preheated water for high-pressure economizer input	

<p>Scn.E Vs. Scn.A</p>		
<p>High-pressure economizer placement before low-pressure evaporator and low-pressure superheater after high-pressure evaporator</p>		
<p>Scn. F Vs. Scn. E</p>		
<p>Using low-pressure economizer preheated water for high-pressure economizer input</p>		
<p>Scn. G Vs. Scn. A</p>		
<p>Placement of high-pressure economizer before the superheater</p>		
<p>Scn. H Vs. Scn G</p>		
<p>Using low-pressure economizer preheated water for high-pressure economizer input</p>		
<p>Scn. I Vs. Scn A</p>		
<p>Low-pressure superheater placement before high-pressure superheater</p>		
<p>Scn. J Vs. Scn. I</p>		
<p>Using low-pressure economizer preheated water for the high-pressure economizer input</p>		

4. RESULTS AND DISCUSSION

In this section, the effect of different heat exchanger arrangements based on various scenarios on the system performance is determined and thoroughly discussed. The temperatures of hot exhausted gas flow passing through the

HRSG for all scenarios are presented in Table 8. Also, the thermodynamic properties of flue gas for the base scenario (A) are presented in Table 9 (A) and water and steam flows are presented in Table 9 (B).

Table 8. Flue gas temperature in each section of the proposed HRSG scenarios

Flue gas stream line	Scn. A T [K]	Scn. B T [K]	Scn. C T [K]	Scn. D T [K]	Scn. E T [K]	Scn. F T [K]	Scn. G T [K]	Scn. H T [K]	Scn. I T [K]	Scn. J T [K]
a	796.7	796.7	796.7	796.7	796.7	796.7	796.7	796.7	796.7	796.7
b	735.7	735.7	735.7	735.7	737.1	737.1	735.7	735.7	736.1	736.4
c	552.1	552.1	552.1	552.1	731.4	731.4	552.1	552.1	734.6	733.5
d	503.1	519.2	546.8	546.8	552.1	552.1	550.8	549.5	552.1	552.1
e	501.7	516.5	486.5	486.5	486.5	486.5	501.7	516.5	503.4	519.6
f	486.5	486.5	437.4	453.5	438.6	454.3	486.5	486.5	486.5	486.5
g	485.3	468.2	432.9	433.0	433.7	433.8	485.3	468.2	485.2	468.2

Table 9 (A). Gas thermodynamic properties of dual-pressure HRSG scenario (A)

Heat exchanger	T _{gi} [K]	T _{go} [K]	M _{g,i} [kg/s]	Q [kJ]
LP Economizer	485.3	486.5	508.3	683
LP Evaporator	486.5	501.7	508.3	9116
LP Super heater	501.7	503.1	508.3	810
HP Economizer	503.1	552.1	508.3	29541
HP Evaporator	552.1	735.7	508.3	109077
HP Super heater	735.7	796.7	508.3	36743

Table 9 (B). Water & steam thermodynamic properties of dual-pressure HRSG

HP Stream	Temperature [°C]	Pressure [kPa]	Enthalpy [kJ/kg]	Mass flow rate [kg/s]
12	470.0	5000	3364	64.48
11	264.0	5000	2794	64.48
10	264.0	5000	2794	64.48
9	264.0	5000	1154	64.48
8	249.0	2112	1080	65.77
7	149.5	2112	631.2	65.77
LP Stream	Temperature [°C]	Pressure [kPa]	Enthalpy [kJ/kg]	Mass flow rate [kg/s]
6	270.0	1500	2969	4.56
5	198.3	1500	2792	4.56
4	198.3	1500	2792	4.56
3	198.3	1500	844.9	4.56
2	183.3	2112	778.0	4.65
1	149.5	2112	631.2	4.65

4.1. Steam generation evaluations at high pressure and low pressure in HRSG

A comparison of steam generation at high and low pressures in HRSG in each designed scenario is illustrated in Figure 4.

As it can be clearly observed from the results, the scenarios (E) and (F) generate considerably more steam in the default state which is equal to approximately 20 kg/s at LP steam generation rate, while in worse scenarios which are (G) and (H), the LP steam generation rates correspond to 4.56 kg/s. The main reason behind this is the suitable arrangement of heat exchangers within the HRSG. It is worth noting that the steam produced in scenarios (E) and (F) is substantially greater than that in scenario (A) which is a presented conventional layout of heat exchangers in the HRSG. Moreover, LP steam production of scenarios (G) and (H) which are studied and suggested in the previous literature is considerably lower than that in the proposed scenarios in this study. Superior results conspicuously result from the proposed scenarios of (E) and (F) as they demonstrate the highest levels of LP steam production.

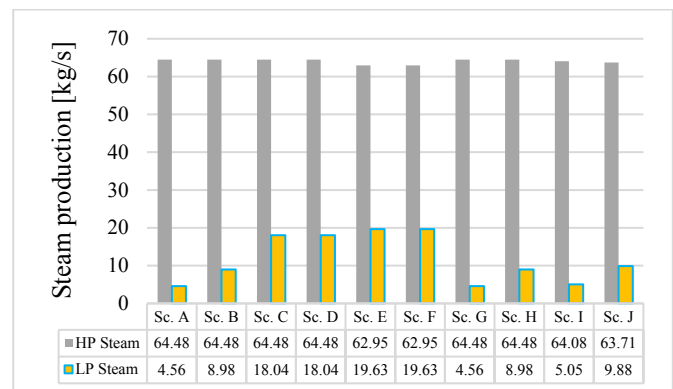


Figure 4. LP & HP steam generation in different scenarios without duct burner

4.2. Fuel consumption of duct burner for steam generation

There is no doubt that fuel consumption in the thermal systems is of particular interest of examination to not only achieve higher efficiency but also lessen the operation cost as well as environmental side effects associated with it. Considering that all HRSG scenarios are designed to produce

a specific amount of steam at specific pressures as illustrated in Table 1, the supplemental firing unit enables the system to track demand (i.e., producing more steam when the load swings upward than the unfired unit can produce). The duct burner must compensate for providing needed heat (temperature and mass flow rate) to the stream passing through the HRSG. If the heat rate at HRSG is not sufficient to generate a specific amount of steam, it operates to provide the required energy using auxiliary fuel.

In Table 10, fuel consumption of different configurations of HRSG with and without supplemental firing unit is illustrated. As can be observed, maximum fuel consumption belongs to scenarios (A), (G), and (I) in which duct burner used 1.055

kg/s while superior results regarding fuel consumption belonged to scenarios (C), (D), (E), and (F) where duct burner consumed 0.317 kg/s and total amount of fuel consumption was equal to 9.884 kg/s to produce a specific and stable amount of steam at HP and LP pressures. This delivers significantly better results due to low fuel consumption corresponding to about 7 % saving in fuel. The main reason behind this fuel saving can be more efficient heat exchanger arrangement in related scenarios. This achievement can be more tangible when it comes to annual scale which immensely improves operation costs and mitigates the environmental side effects, finally resulting in huge annual cost saving.

Table 10. Fuel consumption of CCGTs power plant in different configurations of dual-pressure HRSG

Scenarios	Fuel consumption (kg/s)	Gas turbine (kg/s)	Duct burner (kg/s)
A	10.622	9.567	1.055
B	10.38	9.567	0.813
C	9.884	9.567	0.317
D	9.884	9.567	0.317
E	9.884	9.567	0.317
F	9.884	9.567	0.317
G	10.622	9.567	1.055
H	10.38	9.567	0.813
I	10.622	9.567	1.055
J	10.38	9.567	0.813

Also, scenarios (B), (C), and (I) exhibit better results than the base scenario (A). The total fuel consumption in the mentioned scenarios is 10.38 kg/s, which corresponds to approximately 3 % saving.

4.3. Electrical power and efficiency

The power generation capacity of the steam cycle in both high-pressure and low-pressure steam turbines regarding different scenarios is illustrated in Figure 5. As can be seen, scenarios (C) and (D) produced maximum power in the steam cycle equal to 68.54 MW that causes approximately 12 % improvement in comparison with scenario (A) where it generates 61.17 MW. This enhancement is mainly due to better performance in low-pressure steam turbine power production which increased from 2.5 MW to 9.87 MW.

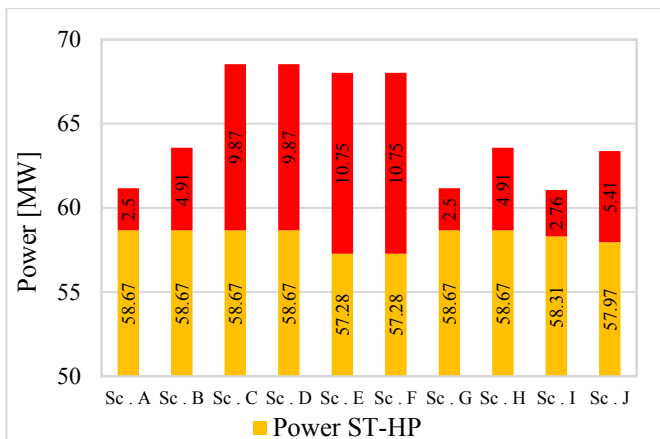


Figure 5. Power production of steam cycle considering different scenarios

Further, scenarios (A), (G), and (I) exhibited approximately similar performance, while slight improvements can be seen in scenarios (B) and (H). An improvement in total steam production from 61.17 MW to 63.58 MW can be observed. This delivers significantly better results due to a more efficient heat exchanger arrangement in the HRSG.

Figure 6 shows the total net power production in both GC and SC for different proposed scenarios. As discussed earlier, from obtained results, it can be clearly understood that scenarios (C) and (D) had a greater level of power production equal to 218.33 MW. Also, it should be noted that the scenario (I), the most unfavorable one, can produce the net electrical power of 210.89 MW.

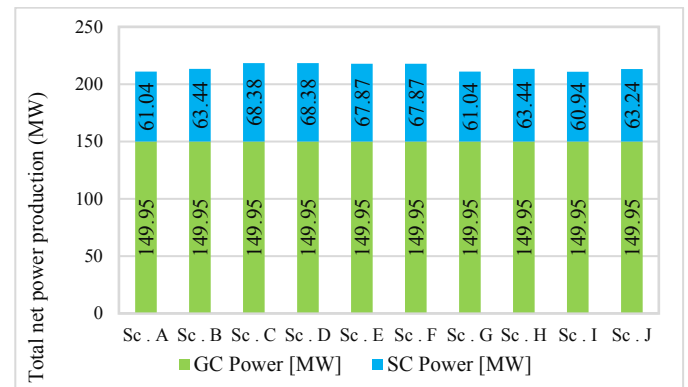


Figure 6. Total net power production of gas cycle and steam cycle for different scenarios

Total net power and efficiency of CCGT, GC, and ST for different designed scenarios are illustrated in Figure 7. As can be seen, the designed heat exchanger arrangement of scenario

(C) has not only the best thermal and electrical efficiency of the system, but also produces the maximum power of 218.3 MW, while the scenario (A) produces 210.98 MW electricity. Based on a comparison of different scenarios, it was found that the best performance in both power and efficiency belonged to scenarios (C) and (D).

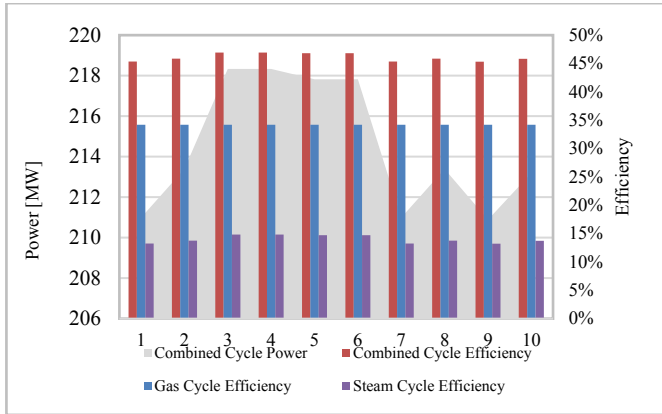


Figure 7. Total net power and efficiency of CCPP, GC, and ST for different scenarios

Further, Figure 8 shows a comparison between produced and consumed power in two scenarios (A) as base configuration and scenario (C) as the best designed heat exchanger arrangement. As is illustrated in two pie charts, the most striking difference in power production is related to the low-pressure steam turbine power production in scenario (C), which is remarkably enhanced due to new configuration design.

The low-pressure steam turbine power generation is improved from 2.5 MW in base scenario (A) to 9.87 MW in the best scenario (C) where the power production in low-pressure steam cycle has been approximately quadrupled. In addition, overall power production of CCPP has been significantly improved from 210.98 MW to 218.3 MW, while consumed fuel has proved to be almost 7 % saving potential. The energy consumption in compressor is maintained constant, as expected.

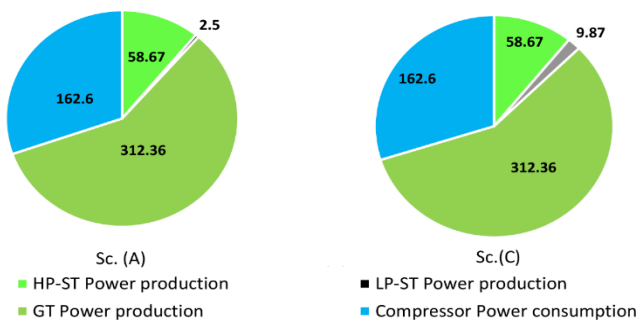


Figure 8. A comparison between produced and consumed power in scenarios (A) and (C)

In addition, the two T-Q diagrams with regard to scenarios of (A) as base configuration and scenario (C) as the best performed scenario are shown in Figures 9 and 10, respectively.

According to Figure 9, the GT hot flue gas at point (a) is incorporated into the HRSG at a temperature of 796.7 K and after passing LP as well as HP units leave the HRSG unit at point (g) with a temperature of 485.4 K. At the same time, feed water enters the HRSG unit at points (g) and (d).

Moreover, after heat exchange, the superheat steam will leave the unit at the point (d) with a temperature of 543.2 K for LP-steam and at the point of (a) with a temperature of 743.2 K for HP-steam.

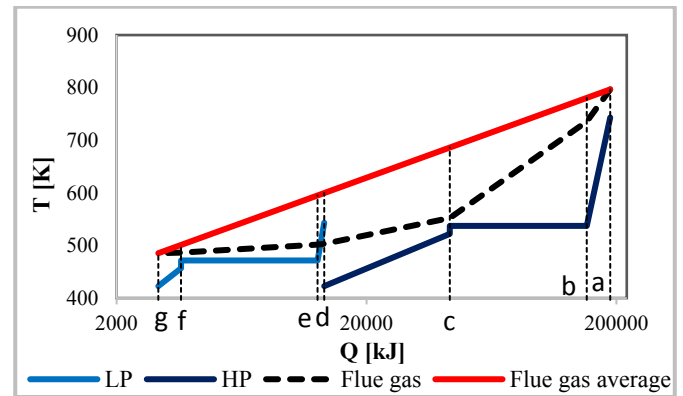


Figure 9. T-Q profile of scenario (A)

This diagram clearly shows the amount of heat exchanged in each heat exchanger. It is observed that the highest amount of heat exchange belongs to the HP section of the HRSG and the highest value is in the HP evaporator heat exchanger. By comparing the temperature profile of hot flue gas passing through the HRSG from point (a) to (g) and temperature profiles of produced steam, it can be observed that there is still a great energy potential to be recovered and saved from the outlet gases. The higher the energy recovery is, the closer the temperature profile of the steam produced is to the temperature profile of the hot gas.

Figure 10 shows the temperature profile of scenario (C). It can be seen that in this scenario, compared to the base scenario (A), the steam temperature profile is much closer to the outlet gas temperature profile, which means higher and more efficient heat exchange and, consequently, more heat recovery from the hot outlet-gas flow. In scenario (C), the outlet gas temperature declines to 432.9 K, where its temperature is reduced by almost 53 K in comparison to the base scenario. Besides, in the LP unit, more heat is observed rather than the base scenario which leads to more steam production at 295.6 %. Ultimately, more power will be produced in the LP-steam turbine of the CCGT power plant.

By comparing these two diagrams, it is concluded that by changing the configuration of heat exchangers in HRSG, the amount of heat exchanged between the hot stream (flue gas from the gas turbine) and the cold streams (high-pressure and low-pressure steam flows) increases. This value will be at the highest possible value due to the minimization of the pinch point temperature difference.

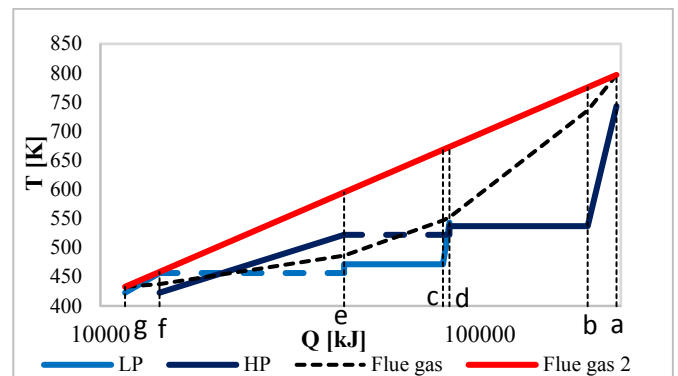


Figure 10. T-Q profile of scenario (C)

5. ENVIRONMENTAL ASSESSMENT

It is necessary to assess the environmental effects on thermal and power generation systems that generally provide their required energy using fossil fuels. In this study, the amount of fuel combustion products at the combined cycle power plant for a scenario with the lowest fuel consumption is studied and the results are presented in Table 11.

In terms of environmental analysis, the benefits of the proposed configurations are investigated and compared with the environmental damage triggered by a base scenario of (A) as reference. The CO₂ emission cost rate of the scenario (C) is about 461.521 kgCO₂/MWh which is considerably lower than

the base scenario which is equal to 512.89 kgCO₂/MWh. Moreover, Ω_{CO_2} potential of the system is 51.37 kgCO₂/MWh; consequently, BEN_{ENV} of the system is equal to 133,418 \$/MWh. Accordingly, for fuel consumption of 10.61 kg/s in base configuration of gas turbine cycle with HRSG, scenario (A), the amount of 30.06 kgCO₂/s is generated, equal to 2597 ton/day. Since the designed configurations in scenarios (C), (D), (E), and (F) have the lowest fuel consumption, lower CO₂ production of about 2418 ton is the result. This value shows 178.8 ton/day reduction in comparison with the base scenario of (A).

Table 11. Calculated flue gas components of gas turbine for all the proposed scenarios

Component	Value Sc. A [kg/s]	Value Sc. B [kg/s]	Value Sc. C [kg/s]	Value Sc. D [kg/s]	Value Sc. E [kg/s]	Value Sc. F [kg/s]	Value Sc. G [kg/s]	Value Sc. H [kg/s]	Value Sc. I [kg/s]	Value Sc. J [kg/s]
CO ₂	30.06	29.38	27.99	27.99	27.99	27.99	30.06	29.38	30.06	29.38
H ₂ O	22.31	21.80	20.76	20.76	20.76	20.76	22.31	21.80	22.31	21.80
O ₂	78.38	78.38	78.38	78.38	78.38	78.38	78.38	78.38	78.38	78.38
N ₂	390.4	387.3	381.0	381.0	381.0	381.0	390.4	387.3	390.4	387.3
Ar	5.986	5.939	5.843	5.843	5.843	5.843	5.968	5.939	5.986	5.939

5. CONCLUSIONS

Scenario base modeling was undertaken for different dual-pressure HRSG configurations considering operational flue gas temperature and related initial values that represent the new evaluation approach of combined cycles. The expressed scenarios were selected due to the steam demand of the considered power plant and the technical possibility of the heat exchanger arrangement. Therefore, the primary purpose of this study was to present a method to increase the productivity of the HRSG systems. Results demonstrated that four of the ten considered HRSG models had a better operation in fuel consumption, steam production, power, and electrical efficiency than the conventional configuration. Besides, the environmental benefit of the best scenario proved to be a remarkable improvement. Eventually, concerning the HRSG model development, low-pressure steam generation of the scenarios of (C), (D), (E), and (F) was about four times higher than that in the base scenario of (A). It was shown that more energy could be absorbed in the HRSG by relocating super heaters and evaporators of the LP section. So, the following outputs were obtained:

- Fuel consumption of duct burner of the selected configurations was almost 30 % less than the conventional type.
- HRSG efficiency using four selected configurations was approximately 9 % higher than the base model.
- Reduction of CO₂ emission in the best scenario of (C) was about 6.88 % in comparison with the base model.
- The environmental benefit of the best scenario was equal to 133,418 \$/MWh.

6. ACKNOWLEDGEMENT

The authors appreciatively acknowledge the Iranian Research Organization for Science and Technology (IROST) for providing the input data of Fars power plant.

NOMENCLATURE

Symbols

a, b, c	Specific heat constants of steam
a', b', c'	Specific heat constants of flue gas
BLD	Blow down (%)
C _p	Specific heat capacity at constant pressure (kJ/kg K)
dT	Temperature division
h	Specific enthalpy (kJ/kg)
H	Enthalpy at actual state (kJ)
H'	Enthalpy at ideal state (kJ)
LHV	Lower heating value (kJ/kg)
mf	Mass fraction
m	Mass flow rate (kg/s)
m'	Demand mass flow rate (kg/s)
m _{ole}	Mole flow rate (kmole/s)
MW	Molecular weight (kg/kmole)
n	Mole of air in combustion reaction (kmole)
n _{1, ..., n₅}	Mole of products in combustion reaction (kmole)
P	Pressure (bar)
PW	Power (kW)
Q	Heat transferred (kJ)
Q̇	Heat transferred rate (kJ/kg)
R	Gas constant (kJ/kg K)
RPC	Compressor pressure ratio
RPT	Turbine pressure ratio
S	Entropy at actual state (kJ/kg K)
S'	Entropy at ideal state (kJ/kg K)
T	Temperature at actual state (K)
T'	Temperature at ideal state (K)
W	output work (kJ)
Ẇ	Specific output work (kJ/kg)
ΔP	Pressure difference (%)

Greek Letter

η	Efficiency
γ	Specific heat ratio

Subscripts and superscripts

air	Air
AC	Air compressor
Act	Actual
CC	Combustion chamber

CCPP	Combined cycle power plant
DB	Duct burner
Demand	Demand
Electrical	Electrical
Fuel	Fuel
FA	Fresh air
FG	Flue gas
FW	Feed water
GC	Gas cycle
GT	Gas Turbine
HP	High pressure
Eco	Economizer
Sup	Super heater
Sp	Splitter
HX	Heat Exchanger
in	Inlet
isen	Isentropic state
LP	Low pressure
net	Net
new	New state
out	Outlet
p	Pump
Ref	Reference
ST	Steam turbine
th	Thermal
theo	Theoretical
0	Initial state

Acronyms and abbreviation

AP	Approach point temperature
CCPP	Combined cycle power plant
CHP	Combined heat and power
EES	Engineering equation solver
LP	Feed water
PP	Gas turbine
HP	High pressure
HRSRG	Heat recovery steam generator
LP	Low pressure
PP	Pinch point
TIT	Turbine inlet temperature
TOT	Turbine outlet temperature

REFERENCES

- Moghadas, M., Ozgoli, H.A. and Farhani, F., "A machine learning-based operational control framework for reducing energy consumption of an amine-based gas sweetening process", *International Journal of Energy Research*, Vol. 45, No. 1, (2021), 1055-1068. (<https://doi.org/10.1002/er.6159>).
- Ozgoli, H.A. and Ghadamian, H., "Energy price analysis of a biomass gasification-solid oxide fuel cell-gas turbine power plant", *Iranian Journal of Hydrogen & Fuel Cell*, Vol. 3, No. 1, (2016), 45-58. (<https://doi.org/10.22104/ijhfc.2016.327>).
- Ozgoli, H.A., Safari, S. and Sharifi, M.H., "Integration of a biomass-fueled proton exchange membrane fuel cell system and a vanadium redox battery as a power generation and storage system", *Sustainable Energy Technologies and Assessments*, Vol. 42, (2020), 100896. (<https://doi.org/10.1016/j.seta.2020.100896>).
- Moghadas, M., Ozgoli, H.A. and Farhani, F., "Gas sweetening process simulation - Investigation on recovering waste hydraulic energy", *International Journal of Mechanical, Industrial and Aerospace Sciences*, Vol. 12, No. 8, (2018), 789-804. (<https://doi.org/10.5281/zenodo.1340566>).
- Ozgoli, H.A., Elyasi, S. and Mollazadeh, M., "Hydrodynamic and electrochemical modeling of vanadium redox flow battery", *Mechanics & Industry*, Vol. 16, No. 2, (2015), 201-213. (<https://doi.org/10.1051/meca/2014071>).
- Ozgoli, H.A., Ghadamian, H. and Farzaneh, H., "Energy efficiency improvement analysis considering environmental aspects in regard to biomass gasification PSOFC/GT power generation system", *Procedia Environmental Sciences*, Vol. 17, (2013), 831-841. (<https://doi.org/10.1016/j.proenv.2013.02.101>).
- Ozgoli H.A., Moghadasi, M., Farhani, F. and Sadigh, M., "Modeling and simulation of an integrated gasification SOFC-CHAT cycle to improve power and efficiency", *Environmental Progress & Sustainable Energy*, Vol. 36, No. 2, (2016), 610-618. (<https://doi.org/10.1002/ep.12487>).
- Safari, S., Ghasedi, A.H. and Ozgoli, H.A., "Integration of solar dryer with a hybrid system of gasifier-solid oxide fuel cell/micro gas turbine: Energy, economy, and environmental analysis", *Environmental Progress & Sustainable Energy*, Vol. 40, No. 3, (2020), e13569. (<https://doi.org/10.1002/ep.13569>).
- Safari, S., Hajilounezhad, T. and Ehyaei, M.A., "Multi-objective optimization of solid oxide fuel cell/gas turbine combined heat and power system: A comparison between particle swarm and genetic algorithms", *International Journal of Energy Research*, Vol. 44, No. 11, (2020), 9001-9020. (<https://doi.org/10.1002/er.5610>).
- Ozgoli, H.A. and Yazdani, H., "Integration of a vanadium redox flow battery with a proton exchange membrane fuel cell as an energy storage system", *Iranian Journal of Hydrogen and Fuel Cell*, Vol. 1, (2017), 53-68. (<https://doi.org/10.22104/ijhfc.2017.2281.1140>).
- Abanades, S., Abbaspour, H., Ahmadi, A., Das, B., Ali Ehyaei, M., Esmailion, F., El Haj Assad, M., Hajilounezhad, T., Hmida, A., Rosen, M.A., Safari, S., Shabi, M.A. and Silveira, J.L., "A conceptual review of sustainable electrical power generation from biogas", *Energy Science & Engineering*, Vol. 10, No. 2, (2021), 630-655. (<https://doi.org/10.1002/ese3.1030>).
- Ozgoli, H.A., "Simulation of integrated biomass gasification-gas turbine-air bottoming cycle as an energy efficient system", *International Journal of Renewable Energy Research*, Vol. 7, No. 1, (2017), 276-284. (<https://doi.org/10.20508/ijrer.v7i1.5428.g6986>).
- Ozgoli, H.A., Ghadamian, H. and Pazouki, M., "Economic analysis of biomass gasification-solid oxide fuel cell-gas turbine hybrid cycle", *International Journal of Renewable Energy Research*, Vol. 7, No. 3, (2017), 1007-1018. (<https://doi.org/10.20508/ijrer.v7i3.5814.g7131>).
- Safari, S. and Ozgoli, H.A., "Electrochemical modeling and techno-economic analysis of solid oxide fuel cell for residential applications", *Journal of Renewable Energy and Environment (JREE)*, Vol. 7, No. 1, (2020), 40-50. (<https://doi.org/10.30501/jree.2020.105451>).
- Kaviri, A.G., Jaafar, M.N.M., Lazim, T.M. and Barzegaravval, H., "Exergoenvironmental optimization of heat recovery steam generators in combined cycle power plant through energy and exergy analysis", *Energy Conversion and Management*, Vol. 67, (2013), 27-33. (<https://doi.org/10.1016/j.enconman.2012.10.017>).
- Kumar, A., Kachhwaha, S. and Mishra, R., "Thermodynamic analysis of a regenerative gas turbine cogeneration plant", *Journal of Scientific and Industrial Research*, Vol. 69, No. 3, (2010), 225-231. (<http://nopr.niscares.in/bitstream/123456789/7384/1/JSIR%2069%283%29%20225-231.pdf>).
- Khaliq, A. and Kaushik, S.C., "Second-law based thermodynamic analysis of Brayton/Rankine combined power cycle with reheat", *Applied Energy*, Vol. 78, No. 2, (2004), 179-197. (<https://doi.org/10.1016/j.apenergy.2003.08.002>).
- Ahmadi, P. and Dincer, I., "Thermodynamic analysis and thermoeconomic optimization of a dual pressure combined cycle power plant with a supplementary firing unit", *Energy Conversion and Management*, Vol. 52, No. 5, (2011), 2296-2308. (<https://doi.org/10.1016/j.enconman.2010.12.023>).
- Franco, A. and Casarosa, C., "On some perspectives for increasing the efficiency of combined cycle power plants", *Applied Thermal Engineering*, Vol. 22, No. 13, (2002), 1501-1518. ([https://doi.org/10.1016/S1359-4311\(02\)00053-4](https://doi.org/10.1016/S1359-4311(02)00053-4)).
- Bassily, A.M., "Modeling, numerical optimization, and irreversibility reduction of a triple-pressure reheat combined cycle," *Energy*, Vol. 32, No. 5, (2007), 778-794. (<https://doi.org/10.1016/j.energy.2006.04.017>).
- Tajik Mansouri, M., Ahmadi, P., Ganjeh Kaviri, A. and Mohd Jaafar, M.N., "Exergetic and economic evaluation of the effect of HRSRG configurations on the performance of combined cycle power plants", *Energy Conversion and Management*, Vol. 58, (2012), 47-58. (<https://doi.org/10.1016/j.enconman.2011.12.020>).
- Antonanzas, J., Alia Martínez, M., Ascacibar, F.J. and Antonanzas, F., "Towards the hybridization of gas-fired power plants: A case study of Algeria", *Renewable and Sustainable Energy Reviews*, Vol. 51, (2015), 116-124. (<https://doi.org/10.1016/j.rser.2015.06.019>).
- Erdem, H. and Sevilgen, S., "Case study: Effect of ambient temperature on the electricity production and fuel consumption of a simple cycle gas

- turbine in Turkey", *Applied Thermal Engineering*, Vol. 26, (2006), 320-326. (<https://doi.org/10.1016/j.applthermaleng.2005.08.002>).
24. Ibrahim, T.K., Kamil Mohammed, M., Awad, O.I., Rahman, M.M., Najafi, G., Basrawi, F., Abd Alla, A.N. and Mamat, R., "The optimum performance of the combined cycle power plant: A comprehensive review", *Renewable and Sustainable Energy Reviews*, Vol. 79, (2017), 459-474. (<https://doi.org/10.1016/j.rser.2017.05.060>).
25. Feng, H., Zhong, W., Wu, Y. and Tong, S., "Thermodynamic performance analysis and algorithm model of multi-pressure heat recovery steam generators (HRSG) based on heat exchangers layout", *Energy Conversion and Management*, Vol. 81, (2014), 282-289. (<https://doi.org/10.1016/j.enconman.2014.02.060>).
26. Razak, A.M.Y., *Industrial gas turbines*, 1st Edition, Woodhead Publishing, Elsevier, (2007), 624-650.
27. Ahmadi, A., Das, B., Ehyaei, M.A., Esmaeilion, F., El Haj Assad, M., Jamali, D.H., Koohshekan, O., Kumar, R., Rosen, M.A., Negi, S., Sekhar Bhogilla, S. and Safari, S., "Energy, exergy, and techno-economic performance analyses of solar dryers for agro products: A comprehensive review", *Solar Energy*, Vol. 228, (2021), 349-373. (<https://doi.org/10.1016/j.solener.2021.09.060>).
28. Abanades, S., Abbaspour, H., Ahmadi, A., Das, B., Ehyaei, M.A., Esmaeilion, F., El Haj Assad, M., Hajilounezhad, T., Jamali, D.H., Hmida, A., Ozgoli, H.A., Safari, S., AlShabi, M. and Bani-Hani, E.H., "A critical review of biogas production and usage with legislations framework across the globe", *International Journal of Environmental Science and Technology*, Vol. 19, (2022), 3377-3400. (<https://doi.org/10.1007/s13762-021-03301-6>).
29. Hosseinpour, J., Chitsaz, A., Liu, L. and Gao, Y., "Simulation of eco-friendly and affordable energy production via solid oxide fuel cell integrated with biomass gasification plant using various gasification agents", *Renewable Energy*, Vol. 145, (2020), 757-771. (<https://doi.org/10.1016/j.renene.2019.06.033>).

ABSTRACTS

Energy Potential of Agricultural and Forestry By-Products in Peru

Roxana Isabel Bernola Flores, Carmen Elena Flores Barreda, Diana Carolina Parada Quinayá, Ursula Fabiola Rodríguez Zúñiga*

Department of Chemical Engineering, University of Engineering and Technology, Jr. Medrano Silva 165, Barranco, Lima, Peru.

PAPER INFO

Paper history:

Received: 11 January 2022

Revised in revised form: 31 March 2022

Scientific Accepted: 07 April 2022

Published: 27 July 2022

Keywords:

Energy from Agriculture,
Renewable Biofuels,
Circular Economy,
Calorific Value

ABSTRACT

Reducing the demand for fossil fuels and the derived products can be achieved through the development of alternative energy sources. This work presents a countrywide study of the energy potential of lignocellulosic biomass sourced from agro-industrial by-products in the country of Peru. Ranking of the crops that produce the most waste was followed by an energy potential evaluation of carbohydrate conversion and thermochemical conversion. The crops with high calorific values were sugar cane bagasse, wood waste, and coffee husk. The energy potential of the principal lignocellulosic by-products, in terms of tons of oil equivalents per year, resulted from rice straw at 1.45 M, followed by corn residue at 1.13 M and sugar cane residue at 1.10 M. The northern region of Peru generated the highest quantities of rice (straw and husk), banana (husk and rachis), and sugar cane (bagasse and straw) by-products and the southern regions generated the greatest quantities of quinoa residue, all of which could be used as raw materials for biofuels and aggregates for materials. These results indicate that theoretically, this readily available biomass could meet the country's energy demands while promoting sustainability and national energy security.

<https://doi.org/10.30501/jree.2022.323731.1310>

2423-7469/© 2023 The Author(s). Published by MERC. This is an open access article under the CC BY license (<https://creativecommons.org/licenses/by/4.0/>).



چکیده

کاهش تقاضا برای سوخت‌های فسیلی و محصولات مشتق شده، از طریق توسعه منابع انرژی جایگزین قابل دستیابی است. این مقاله یک مطالعه کشوری در مورد پتانسیل انرژی منابع زیست‌توده لیگنوسلولزی از محصولات جانبی کشاورزی و صنعتی در کشور پرو ارائه می‌دهد. سپس در ادامه به رتبه بندی محصولاتی با بیشترین تولید ضایعات با ارزیابی پتانسیل انرژی تبدیل کربوهیدرات و تبدیل ترموشیمیایی پرداخته شده است. محصولاتی که ارزش گرمایی بالا داشتند شامل: باگاس نیشکر، ضایعات چوب و پوسته قهوه بودند. پتانسیل انرژی محصولات جانبی لیگنوسلولزی اصلی، بر حسب یک تن نفت در سال، از کاه برنج با 1/45 M، به دنبال آن ضایعات ذرت با 1/13 M و ضایعات نیشکر با 1/10 M انرژی حاصل می‌شود. منطقه شمالی پرو بیشترین مقدار محصولات جانبی برنج (کاه و پوسته)، موز (پوسته و ساقه) و نیشکر (باگاس و کاه) و مناطق جنوبی بیشترین مقدار ضایعات کینوا را تولید می‌کنند. همه ضایعات نامبرده شده می‌توانند به عنوان مواد خام برای سوخت‌های زیستی و مواد توده ای استفاده شوند. این نتایج نشان می‌دهد که از نظر تئوری، این زیست‌توده به راحتی می‌تواند نیازهای انرژی کشور را برآورده کند و در عین حال پایداری و امنیت انرژی ملی را ارتقا دهد.

Improvement of Frequency Stability in the Power System Considering Wind Turbine and Time Delay

Farhad Amiri, Mohammad Hassan Moradi*

Department of Electrical Engineering, Bu-Ali Sina University, P. O. Box: 65178-38695, Hamedan, Hamedan, Iran.

PAPER INFO

Paper history:

Received: 17 January 2022

Revised in revised form: 08 March 2022

Scientific Accepted: 20 March 2022

Published: 06 August 2022

Keywords:

Wind Turbine,
Time Delay,
Load-Frequency Control,
Virtual Damping,
Power System

ABSTRACT

In the power system, frequency stability is critical. The wind turbine oscillates (depending on the wind speed) and is of low inertia. Thus, wind turbines face the issue of power system frequency stability. Since the power system's resources are interconnected via communication networks, the presence of time delay also affects the frequency stability of the power system. When a disturbance occurs in the power system due to load or distributed generation sources (wind turbine), it leads to frequency deviations in the power system, exhibiting low damping speed. Although large conventional generators in the power system provide sufficient inertia and reduce frequency deviation, the damping speed of frequency fluctuations is slow, which may be due to time delays between power system resources. In this paper, virtual damping (a proposed method) is used to accelerate the damping of frequency deviations caused by load disturbances, distributed generation source disturbances, and the time delay between power system resources. The results of the proposed method are compared to those obtained using the conventional method in this field, demonstrating the superiority of the proposed method. The proposed method reduced frequency deviations in the power system caused by disturbances and time delays by 67 % (a 67 % improvement over existing methods in this field) and increased the damping speed of the frequency deviations by 62 % (a 62 % improvement over the methods used in this field).

<https://doi.org/10.30501/jree.2022.321859.1308>

2423-7469/© 2023 The Author(s). Published by MERC. This is an open access article under the CC BY license (<https://creativecommons.org/licenses/by/4.0/>).



چکیده

پایداری فرکانسی در سیستم قدرت اهمیت فراوانی دارد. توربین بادی، طبیعت نوسانی (وابسته به سرعت باد) و اینرسی پایین دارد. بنابراین توربین بادی، مسئله پایداری فرکانسی در سیستم قدرت را با مشکلاتی مواجه می‌کند. وجود تأخیر زمانی در سیستم قدرت، به علت اینکه منابع سیستم قدرت از طریق شبکه‌های مخابراتی با هم ارتباط دارند نیز پایداری فرکانسی سیستم قدرت را به خطر می‌اندازد. زمانی که در سیستم قدرت، اغتشاش ناشی از بار یا منابع تولید پراکنده (توربین بادی) به وجود می‌آید، باعث می‌شود که فرکانس سیستم انحراف پیدا کند و همچنین این نوسانات فرکانس ناشی از اغتشاشات، سرعت میرای کندی دارند. وجود ژنراتورهای بزرگ مرسوم در سیستم قدرت، اینرسی کافی را برای سیستم قدرت فراهم می‌کند و باعث می‌شود انحراف فرکانس کمتر شود، اما سرعت میرایی نوسانات فرکانس کند است که می‌تواند ناشی از تأخیر زمانی بین منابع سیستم قدرت باشد. در این مقاله، برای توربین های بادی موجود در سیستم قدرت، یک میرایی مجازی (روش پیشنهادی) به کار برده شده است که باعث می‌شود انحراف فرکانس ناشی از اغتشاشات بار، اغتشاشات منابع تولید پراکنده و تأخیر ارتباطی بین منابع سیستم قدرت، سریعتر میرا شود. نتایج روش پیشنهادی با روش مرسوم به کار برده شده در این زمینه مقایسه شده است و برتری روش پیشنهادی نشان داده شده است. روش پیشنهادی، انحرافات فرکانس ناشی از اغتشاشات و تأخیر زمانی سیستم قدرت را به میزان ۶۷٪ کاهش داده است (۶۷٪ بهبود نسبت به روشهای به کار برده شده در این زمینه) و سرعت میرایی انحرافات فرکانس را به میزان ۶۲٪ افزایش داده است (۶۲٪ بهبود نسبت به روشهای به کار برده شده در این زمینه).

Deriving an Alternative Energy Using Anaerobic Co-Digestion of Water Hyacinth, Food Waste, and Cow Manure

Sapna Kinattinkara ^a, Thangavelu Arumugam ^{b*}, Nandhini Samiappan ^a, Vivek Sivakumar ^c, Sampathkumar Velusamy ^d, Mohanraj Murugesan ^e, Manoj Shanmugamoorthy ^d

^a Department of Environmental Science, PSG College of Arts and Science, P. O. Box: 641014, Coimbatore, India.

^b Department of Environmental Studies, Kannur University, P. O. Box: 670567, Kerala, India.

^c Department of Civil Engineering, Hindustan College of Engineering, P. O. Box: 641032, Coimbatore, India.

^d Department of Civil Engineering, Kongu Engineering College, P. O. Box: 638060, Erode, India.

^e Department of Mechanical Engineering, Hindustan College of Engineering, P. O. Box: 641032, Coimbatore, India.

PAPER INFO

Paper history:

Received: 14 February 2022

Revised in revised form: 07 April 2022

Scientific Accepted: 13 April 2022

Published: 06 August 2022

Keywords:

Anaerobic Digestion,

Bioenergy,

Biogas,

Cow Dung,

Eichhornia Crassipes

ABSTRACT

Increased global energy consumption demands the use of more energy resources, aggravating environmental issues. This study focused on analyzing biogas production from a mixture of cow dung, water hyacinth, and food waste and checking the efficiency of the biogas. The efficiency of biogas production was tested using two alternative settings in the study. The first setup employs Eichhornia crassipes that have been NaOH-treated and mixed with co-digestion substrates such as cow manure and food waste which have been stored at room temperature for 32 days. The second setup contains five different types of substrates such as L1-cow dung, L2-cow dung: water hyacinth, L3-cow dung: food waste, L4-cow dung: water hyacinth: food waste, and L5-water hyacinth. The properties of the Eichhornia crassipes were studied on several biogas substrates, such as pH, temperature, COD, TOC, and NPK tests, as well as total biogas output and methane percentage. The results of the comparison analysis show that the substrate L4 has a high level of NPK (4.7 %) and a higher amount of COD (137600 mg/l). These characteristics enhance the gas yield and methane percentage (85 %). Overall, the water hyacinth mixed with cow dung and food waste exceeded the other four substrates. The total yield of biogas from the first setup was 8.5 litres, the flammability was tested on the 28th day, and the blue flame was obtained. Water hyacinth was removed from aquatic areas and used as an alternative energy source, hence being environmentally friendly.

<https://doi.org/10.30501/jree.2022.327715.1325>

2423-7469/© 2023 The Author(s). Published by MERC. This is an open access article under the CC BY license (<https://creativecommons.org/licenses/by/4.0/>).



چکیده

افزایش مصرف جهانی انرژی مستلزم استفاده بیشتر از منابع انرژی است که مسائل زیست‌محیطی را تشدید می‌کند. تمرکز این مطالعه بر تجزیه و تحلیل تولید بیوگاز از مخلوطی از کود گاو، سنبل آبی و ضایعات غذایی و بررسی کارایی بیوگاز می‌باشد. تأثیر تولید بیوگاز بر روی دو سیستم جایگزین در این مطالعه مورد آزمایش قرار گرفت. اولین سیستم از سنبل آبی با افزودن هیدروکسید سدیم (NaOH) و ترکیب با لایه‌های مشترک مانند کود گاوی و ضایعات غذایی که به مدت ۳۲ روز در دمای اتاق ذخیره شده‌اند، استفاده می‌کند. سیستم دوم شامل پنج نوع مختلف بستر مانند کود گاوی L1، کود گاوی L2: سنبل آبی، کود گاوی L3: ضایعات غذا، کود گاوی L4: سنبل آبی: ضایعات غذا و کود گاوی L5: سنبل آبی است. خواص سنبل‌های آبی بر روی چندین بستر بیوگاز، مانند pH، دما، COD، TOC و تست‌های NPK و همچنین کل خروجی بیوگاز و درصد متان مورد مطالعه قرار گرفت. نتایج پس از تجزیه و تحلیل و مقایسه نشان می‌دهد که بستر L4 دارای سطح بالایی از NPK (۴/۷٪) و مقدار بالایی از COD (۱۳۷۶۰۰ میلی گرم در لیتر) است. این ویژگی‌ها باعث افزایش بازده گاز و درصد متان (۸۵٪) می‌شود. به طور کلی، سنبل آبی مخلوط با فضولات گاو و ضایعات غذایی از چهار بستر دیگر فراتر رفت. بازده کل بیوگاز از اولین سیستم ۸/۵ لیتر بود، اشتعال پذیری در روز ۲۸ آزمایش شد و شعله آبی به دست آمد. سنبل آبی از مناطق آبی حذف شد و به عنوان منبع انرژی جایگزین مورد استفاده قرار گرفت و از این رو دوستدار محیط‌زیست است.

Effect of Pretreatment on the Physical Properties and Heating Values of Briquettes

Toyese Friday Oyewusi ^{a*}, Gabriel Alebiowu ^b, Elizabeth Funmilayo Aransiola ^c, Ayowumi Rita Soji-Adekunle ^d, Busayo Sunday Adeboye ^e

^a Department of Agricultural Engineering, Faculty of Engineering, Adeleke University, P.M.B. 250, Ede, Osun State, Nigeria.

^b Department of Pharmaceutics, Faculty of Pharmacy, Obafemi Awolowo University, P.M.B. 13, Ile-Ife, Osun State, Nigeria.

^c Department of Chemical Engineering, Faculty of Technology, Obafemi Awolowo University, P.M.B. 13, Ile-Ife, Osun State, Nigeria.

^d Department of Mechanical Engineering, Faculty of Engineering, Adeleke University, P.M.B. 250, Ede, Osun State, Nigeria.

^e Department of Mechanical Engineering, College of Science, Engineering and Technology, Osun State University, P.M.B. 4494, Osogbo, Osun State, Nigeria.

PAPER INFO

Paper history:

Received: 17 February 2022

Revised in revised form: 12 April 2022

Scientific Accepted: 24 April 2022

Published: 15 August 2022

Keywords:

Carbonized Briquette,
Uncarbonized Briquette,
Density,
Compressive Strength,
Heating Value

ABSTRACT

Briquettes from agro-residues have been promoted as a better alternative to firewood and charcoals for heating and cooking in the rural communities. In this light, a study was carried out to investigate the effect of pretreatment methods on physical properties and heating values of briquettes produced from corncob. To accomplish this work, an experiment was designed as a $2 \times 3 \times 3 \times 3$ completely randomized with three replicates. The parameters are pretreatment methods (carbonized and uncarbonized), binder types (cassava, corn, and gelatin), binder concentrations (10, 20, 30 %), and compacting pressures (50, 100, and 150 kPa). A charcoal kiln was fabricated to obtain the pretreatment through pyrolysis and a punch and die was also fabricated to facilitate briquette densification. The physical properties tested were limited to moisture content (MC), density and compressive strength and were determined using a conventional method. The heating value of the briquettes produced was determined using bomb calorimeter. The results demonstrated that average moisture content ranged between 5.29-6.58 % and 12.75-13.72 %, mean relaxed density varied from 813-925 kgm^{-3} and 963-1166 kgm^{-3} , compressive strength ranged between 2.27-5.07 MPa and 5.97-10.12 MPa, and heating value ranged between 28.85-32.36 MJkg^{-1} and 27.58-28.80 MJkg^{-1} for carbonized and uncarbonized briquettes, respectively. Briquettes produced from carbonized corncob had a better moisture content and heating value, while briquettes produced from uncarbonized corncob had higher density and compressive strength. The study shows that pretreatment methods under different binder types and concentrations and the compacting pressure significantly affected the briquettes physical properties and heating values. Therefore, this technology can be successfully applied in rural off-grid areas by the government and other stakeholders in the energy sector as part of renewable energy technologies.

<https://doi.org/10.30501/jree.2022.327453.1329>

2423-7469/© 2023 The Author(s). Published by MERC. This is an open access article under the CC BY license (<https://creativecommons.org/licenses/by/4.0/>).



چکیده

قالبهای تهیه شده از پسماندهای کشاورزی به عنوان جایگزین بهتری برای هیزم و زغال چوب برای گرم کردن و پخت و پز در جوامع روستایی ترویج یافته است. در این راستا، مطالعه‌ای به منظور بررسی تأثیر روش‌های پیش تصفیه بر خواص فیزیکی و ارزش حرارتی قالبهای تولید شده از ذرت انجام شد. برای انجام این کار، آزمایشی به صورت کاملاً تصادفی با سه تکرار در قالب $2 \times 3 \times 3 \times 3$ طراحی شد. پارامترها عبارتند از روش‌های پیش تیمار (کربنیزه و بدون کربن)، انواع بایندر (کاساوا، ذرت و ژلاتین)، غلظت چسب (۱۰، ۲۰، ۳۰ درصد)، و فشارهای فشردن (۵۰، ۱۰۰ و ۱۵۰ کیلو پاسکال). یک کوره زغال چوب برای به دست آوردن پیش تیمار از طریق پیرولیز و یک پانچ و قالب نیز برای تسهیل تراکم قالبهها ساخته شد. خواص فیزیکی آزمایش شده به محتوای رطوبت (MC)، چگالی و مقاومت فشاری محدود بود و با استفاده از روش معمولی تعیین شد. مقادیر گرمایی قالبههای تولید شده با استفاده از کالریمتر بمب تعیین شد. نتایج نشان داد که میانگین رطوبت بین ۵/۲۹-۶/۵۸ درصد و ۱۲/۷۵-۱۳/۷۲ درصد، میانگین چگالی شل بین ۸۱۳-۹۲۵ kgm^{-3} و ۹۶۳-۱۱۶۶ kgm^{-3} و مقاومت فشاری بین ۲/۲۷-۵/۰۷ MPa و ۵/۹۷-۱۰/۱۲ MPa متغیر است. ارزش حرارتی بین ۲۸/۸۵-۳۲/۳۶ MJkg^{-1} و ۲۷/۵۸-۲۸/۸۰ MJkg^{-1} برای قالبههای کربنیزه و غیر کربنی شده به ترتیب در بازه زمانی قرار داشت. قالبههای تولید شده از ذرت کربن‌دار دارای رطوبت و مقادیر گرمایی بهتری بودند، در حالی که قالبههای تولید شده از ذرت بدون کربن دارای چگالی و مقاومت فشاری بالاتری بودند. این مطالعه نشان می‌دهد که روش‌های پیش تیمار تحت انواع بایندر و غلظت‌های مختلف و فشار فشردن‌سازی به‌طور قابل‌توجهی بر خواص فیزیکی و ارزش حرارتی قالبهها تأثیر می‌گذارد. بنابراین، این فناوری می‌تواند با موفقیت در مناطق روستایی خارج از شبکه توسط دولت و سایر ذینفعان در بخش انرژی به عنوان بخشی از فناوری‌های انرژی تجدیدپذیر به کار گرفته شود.

Potential for Battery Energy Storage System in Zimbabwe

Allen G. Njovana, Wenying Yu*, Qiyang Shen, Jiarui Li, Yanyan Zhu, Yongsheng Liu*

Institute of Solar Energy, Shanghai University of Electric Power, P. O. Box: 200090, Shanghai, China.

PAPER INFO

Paper history:

Received: 24 August 2021

Revised in revised form: 28 December 2021

Scientific Accepted: 08 January 2022

Published: 20 August 2022

Keywords:

Battery Energy Storage System,

Solar Photovoltaic,

BESS Investments,

Levelized Cost of Energy Storage,

Lithium-Iron Phosphate,

Zimbabwe

ABSTRACT

This study aims to assess the potential of coupling solar PV power plants with Battery Energy Storage System (BESS) to curtail load-shedding and provide a stable and reliable baseload power generation in Zimbabwe. Data from geographical surveys, power plant proposals, and investment information from related sources were reviewed and applied accordingly. Areas considered to be of good potential to employ the use of BESS were identified considering such factors as feasibility of PV plants, proximity to transmission lines, the size of a town or neighborhood, and energy demands for BESS Return On Investment (ROI) calculations. Previous studies have proven that 10 % of the suitable land for PV systems has the capability to generate thirty times the current power demand of the nation operating even with the least efficiency. In recent years, coupling renewable energy sources with a suitable energy storage system yielded improved performances, giving consumers a reliable, stable, and predictable grid. BESS technologies on the utility scale have improved in recent years, giving more options with improved safety, and decreasing the purchase costs, too.

<https://doi.org/10.30501/jree.2022.294957.1230>

2423-7469/© 2023 The Author(s). Published by MERC. This is an open access article under the CC BY license (<https://creativecommons.org/licenses/by/4.0/>).



چکیده

هدف از این مطالعه، ارزیابی پتانسیل اتصال نیروگاه‌های فتوولتائیک خورشیدی با سیستم ذخیره‌سازی انرژی باتری (BESS) برای کاهش بار و تولید برق پایدار و قابل اعتماد در زیمبابوه است. داده‌های بررسی‌های جغرافیایی، پیشنهادهای نیروگاهی و اطلاعات سرمایه‌گذاری از منابع مرتبط بررسی و بر این اساس اعمال شده است. مناطقی که پتانسیل خوبی برای استفاده از BESS دارند، در نظر گرفته شده‌اند و با در نظر گرفتن عواملی مانند امکان‌سنجی نیروگاه‌های فتوولتائیک، نزدیکی به خطوط انتقال، اندازه یک شهر یا محله و تقاضای انرژی برای محاسبات بازگشت سرمایه BESS (ROI) شناسایی شدند. مطالعات قبلی ثابت کرده است که ۱۰ درصد از زمین‌های مناسب برای سیستم‌های فتوولتائیک توانایی تولید ۳۰ برابر برق فعلی کشور را دارد که حتی با کمترین بازده کار می‌کنند. در سال‌های اخیر، اتصال منابع انرژی تجدیدپذیر با یک سیستم ذخیره‌ساز انرژی مناسب، عملکرد بهتری را به همراه داشته و به مصرف‌کنندگان، یک شبکه قابل اعتماد، پایدار و قابل پیش‌بینی ارائه داده است. فناوری‌های BESS در مقیاس سودمند در سال‌های اخیر بهبود یافته‌اند و گزینه‌های بیشتری را با ایمنی بهبود یافته و همچنین هزینه‌های خرید کاهش داده‌اند.

A Brief Overview of Microgrid Performance Improvements Using Distributed FACTS Devices

Ghazanfar Shahgholian ^{a,b*}

^a Department of Electrical Engineering, Najafabad Branch, Islamic Azad University, Najafabad, Iran.

^b Smart Microgrid Research Center, Najafabad Branch, Islamic Azad University, Najafabad, Iran.

PAPER INFO

Paper history:

Received: 26 December 2021

Revised in revised form: 28 February 2022

Scientific Accepted: 24 March 2022

Published: 27 August 2022

Keywords:

Microgrid,
Distributed Flexible AC Transmission
System,
Performance,
Connection Mode

ABSTRACT

Distributed flexible ac transmission system (D-FACTS) is a light-weight version of FACTS, which it is easily allocated and costs less than flexible ac transmission system (FACTS) devices. They have potential benefits to improve the system stability and improvement in power quality in microgrid (MG). The integration of distributed energy sources, loads, electrical energy storage devices, and electronic power devices, as well as the operation of microgrids in connected or island-connected modes has expanded their use. It is a small main grid that can generate electricity when disconnected from the main network. In addition, microgrids reduce the high investment costs required to upgrade the network. The application of DFACTS devices for improving the microgrid operation has been investigated by some researches. This paper provides a review of impact and role of various DFACTS devices in the function of microgrids, which has been reported in recent years in various pieces of the literature. DFACTS devices with their properties are described. Finally, a useful reference and framework for the study is provided for future expansion of DFACTS devices so as to improve the performance of the microgrid.

<https://doi.org/10.30501/jree.2022.321435.1305>

2423-7469/© 2023 The Author(s). Published by MERC. This is an open access article under the CC BY license (<https://creativecommons.org/licenses/by/4.0/>).



چکیده

سیستم انتقال جریان متناوب توزیع شده^۱ (D-FACTS) یک نمونه اقتصادی از ادوات FACTS است که به راحتی قابل تخصیص است و هزینه کمتری نسبت به دستگاه‌های سیستم انتقال جریان متناوب (FACTS) دارد. آنها مزایای بالقوه‌ای برای بهبود پایداری سیستم و بهبود کیفیت توان در ریزشبكة (MG) دارند. ادغام منابع انرژی توزیع شده، بارها، دستگاه‌های ذخیره انرژی الکتریکی و دستگاه‌های برق الکترونیکی، و همچنین عملکرد ریزشبكة‌ها در حالت‌های متصل یا متصل به جزیره، استفاده از آنها را گسترش داده است. این یک شبکه اصلی کوچک است که می‌تواند در صورت قطع شدن از شبکه اصلی برق تولید کند. علاوه بر این، ریزشبكة‌ها هزینه‌های بالای سرمایه‌گذاری مورد نیاز برای ارتقاء شبکه را کاهش می‌دهند. کاربرد دستگاه‌های DFACTS برای بهبود عملکرد ریزشبكة توسط برخی تحقیقات بررسی شده است. این مقاله مروری بر تأثیر نقش دستگاه‌های مختلف DFACTS در ریزشبكة‌ها ارائه می‌کند که در سال‌های اخیر در ادبیات مختلف گزارش شده است. دستگاه‌های DFACTS با ویژگی‌های آنها شرح داده شده است. در نهایت، یک مرجع و چارچوب مفید جهت مطالعه برای گسترش آینده دستگاه‌های DFACTS برای بهبود عملکرد ریزشبكة ارائه شده است.

¹ Distributed Flexible AC Transmission System

Improving the Efficiency of a Cantilever Energy Scavenger

Mohammad Rahimzadeh ^{a*}, Hamid Samadi ^b, Nikta Shams Mohammadi ^c

^a Department of Mechanical Engineering, Faculty of Engineering, Golestan University, P. O. Box: 49138-15759, Gorgan, Golestan, Iran.

^b Department of Mechanical Engineering, Babol University of Technology, P. O. Box: 47148-73113, Babol, Mazandaran, Iran.

^c Department of Electrical Engineering, Shahrood University of Technology, P. O. Box: 36199-95161, Shahrood, Semnan, Iran.

PAPER INFO

Paper history:

Received: 16 December 2021

Revised in revised form: 01 May 2022

Scientific Accepted: 21 May 2022

Published: 27 August 2022

Keywords:

Piezoelectric,
Cantilever Beam,
Energy Harvesting,
Voltage,
Unimorph

ABSTRACT

Energy harvesting from ambient vibrations using piezoelectric cantilevers is one of the most popular mechanisms for producing electrical energy. Recently, efforts have been made to improve the performance of energy harvesters. The output voltage dramatically depends on the geometrical and physical parameters of these devices. In addition, improved performance is often achieved by operating at or near the resonance point. So, this paper aims to reduce the natural frequency to match the environmental excitation frequency and increase the harvested energy. For this purpose, different geometrical and physical parameters are studied to determine the impact of each parameter. These parameters include the length, thickness, density, and Young's modulus of each layer. The beam is considered a unimorph cantilever with rectangular configuration and the study is performed using COMSOL Multiphysics software. The results are compared with those obtained by an analytical approach. The results show that changing the parameters made the natural frequency of the system vary in the range of 20 Hz to 200 Hz and increased the output voltage up to 20 V.

<https://doi.org/10.30501/jree.2022.320113.1300>

2423-7469/© 2023 The Author(s). Published by MERC. This is an open access article under the CC BY license (<https://creativecommons.org/licenses/by/4.0/>).



چکیده

برداشت‌کننده های انرژی مورد استفاده در هر محیط، متفاوت هستند. طراحی یک سیستم مناسب به منظور برداشت انرژی از یک محیط خاص نیازمند مطالعه و بررسی شرایط آن می‌باشد. لذا انتخاب مناسب پارامترهای هندسی و فیزیکی سیستم برداشت‌کننده، بسیار مهم است. اصلی ترین هدف از این طراحی، پایین آوردن فرکانس طبیعی برای تطابق با فرکانس تحریک در محیط موردنظر و افزایش میزان انرژی برداشتی می‌باشد. در این تحقیق با تغییر پارامترهای مختلف هندسی و فیزیکی، میزان تأثیر هر یک در فرآیند برداشت انرژی سنجیده شد. از جمله این پارامترها می‌توان به طول تیر، ضخامت، چگالی و مدول الاستیسیته هر یک از لایه‌ها اشاره نمود. تیر به صورت مستطیلی و دارای یک لایه پیزوالکتریک در نظر گرفته شد. شبیه‌سازی به دو روش تحلیلی و اجزای محدود انجام شد که از تطابق بسیار خوبی برخوردار بودند. نتایج نشان دادند که با تغییر پارامترهای مختلف، می‌توان فرکانس طبیعی اول سیستم را بین ۲۰ تا ۲۰۰ هرتز و ولتاژ استحصالی را تا ۲۰ ولت تغییر داد.

Investigation of a Set of Novel Heat Exchanger Configurations of a Heat Recovery Steam Generator to Improve the Energy Efficiency of Combined Cycle Power Plant

Mohammad Rasooli Mavini ^a, Hassan Ali Ozgoli ^{b*}, Sadegh Safari ^a

^a Department of Energy Engineering, Faculty of Natural Resources and Environment, Science and Research Branch, Islamic Azad University (IAU), P. O. Box: 14515-775, Tehran, Tehran, Iran.

^b Department of Mechanical Engineering, Iranian Research Organization for Science and Technology (IROST), P. O. Box: 33535-111, Tehran, Tehran, Iran.

PAPER INFO

Paper history:

Received: 24 January 2022

Revised in revised form: 08 May 2022

Scientific Accepted: 28 May 2022

Published: 28 September 2022

Keywords:

HRSG,

CHP,

Configuration Analysis,

Energy Efficiency,

Environment Analysis

ABSTRACT

In this study, various configuration designs of a Heat Recovery Steam Generator (HRSG) are examined to enhance the energy efficiency of a Combined Cycle Power Plant (CCPP). A novel approach to investigating ten applicable configurations of a dual pressure HRSG is used thoroughly to explore the best practice models from the energy-conserving perspective. Further, a fuel consumption assessment has been conducted to identify the best performance of the cycle and investigate the minimum pollutants released by each Heat Recovery Steam Generator (HRSG). The results revealed that four out of ten scenarios expressed considerably better performance in terms of fuel consumption, steam production, energy efficiency, and environmental considerations. Further, it was found that compared to conventional configurations, not only the selected scenarios managed to improve the low-pressure steam generation, but also 30 % fuel consumption saving in supplementary firing was achieved as both economic and environmental benefits. Moreover, the carbon dioxide saving potential for the best scenario is $51.37 \text{ kgCO}_2 \text{ MWh}^{-1}$; consequently, the environmental benefit of it is calculated to be about $133,418 \$ \text{ MWh}^{-1}$.

<https://doi.org/10.30501/jree.2022.326260.1317>

2423-7469/© 2023 The Author(s). Published by MERC. This is an open access article under the CC BY license (<https://creativecommons.org/licenses/by/4.0/>).



چکیده

در این مطالعه، طرح‌های پیکربندی مختلف یک دیگ بخار بازیافت حرارت به منظور افزایش کارایی انرژی یک نیروگاه سیکل ترکیبی مورد بررسی قرار گرفته است. یک رویکرد جدید برای بررسی کامل ده پیکربندی مختلف یک دیگ بخار بازیافت حرارت استفاده شده تا بهترین مدل یا مدل‌های عملی یک بویلر بازیافت حرارت با در نظر گرفتن ملاحظات صرفه‌جویی در مصرف انرژی شناسایی شود. علاوه بر این، ارزیابی مصرف سوخت برای شناسایی بهترین عملکرد چرخه و بررسی حداقل آلاینده‌های منتشر شده از هر پیکربندی دیگ بخار بازیافت حرارت انجام شده است. نتایج نشان داده است که چهار سناریو از بین ده سناریو، عملکرد قابل توجه بهتری را در زمینه‌های: مصرف سوخت، تولید بخار، بهره‌وری انرژی و در نهایت ملاحظات زیست‌محیطی داشته‌اند. علاوه بر این، مشخص شده است که در مقایسه با پیکربندی متعارف، نه تنها سناریوهای انتخاب شده تقریباً چهار برابر بهبود در تولید بخار کم‌فشار را نشان داده‌اند، بلکه ۳۰ درصد صرفه‌جویی در مصرف سوخت در بخش فشار بالا حاصل شده است که از هر دو منظر اقتصادی بودن و داشتن مزایای زیست‌محیطی برتری دارد. علاوه بر این، پتانسیل صرفه‌جویی در دی‌اکسیدکربن برای بهترین سناریو $51.37 \text{ kgCO}_2 \text{ MWh}^{-1}$ کیلوگرم $\text{CO}_2 \text{ MWh}^{-1}$ است که در نتیجه سود ناشی از مسائل زیست‌محیطی آن در حدود $133,418 \$ \text{ MWh}^{-1}$ محاسبه شده است.

CONTENTS

<p>Roxana Isabel Bernaola Flores Carmen Elena Flores Barreda Diana Carolina Parada Quinayá Ursula Fabiola Rodríguez Zúñiga</p>	<p>Energy Potential of Agricultural and Forestry By-Products in Peru</p>	<p>1-8</p>
<p>Farhad Amiri Mohammad Hassan Moradi</p>	<p>Improvement of Frequency Stability in the Power System Considering Wind Turbine and Time Delay</p>	<p>9-18</p>
<p>Sapna Kinattinkara Thangavelu Arumugam Nandhini Samiappan Vivek Sivakumar Sampathkumar Velusamy Mohanraj Murugesan Manoj Shanmugamoorthy</p>	<p>Deriving an Alternative Energy Using Anaerobic Co-Digestion of Water Hyacinth, Food Waste, and Cow Manure</p>	<p>19-25</p>
<p>Toyese Friday Oyewusi Gabriel Alebiowu Elizabeth Funmilayo Aransiola Ayowumi Rita Soji-Adekunle Busayo Sunday Adeboye</p>	<p>Effect of Pretreatment on the Physical Properties and Heating Values of Briquettes</p>	<p>26-33</p>
<p>Allen G. Njovana Wenying Yu Qiyang Shen Jiarui Li Yanyan Zhu Yongsheng Liu</p>	<p>Potential for Battery Energy Storage System in Zimbabwe</p>	<p>34-42</p>
<p>Ghazanfar Shahgholian</p>	<p>A Brief Overview of Microgrid Performance Improvements Using Distributed FACTS Devices</p>	<p>43-58</p>
<p>Mohammad Rahimzadeh Hamid Samadi Nikta Shams Mohammadi</p>	<p>Improving the Efficiency of a Cantilever Energy Scavenger</p>	<p>59-67</p>
<p>Mohammad Rasooli Mavini Hassan Ali Ozgoli Sadegh Safari</p>	<p>Investigation of a Set of Novel Heat Exchanger Configurations of a Heat Recovery Steam Generator to Improve the Energy Efficiency of Combined Cycle Power Plant</p>	<p>68-82</p>

